



CREEP AND PLASTICITY PARAMETER DETERMINATION OF SAND-TDA MIXTURES FOR THE PURPOSE OF CONSTITUTIVE MODELING

Thèse

Nima Ghafari

Doctorat en génie civil
Philosophiæ doctor (Ph. D.)

Québec, Canada

© Nima Ghafari, 2022

**CREEP AND PLASTICITY PARAMETER
DETERMINATION OF SAND-TDA MIXTURES FOR
THE PURPOSE OF CONSTITUTIVE MODELING**

Thèse

Doctorat en génie civil
Philosophiae Doctor (Ph. D.)

Nima Ghafari

Sous la direction de :

Adolfo Foriero, ing., PhD, directrice de recherche

RÉSUMÉ

L'objectif de cette étude est le développement d'une base de connaissances pour la conversion d'un déchet problématique en matériau de construction pour des projets de génie civil. Le phénomène de mécanisation des sociétés, la croissance rapide de la population, ainsi que le développement du réseau de transport terrestre par la construction des nouvelles routes et autoroutes ont entraîné une croissance sans cesse de l'industrie automobile à travers le monde et par conséquent l'accumulation de gros volumes de pneus usés. Chaque année, les Américains et les Canadiens éliminent en moyenne environ 300 millions de pneus (respectivement 250 et 30 millions de pneus), ce qui a accru les préoccupations environnementales liées à l'élimination de ces déchets non biodégradables et polluants. Par conséquent, la gestion des déchets de pneus nécessite des méthodes innovantes et efficaces d'élimination et de réutilisation des pneus.

Un pneu est généralement composé de trois composants principaux, notamment le caoutchouc, le métal et le tissu. Le cycle de vie des pneus est généralement composé de cinq étapes principales : extraction, production, consommation, collecte des pneus usagés et enfin la gestion des déchets qui comprend les sites enfouissement et la récupération.

Grâce à l'un des processus de récupération, les pneus usagés sont découpés en différentes formes et tailles appelées agrégats dérivés de pneus (ADP). Actuellement, des efforts considérables sont en cours au niveau mondial pour recycler les pneus usagés sous forme d'agrégats dérivés de pneus (ADP) à des fins d'ingénierie civile et géotechnique différentes. En tant que géo-matériau, les formes déchiquetées et granulées des pneus usés sont généralement mélangées avec du sable et / ou du limon pour former ce que l'on appelle communément des mélanges sol-ADP. En raison de leur faible poids, de leur bon drainage, de leurs propriétés d'isolation thermique satisfaisantes, de leur atténuation des vibrations, etc., les géo-matériaux d'ingénierie contenant du ADP sont devenus intéressants pour les ingénieurs concepteurs. Cependant, en raison de leur faible module d'élasticité, les mélanges ADP-sol présentent une compressibilité significative par rapport à celle des sols conventionnels. Spécifiquement, la compressibilité excessive des mélanges sol-ADP, qui est composé à la fois de la partie immédiate et celle dépendante du temps est extrêmement difficile à cerner dans les applications où de lourdes charges sus-jacentes sont appliquées. Afin de maximiser leur fiabilité et de minimiser la possibilité de ruptures, il est nécessaire d'avoir une compréhension précise du comportement

mécanique (par exemple, élastique, plastique et fluage) des mélanges sol-ADP lorsqu'ils sont soumis à une charge.

La présente étude comprend deux phases. Les phases consistent en un programme expérimental qui a été mené pour déterminer les paramètres essentiels d'élasticité, de plasticité et de fluage des mélanges granulés ADP-sable. Des simulations MEF ont ensuite été réalisées aux fins de la validation des résultats des essais.

Les valeurs des paramètres obtenus grâce aux observations expérimentales ont été utilisées dans le développement de modèles de comportement qui sont proposés pour les comportements de fluage et de déformation plastique des mélanges sable-ADP. En ce qui concerne le fluage, les résultats indiquent une phase de fluage primaire qui est rapidement passée à une phase de fluage stationnaire secondaire, n'atteignant jamais la phase tertiaire. Il a également été observé que l'ampleur de la déformation de fluage est fortement affectée par la teneur en fraction volumique de l'ADP et la charge appliquée. Cette observation a conduit à l'adoption de la loi Norton-Bailey comme modèle constitutif possible du fluage des mélanges ADP-sable. En outre, un modèle complet de comportement sol-ADP doit également englober la plasticité. Ceci a été réalisé grâce au développement d'un modèle d'état critique, basé sur les paramètres de plasticité obtenus expérimentalement des tests triaxiaux. Les courbes de contrainte déviatorique en fonction de la déformation axiale obtenues avec le modèle d'état critique ont capturé la réponse élastoplastique non linéaire obtenue dans les essais. Les résultats ont indiqué que le niveau de résistance au cisaillement dépend fortement de l'angle de frottement à l'état critique qui à son tour dépend de la teneur en ADP. Pour les mélanges ADP-sable utilisés dans cette étude, l'effet de la teneur en ADP démontre un renforcement de la matrice de sable. Cependant, ce renforcement diminue à mesure que la teneur en ADP augmente.

Mots clés: équation constitutive, paramètre de fluage, déformation, géo-matériau, pneu usé, ADP.

ABSTRACT

The aim of this study is the development of a knowledge base for the conversion of a problematic waste product into a construction material for civil engineering projects. The phenomenon of mechanization of the societies, rapidly growing population, and also the development of the land transportation network through the construction of the new roads and highways have resulted in an unceasingly growing of auto industry across the world and consequently accumulation of large volumes of scrap automobile tires.

Every year Americans and Canadians together average disposal of approximately 300 million tires (respectively 250 and 30 million tires) which consequently has increased environmental concerns over the disposal of such non-biodegradable and pollutant waste materials. Hence, scrap tire management requires innovative and efficient methods of tire disposal and reuse.

A tire is generally made from three main components including rubber, metal, and fabric. The tire life cycle is generally composed of five main stages including extraction, production, consumption, collection of used tires and finally waste management which is comprised of landfilling and recovery.

Through one of the recovery processes, scrap tires are cut into different shapes and sizes called tire-derived aggregate (TDA). Presently, global extensive efforts are underway in order to recycle the waste tires in the form of tire-derived aggregate (TDA) for different civil and geotechnical engineering purposes. As a geomaterial, usually the shredded and granulated forms of scrap tires are mixed with sand and/or silt to form what is commonly referred to as soil-TDA mixtures. Due to their lightweight, good drainage, satisfactory thermal insulation properties, vibration mitigation, etc., engineered geomaterials containing TDA have become of interest to design engineers. However, due to their low elastic modulus, TDA-soil mixtures exhibit significant compressibility compared to that of conventional soils. Specifically, the excessive compressibility of soil-TDA mixtures which is composed of both immediate and time-dependent portions is extremely challenging in such applications wherein heavy overlying loads are applied. In order to maximize their reliability and to minimize the possibility of failures, it is necessary to have an accurate understanding on the mechanical behavior (e.g., elastic, plastic and creep) of the soil-TDA mixtures when subjected to loading.

The present study consists of two phases. These phases consist of an experimental program that was conducted to determine the elastic, plastic, and creep parameters of TDA-sand granulated mixtures. FEM simulations were subsequently conducted for the purposes of test result validation.

Values of the parameters obtained through the experimental observations were used in the development of constitutive models which are proposed for the creep and plastic deformation behaviors of the sand-TDA mixtures. In regard to creep, the results indicate a primary creep phase that rapidly transitioned into a secondary stationary creep phase, never attaining the tertiary phase. It has been also observed that the magnitude of the creep strain is strongly affected by the TDA volume fraction content and the applied load. This observation conducted the adoption of the Norton-Bailey law as a possible constitutive model for creep of TDA-sand mixtures. Furthermore, a complete model of soil-TDA behavior must also encompass plasticity. This was achieved through the development of a critical state model, based on the experimentally obtained plasticity parameters of triaxial tests. The calculated deviatoric stress versus axial strain curves obtained with the critical state model captured the non-linear elastoplastic response obtained in the tests. Results indicated that the level of the shear strength is highly dependent on the critical state friction angle which in turn depends on the TDA content. For the loose TDA-sand mixtures used in this study, the effect of the TDA content demonstrates a reinforcement of the sand matrix. However, this reinforcement diminishes as the TDA content increases.

Keywords: Constitutive equation, creep parameter, deformation, geomaterial, scrap tire, TDA.

TABLE OF CONTENT

<u>RÉSUMÉ</u>	<u>II</u>
<u>ABSTRACT</u>	<u>IV</u>
<u>TABLE OF CONTENT</u>	<u>VI</u>
<u>LIST OF TABLES</u>	<u>X</u>
<u>LIST OF FIGURES</u>	<u>XI</u>
<u>LIST OF SYMBOLS</u>	<u>XVI</u>
<u>DEDICATION</u>	<u>XVIII</u>
<u>ACKNOWLEDGEMENTS</u>	<u>XIX</u>
<u>FOREWORD</u>	<u>XX</u>
<u>INTRODUCTION</u>	<u>1</u>
CONTEXT OF THE STUDY	1
UTILIZATION OF TDA IN EARTHWORK APPLICATIONS	6
PROBLEM STATEMENT	8
GENERAL OBJECTIVES OF THE STUDY	10
ORIGINALITY OF THE STUDY	11
MOTIVATION AND SIGNIFICANCE OF THE STUDY	12
THESIS ORGANIZATION	13
<u>CHAPTER 1</u>	<u>14</u>
<u>1 LITERATURE REVIEW</u>	<u>14</u>
1.1 MOTORIZED VEHICLE TIRE	15
1.2 TIRE COMPOSITION AND STRUCTURE	15
1.3 SCRAP TIRE DEFINITION	17
1.4 ENVIRONMENTAL ISSUES CAUSED BY STOCKPILING OF SCRAP TIRES	17
1.4.1 CONTROLLED COMBUSTION OF WASTE TIRE	19
1.4.2 OPEN AIR COMBUSTION OF WASTE TIRE	19

1.5	HISTORY OF THE TIRE FIRE INCIDENTS IN CANADA	19
1.5.1	HAGERSVILLE TIRE FIRE – ONTARIO, FEBRUARY 1990	19
1.5.2	SAINT AMABLE TIRE FIRE – QUÉBEC, MAY 1990	20
1.6	TIRE DERIVED AGGREGATE (TDA)	20
1.7	FUNDAMENTAL MECHANICAL CHARACTERISTICS OF SAND-TIRE MIXTURES	21
1.7.1	UNIT WEIGHT AND VOID RATIO OF SAND-TIRE MIXTURES	22
1.7.2	COMPRESSIBILITY CHARACTERISTICS OF DRY SAND-TIRE MIXTURES	24
1.7.3	SHEAR STRENGTH AND DILATANCY CHARACTERISTICS OF SAND-TIRE MIX	28
1.8	CIVIL ENGINEERING APPLICATIONS OF TDA	34
1.9	GEOTECHNICAL ENGINEERING APPLICATIONS OF TDA	35
1.10	SPECIFICATIONS AND GUIDELINES FOR USE OF SCRAP TIRE IN CIVIL ENGINEERING	36
1.11	EXISTING MODELS TO PREDICT CREEP BEHAVIOR OF TDA AND TDA-SAND MIXTURES	37
1.11.1	THE MODEL RECOMMENDED BY NGO AND VALDES IN 2007	37
1.11.2	THE MODEL RECOMMENDED BY WARTMAN ET AL. IN 2007	38
1.12	BAILEY-NORTON CREEP LAW	39
1.13	GENERAL CONCLUSION OF CHAPTER 1 (LITERATURE REVIEW)	40
<u>CHAPTER 2</u>		<u>42</u>
2	<u>METHODOLOGY</u>	<u>42</u>
2.1	INTRODUCTION	42
2.2	TEST MATERIALS	42
2.2.1	SAMPLE PREPARATION PROCEDURES	45
2.3	DESCRIPTION OF THE CREEP TEST FOR DETERMINING THE CREEP PARAMETERS OF THE NORTON-BAILEY CONSTITUTIVE MODEL	46
2.3.1	DESCRIPTION OF THE SAMPLES AND TEST APPARATUS SETUP	47
2.4	DESCRIPTION OF THE TRIAXIAL TEST FOR DETERMINATION OF THE PLASTICITY PARAMETERS FOR THE CONSTITUTIVE CRITICAL STATE MODEL	51
2.4.1	TEST APPARATUS AND EXPERIMENTAL PROCEDURE	51
2.5	DIRECT SHEAR TESTS FOR DETERMINATION OF THE TRUE STRESSES OF THE CREEP TESTS	53
2.5.1.1	Shear Box Test Procedure	54
2.6	SMALL-SCALE FOUNDATION TEST	57
<u>CHAPTER 3 : FOREWORD</u>		<u>60</u>
AUTHORS AND AFFILIATIONS		60
AUTHOR CONTRIBUTIONS		60
RÉSUMÉ FRANÇAIS		61
<u>3 LABORATORY CREEP PARAMETER DETERMINATION OF SAND-TDA MIXTURES WITH SUBSEQUENT FEM VALIDATION</u>		<u>63</u>

3.1	ABSTRACT	63
3.2	LIST OF SYMBOLS	63
3.3	INTRODUCTION	64
3.4	SAND-TDA MIXTURES OF THE CREEP TESTS	66
3.5	APPARATUS FOR THE CREEP TESTS	66
3.6	TESTING PROCEDURE	68
3.7	DISCUSSION OF THE CREEP TEST RESULTS	71
3.8	EQUATION OF STATE APPROACH TO MODEL CREEP OF SAND-TDA MIXTURES	75
3.9	BACK-CALCULATION OF THE CREEP PARAMETERS BASED ON THE TEST RESULTS	77
3.10	ASSESSMENT OF THE CREEP LAW BASED ON THE BACK-CALCULATED CREEP PARAMETERS	82
3.11	EXTENSION OF THE CREEP LAW FOR MULTI-AXIAL DEVIATORIC CREEP FEM FORMULATIONS	84
3.12	FEM MODEL TO SIMULATE A SMALL-SCALE FOUNDATION CREEP TEST	85
3.13	CONCLUSIONS	95
3.14	ACKNOWLEDGMENTS	95
3.15	APPENDIX	95
3.16	REFERENCES	96
<u>CHAPTER 4 : FOREWORD</u>		<u>99</u>
	AUTHORS AND AFFILIATIONS	99
	AUTHOR CONTRIBUTIONS	99
	RÉSUMÉ FRANÇAIS	101
<u>4 A CRITICAL STATE MODEL OF SAND-TDA MIXTURES BASED ON TRIAXIAL TESTS</u>		<u>102</u>
4.1	ABSTRACT	102
4.2	INTRODUCTION	102
4.3	SAND-TDA MIXTURES OF THE TRIAXIAL TESTS	104
4.4	TEST EQUIPMENT AND EXPERIMENTAL PROCEDURE	106
4.5	TEST RESULTS AND OBSERVATIONS	106
4.6	A CRITICAL STATE MODEL TO INTERPRET TDA-SAND MIXTURES	112
4.7	CALCULATION PROCEDURE FOR THE STRESS-STRAIN RESPONSE OF THE SAND-TDA MIXTURE	116
4.8	COMPARISON OF THE CRITICAL STATE MODEL WITH THE TRIAXIAL TEST RESULTS	116
4.9	CONCLUSIONS	124
4.10	LIST OF SYMBOLS	125
4.11	ACKNOWLEDGMENTS	126
4.12	AUTHOR CONTRIBUTIONS	126
4.13	DECLARATION OF CONFLICTING INTERESTS	126
4.14	REFERENCES	126

CHAPTER 5	129
5 RESULTS AND DISCUSSION	129
5.1 RESULTS OF CREEP PARAMETER DETERMINATION	129
5.1.1 RESULTS OF DIRECT SHEAR TESTS FOR DETERMINATION OF THE NOMINAL STRESSES	129
5.1.2 DISCUSSION ON THE CREEP TEST RESULTS	131
5.2 EVALUATION OF THE CREEP LAW BASED ON THE BACK-CALCULATED CREEP PARAMETERS	139
5.3 REBOUND BEHAVIOR OF A SAND-TDA SAMPLE UNDER TRIAXIAL TESTING	141
5.4 SIMULATION OF THE BEHAVIOR OF THE SAND-TDA MIXTURES DURING A TUNNEL EXCAVATION	142
5.4.1 INTRODUCTION	142
5.4.2 FINITE ELEMENT MESH	143
5.4.3 SOIL PROPERTIES AGGREGATE	143
5.4.4 PROPERTIES OF SOIL-TIRE AGGREGATE MIXTURE	143
5.4.5 RESULTS AND DISCUSSION	144
CONCLUSION	149
REFERENCES	153

LIST OF TABLES

Table 1.1 Composition of passenger car and truck/bus tires (Rahman, 2004; Presti, 2013) _____	15
Table 2.1 Test sample specifications. _____	45
Table 3.1 Friction angle: shear box tests results (aluminum–Ottawa sand–TDA mixture) _____	70
Table 3.2 Net force calculation, based on the estimated wall friction obtained in shear box tests _	70
Table 3.3 True Stress*, Based on Net Force Calculations _____	71
Table 3.4 Creep parameters obtained from long duration tests at the reference strain rate ($\dot{\epsilon}_c =$ 0.0001 <i>min</i> – 1) and room temperature. _____	81
Table 4.1 Initial void ratio and unit weight of Ottawa Sand-TDA mixture _____	105

LIST OF FIGURES

Figure 1.1 Typical vehicle tire structure	16
Figure 1.2 Typical tire sidewall information (Les Schwab Tire Center 2020)	16
Figure 1.3 Stockpiled scrap tires occupying a large dumping area and imposing ecological pollution	17
Figure 1.4 Garner/Brandywine Scrap Tire Stockpile.	18
Figure 1.5 Influence of tire content on unit weight of soil-TDA mixtures	23
Figure 1.6 Influence of mixing ratio on dry unit weight of sand-tire mixed materials	24
Figure 1.7 Axial strain vs. vertical effective stress for sand-tire mixtures with different tire content	26
Figure 1.8 Variation of vertical compressive strain at 100 <i>kPa</i> for various TDA content.	27
Figure 1.9 Variation of total, plastic and elastic strains at 458 <i>kPa</i> vertical stress.	27
Figure 1.10 Influence of tire content on the value of initial friction angle (f'_1) of sand-tire mixtures	31
Figure 1.11 Influence of normal stress and tire content on shear strength of sand-tire mix.	31
Figure 1.12 Influence of tire content and normal stress on friction angel of sand-tire mixtures	32
Figure 1.13 Influence of tire content and confining pressure on the peak deviator stress	33
Figure 2.1 TDA granular material employed in this study	43
Figure 2.2 Grain-size distribution curves of TDA and Ottawa sand used in this study	43
Figure 2.3 TDA particle size distribution by percentage	44
Figure 2.4 Graded Ottawa sand used in this study	44
Figure 2.5 Phase diagram of TDA–sand mixture	46
Figure 2.6 Preparation of the cylindrical aluminum cell	48
Figure 2.7 The cylindrical aluminum cell and loading cap with their dimensions	48
Figure 2.8 Placement of specimens inside the cylindrical cell before mixing	49
Figure 2.9 Measurement and preparation of the weights	49
Figure 2.10 Creep test illustration	50
Figure 2.11 A whole perspective of the triaxial test	52
Figure 2.12 Test materials (sand and TDA) and triaxial test sample preparation	52
Figure 2.13 Illustration of the sample under triaxial testing while LVDT is connected to the PC to measure and record the vertical deformations occurred during the experiment	53
Figure 2.14 Illustration of direct shear test using shear box apparatus	54

Figure 2.15 Shear box and the Al 6061 plate which is placed at the bottom of the box	55
Figure 2.16 Illustration of the shear box and LVDTs positions as well as the data recording by computer during the direct shear testing	55
Figure 2.17 Flattening of surface of the sample before placement of the loading cap	56
Figure 2.18 Test materials (sand and TDA) and the testing cell before and after the sample preparation and placement	58
Figure 2.19 Illustration of the small-scale test and the condition of the sample during the test	59
Figure 2.20 Data recording procedure during small-scale foundation test	59
Figure 3.1 Grain-size distribution curves of materials used in the present study	67
Figure 3.2 Phase diagram of TDA–sand mixture	67
Figure 3.3 Consolidometer loading frame used for the creep tests	68
Figure 3.4 Loading cap and cylindrical aluminum cell (adapted for the consolidometer)	69
Figure 3.5 Typical shear box test setup to determine the friction angle between TDA–soil mixture and aluminum alloy 6061	69
Figure 3.6 Typical shear box test result of a TDA–sand mixture resting	70
Figure 3.7 Constant stress logarithmic creep curves of the total strains (40% TDA)	72
Figure 3.8 Total strain as a function of the applied vertical stress for specific times (40% TDA)	72
Figure 3.9 Constant stress creep curves of the creep strains (80% TDA)	73
Figure 3.10 Constant stress creep curves of the creep strains (100% TDA)	73
Figure 3.11 Determination of the time creep parameter b (60% TDA)	79
Figure 3.12 Determination of the time creep parameter b (100% TDA)	80
Figure 3.13 Determination of the creep parameter n (60% TDA)	80
Figure 3.14 Determination of the creep modulus for the power law	81
Figure 3.15 A comparison of the creep law with the test results for $\sigma_v = 75 \text{ kPa}$ (40% TDA)	83
Figure 3.16 A comparison of the creep law with the test results for $\sigma_v = 75 \text{ kPa}$ (100% TDA)	83
Figure 3.17 Axisymmetric finite element mesh used for the test	87
Figure 3.18 Triaxial test results of initial elastic modulus as a function of %TDA for $\sigma_v = 100 \text{ kPa}$	87
Figure 3.19 Comparison of a finite element simulation and test results for $\sigma_v = 100 \text{ kPa}$ at $\theta = 80\%$ TDA	89
Figure 3.20 Comparison of a finite element simulation and test results for $\sigma_v = 100 \text{ kPa}$ at $\theta = 100\%$ TDA	89
Figure 3.21 Typical result of vertical displacements obtained by finite element simulation for $\sigma_v = 100 \text{ kPa}$ at $\theta = 80\%$ TDA	90

Figure 3.22 Comparison of a finite element simulation and test results for $\sigma_v = 50 \text{ kPa}$ at $\theta = 60\%$ TDA _____	90
Figure 3.23 Comparison of a finite element simulation and test results for $\sigma_v = 35 \text{ kPa}$ at $\theta = 40\%$ TDA _____	91
Figure 3.24 Rigid circular plate resting on a TDA–sand mixture _____	91
Figure 3.25 Laboratory setup for small-scale circular rigid plate resting on a TDA–sand mixture_	92
Figure 3.26 Axisymmetric finite element mesh used for the small-scale foundation simulations__	93
Figure 3.27 FEM simulation of rigid circular plate resting on a TDA–sand mixture _____	93
Figure 3.28 Vertical strain after 18,655 min: FEM simulation of rigid circular plate resting on a TDA– sand mixture _____	94
Figure 3.29 Total vertical displacements at 200 min: FEM simulation of rigid circular plate resting on a TDA–sand mixture _____	94
Figure 4.1 Grain-size distribution curves of materials used in the present study_____	105
Figure 4.2 Phase diagram of TDA–sand mixture_____	105
Figure 4.3 Triaxial test configuration_____	106
Figure 4.4 Test results of deviatoric stress versus axial strain at 50 % TDA_____	107
Figure 4.5 Test results of deviatoric stress versus axial strain at 75 % TDA_____	107
Figure 4.6 The shape of the sand-TDA sample having 75% TDA at the end of the triaxial test __	108
Figure 4.7 Test results of deviatoric stress versus axial strain at 100 % TDA_____	109
Figure 4.8 Deviatoric stress versus axial strain at failure for $\sigma_3 = 50 \text{ kPa}$ _____	109
Figure 4.9 Deviatoric stress versus axial strain at failure for $\sigma_3 = 100 \text{ kPa}$ _____	110
Figure 4.10 Deviatoric stress versus axial strain at failure for $\sigma_3 = 150 \text{ kPa}$ _____	110
Figure 4.11 Secant elastic modulus versus axial strain at failure for $\sigma_3 = 50 \text{ kPa}$ _____	111
Figure 4.12 Secant elastic modulus versus axial strain at failure for $\sigma_3 = 100 \text{ kPa}$ _____	111
Figure 4.13 Secant elastic modulus versus axial strain at failure for $\sigma_3 = 150 \text{ kPa}$ _____	112
Figure 4.14 Determination of the frictional constant M at a TDA of 50 % and $\epsilon_v = 20 \%$ _____	117
Figure 4.15 Determination of the frictional constant M at a TDA of 50 % and $\epsilon_v = 23 \%$ _____	118
Figure 4.16 Determination of the frictional constant M at a TDA of 75 % and $\epsilon_v = 20 \%$ _____	118
Figure 4.17 Determination of the frictional constant M at a TDA of 75 % and $\epsilon_v = 23 \%$ _____	119
Figure 4.18 Mobilized friction angle versus vertical strain at TDA = 50 % _____	119
Figure 4.19 Mobilized friction angle versus vertical strain at TDA = 75 % _____	120
Figure 4.20 Modified Cam Clay Model in p-q Space for Ottawa Sand_____	121
Figure 4.21 Deviatoric stress versus axial strain, void ratio versus axial strain, and deviatoric strain versus volumetric strain at 50% tire derived aggregate (TDA) and $\sigma_3 = 100 \text{ kPa}$. _____	121

Figure 4.22 Deviatoric stress versus axial strain, void ratio versus axial strain, and deviatoric strain versus volumetric strain at 50% tire derived aggregate (TDA) and $\sigma_3 = 150 \text{ kPa}$.	122
Figure 4.23 Deviatoric stress versus axial strain, void ratio versus axial strain, and deviatoric strain versus volumetric strain at 75% tire derived aggregate (TDA) and $\sigma_3 = 100 \text{ kPa}$.	122
Figure 4.24 Deviatoric stress versus axial strain, void ratio versus axial strain, and deviatoric strain versus volumetric strain at 75% tire derived aggregate (TDA) and $\sigma_3 = 150 \text{ kPa}$.	123
Figure 5.1 Direct shear test results of sand-TDA mixture ($\theta_p = 0.6$) resting on a plate made of aluminum alloy 6061	130
Figure 5.2 Calculation of true stresses based on the nominal stresses and friction stresses (Ac: area of cylinder (cap) As: cross-section area of soil)	131
Figure 5.3 Instantaneous strain occurs simultaneously with applying the vertical load	132
Figure 5.4 Illustration of the total strain which is sum of Instantaneous strain and creep strain	132
Figure 5.5 Creep strain versus time curves of sample having 40% TDA under 5 constant stresses	133
Figure 5.6 Creep strain versus time curves of sample having 60% TDA under 5 constant stresses	133
Figure 5.7 Creep strain versus time curves of sample having 80% TDA under 5 constant stresses	134
Figure 5.8 Creep strain versus time curves of sample having 100% TDA under 5 constant stresses	134
Figure 5.9 Determination of the time creep parameter b (40% TDA)	137
Figure 5.10 Determination of the time creep parameter b (80% TDA)	137
Figure 5.11 Determination of the creep parameter n (40% TDA)	138
Figure 5.12 Determination of the creep parameter n (80% TDA)	138
Figure 5.13 Determination of the creep parameter n (100% TDA)	139
Figure 5.14 A comparison of the creep law with the test results for $\sigma_v = 75 \text{ kPa}$ (60% TDA)	140
Figure 5.15 A comparison of the creep law with the test results for $\sigma_v = 75 \text{ kPa}$ (80% TDA)	140
Figure 5.16 Rebound behavior of sand-TDA mixture having $\theta_p = 0.6$ under $\sigma_3 = 300 \text{ kPa}$ triaxial loading	141
Figure 5.17 Axial strain vs time during triaxial loading and rebound for sand-TDA mixture of $\theta_p = 0.6$ under $\sigma_3 = 300 \text{ kPa}$	142
Figure 5.31 Finite Element Mesh	143
Figure 5.32 The initial stress field for a soil deposit with no TDA	144
Figure 5.33 The initial stress field at 50% TDA	144
Figure 5.34 The stress field after excavation with no TDA	145
Figure 5.35 The stress field after excavation at 50% TDA	145
Figure 5.36 The effective plastic deformations after excavation with no TDA	146

Figure 5.37 The effective plastic deformations after excavation with 50 % TDA_____	146
Figure 5.38 Horizontal displacement from the axis of symmetry of tunnel after excavation with no TDA _____	147
Figure 5.39 Horizontal displacement from the axis of symmetry of tunnel after excavation with 50% TDA _____	147
Figure 5.40 Surface displacement of tunnel after excavation with no TDA _____	148
Figure 5.41 Surface displacement of tunnel after excavation with 50% TDA_____	148

LIST OF SYMBOLS

A	Creep parameter in the Norton-Bailey Law having units $(kPa)^{-n}(min)^{-b}$
β	Proportionality factor of the creep flow law
b	Creep parameter associated to time
δ_{ij}	The Kronecker delta
ϵ_{ij}^c	Tensorial representation of the creep strains
$\dot{\epsilon}_{ij}^c$	Tensorial representation of the creep strain rates
ϵ_e^c	The effective creep strain
$\dot{\epsilon}_e^c$	The effective creep strain rate having unit (min^{-1})
$\dot{\epsilon}_1^c$	The vertical creep strain rate having unit (min^{-1})
$\dot{\epsilon}_c$	Arbitrary reference strain rate having unit (min^{-1})
K_0	Coefficient of earth pressure at rest
n	Creep parameter associated with stress
S_{ij}	Tensorial representation of the deviatoric stress in (kPa)
σ_1	The total axial stress in (kPa)
σ_3	The total lateral stress in (kPa)
σ_{ij}	Tensorial representation of the total stress in (kPa)
σ_{co}	Extrapolated creep modulus σ_{cp} having units (kPa)
σ_{cp}	Power law creep parameter or creep modulus having units (kPa)
σ_e	The effective stress having units (kPa)
T	Variable representing the temperature in $(^\circ C)$
t	Variable representing time in minutes

e_o	Initial void ratio
e_f	Void ratio at failure
e_{Γ}	Void ratio on the critical state line when $\ln(p_f) = 1$
ϵ_s	Total deviatoric strain
ϵ_s^e	Elastic deviatoric strain
ϵ_s^p	Plastic deviatoric strain
ϵ_v	Total volumetric strain
ϵ_v^e	Elastic volumetric strain
ϵ_v^p	Plastic volumetric strain
ϕ'_{cs}	Friction angle at the critical state
γ	Unit weight having unit $\frac{kN}{m^3}$
κ	Unloading/reloading index
p'	Mean effective stress in (kPa)
p'_o	Initial mean effective stress in (kPa)
p'_y	The mean effective stress at yield in (kPa)
p'_c	Maximum past mean effective stress in (kPa)
p'_f	Mean effective stress at failure in (kPa)
λ	Compression index
M	Friction constant
q	Deviatoric stress in (kPa)
q_f	Deviatoric stress at failure in (kPa)
q_y	Deviatoric stress at yield in (kPa)
θ_p	TDA percentage volume ratio

DEDICATION

*Dedicated to my beloved parents, Ali & Mitra
for their love, endless supports,
encouragement & sacrifices*

ACKNOWLEDGEMENTS

To start with, I would like to sincerely thank my research director Prof. Adolfo Foriero for being greatly patient and supportive throughout the entire years of my doctorate research project. I really appreciate your wonderful supervision, support, and leadership during my studies at Laval University.

Moreover, I would like to acknowledge *Shercom Industries Inc.* in Saskatoon, Saskatchewan, Canada for their provision of the TDA materials used in the experimental part of this study.

I also acknowledge the technical supports of Mr. Christian Juneault, the research and laboratory technician at the Department of Civil and Water Engineering, Laval University.

Finally, I want to express my deep gratitude to my wonderful parents for their comprehensive supports. They have done special efforts in order to provide me with sufficient financial supports throughout the entire years of my doctorate studies in Canada.

FOREWORD

This dissertation is written in a manuscript-based format and it is comprised of five chapters. This thesis is written in accordance with a Ph.D. research project aiming to provide the critical tools for *the creep and plasticity parameter determination of sand-TDA mixtures for the purpose of constitutive modeling*. At the beginning, the introduction section provides explanations on Tire Derived Aggregates (TDAs), the knowledge gaps, general objective and originality of the study, as well as the thesis organization. **Chapter 1** consists of several sections that present useful information on the physical and mechanical characteristics and current geotechnical applications of pure TDA and sand-TDA mixtures in accordance with the literature review. The methodology of this research thesis discusses the implementation of four laboratory experiments provided in **Chapter 2**. For **Chapter 3** and **Chapter 4** relevant Forewords have been provided at the beginning of each of these mentioned chapters. **Chapters 5** presents the readers a discussion on the findings and experimental results mostly other than those previously presented within chapters 3 and 4, as well as a simulation of the behavior of the sand-TDA mixtures during a tunnel excavation. The conclusion section at the end of this manuscript provides readers with a general conclusion of this study.

Chapter 3

This chapter emphasizes the obtention of creep parameters for use in constitutive equations. This has been accomplished by considering sand specimens, at a predetermined TDA volumetric content, which were confined laterally and loaded axially with a total stress increment of a long duration. The experimental observations led to the approval of the Norton-Bailey law as a likely constitutive model for the estimation of the creep of such granular materials containing sand and TDA.

Chapter 4

This chapter emphasizes the plasticity parameters through the development of a critical state model based on the results of triaxial tests. This was achieved by considering loose sand specimens, at a predetermined TDA volumetric content, subject to various confining pressures under a constant axial displacement rate.

Chapters 5

Besides providing discussions on experimental results, this chapter also presents an example in which a 2D simulation has been conducted on the behavior of the soil with and without TDA during tunnel excavation. In order to calculate the in-situ stresses, two steps were performed in COMSOL. In the first step of this study, the state of the soil before the excavation of the tunnel is computed. In the second step, the elastoplastic behavior is examined once the soil is removed. As mentioned above this example considers both the soil and soil-TDA mixture for the comparison purpose.

INTRODUCTION

The introduction section of the thesis aimed to provide the readers with an overview of the whole study including general idea, problems and knowledge gaps that were observed before completion of this study, objectives of the study that were defined in accordance with the existing knowledge gaps, brief explanation of scrap tire together with its disposal difficulties and environmental issues impose to our nature and society, a brief explanation of tire-derived aggregates (TDAs) and their applications in geotechnical engineering projects, and a brief description on the methods employed to achieve the objectives of the present study. In addition, relevant statistical information has been provided in the first subsection in order to compare the scrap tire generation volume in Canada and the United States (North America) with other regions of the world. This may offer a more perceptible and brighter background of the existing problems associated with the illegal stockpiles of millions of end-of-life tires (ELT) that are thrown out every day in our environment.

Context of The Study

Due to the phenomenon of mechanization of the societies, rapidly growing population, and also the development of the land transportation network through the construction of the new roads and highways across the world, the auto industry is growing faster than ever producing massive amounts of waste tires. According to the annual reports, more than 2.9 billion tires were manufactured across the world only during the year 2017 (Raffoul et al. 2017; Siddika et al. 2019). The World Business Council for Sustainable Development has also estimated the generation of 1 billion waste tires every year (WBCSD 2020). Although some parts of these scrap tires such as steel are being recycled all over the world, the main portion including rubber tire may not be easily reused or recycled. This has resulted in the accumulation of enormous amounts of scrap automobile tires which are unusable, non-biodegradable, and pollutant.

The vast amounts of end-of-life tires that have been already stockpiled or landfilled are estimated to be 3 billion tires in the European Community, and approximately a total of 1 billion tires in the United States and Canada. (Oikonomou and Mavridou 2009). Estimations provided by the U.S. Tire Manufacturers Association indicate an annual generation of 14.5 kg scrap tire per resident in 2015 (USTMA 2018) and 14.75 kg during 2017 in the United States (USTMA 2018) which represents a 1.7% increase within two years.

The Canadian Association of Tire Recycling Agencies has reported the collection of 440,880 tonnes of scrap tires across Canada in the year 2018 representing 11.9 kg per resident (CATRA 2019). In the province of Québec this per capita rate is reported to be a bit lower by 11.55 kg in the year 2019 (RECYC-QUÉBEC 2019).

The European Tyre & Rubber Manufacturers Association (ETRMA 2016) describes EU28 countries annual waste tire generation to be 6.4 kg per resident (Rodríguez et al. 2018) while the Japan Automobile Tyre Manufacturers Association 2019 annual report indicates the generation of 96 million scrap tires by quantity or 1.032 thousands of tones by weight representing a per capita rate of 8.16 kg in the year 2018 (JATMA 2019).

By comparison between the amount of scrap tire generated per resident in the US and Canada and the generation rates in EU28 and Japan, one can simply conclude that the yearly per capita generation of waste tires in North America is close to being twice the rates reported for other regions in the world.

For example, in Québec province, the growing sale of SUVs due to the increasing public interest in this class of automobile since 2012 is leading to a significant increase in the average weight of used tires (tires of SUVs are larger and heavier than other types of passenger cars). Additionally, the growing public interest to extensive use of "China made tires" which are comparatively less expensive while having lower quality, in contrast, could be the other reason to the high quantities of scrap tire generation in province of Québec and also across Canada and the United States (RECYC-QUÉBEC 2019). In the province of Québec, between the years 2015 to 2019 the annual increase in the quantities of collected scrap tires is on average 6% whereas the increase in the number of registered vehicles is growing by 1.5% per year. This certainly proves the significant influence of the two above-mentioned factors on the increasing rate of scrap tire generation in Quebec as a region of North America.

Furthermore, the lower population density in vast areas of North America as well as the long duration of winter within the cold regions of the United States and Canada compared to other regions such as Europe and Japan could be considered as the other two main sensible reasons for this significant difference. The low population density in a vast region leads to longer distance travels causing tires to wear in a short time. In addition, due to the cold and long winter drivers have to buy two sets of tires including winter tires (snow tires) for use in cold seasons and summer tires (regular type) for use during the summer season. Moreover, the lower population density

together with the extended cold winter consequently result in mandatory dependence of people's everyday life to traveling in passenger vehicles.

In conclusion, the above-mentioned reasons are the most plausible and important factors affecting the high per capita rate of scrap tire generation in North America.

To obtain an overview of the past and future situation in the United States, it can be noted that according to the FHWA/NY/SR-86/85 published by the New York State Department of Transportation (Chamberlin and Gupta 1986) only 200 million automobile tires and 40 million truck tires were discarded across the United States in the year 1985. With respect to observed increasing rates, the quantities of scrap automobile tires that will be generated in the year 2030 are expected to become 1200 million tires resulting in the accumulation of approximately 5 billion waste tires across the world (Pacheco-Torgal, Ding, and Jalali 2012).

Hence, the state of New York is one of the first places in the world to take action in order to accelerate the use of recycled waste tire. Consequently, in 1997 the New York State Department of Transportation (NYSDOT) initiated the preparation of new regulations in which accordingly the design and construction sectors were mandated to use higher volumes of waste materials in transportation projects. Although, scrap tires were in the frontline of these new waste management regulations. Therefore, in the same year, the Geotechnical Engineering Bureau (GEB) started the development and implementation of a pilot project which enabled the NYSDOT to achieve appropriate design and construction guidelines on the use of scrap tires in geotechnical engineering applications (Dickson, Dwyer, and Humphrey 2001).

Currently, there are three common methods for the disposal of scrap tires including discarding, burning, and recovery. In the first method, waste tires are stockpiled in scrapyards which unfortunately imposes various issues to nature and the environment. Numerous studies conducted previously have reported on the ecological threats caused by unsafely stockpiling or landfilling of waste tires in an uncontrolled manner (Chamberlin and Gupta 1986; Williams, Besler, and Taylor 1990; B. N. N. Eldin and Senouci 1992; Jang et al. 1998; Garga and O'Shaughnessy 2000; Mujibur Rahman 2004; Lo Presti 2013; Torretta et al. 2015). The most important one is that due to the utilization of high amounts of carbon black during the tire manufacture process, tire landfills are often subjected to combustion risk. Another is the undesirable fact that they accumulate rainwater and consequently provide a breeding ground for the disease-carrying mosquitoes and rodents. In the second method, scrap tires are burned in open areas which lead to air emissions, soil

contamination, surface water and groundwater pollution (more information is available within chapter 1 “Literature Review”).

The two above-mentioned disposal methods (discarding and burning of tires) have been an ongoing challenge to environmentalists and regulators who are concerned over environmental issues. For instance, in Québec, the 100% of the scrap tires are intended to be accumulated and recycled since the disposal in landfill or incineration are prohibited within this province of Canada. Under the regulations of this province, an environmental fee of \$ 3 is paid simultaneously with the purchase of a new tire for its collection and treatment. Taking into account that the average tire life is estimated to be 6 years, the environmental fee (\$ 3) was paid 6 years prior to the time of collection and recycling (RECYC-QUÉBEC 2019).

Finally, in the third method, the scrap tires are either recovered to be reused for its original purpose (automobile tire) via re-treading and re-fitting processes while retaining the original shape, or ignited as fuel to produce heat energy, or recycled for multiple purposes such as civil engineering applications.

A tire is generally made from three main components including rubber, metal, and fabric. The tire life cycle is generally composed of five main stages including extraction, production, consumption, collection of used tires and finally waste management which, as mentioned above, is comprised of landfilling and recovery.

The most common forms of recycled scrap tires are whole, halved, shredded, and granulated. Through a recycling process, where large chipper/shredder machinery is used, scrap tires are cut into different shapes and sizes called tire-derived aggregate (TDA).

In civil engineering applications, TDAs are usually added to conventional materials in order to produce a superior construction material with improved mechanical and thermal characteristics. In particular, the geo-environmental field has a variety of uses for these mixtures. This ranges from reactive barriers to leachate collection layers (Thakur and Kaushik 2016). Another application of TDA-granular soil mixture consists in barriers for golf courses and athletic fields. Besides its lightweight advantages, the presence of tire rubber offers several improvements in mechanical and thermal characteristics of soil-tire mixtures such as good draining, thermal insulation, and vibration mitigation. Moreover, in the production of lightweight concrete, TDA is mixed with concrete materials as a substitute for the conventional construction aggregates (crushed stone).

In geotechnical applications, TDAs are mixed with sand and/or silt to form what is commonly referred to as soil-TDA mixture. For the purpose of geotechnical engineering applications, scrap tires are used either in whole tire or aggregates form. In order to produce the tire-made aggregates, the scrap tires are cut into small particles which are commonly known as Tire Derived Aggregate (TDA).

In addition to the above-mentioned advantages which are even alone looking sufficient to encourage the design engineers and the contractors in order to consider the use of recycled scrap tires in geotechnical engineering projects, these by-product materials are considerably cheaper (four times cheaper) than conventional geomaterials such as typical backfill aggregates (Mahgoub and El Naggar 2019). The presence of economic motives leads to higher persuasion of the geotechnical firms to utilize recycled tires as inexpensive geomaterials.

From the geotechnical engineering point of view, the compressibility of materials is one of the most important factors affecting the mechanical properties of the designed geomaterials particularly when these materials are used as backfill geomaterials, subbase materials for road and highways, and foundation materials beneath the heavy structures where the section is subjected to the high intensity of loads. Although in geotechnical engineering applications, TDA materials exhibit unique mechanical and thermal characteristics compared with conventional soil and gravel, the soft and flexible nature of the rubber makes it very compressible. This includes immediate and delayed compressions (instantaneous and long-term deformations). The high compressibility of tire rubber reasonably caused it immediate deformation under pressure, however, the time-dependent deformation of such geomaterials must be also determined and considered as one of the key-factors from very early stages of the design.

One of the main and everlasting concerns of geotechnical engineers about the utilization of new geomaterials as the alternative to the conventional ones is often the lack of knowledge on the long-term behavior of those materials, a key-factor which directly affect the long-term performance and consequently the sustainability of the structure.

Currently, the presence of a considerable lack of knowledge in the modeling of time-dependent deformation (creep) of sand-tire materials is highly felt. Precise modeling of the long-term behavior of construction materials/geomaterials is a necessary and critical tool to enable the designers to predict the time-dependent settlement of such materials as sand-tire mixtures when subjected to overlying loads. Appropriate prediction on delayed deformation (creep) of materials enables the design engineers to take necessary measures in their designs in order to prevent a wide range of

future irreparable failures. This will significantly increase the service life of the structure and simultaneously reduce the excessive costs associated with maintenance, repair, or future reconstruction.

The present study consists of three phases. In the first phase of this study, a new application of soil-TDA mixtures following with the recommended design chart and specifications have been proposed. The second and third phases consist of an experimental program that was conducted to determine the essential elastic, plastic, and creep parameters of TDA-sand granulated mixtures and FEM simulations conducted for the purpose of validation of the obtained test results. The experimental program and relevant FEM simulations themselves consist of four different sections in which a series of laboratory tests and FEM simulations have been carried out in each section. The values of the parameters achieved through the experimental observations were used in the development of constitutive equations which are proposed aiming to model the creep and plastic deformation behaviors of the sand-TDA mixtures.

Utilization of TDA in Earthwork Applications

Tire derived aggregates (TDAs) are increasingly used in geotechnical engineering applications. In most of these operations the TDAs, as alternative aggregates, are mixed with different types of granular soil such as sand or clay at various volumetric ratios to form soil-TDA mixture. Utilization of soil-TDA mixtures in earthwork applications offers unique advantages, which among those, their lightweight nature is the most highlighted benefit. The average specific gravity of processed scrap tires has been reported to be 1.22, which is equal to 46% of the specific gravity of sand. Hence, the relative fraction content of soil and tire particles is the major factor affecting the unit weight of the soil-TDA mixtures (Youwai and Bergado 2003). The unit weight of recycled scrap tire lies between 3 and $6 \frac{kN}{m^3}$ which is a desirable value when used in different volume fraction mixtures. As a comparison, a soil-TDA mixture with a volume ratio of 50% TDA has a unit weight that lies somewhere between 10 and $13 \frac{kN}{m^3}$.

Numerous studies have already investigated the performance of TDA materials in various earthwork applications leading to provide a list of benefits as well as to propose useful guidelines, recommendations, and vast volumes of test results related to both pure TDA and soil-TDA mixture properties. ASTM D6270 “*Standard Practice for Use of Scrap Tires in Civil Engineering Applications*” The employment of such mixtures as lightweight fill material for embankments (Bosscher, Edil, and Eldin 1992; Bosscher, Edil, and Kuraoka 1997; D. N. Humphrey 2008); bridge

abutments (Apex-Companies 2008), backfilling retaining walls and also drainage layers for roads and landfills, as well as low-cost lightweight backfill materials used in the construction of shallow foundations (Mahgoub and El Naggar 2019) and insulation of basements in residential buildings (ASTM 2008) are well documented.

Moreover, in northern regions, TDA-granular soil mixtures are employed in pavement design. They primarily serve as an insulating layer (Dana N. Humphrey and Eaton 1995; Edeskar 2006) in order to prevent frost heave and hence degradation of the road surface. In addition, a serendipity condition arises because this overlays mixture also acts as a damping layer against vibrations from the resulting traffic flow.

Taking into account the low unit weight together with other unique mechanical properties of TDAs as geomaterial on one hand and on the other hand the urge for immediate recovery of huge volumes of waste tires, the questions may arise a) why the recycled tires are mixed with conventional soils such as sand or clay, and b) why they are not used alone in geotechnical engineering applications. Indeed, the pure TDAs are highly compressible due to their high rubber content and high porosity causing extensive settlement and compaction problems (Edil and Bosscher 1994; Youwai and Bergado 2003; Sodom Bali Reddy and Krishna 2017; Platzer et al. 2018; Madhusudhan, Boominathan, and Banerjee 2019a) particularly when used in such applications as highway embankment fill. Furthermore, the primary constituents of tires include carbon black, polymers, and softeners. This combination provides the tire with an extremely high heating value (Bernal, Lovell, and Salgado 1996) thus, when exposed to air, TDAs are combustible materials (Garga and O'Shaughnessy 2000) as a result of self-heating (internal heating).

When subjected to vertical load, sand exhibits significantly lower compression compared to rubber tire materials and is one of the most suitable types of soils to be mixed with tire particles at various fraction content in order to modify the compressibility characteristics of the TDAs. Additionally, sand particles are finer than that of typical TDA particles (except tire powder), thus filling the existing voids when mixed with pure TDA leading to decrease compressibility through densifying the resultant mixture. Therefore, the inclusion of sand may considerably increase the mechanical strength of the sand-TDA mixture through the improvement in deformation characteristics of the rubber tire materials. Moreover, the presence of sand in the mixture significantly reduces the risk of self-ignition in tire embankment fills (Bosscher, Edil, and Eldin 1992; Youwai and Bergado 2003).

In Addition to the soil-TDA mixing treatments aiming to reduce the compressibility and the fire hazard of pure TDA, guidelines (ASTM 2008; GeoSyntec 2008; CalRecycle 2016) and previously published studies (Bosscher et al.1992; Bernal et al. 1996; Masad et al. 1996; Kiran Sonti et al. 2003; Nantung et al. 2009; Hoppe and Oman 2013; Ehsani et al. 2015) have strongly recommended the use of a soil-coverage at the top of the soil-tire embankments.

The presence of a soil cap limits the exposure of tire materials to air and consequently minimizes the risk of ignition. As a possible solution to minimize the infiltration of water and air into the tire-based fill materials, ASTM D6270 (2008) has specified a 0.5-m thick compacted topsoil layer separated from TDA fill through a geotextile. Extensive precautions must be undertaken along the construction stages in order to prevent fire ignition either in stockpiles or tire embankment that have not yet been properly covered by soil (Masad et al. 1996).

Furthermore, the implementation of a soil cover with an appropriate thickness may properly control the compressibility and settlement of the tire based geomaterials. It is even reported that the pure tire embankments adequately equipped with soil cap exhibit similar performance to that of soil-tire embankments (Bernal et al.1996). For the road embankment application, ASTM D6270 (2008) has specified 0.8-m thick topsoil for paved roads having light traffic and 1 to 2 m thickness for paved roads subjected to heavy traffic loads. Though, unpaved roads require a topsoil thickness as low as 0.3 to 0.5 m based on their traffic flow. When soil-TDA mixtures are used beneath the foundation, the presence of a soil cap having thickness equal to one-fourth of the foundation width is recommended at the top of the tire-modified section (Moghaddas Tafreshi and Norouzi 2012).

Generally, for road construction purposes the actual thickness of the soil cap is predominantly investigated in accordance with such parameters as loading conditions and load magnitude, TDA or soil-TDA layer thickness, pavement thickness, etc. (ASTM 2008).

Problem Statement

Of the main and all-time concerns of design engineers regarding utilization of new geomaterials are the mechanical characteristics (especially long-term performance) of the material which directly affect the service life of dependent structures.

Due to its low elastic modulus ($E \approx 1 \text{ MPa}$, depending on overlaying pressure), tire-derived aggregates exhibit a significant compressibility behavior compared to that of conventional soils (Wartman et al. 2007). Although, due to the lightweight, good drainage, vibration mitigation, etc.,

engineered soils containing TDA have become of interest to design engineers but the excessive compressibility of the rubber materials which is composed of both immediate and time-dependent (creep) deformation portions seems to be extremely challenging in such applications wherein heavy overlying loads are applied (e.g., embankment filling applications).

In particular, the influences of the high-compressibility induced secondary compression phase on the long-term mechanical stability of the soil structures containing TDA has been overlooked to date. From the review of the related past studies, a lack of both experimental and numerical investigations on creep deformation behavior of sand-TDA mixtures is highly perceptible. The narrow studies that have been so far conducted on the engineering characteristics of sand-TDA mixtures are mostly limited to the assessment of shear strength through regular or large size direct shear tests (Madhusudhan et al. 2019a). Consequently, the available knowledge is not sufficient to enable the researchers and the engineers in order to satisfactorily evaluate the elastic, plastic, and creep behaviors of the sand-TDA mixed geomaterials.

Therefore, in order to minimize the possible future failures and consequently maximize the reliability of using soil-TDA mixtures as a novel geomaterial, it is necessary to have an accurate understanding of the elastic, plastic, and creep behaviors of such materials when used in geotechnical engineering applications.

Nevertheless, as mentioned earlier, only limited number of published studies have emphasized the importance of time-dependent creep behavior of soil-rubber materials for use in geotechnical engineering applications and hence, urged the need for a comprehensive investigation in this field, the few existing constitutive equations that have developed to model the behavior of soil-TDA mixtures are not able to predict both elastoplastic and creep behaviors of these geomaterials. Furthermore, based on the literature review presented in CHAPTER 1, the proposed models for the creep behavior of soil-tire mixed materials are unable to predict both volumetric and deviatoric time-dependent deformations and are limited to predict only the volumetric creep.

Therefore, in accordance with the above-mentioned problem statement the following is a list of limitations of using sand-tire granular materials in geotechnical engineering applications.

1. This study has shown that the shear strength of sand-TDA mixtures increases with TDA content. Moreover, this study has also shown that tires have a very low elastic modulus and that consequently a typical sand-tire granular mixture exhibits a high initial and time-dependent (creep) compressibility behavior. Consequently, precautions must be taken in

- order to guaranty the serviceability of geotechnical structures. Previous models in the literature have not contextually addressed this fact.
2. Only limited number of studies have emphasized the importance of time-dependent creep behavior of soil-tire rubber materials for use in geotechnical engineering applications. These include studies conducted by Wartman et al. and Anh and Valdez in 2007. The limitations of such studies are *a)* the constitutive equations, that have been developed, address the creep behavior of soil-TDA mixtures only and are not able to predict both the elastoplastic and creep behaviors of geomaterials. *b)* they are unable to predict both volumetric and deviatoric time-dependent deformations and are limited to predict only the volumetric creep.
 3. The evaluation of immediate and time-dependent deformations, as well as plastic deformations, under vertical and lateral pressures are components of the total deformation which have not been thoroughly investigated in past studies. In this investigation a creep and plasticity models are developed for this purpose.
 4. Most past studies have considered investigation of the mechanical behavior of the mixtures consisting of sand and tire derived aggregates sized between 75 to 600 mm. This study has emphasized the investigation of the short and long-term mechanical behavior of granular tire rubber with an approximate size ranging between 1 to 2.5 mm.

General Objectives of The Study

The principal objective of this study is to determine the creep and plasticity parameters for the sand-TDA mixtures aimed at the development of appropriate constitutive models in order to estimate both instantaneous and long-term mechanical behaviors of such mixtures. Therefore, to obtain the mentioned principal objective this study aims to determine the creep parameters of the Norton-Bailey constitutive model for sand-TDA mixtures through conducting a series of laboratory creep and direct shear tests with subsequent FEM validation. The Norton-Bailey constitutive model has been chosen because it is widely utilized in practice to capture primary and secondary creep.

Moreover, to complete the obtention of principal objective this study is aiming to determine the plasticity parameters in order to propose a critical state model for sand-TDA mixtures based on the results of triaxial tests.

Originality of The Study

To this date, this research study is the very first study to address the creep behavior investigation of sand-tire granular mix materials via the Baily-Norton Creep Model. Moreover, this is the very first study to model the plasticity behavior of sand-tire granular mix materials through a modified Cam Clay Critical State Model.

The outcomes of this study improve the knowledge on the mechanical response of sand-TDA mixtures used as lightweight materials in geotechnical engineering applications. The constitutive models proposed in this study enable researchers and geotechnical engineers to predict the creep and plastic behaviors of sand-TDA mixtures.

The soft and flexible nature of the tire materials together with their lightweight privileges may offer multiple exclusive advantages of TDA materials to the design engineers and contractors. Although, simultaneously the high compressibility behavior of engineered geomaterials containing TDA is leading to a large settlement particularly when used as filling materials in the construction of underground structures such as subway tunnels and stations. On the other hand, underground transportation infrastructures are often expensive to build, repair, and reconstruct. These valuable structures are directly responsible for the quality of humans' life and consequently social sustainability in metropolitan areas. Hence, they are expected to be designed and constructed for a long-term service life usually above 50 years.

Presence of the modeling tools capable to estimate the elastic, plastic, and creep deformation characteristics of sand-TDA geomaterials are critical in order to predict the mechanical behaviors of the backfill sections placed at the top of underground structures. The availability of sufficient knowledge on the mechanical behaviors of the geomaterials under overlying pressures leads to the development of an accurate design of the backfill section. The stability of the backfill section is the most important factor influencing the structural health and consequently service life of the underground infrastructures.

Additionally, facilitated access to the sufficient and reliable information on the mechanical properties of tire-derived aggregate as well as TDA-soil mixtures is obviously leading to simultaneously encourage the design engineers and the contractors in order to consider the use of recycled scrap tire as an inexpensive lightweight alternative aggregate in civil engineering applications. This will prevent the discarding of these valuable materials to the dumping grounds

and consequently help to the removal of challenging and non-biodegradable waste from the environment.

For instance, in accordance with literature (Zornberg et al. 2004; M. S. Mashiri et al. 2015) the addition of 35% of the tire to sand by mass (mixture consist of 35% tire and 65% sand) is defined as the optimum mix ratio which leads to the highest level of mechanical reinforcement within the sand-tire mixture. The inclusion of this amount of tires reduces the mass of sand by approximately 17% whereas simultaneously it results in recycling of nearly 460 kg of scrap tires for the production of each cubic meter of sand-tire mixed materials.

Motivation and Significance of the Study

The modeling of elastic, plastic and creep behaviors of granulated waste tire for the purposes of analysis in geotechnical engineering projects, which is the principal objective of this study, leads to a better understanding of the mechanical properties of a soil-tire mix. Consequently, this will better characterize the medium and consequently reduce the failure as a result of the design and construction of the geotechnical structures. A knowledge improvement of the mechanical behaviors of such geomaterials leads to a risk reduction which may help increase the use of waste tires in civil engineering projects. From the Environmental point of view this may help with the disposal of these waste materials. At the same time, we could take advantage of the unique mechanical and thermal properties of tire-soil mixtures, including advantages related to their lightweight nature, shear strength improvement, their good insulating properties, damping and drainage performances.

Of all the above-mentioned advantages of using soil-tire mixture as geomaterial, two of them are the principal motivators. These two advantages inspired the conduction of these studies and are: the shear strength improvement and lightweight nature of TDA.

The lightweight nature of the tire rubber is considered as the main motivation for using this type of waste materials in geotechnical engineering applications. The average specific gravity of processed scrap tires has been reported to be 1.22, which is equal to 46% of the specific gravity of sand. Hence, the relative fraction content of soil and tire particles is the major factor affecting the unit weight of the soil-TDA mixtures (Youwai and Bergado 2003). The unit weight of recycled scrap tire lies between 3 and $6 \frac{kN}{m^3}$ which is a desirable value when used in different volume fraction mixtures. As a comparison, a soil-TDA mixture with a volume ratio of 50% TDA has a unit weight that lies somewhere between 10 and $13 \frac{kN}{m^3}$. Typically, the unit weight of processed tire is equal to

$\frac{1}{3}$ of that of sand. The importance of unit weight is even more evident when used as backfill material overlaying underground structures such as subway tunnels and stations.

The results obtained in the present study have shown that the use of an appropriate amount of granular tire increases the shear strength of the resulting sand-tire mix when compared to that of sand alone. However, the use of excessive amounts of tire within a sand-tire mixture may reduce the shear strength of the resulting material.

Thesis Organization

This dissertation is written in a manuscript-based format and it is comprised of five chapters. Chapter 1 consists of several sections that present useful information on the physical and mechanical characteristics and current geotechnical applications of pure TDA and sand-TDA mixtures in accordance with the literature review. In Chapter 2, the methodology of this work is discussed via explanations of the test material composition and sample preparation procedures along with descriptions of the implementation of four laboratory experiments. The content of Chapter 3 is published as a peer-reviewed paper in the “*Indian Geotechnical Journal (IGJ)*”. The content of Chapter 4 is published as a peer-reviewed paper in the “*Transportation Research Record (TRR)*”. Chapter 5 discusses the experimental results obtained in two previous chapters (3 and 4).

CHAPTER 1

1 Literature Review

The present chapter of the thesis has been designed to provide the readers with necessary information collected from a variety of past related studies on the properties of automobile tires as well as their production and lifecycle and also their possible risks to the environment and consequently humans life, the definition of scrap tire and its collection methods, recovery or recycling processes, the definition of tire-derived aggregates (TDAs), their classifications and physical properties, as well as their applications in civil and geotechnical engineering and their possible reaction in contact with water. Furthermore, useful information on the existing constitutive models for sand-rubber materials as well as creep models to predict the long-term settlement of geomaterials with the inclusion of tire rubber are discussed in this chapter. This will help to facilitate a better understanding of the general idea of the present study by providing an appropriate comprehensive background for the readers before going forward to the next chapters of the study. A list of discussed sections has been provided below.

1. Motorized Vehicle Tire
2. Tire Composition and Structure
3. Scrap Tire
4. Environmental Issues Caused by Stockpiling of Scrap Tires
5. History of the Tire Fire Incidents in Canada
6. Tire Derived Aggregate (TDA)
7. Fundamental Mechanical Characteristics of Sand-Tire Mixtures
8. Civil Engineering Applications of TDA
9. Specifications and Guidelines for Use of Scrap Tire in Civil Engineering
10. Existing Models to Predict Creep Behavior of TDA and TDA-Sand Mixtures

1.1 Motorized Vehicle Tire

Tire (North American English) or tyre (British English) is a circular item that is made from rubber or polymer materials reinforced by synthetic fibers and high-strength steel. These components together form an advanced strong structure beneficial from high levels of tensile strength, flexibility, resilience, and frictional resistance (Garga and O'Shaughnessy 2000). The importance of automobile tires is more highlighted when we realize the fact that these unique mechanical characteristics remain even for many years after the end of their efficient service life.

The following subsections provide the readers with useful information on tire composition, tire lifecycle, and effects of temperature on properties of the tire.

1.2 Tire Composition and Structure

Generally, a tire is composed of 40-50% rubber, 20-30% carbon black and reinforcing material, and 20% adhesive cord and steel wires (Mujibur Rahman 2004; Lo Presti 2013). Figure 1.1 shows different parts of a typical vehicle tire.

The main sources of rubber used in the manufacture of tire are including natural rubber (obtain from the sap of the *Hevea brasiliensis* tree), synthetic rubber (produce from petrochemical materials), and recycled rubber (mostly supplied through the recovery of waste tires). The other main components used in the production of tires include but are not limited to carbon black, zinc oxide, sulfur, copper, tin, zinc, chromium, and reinforcing steel and fabrics (Atech Group 2001; Basel Convention 2007).

Table 1.1 Composition of passenger car and truck/bus tires (Rahman, 2004; Presti, 2013)

Material (Contents)	Car (%)	Truck/Buses (%)
Rubber/Elastomers	48	43
Carbon black	22	21
Metal	15	27
Textile	5	–
Zinc oxide	1	2
Sulphur	1	1
Additives	8	6

One of the most frequent questions that might be raised in all people's mind is "*why are all manufactured automobile tires black color?*". The answer is very short but precise and complete.

In fact, the black color of the tires comes from the addition of “carbon black” an additive which improves the corrosion control and heat reduction capabilities of manufactured tires.

Figure 1.2 illustrates a typical tire sidewall containing technical information provided by the manufacturer of the tire for both sellers and consumers in order to facilitate the selection of an appropriate type of tire in accordance with their cars requirements as well as their different usage purposes (on-road off-road, racing, etc.), (Basel Convention 2007).

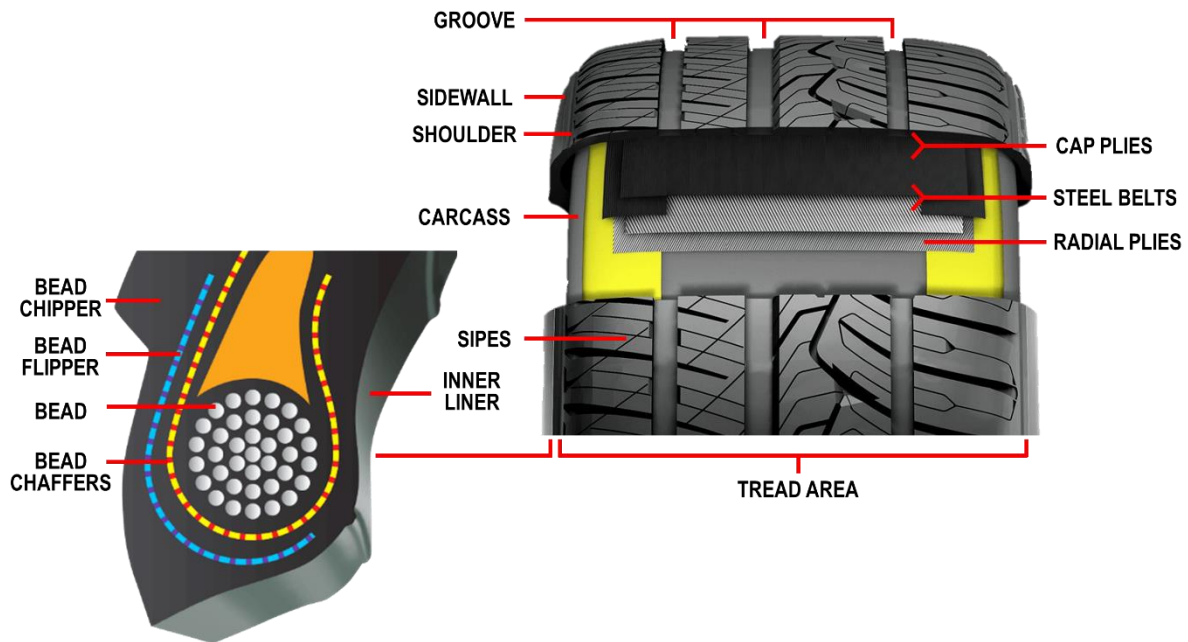


Figure 1.1 Typical vehicle tire structure
 Modified from: (CARID 2020) and (Computype 2020)

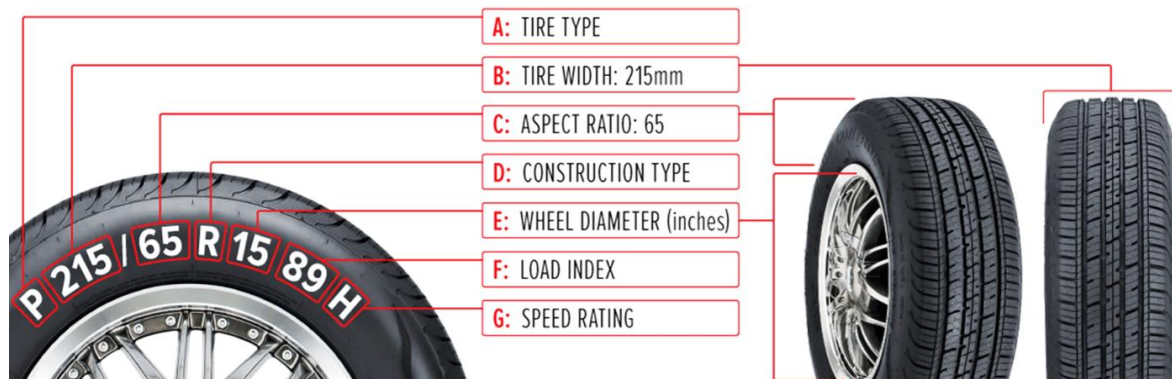


Figure 1.2 Typical tire sidewall information (Les Schwab Tire Center 2020)
 Modified from: (Les Schwab Tire Center 2020)

1.3 Scrap Tire Definition

A scrap tire, which is also known as waste tire, discarded tire or end-of-life tire (ELT), is defined as a used tire, which due to technical defecting problems, serious damages or wearing issues, is no longer suitable for its original use even after being retreaded or regrooved (used tires can be regrooved and retreaded in accordance with the manufacturer recommendations).

1.4 Environmental Issues Caused by Stockpiling of Scrap Tires

When scrap tires are inappropriately stockpiled within illegal landfills, they impose significant vexing issues on nature and the environment. The scrap tires that are illegally discarded when allowed to accumulate rainwater and organic debris, provide a breeding ground for a variety of disease-carrying mosquitoes and insects (Figure 1.3). Hence, these non-biodegradable wastes are responsible for the direct threat to public health (Eldin and Piekarski 1994). Figure 1.4 shows the Garner/Brandywine scrap tire stockpile before, during, and after cleanup. The Garner/Brandywine scrap tire stockpile is located in Prince George's County, Maryland, United States.



Figure 1.3 Stockpiled scrap tires occupying a large dumping area and imposing ecological pollution

Modified from: (World Business Council for Sustainable Development (WBCSD), Geneva 2020)

The cleanup process in this stockpile which consists of approximately 1.5 to 2 million tires began in 2010 and was completed in June 2011 after completion of stabilization activities (MDE 2011).



Figure 1.4 Garner/Brandywine Scrap Tire Stockpile.

Modified from: (MDE 2011)

Moreover, owing to their chemical composition (utilization of high amounts of carbon black during the tire manufacture processes), tires have a combustible nature. Therefore, illegal scrap tire stockpiles are always intended to combustion risk. Since the tire associated fires are technically difficult and economically expensive to extinguish, they are often uncommonly noxious consequences for societies (Chamberlin and Gupta 1986). Furthermore, tire fires may cause serious air, soil, and water quality issues in the surrounding nature and environment. During combustion, tires generate enormous quantities of toxic dense black smoke leading to air pollution which is responsible for different types of cancers (Ashish Singh et al. 2015).

In addition to black smoke generation, the melting tires produce significant amounts of oil which are released and penetrate the soil and groundwater aquifer of the tire fire location and surrounding areas. Due to the presence of various heavy metals, upon access to either groundwater or surface water, this tire fire generated oil is classified as a toxic contaminant for human life as well as animal and aquatic life. When the toxic contaminants reach the running waters such as rivers, they could be simply transported everywhere even kilometers away from their origin. However, since they travel in running water, the concentration of the contaminants decreases exponentially in accordance with the time and distance of transportation (Senoro et al. 2016).

Besides environmental impacts, tire fires pose serious economic problems to the governments leading to the initiation of excessive costs for taxpayers. For instance, in the Hagersville fire accident in southern Ontario in Canada which occurred in February 1990, 200 firefighters efforted for the duration of 17 days in order to extinguish the fire. The Canadian government spent a budget of nearly \$1,000,000 only for the implementation of necessary site cleanups and limited

environmental experiments (Mawhinney 1990a; N. N. Eldin and Piekarski 1994). Undesirably these expenses applied to the taxpayers later on.

1.4.1 Controlled Combustion of Waste Tire

Across the world, tires are being combusted as fuel for power generation or heating purposes. This method is called tire-derived fuel (TDF). The laboratory test results on the controlled combustion of TDF in a Rotary Kiln Incinerator Simulator (RKIS) have demonstrated that, even by using an appropriate combustion device, in any case, the amount of zinc emissions generated from burning of a tire is much higher than those generated by conventional fossil fuels (EPA 1997).

1.4.2 Open Air Combustion of Waste Tire

Air, soil, and water pollution caused by open burning of tires are more toxic and hazardous than those of controlled combustions in the TDF recycling method. Open burning emissions consist of either particulate pollutant such as carbon monoxide (CO), sulfur oxides (SO_x), oxides of nitrogen (NO_x), and volatile organic compounds (VOC_s) or hazardous air pollutants (HAP_s) such as polynuclear aromatic hydrocarbons (PAH_s), dioxins, furans, hydrogen chloride, benzene, polychlorinated biphenyls (PCB_s); and metals for instance arsenic, mercury, nickel, zinc, cadmium, chromium, and vanadium (EPA 1997; Downard et al. 2015; Singh et al. 2015).

Both types of above-mentioned pollutions may lead to serious and undeniable acute (short-term) and chronic (long-term) health issues for firefighters and adjacent inhabitants including humans, aquatic, and animals (EPA 1997).

1.5 History of the Tire Fire Incidents in Canada

Although, it is noted that since 1983 Canada and the United States together have experienced over a dozen large tire fires, in accordance with the news and available information there are only two major tire fire accidents in the history of Canada. Based on the published reports, in 1990 these two fire accidents took place in Ontario and Quebec respectively (Mawhinney 1990a; 1990b; CBC 2019).

1.5.1 Hagersville Tire Fire – Ontario, February 1990

The fire initiated on February 12, 1990, within an outdoor storage yard in the vicinity of Hagersville in southern Ontario. According to the report (Mawhinney 1990a) provided in May 1990 by the National Research Council of Canada (NRC), several millions of stockpiled waste tires burned in 17 days posing substantial damaging impacts to the people of the neighborhood, agricultural

activities, and environment. The airborne pollution followed by dense black smoke generation induced the evacuation of a zone of 3 kilometers radius around the fire spot. Massive amounts of oil (containing benzene, toluene, and other contaminants) were generated during the breakdown of the burning tires and spread into the soil and surface water leading to contaminate the groundwater aquifer. Up to the date of the report preparation by NRC in May 1990, approximately 700,000 liters of burned tire associated oil as well as nearly 1,400,000 liters of contaminated water were collected from the site and adjacent areas. Eventually, as an important lesson learned from this crisis, the NRC urged the reduction in the volume of the stockpiled scrap tires aiming to limit the risk of further tire fire accidents in the future.

1.5.2 Saint Amable Tire Fire – Québec, May 1990

About two and a half months after the fire quench in Ontario, it was time for Québec to experience a historical tire fire disaster. In the afternoon of May 16, 1990, a fire initiated in a large scrap tire storage in the vicinity of the town of Saint Amable located in Québec province. The storage has a distance of fewer than 700 m from the town on the south shore of the Saint Lawrence River. According to the report (Mawhinney 1990b) provided in July 1990 by the National Research Council of Canada (NRC), the column of dense black smoke was visible from 40 km away in the metropolitan area of Montreal. A wide range of negative environmental influences including immediate air pollution, soil contamination, and damage to plants within the few kilometers of the smoke fallout zone as well as the surface and groundwater contamination, have been mentioned within the report prepared by NRC in the same year. It has been reported that the surface water in the adjacent areas very close to the fire was severely contaminated with hydrocarbons, heavy metals, and minimal quantities of dioxin. The Saint Amable municipality estimated the fire associated total cost of nearly \$500,000.

1.6 Tire Derived Aggregate (TDA)

Tire derived aggregate (TDA) refers to processed scrap tires with a basic geometrical shape. Generally, the production of one ton of TDA requires 100 automobile tires to be recycled. According to ASTM D6270, the “*standard practice for use of scrap tires in civil engineering applications*”, TDAs are classified into three different categories including rough shreds with the maximum size of 600 millimeters, the medium size consists of TDA with a maximum size of 300 millimeters and the small version of TDA with the maximum particle size of 75 millimeters.

There are also other methods of classification (Dana N. Humphrey and Eaton 1995; FHWA 2016; Recycling Research Institute 2020) in which TDAs have classified again into three different categories including, tire shreds with particle sizes ranging between 50 to 305 millimeters, tire chips with particle sizes ranging between 12 to 50 millimeters and granulated rubber containing particles with sizes greater than 12 millimeters. Although, TDAs may be produced in different sizes other than those mentioned above in accordance with the different usage purposes. As an example, in civil engineering applications TDAs can be ordered based on the project requirements.

There is a third version of TDA classification (Xiao, Ledezma, and Hartman 2014; Cheng and Ahn 2014; Apex-Companies 2008; EPA 2010; Hoppe and Oman 2013; CalRecycle 2016) in which TDA is categorized into type A with a maximum size ranging between 3 to 8 in. (75 to 200 mm) and type B with a maximum size ranging between 12 to 18 in. (305 to 450 mm).

1.7 Fundamental Mechanical Characteristics of Sand-Tire Mixtures

As stated earlier, sand-tire mixtures are produced through the addition of recycled tire in the form of tire-derived aggregate to the sand. In this process, the addition of tire to sand is accomplished in accordance with either the weight/volume of the sand or total weight/volume of the resultant mixture. Despite the influence of the magnitude of the applied stress, due to the flexibility of rubber compared to sand, the mechanical properties of the resulting sand-tire mixtures are highly dependent on the tire fraction content within the mixture.

Multitudinous studies have already aimed at investigating the physical and mechanical properties of tire-sand composite geomaterials (Bosscher et al. 1992; Ahmed 1993; Bernal et al. 1996; Foose et al. 1996; Masad et al. 1996; Tatlisoz et al. 1997; Tatlisoz et al. 1998; Lee et al. 1999; Feng and Sutter 2000; Youwai and Bergado 2003; Y. W. Yoon, Cheon, and Kang 2004; Zornberg et al. 2004; Abdrabbo et al. 2005; Ghazavi and Sakhi 2005; Attom 2006; Rao and Dutta 2006; S. Yoon et al. 2006; Wartman et al. 2007; Y. W. Yoon, Heo, and Kim 2008; Tanchaisawat et al. 2008; Hazarika et al. 2010; Edinçliler et al. 2010; Anastasiadis et al. 2012; Moghaddas Tafreshi and Norouzi 2012; Senetakis et al. 2012; Xiao et al. 2012; Marto et al. 2013; Mohamad et al. 2013; Sheikh et al. 2013; Maria Soledad Mashiri 2014; Balunaini et al. 2014; Dammala et al. 2015; M. S. Mashiri et al. 2015; Ehsani et al. 2015; Perez et al. 2016; M. S. Mashiri, Vinod, and Sheikh 2016; H. El Naggar, Soleimani, and Fakhroo 2016; Perez et al. 2017a; 2017b; Ehsani et al. 2017; Jamshidi Chenari et al. 2017; Noorzad and Raveshi 2017; AbdelRazek, El-Sherbiny, and Lotfi 2018; Asadi et al. 2018; Edinçliler et al. 2018; Platzer et al. 2018; S. Bali Reddy et al. 2018; Wang et al. 2018; Asadi and

Mahboubi 2019; Benessalah et al. 2019; Jamshidi Chenari et al. 2019; Li et al. 2019; Madhusudhan et al. 2019a; 2019b; Tsiavos et al. 2019; Foriero and Ghafari 2020).

Numerous studies have reported on the influence of tire content on the fundamental mechanical characteristics of sand-tire mixtures such as Void Ratio, Density and Unit Weight of the mixture (Bosscher et al. 1992; Dana N. Humphrey et al. 1993; Masad et al. 1996; Tatlisoz et al. 1998; Youwai and Bergado 2003; Ghazavi and Amel Sakhi 2005; Garcia et al. 2011; Tatlisoz et al. 1997; Dammala et al. 2015; AbdelRazek et al. 2018), Compressibility (B. N. N. Eldin and Senouci 1992; Ahmed 1993; Rao and Dutta 2006; Wartman et al. 2007; Zornberg et al. 2004; Youwai and Bergado 2003; Edil and Bosscher 1994; Jamshidi Chenari et al. 2017; Sodom Bali Reddy and Krishna 2017; Platzer et al. 2018; AbdelRazek et al. 2018; Benessalah et al. 2019; Madhusudhan et al. 2019a) Shear Strength (Ahmed 1993; Dana N. Humphrey et al. 1993; Edil and Bosscher 1994; Bernal et al. 1996; Foose et al. 1996; Ghazavi and Sakhi 2005; Sheikh et al. 2013; M. S. Mashiri et al. 2015; Naggar et al. 2016).

1.7.1 Unit Weight and Void Ratio of Sand-Tire Mixtures

The geotechnical engineering applications of TDA stem from the unique properties attributed to rubber tire. As stated earlier the unit weight of TDA materials is significantly lower than typical sand whereas the void ratio of TDA is higher than sand. Hence, of particular importance is the fact that the unit weight of the mixture is rendered low by that of the TDA component (Edil and Bosscher 1994). Specifically, the unit weight of pure (100%) TDA lies between 3 and 6 $\frac{kN}{m^3}$ which is a desirable value when used in different volume fraction mixtures. As a comparison, a TDA-soil mixture with a volume ratio of 50% TDA has a unit weight that lies somewhere between 10 and 13 $\frac{kN}{m^3}$.

Bosscher et al. (1992) measured the void ratios for various sand-TDA mixtures using their values of unit weight and concluded that the higher the sand content the lower the void ratio. This is because of the presence of fine sand particles within the void spaces between the tire particles which consequently lead to a decrease in the total pore volume of the mixture.

Pincus, Edil, and Bosscher (1994) investigated the engineering properties and behavior of the pure tire chips and tire chips-soil mixtures. They noticed that the unit weight of sand-tire mixtures is predominantly a function of tire (or sand) content. Moreover, it can be observed from the results

that the increase in the tire percentage, either by volume or weight of sand, resulting in a reduction of unit weight of the mixture.

Tatlisoz et al. (1997) evaluated the mechanical characteristics and behavior of scrap tire chips as well as their mixtures with sand and clay. It was observed from the test results that the unit weight of the soil-TDA mixtures decreases as the TDA content increases, at a rate of nearly 1.5 kN/m^3 per 10% TDA inclusion growth (Figure 1.5).

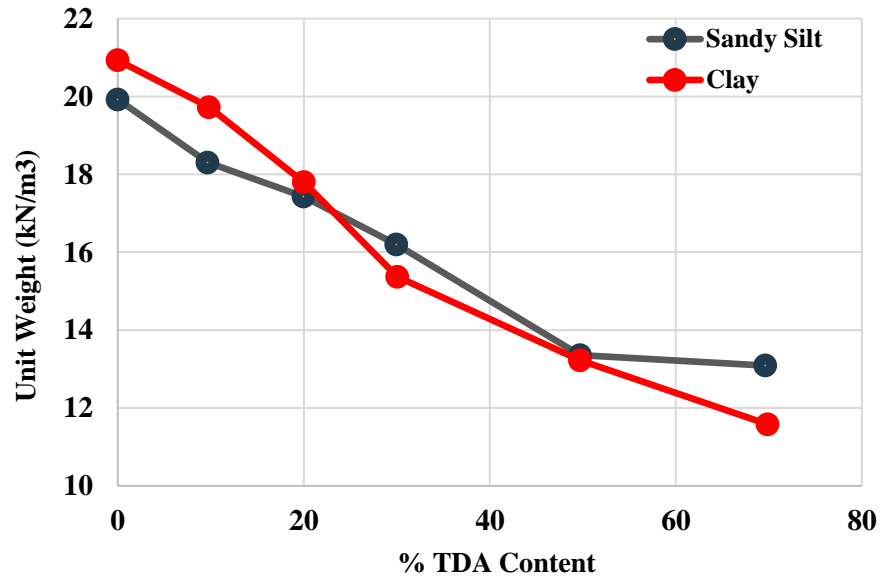


Figure 1.5 Influence of tire content on unit weight of soil-TDA mixtures

Modified from: (Tatlisoz, Benson, and Edil 1997)

Youwai and Bergado (2003) carried out a series of drained triaxial tests on compacted sand-tire mixtures having different mixing ratios of sand and tire. They concluded that the strength, density and unit weight of mixtures decrease when the proportion of tire in increased within the mixture. Furthermore, the results indicated that the unit weight of sand-tire mixed materials is approximately 13-60% lower in comparison with the compacted pure sand, based on the mixing ratio (Figure 1.6).

AbdelRazek et al. (2018) assessed the mechanical properties of sand-rubber through conducting a series of drained triaxial tests and one-dimensional compression tests. During the test material preparation, they produced samples of TDA having different particle sizes mixed with poorly graded coarse-to-medium siliceous sand at a constant relative density of 80%.

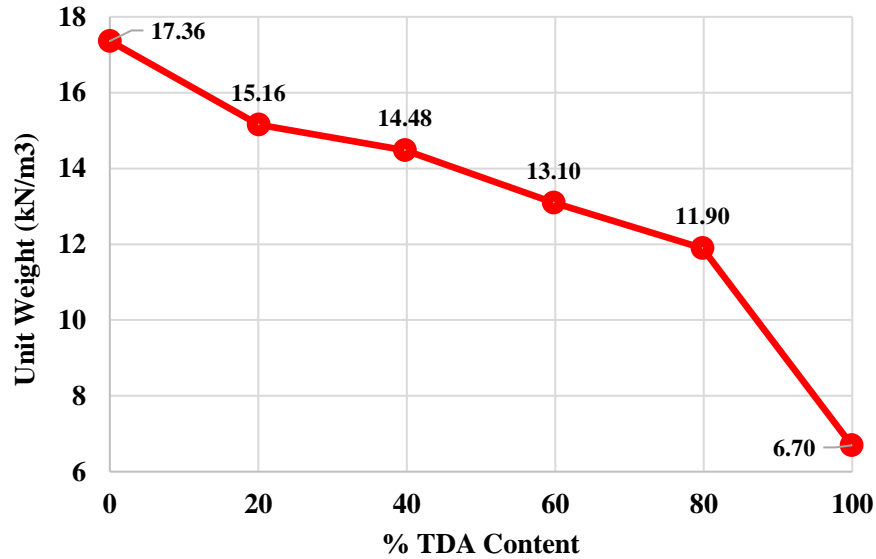


Figure 1.6 Influence of mixing ratio on dry unit weight of sand-tire mixed materials

Modified from: (Youwai and Bergado 2003)

As described the measured unit weight of the resulting mixtures included 17.2 kN/m^3 for pure sand (0% TDA content), 16.6 kN/m^3 for 5% TDA content, 15.86 kN/m^3 for 10% TDA content, 13.6 kN/m^3 for 20% TDA content, 11.8 kN/m^3 for 30% TDA content and 5 kN/m^3 for pure TDA material (100% rubber). These measured values clearly indicated that the increase of the TDA percentage within the sand-tire mixtures significantly reduced the unit weight of mixed materials.

1.7.2 Compressibility Characteristics of Dry Sand-Tire Mixtures

In geotechnical engineering applications, compared with other types of granular soils, sand has received more attention in order to be mixed with TDA. The inclusion of appropriate amounts of sand may significantly modify the compressibility behavior of granular tire materials. It has been reported (Tatlisoz et al. 1997) that sand-tire mixtures exhibit somewhat lower compressibility in comparison with soil-tire mixtures containing silt or clay whereas the tire alone exhibits the highest compressibility in absence of a soil modifier (e.g., sand, clay or silt). TDA content enhancement results in an increase of tire particles in the sand-tire matrix which consequently leads to an increase in compressibility of the sand-TDA mixture. The reason could be explained as the pure TDAs are highly compressible due to their high rubber content and high porosity. This may impose an extensive settlement and compaction problems particularly in tire modified embankments filled by sand-TDA mixed materials (Edil and Bosscher 1994; Youwai and Bergado 2003; Sodom Bali Reddy and Krishna 2017; Platzer et al. 2018; Madhusudhan et al. 2019a). Numerous studies have

already examined the compression behavior of sand mixed with different percentages of tire particles and mentioned the tire friction as one of the most important factors affecting the compressibility of the resultant sand-tire mixture. The majority of these studies (B. N. N. Eldin and Senouci 1992; Ahmed 1993; Rao and Dutta 2006; Wartman, Natale, and Strenk 2007; Zornberg, Cabral, and Viratjandr 2004; Jamshidi Chenari et al. 2017) have reported a considerable increase in compressibility of the sand-tire mixture through an increase in tire content (either by total volume or the total weight of the resultant mixture). There are a few studies that have reported the opposite trend (Benessalah et al. 2019) however, almost all of the previous studies agree that in high ranges of vertical stress the influence of tire content on the compressibility of the mixture decreases (Jamshidi Chenari et al. 2017).

Rao and Dutta (2006) investigated the mechanical behavior of sand mixed with different percentages of tire by conducting 28 compressibility tests, 4 repeated load tests and 52 triaxial compression tests. They concluded that sand-tire mixtures having tire content of less than 20% behave similarly to gravel-sand mixtures. However, excessive compressibility was observed for those mixtures containing more than 20% of tire.

Wartman et al. (2007) investigated the immediate and time-dependent compression of sand mixed with tire-derived aggregate. They realized that the magnitude of both immediate and time-dependent compression of the sand-TDA mixtures are highly dependent on the tire content and the time. They also concluded that both immediate and time-dependent compressibility of the sand-TDA mixtures increases with addition in the tire fraction content.

AbdelRazek et al. (2018) have investigated the compressibility of sand-tire materials with different tire fraction content. They conducted a series of 24-hour loading one-dimensional consolidation tests. According to the results they have reported, samples containing 5%, 10%, 20%, and 30% rubber which were subjected to 200 *kPa* vertical effective stress, reached axial strains of 2.2%, 2.5%, 9%, and 15.6%, respectively. (Figure 1.7). Test results demonstrated that a considerable jump occurred between the magnitude of axial strain recorded for the soil samples having 10% and 20% tire inclusion. The same trend can be observed between the samples containing 20% and 30% tire materials.

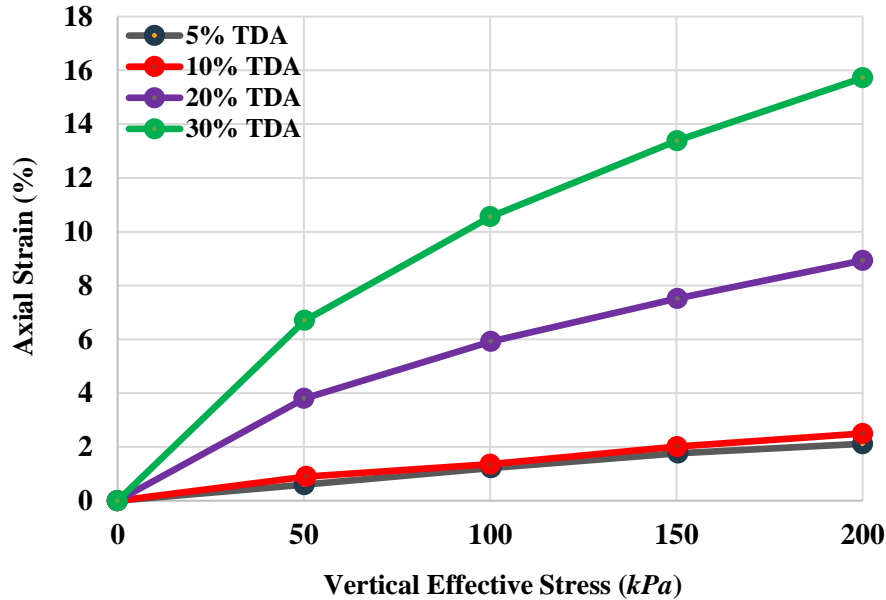


Figure 1.7 Axial strain vs. vertical effective stress for sand-tire mixtures with different tire content

Modified from: (AbdelRazek, El-Sherbiny, and Lotfi 2018)

Madhusudhan et al. (2019) carried out a series of triaxial and direct shear tests on dry sand-tire mixtures. They also observed an increase in the compressibility of the soil mixture as a result of the increase in the tire content.

Benessalah et al. (2019) conducted a series of odometer tests in order to investigate the effect of inclusion of rubber particles on the sand compaction and consolidation with a concentration on the compressibility parameters. Based on the experimental results with an increase in the tire fraction content the compressibility of sand-tire mixtures decreases, whereas both the compression index C_c and the swelling index C_s were increased. Moreover, a slight decrease for both preconsolidation pressure and the oedometric modulus was observed.

Madhusudhan et al. (2019a) investigated the engineering properties of fully saturated mixtures containing river sand and fine tire particles having dense condition. In this experimental study, the compressibility behavior of sand-TDA mixtures was examined through a one-dimensional compression test. The test results for the 100 kPa and 458 kPa compressive stress demonstrated the same ascending trend of axial compressive strain with an increase in tire inclusion within the mixture (Figure 1.8). Moreover, as shown in Figure 1.9, under 458 kPa compressive stress the soil sample made of pure sand (0% TDA) experienced a vertical strain equal to 1.2% whereas the sample consist of 100% tire exhibited a vertical strain of 57%.

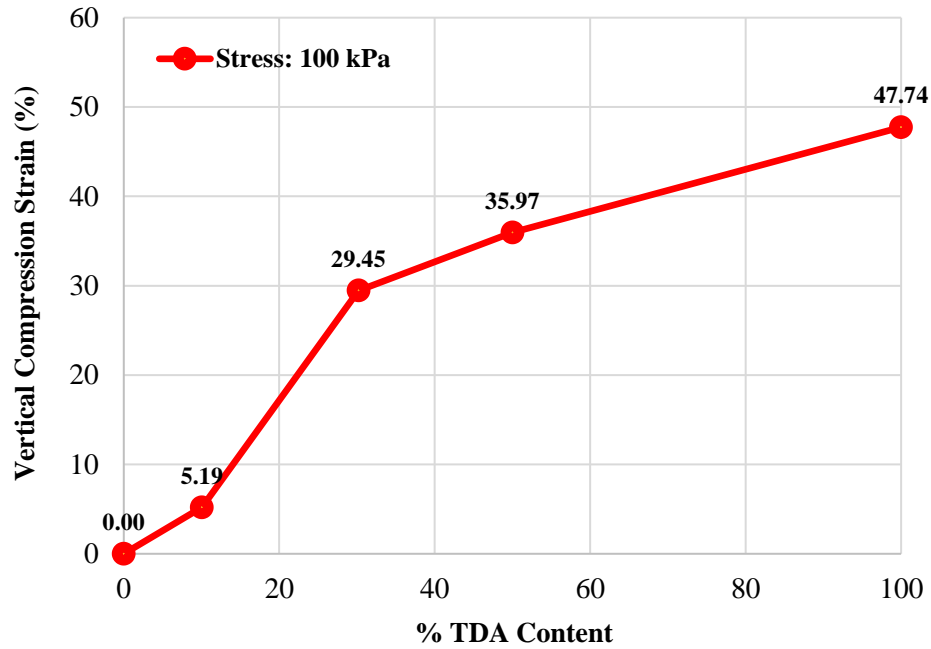


Figure 1.8 Variation of vertical compressive strain at 100 kPa for various TDA content.

Modified from: (Madhusudhan, Boominathan, and Banerjee 2019a)

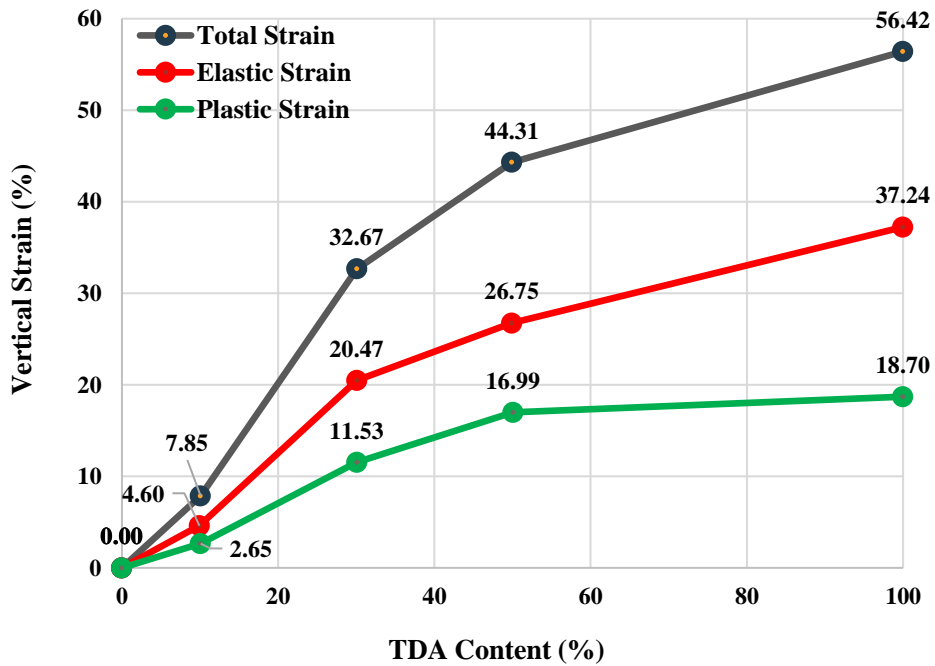


Figure 1.9 Variation of total, plastic and elastic strains at 458 kPa vertical stress.

Modified from: (Madhusudhan, Boominathan, and Banerjee 2019a)

1.7.3 Shear Strength and Dilatancy Characteristics of Sand-Tire Mix

The shear strength and dilatancy characteristics are the key factors affecting the efficiency and performance of processed scrap tires when it is considered to be used (either pure or mixed with soil) in a variety of geotechnical engineering applications such as highway embankments and backfill retaining structures (Wu et al. 1997; Youwai and Bergado 2003; Mashiri et al. 2015). Dilatancy is defined as the “variation of the volumetric strain with the plastic deviatoric strain” (Mashiri et al. 2016). In accordance with volumetric strain, the sign of dilatancy would be either positive in case of a compressive increment which is known as “contraction” or negative in case of an expansive increment which is known as “dilation” (Youwai and Bergado 2003). Hence, as fundamental properties of granular materials, determination of the shear strength and dilatancy of TDAs are of the primary measures to take before the beginning of the design of both soil materials and soil structures (e.g., number of TDA layers, depth of each TDA layer, depth of soil-cap etc.).

Humphrey et al. (1993) investigated the shear strength of pure tire chips utilizing direct shear apparatus custom-designed and concluded that the friction angle of the pure tire chips is somewhere between 19° and 25°.

Wu et al. (1997) performed a series of triaxial tests on five tire chips having different sizes, shapes, and gradation features aimed at evaluating the shear strength of tire chips materials. The results indicated that physical characteristics such as size, shape, and gradation have no influence on the frictional behavior of rubber tire materials. Moreover, for the five pure tire chips samples, the internal friction angle calculated to be approximately 40° whereas the interparticle friction angle (f_f) measured as 44°-56°.

Foose et al. (1996) carried out a series of direct shear tests on mixtures of dry sand and TDA in order to examine the feasibility of employing tire-derived aggregates to reinforce sand. They observed from the test results that there are three main factors that significantly affect the shear strength of the sand-TDA mixtures which are defined as TDA fraction content, normal stress, and the sand matrix unit weight. Moreover, test results indicated that the addition of TDA to sand increases the shear strength of the resulting sand-TDA mixture and the initial friction angle (f'_1) reaches 67° whereas the initial friction angle in unreinforced sand with the same unit weight is 34 degrees.

Youwai and Bergado (2003) investigated the strength and deformation characteristics of sand mixed with shredded tires through performing drained triaxial tests on compacted sand-tire

mixtures having different mixing ratios of sand and tire. They reported that based on the test results obtained, the strength of the sand-tire mixed materials decreases with an increase in the tire content owing to the fact that shear strength of shredded tires is lower than that of the sand. Moreover, the peak internal friction angle was measured to be variable between 30 to 34° depending on the tire shred content within the mixture. They additionally concluded that the strength characteristics of the sand-tire mixtures are not only a function of the tire fraction content, but they are also influenced by the size and shape of the tire particles. Furthermore, in experimental investigations, the sample preparation method is considered as another factor that affects the shear strength behavior of the resulting sand-tire mix. It has been also observed that similar to cohesionless granular materials, sand-tire mixtures exhibit both positive and negative dilations which are respectively corresponding to expansion and compression of the sample. Accordingly, when confining pressure increased, the tendency of dilatancy decreased owing to an increase in the intensity of confining stress.

Zornberg et al. (2004) performed a series of tests utilizing a large-scale triaxial apparatus aiming to investigate the optimum dosage as well as the optimum aspect ratio of shredded scrap tires used as granular fill materials. The results revealed that the sand-tire shreds mixtures exhibit a sand-like behavior wherein the tire content is less than 35% by the total weight of the resulting mixture (weight of tire divided by the total weights of tire and sand), while they exhibit tire-like behavior when the tire content is beyond 35% within the mixture. Moreover, it has been observed that the addition of tire shreds up to around 35% leads to an increase in shear strength of the sand-tire mixtures whereas beyond 35% it will result in a reduction of the shear strength. They also concluded that the enhancement of aspect ratio of tire particle (the ratio of the length of tire particles to the width of tire particles) leads to an increase in shear strength of the mixed materials. This shear strength increment is more highlighted when the aspect ratio rises from 4 to 8. Furthermore, the samples containing tire fraction content below 35% exhibit dilatant behavior whereas the samples with tire proportions above 35% demonstrated to be fully contractive. This indicates that the dilatancy of sand- tire mixtures decrease with an increase in tire content. It can be also concluded that the addition of tires with percentages above 35% by weight may completely remove dilatancy within the resulting sand-tire mixed materials. Additionally, the influence of aspect ratio has been observed to be negligible on the volumetric strain at high confining pressures. It has been also noted that the dilatancy decreases with an increase in the aspect ratio of the tire shreds when the specimen is subject to low confining pressures. Finally, based on the results obtained it has been

concluded that the 35% tire shreds content (by weight) is the optimum tire fraction within the sand-tire mixtures.

Ghazavi and Sakhi (2005) performed a series of direct shear tests on the samples of sand reinforced with tire shreds at three different fraction contents including 15%, 30% and 50%. In accordance with the results obtained from the direct shear tests, it was concluded that the key factors affecting the shear strength of the sand-tire mixtures are including normal stress, tire content, tire shred width, tire aspect ratio for a given width and compaction. Furthermore, it has been concluded that the increase in tire content leads to an increase in the initial friction angle of the mixed sand-tire materials. In this study the greatest value acquired for the initial friction angle was approximately $f'_1 = 67^\circ$ at 50% tire content (Figure 1.10) whereas, previously Foose, Benson, and Bosscher (1996) have reported the same value of $f'_1 = 67^\circ$ that was obtained for the mixture with 35% tire content. In addition, Balunaini et al. (2014) have reported that the end-of-test friction angle of sand mixed with large tire shreds lies somewhere between 30-33°.

Attom (2006) investigated the influence of tire inclusion on shear strength properties of sand. Hence, he conducted a series of direct shear tests on 12 soil samples made of 3 different types of sands with varying gradations mixed with tire shreds at 4 different friction content of 10%, 20%, 30% and 40%. He concluded from the results that the increase in tire shreds content will increase both internal friction angle and shear strength of the mixed sand-tire materials. This trend was repeated in all 12 tests. He has also developed a model in order to compute the internal friction angle and consequently predict the shear strength of the sand-tire mixtures. The results of the prediction model almost conformed with those measured during the direct shear tests.

Marto et al. (2013) investigated the shear strength of sand-tire chips mixtures varying in tire content by conducting the standard direct shear test. They have concluded from the results that the shear strength of the mixture increases slightly with an increase in the tire content up to 20% by weight. However, beyond this tire fraction content, the shear strength begins to decrease. Moreover, the severity of this reduction increases with the magnitude of the normal stress (Figure 1.11).

Sheikh et al. (2013) performed triaxial and compression tests in order to investigate the shear and compressibility behaviors of sand-tire crumb (S-TC) mixtures. In accordance with the test results, it has been observed that the shear strength and the corresponding axial strain of the mixed materials are primarily influenced by the tire crumbs content and the magnitude of the confining pressure (Figure 1.12). Furthermore, in contrast with some of the previous conclusions reported by other

studies, the results of this study demonstrated that the friction angle of the sand-tire mixed materials decreases as the tire content increases within the mixture (Figure 1.12).

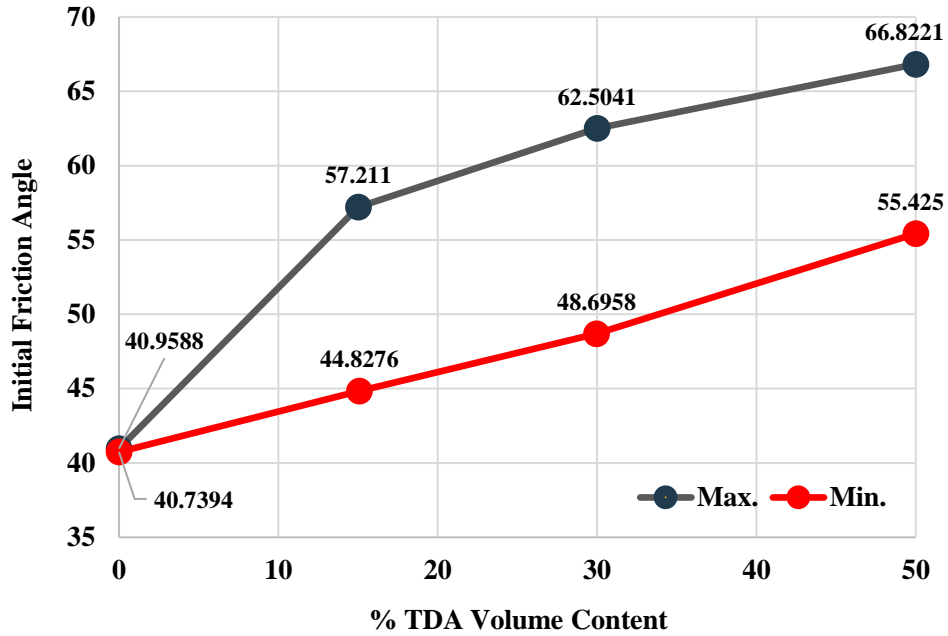


Figure 1.10 Influence of tire content on the value of initial friction angle (f'_1) of sand-tire mixtures
 Modified from: (Ghazavi and Sakhi 2005)

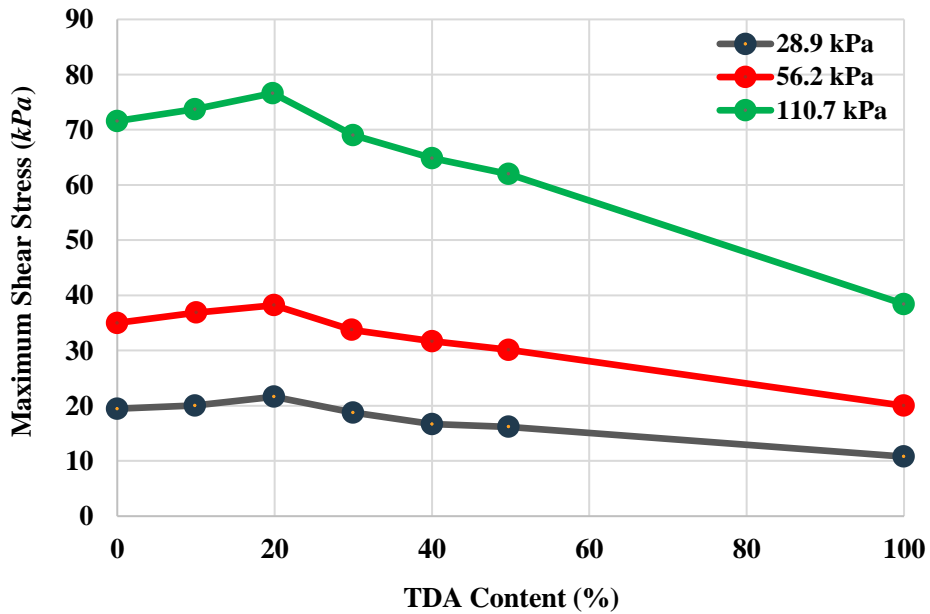


Figure 1.11 Influence of normal stress and tire content on shear strength of sand-tire mix.
 Modified from: (Marto et al. 2013)

Mashiri et al. (2015) conducted a series of monotonic triaxial tests on sand reinforced with different percentages of tire chips. The target was to investigate the shear strength and dilatancy behaviour of sand–tire chips (STCh) mixtures.

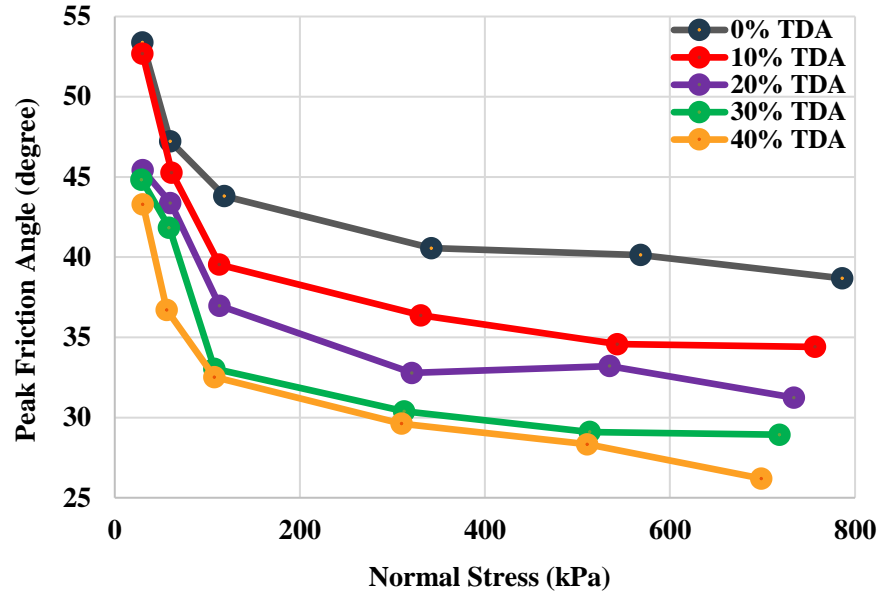


Figure 1.12 Influence of tire content and normal stress on friction angle of sand-tire mixtures
Modified from: (Sheikh et al. 2013)

Considering the substantial reduction in dilatancy followed by a simultaneous increase in the shear strength, they also recognized 35% (by mass) as the optimum percentage of the tire to be mixed with pure sand for the production of STCh mixture. This conforms with the results that have been reported earlier by Zornberg et al. (2004). Moreover, their results depict that the increase in effective confining pressure results in an increase in shear strength and reduction in dilatancy, whereas the increase in the initial relative density leads to an increase in both shear strength and dilatancy characteristics of the mixture.

Noorzad and Raveshi (2017) carried out a series of drained triaxial tests on soil samples of sand mixed with different percentages (by weight) of small tire crumbs aimed at investigation of behavior of the tire-sand mixtures. They concluded that the peak shear strength and the corresponding axial strain of sand-TDA mixtures are primarily influenced by the percentage of tire content and confining pressure (Figure 1.13). In addition, based on their observations from the test results, they concluded that unlike many test results previously reported by other research the increase of tire content within the mixture results in a reduction of shear strength of the sand-tire mixed materials (Figure 1.13).

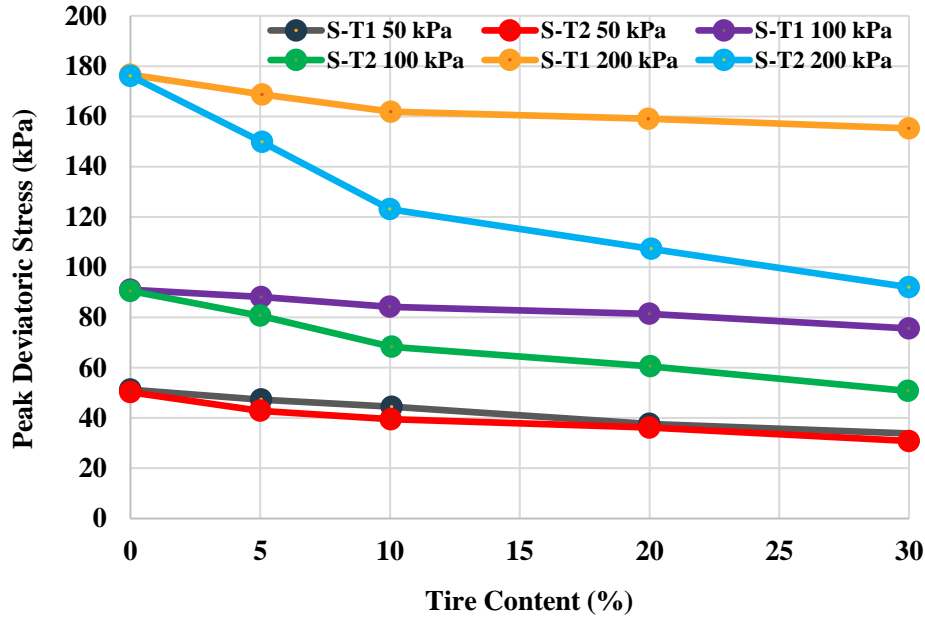


Figure 1.13 Influence of tire content and confining pressure on the peak deviator stress

Modified from: (Noorzad and Raveshi 2017)

As can be observed from the results of the above-mentioned studies, the lack of similar behavior in shear strength of the sand-TDA mixtures based on the TDA content is highly perceptible. Furthermore, the values achieved for the friction angle of the pure tire (100% TDA) varies in different studies. A very likely reason for justifying these discrepancies could be human errors during the experiments as well as the different conditions of the experiments such as room temperature, moisture content of the mixture, initial void ratio of the sample, magnitude of the confining pressure, etc.

Although, it could be concluded from the above studies conducted by different researchers that addition of the TDA to sand up to 35% by total mass of the mixture will result to increase in both the shear strength and internal friction angle while beyond this amount will result in reduction of the mentioned properties of the mix. Hence, the mixture having 35% of TDA and 65% of sand by mass could be considered as the optimum mixture having the highest shear strength and internal friction angle.

Moreover, this can also justify the reason why a pure TDA sample (100% TDA) exhibits the lowest shear strength and internal friction angle compared with the sand-TDA mixtures. In fact, in a sand-TDA matrix, sand particles, which are smaller in size compared to tire particles, act as the texture elements and fill the pore spaces between the tire particles. This will result in an increase in interparticle locking. On the other hand, it has been already proven by past studies (P. Guo and Su

2007) that the presence of interparticle locking is likely to increase both the friction angle and the shear strength of the granular materials. Hence, it is obvious that the addition of sand to TDA may result in an increase in both the friction angle and the shear strength of the resulting mixture.

1.8 Civil Engineering Applications of TDA

Due to the scrap tires' non-biodegradable nature, innovative approaches are needed in order to find new solutions for the recycling of waste tires ever-growing stockpiles. In the past two decades, there have been several initiatives to address this issue. Hitherto, scientists and engineers have come up with the three main applications of scrap tires including tire-derived fuel (TDF), civil engineering applications, and ground rubber applications. Among those civil engineering applications are the most simple, economical and environmentally friendly use of waste tires. Moreover, civil engineering projects tend to be sizeable, creating a massive recycling opportunity for a huge amount of scrap tires to be used as construction materials either in the whole form or in the form of tire-derived aggregates (TDA).

In civil engineering, TDA has received interest in being used in a variety of geotechnical applications such as slope stabilization (Belabdelouahab and Trouzine 2014; Basheer et al. 1996; Grubb et al. 2007), drainage construction (Thakur and Kaushik 2016; Edil and Bosscher 1994), lightweight backfill for retaining walls and bridge abutments (Tweedie et al. 1998; Tatlisoz et al. 1998), vibration mitigation (D. Humphrey 2003; CalRecycle 2016; Cheng and Ahn 2014; Hoppe and Oman 2013), thermal insulation (Dana Humphrey and Blumenthal 2010; Edeskar 2006; Hoor and Rowe 2012), and light-rail construction (Esmaeili and Rezaei 2016; Cal.Recycle 2019). Moreover, it has widespread application as lightweight fill for embankment constructions such as highway and bridge embankments on weak and compressible foundation soils (Apex-Companies 2008; Mahgoub and El Naggat 2019; Foose et al. 1996). In addition, TDA is widely used in production of high-quality asphalt and concrete through a process in which tire particles, as alternative aggregates, are mixed respectively with bituminous and cementitious materials. Waste tires are also processed in order to transform to the form of tire powder. This powder then melted at high temperatures to extract the polymers from the rubber and improve the bitumen properties and the resulting asphalt is called rubber modified asphalt (Dana N Humphrey and Swett 2006; Mujibur Rahman 2004; Presti 2013; Chamberlin and Gupta 1986; Celauro et al. 2012) and rubber modified concrete (Eldin and Senouci 1993; Azizian et al. 2003; Cal-Recycle 2009; Thomas and Gupta 2015; S. Guo et al. 2017; El Naggat et al. 2019), respectively.

1.9 Geotechnical Engineering Applications of TDA

In geotechnical engineering, a common practice in the backfilling process during the construction of underground infrastructures such as subway stations, tunnels, and pipelines, often involves using the same excavated earth materials, such as soil and gravel for backfilling. This construction stage tends to be a low-cost approach however, in the long-term it leads to a considerable reduction in the service life of the buried infrastructures. The reduction in service life is due to a high magnitude of applied loads caused by the inadequate design of backfill materials. These excess applied loads are not only the results of the heavyweight of unsuitable backfill materials but also their improper drainage capacity. The heavy weight of filling materials increases the earth pressure while their poor drainage leads to higher water pressure on the structure.

Tire derived aggregates (TDAs) are made from recycled scrap tires with varying sizes according to the technical, economic, and environmental requirements of the project. Owing to its considerable advantages mentioned earlier, TDAs have been gradually utilized in such geotechnical applications (D. N. Humphrey 2008) as lightweight fill material for embankments construction particularly those built up on weak soils (Apex-Companies 2008; Mahgoub and El Naggar 2019; Foose, Benson, and Bosscher 1996; Bosscher, Edil, and Kuraoka 1997; Dickson, Dwyer, and Humphrey 2001; D. N. Humphrey 2008; S. Bali Reddy, Krishna, and Reddy 2018; Eldin and Senouci 1992), thermal insulation materials used in road and highways pavement design to control and minimize frost penetration (Dana Humphrey and Blumenthal 2010; Edeskar 2006; Hoor and Rowe 2012; Humphrey 2008), subbase drainage materials (Thakur and Kaushik 2016; Edil and Bosscher 1994; Dana N. Humphrey and Eaton 1995; D. N. Humphrey 2008; Hazarika et al. 2010; S. Bali Reddy et al. 2018), pile-supported embankments on soft soil (Jeffrey J. Tweedie et al. 2004; D. N. Humphrey 2008), landfill applications (Dana N Humphrey and Swett 2006; Thakur and Kaushik 2016; D. N. Humphrey 2008), lightweight backfill material to be used in implementation of bridge abutments and retaining walls (Tweedie et al. 1998; Jeffrey J Tweedie et al. 1998; Humphrey 2008; Reddy et al. 2018), and anti-vibration mats for machine foundation and railways (Esmaeili and Rezaei 2016; Cal.Recycle 2019; Humphrey 2008; Ehsani et al. 2015; Hazarika et al. 2010; Reddy et al. 2018). Although, due to its excessive compressibility characteristics TDA is usually mixed with soil (e.g., sand) to form as soil-TDA mixture. The inclusion of soil in TDA materials significantly improves their mechanical properties. The resultant high-strength soil-TDA mixture when used as backfill geomaterial in embankment and retaining wall constructions exhibits unique performance (Tatliso, Benson, and Edil 1997; Edinçliler et al. 2010; Humphrey 2008; Promputthangkoon and Karnchanachetanee 2013; Heimdahl and Drescher 1999; S. Yoon et al. 2006; Masad et al. 1996;

Garga and O'Shaughnessy 2000; Tweedie et al. 1998; Humphrey et al. 1993; FHWA 2016; Basheer et al. 1996; Reddy et al. 2018). It has been reported that compared with conventional foundation materials, utilization of soil-TDA mixture may reduce the settlement of the foundation by 22% (S. Bali Reddy, Krishna, and Reddy 2018).

1.10 Specifications and Guidelines for Use of Scrap Tire in Civil Engineering

The main standard specification currently available for the use of scrap tires in various civil engineering applications is the ASTM D6270. The ASTM specification was published in its initial version in 1998. The last version has been published in 2017. Several publications are currently available addressing the guidelines for the use of processed scrap tire (mainly in form of TDA) in civil engineering projects particularly as geomaterial in geotechnical applications. A selection from these references has been provided below.

1. ASTM D6270
Standard Practice for Use of Scrap Tires in Civil Engineering Applications, *American Society for Testing and Materials*, last version available: ASTM D6270-17.
2. DRRR-2011-038
Civil Engineering Applications of Tire Shreds, a report prepared by Dana N. Humphrey for *California Integrated Waste Management Board*, Orono, Maine, 2003.
3. DRRR-2014-1489
Properties of Tire-Derived Aggregate for Civil Engineering Applications, *California Department of Resources Recycling and Recovery (CalRecycle)*, Sacramento, California, May 2013.
4. DRRR-2016-1545
Usage Guide - TDA (Tire-Derived Aggregate), *California Department of Resources Recycling and Recovery (CalRecycle)*, Sacramento, California, January 2016.
5. EPA530-R-10-010
Scrap Tires: Handbook on Recycling Applications and Management for the U. S. and Mexico, *United States Environmental Protection Agency*, Washington DC, December 2010.
6. FHWA/IN/JHRP-93/04

Laboratory Study on Properties of Rubber-Soils, Joint Transportation Research Program, *Indiana Department of Transportation and Purdue University*, West Lafayette, Indiana, May 1993. DOI: 10.5703/1288284314210.

7. [FHWA/IN/JTRP-2002/35](#)

Construction of Tire Shreds Test Embankment, Joint Transportation Research Program, *Indiana Department of Transportation and Purdue University*, West Lafayette, Indiana, October 2003. DOI: 10.5703/1288284313165.

8. [FHWA-RD-97-148](#)

User Guidelines for Waste and Byproduct Materials in Pavement Construction, Federal Highway Administration Research and Technology, *U.S. Department of Transportation*.

9. [FHWA/TX-03/0-1808-1](#)

Evaluate the Uses for Scrap Tires in Transportation Facilities, Center for Multidisciplinary Research in Transportation, Texas Tech University, A Report Submitted to *Texas Department of Transportation*, Texas, December 2003.

10. [GEM-20](#)

Guidelines for Project Selection, Design, and Construction of Tire Shreds in Embankments, Geotechnical Engineering Manual, *New York State Department of Transportation*, Geotechnical Engineering Bureau, August 2015. (NYSDOT 2015)

11. [ME0012-11/MD04173](#)

Guidance Manual for Engineering Uses of Scrap Tires, Prepared by Geosyntec for *Maryland Department of the Environment*, June 2008.

1.11 Existing Models to Predict Creep Behavior of TDA and TDA-Sand Mixtures

There are only a few numbers of studies to emphasize the modeling of long-term mechanical behavior of TDA and soil-TDA mixture when use as geomaterials in geotechnical engineering applications. The two selected methods of modelling proposed by two different studies which were published in the same year have been briefly discussed below.

1.11.1 The model recommended by Ngo and Valdes in 2007

This creep model has been originally developed by Singh and Mitchell (1968) to predict the behavior of fine-grained soils. Later, in 1997 the model was suggested by Merry and Bray (1997)

to be utilized for prediction of the creep behavior of a wide range of geomaterials. Finally, in 2007 the model was recommended by Ngo and Valdes (2007) for prediction of the time-dependent mechanical response of sand–rubber mixtures. This model is capable of predicting strain versus time via three parameters including α , A , and m , which may be found through the data obtained from creep tests in which at least two different stress magnitudes are applied to independent specimens [Eqs. (1.1) and (1.2)].

$$\varepsilon = \alpha + \frac{A}{1-m} e^{\alpha\sigma} t^{1-m} \quad 1.1$$

where,

$$\alpha = \varepsilon_1 - \frac{A}{1-m} e^{\alpha\sigma} \quad 1.2$$

and ε_1 is equal to the strain at $t = 1 \text{ min}$, whereas m represents the rate at which the strain reduces with time. The value of m is obtained from the slope of the log-log plot of strain rate versus time for any stress intensity (σ). The parameters α and A are achieved from the log-log plot of strain rate versus time for time $t = 1 \text{ min}$. The values of α and A are equal to the slope of the resulting line and the ordinate intercept, respectively. The parameter α designates the stress dependence of the creep rate whereas the parameter A represents strain rate equivalent to $\sigma = 0$. For typical soils the value of m , A and α respectively ranges between 0.75 and 1.0, 0 and 0.004, and 0.001 and 0.006 depending on the over-consolidation ratio (Singh and Mitchell 1968; Ngo and Valdes 2007).

1.11.2 The model recommended by Wartman et al. in 2007

The second model to predict the time-dependent deformation of the pure tire (TDA) or sand-TDA mixtures has been recommended by Wartman et al. (2007) which computes the time-dependent settlement using the following equation:

$$\Delta H_t = H C_{\alpha\varepsilon} \log \frac{t_2}{t_1} \quad 1.3$$

In this equation, H is the thickness of the TDA layer and consequently the ΔH_t is the change in the thickness of the TDA layer; t_1 is the time when time-dependent compression begins (assumed to be 1 day); and t_2 is the time at which the magnitude of time-dependent compression is required (final time-days), $C_{\alpha\varepsilon}$ is the modified secondary compression index which is considered approximately 0.0065 for pure large size TDA (100% tire).

1.12 Bailey-Norton Creep Law

This section briefly provides a background on the constitutive models proposed to explain the deformation of materials especially the Bailey-Norton law.

The creep strain (ε_c) of materials is a function of stress σ , time t , and temperature T , hence it can be written as (Harry 1980; Boyle and Spence 1983; Penny and Marriott 1995; Yao et al. 2007)

$$\varepsilon_c = f(\sigma, t, T), \quad 1.4$$

Then the Eq. (1.4) can be rewritten in its separated form as

$$\varepsilon_c = f_1(\sigma)f_2(t)f_3(T). \quad 1.5$$

Among all expressions suggested in different studies the “Norton power law”, which was proposed by Norton in 1929, received the most attention and was expressed as a stress function where A and n are the materials constants (Norton 1929; Yao et al. 2007)

$$f_1(\sigma) = A\sigma^n. \quad 1.6$$

In order to express the time function the popular “Bailey law” was employed where D and m are the materials constants. The value of m is typically somewhere between $\frac{1}{3}$ and $\frac{1}{2}$ (Bailey 1935).

$$f_2(t) = Dt^m. \quad 1.7$$

Finally, based on the “Arrhenius’s law” the temperature dependence can be written as the following equation while “ $-\Delta H$ ” is activation energy and R is Boltzman’s constant (Dorn 1955)

$$f_3(T) = C \exp\left(\frac{-\Delta H}{RT}\right). \quad 1.8$$

Combining Eq. (1.4) to Eq. (1.8) the creep strain can be rewritten as (Yao et al. 2007)

$$\varepsilon_c = B \exp\left(\frac{-\Delta H}{RT}\right) \sigma^n t^m. \quad 1.9$$

For the special case of an isothermal condition the creep strain can be rewritten as

$$\varepsilon_c = B t^m \sigma^n, \quad 1.10$$

The Eq. (1.10) express the “Norton-Bailey law” that is widely employed for analyzing and modeling the time dependent creep behavior of materials (Harry 1980; Yao et al. 2007). The Bailey-Norton law is capable of properly characterizing the primary and the secondary creep stage from the constant vertical load (uniaxial stress) (Kobelev 2014; Ma et al. 2022; Yao et al. 2007).

1.13 General Conclusion of Chapter 1 (Literature Review)

This section aims to provide a brief discussion on the findings and conclusions related to the review of the past studies stated in the present chapter.

- a) The stockpiling waste tires produce breeding ground for mosquitoes and rodents. Moreover, since petroleum products are used in production of tires, hence they are naturally flammable and therefore they are classified as fire hazardous waste materials. Therefore, tire recycling while it must be economic may help the removal of this type of waste materials from the environment.
- b) New applications of waste tire increase the global demand and consequently better encourage both public and private sectors to produce different types of TDA by making the recycling process profitable.
- c) Tire rubber is classified as lightweight alternative aggregates when added to the different types of soil such as sand to form soil-tire mix materials. The lightweight nature of tire leads to produce a lighter resulting geomaterial when mixed with sand, compare with that of conventional geomaterials. Typically, the unit weight of processed waste tire is equal to $\frac{1}{3}$ of that of sand. This advantage is the principal motivation of using processed waste tires in production of geomaterials.

- d) Only limited numbers of studies have emphasized the importance of time-dependent creep behavior of soil-tire rubber materials for use in geotechnical engineering applications. These include studies conducted by Wartman et al. and Anh and Valdez in 2007. Wartman et al. examined the immediate and time dependent one-dimensional compression of tire chips and shreds. In the same year, Anh and Valdez investigated the one-dimensional compression of specimens, composed of sand and granulated tire rubber. Although even the knowledge improvement on creep behavior of sand-tire materials provided by these mentioned studies is somehow limited. These limitations are as follows, a) The constitutive equations that have developed to model the behavior of soil-TDA mixtures are not able to predict both elastoplastic and creep behaviors of these geomaterials. b) They are unable to predict both volumetric and deviatoric time-dependent deformations and are limited to predict only the volumetric creep.
- e) The Norton-Bailey law is widely used for analysis and modeling of the time dependent creep behavior of materials. Along with all proposed creep models, for the constant stress, the Norton-Bailey law is considered as the most common constitutive equations to model the primary, secondary or tertiary creep stages through the introduction of a power law relationship between creep rate and stress.

CHAPTER 2

2 Methodology

2.1 Introduction

This chapter contains the methodology of the present study. Aimed at the obtention of the proposed objectives of the study efforts were made in order to design an appropriate research program. This research program is comprised of two main portions including an experimental program and a numerical simulation program. In the numerical section of this study, equations have been proposed aiming to provide a satisfactory prediction of shear strength and creep deformation behaviors of the sand-TDA granulated mixed materials. Although the numerical sections have been properly discussed within chapters 3 and 4 of this thesis. The experimental section of this study consists of four different laboratory tests including: 1. Long duration creep tests; 2. Direct shear tests; 3. Triaxial tests; and 4. Small-scale foundation tests. The purpose of conducting the above-mentioned experiments was to determine the elastic, plastic and creep parameters of pure granulated TDA as well as the sand- TDA granulated mixtures.

2.2 Test Materials

The test materials employed in the experimental program within this study incorporate granulated tire-derived aggregate (TDA) and the Ottawa sand. Moreover, the test samples prepared during four experiments can be categorized into two general types including a pure TDA sample made of 100% granulated TDA and sand-TDA samples made of sand-tire mixtures with different mixing ratios. It must be noted that sand does not exhibit significant creep. Sand deformations generally occur instantaneously. Moreover, the objective of this study is to determine the creep and plasticity parameters for the sand-TDA mixtures in order to develop appropriate constitutive models to estimate the instantaneous and the long-term mechanical behaviors of such mixtures. There are numerous studies already conducted to investigate different mechanical properties of sand.

Therefore, for Ottawa sand the mechanical characteristics such as the critical friction angle were obtained from the literature.

The granulated rubber tire used in this study is a by-product of scrap tires which were recycled through a process of size reduction to form as tire-derived aggregate. In 2015, this TDA material (Figure 2.1) had been supplied by the *Shercom Industries Inc.*, and transported from Saskatoon in Saskatchewan to the geotechnical engineering laboratory at Laval University in Québec.



Figure 2.1 TDA granular material employed in this study

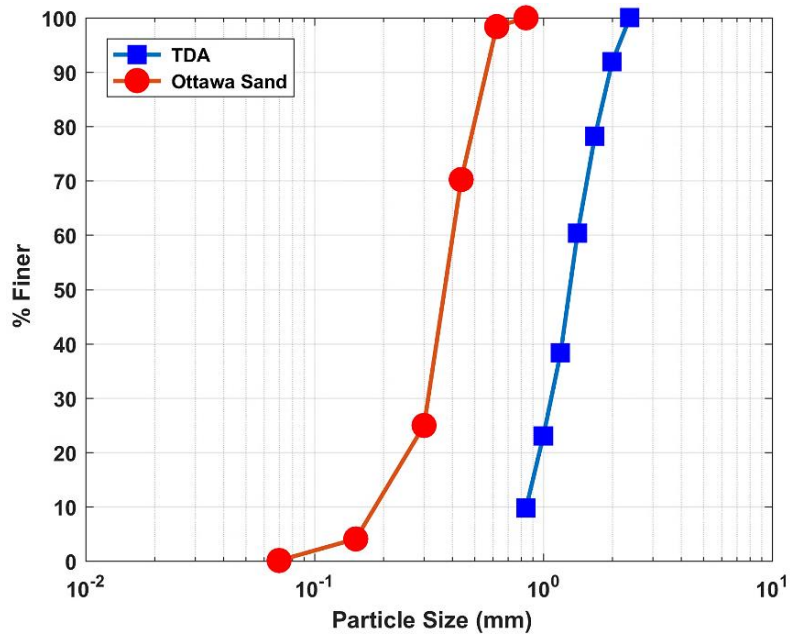


Figure 2.2 Grain-size distribution curves of TDA and Ottawa sand used in this study

The true density of the TDA was measured by the supplier company using a helium pycnometer and reported between 1.14 - 1.24 (g/cm^3). Granulometric and particle size distribution curves for this material is illustrated in Figure 2.2 and Figure 2.3 respectively.

Owing to the calculated values of $C_u = 1.69$ and $C_c = 1.03$ for this type of TDA material and also as it can be observed from its granulometric curve this rubber granular material is considered as poorly graded if classified according to the Unified Soil Classification System.

Furthermore, in this study graded Ottawa sand conforms to ASTM C778 and furnished by U.S. Silica Company (Figure 2.4) has been used in the preparation of those specimens which contain portions of both sand and TDA.

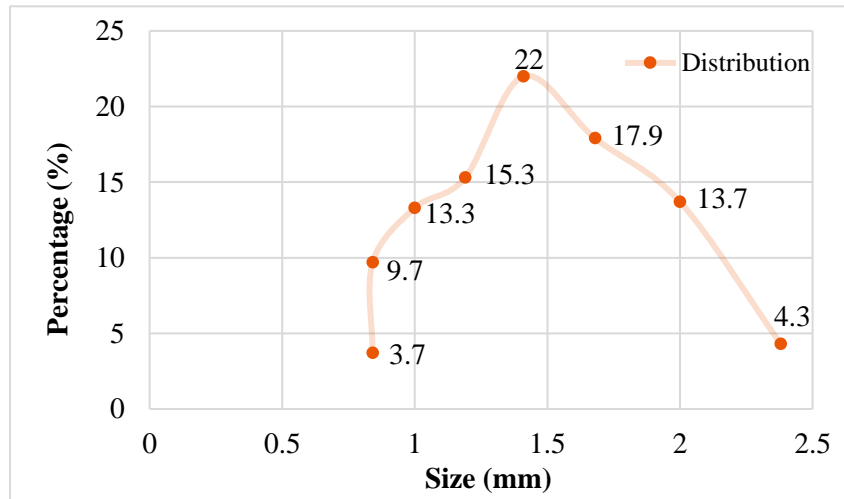


Figure 2.3 TDA particle size distribution by percentage



Figure 2.4 Graded Ottawa sand used in this study

A grain-size distribution curve for Ottawa sand is also illustrated in Figure 2.2. From the shape of this curve and with calculated values of $C_u = 2.1$ and $C_c = 1.26$, this sand is also defined as a poorly graded sand (SP).

2.2.1 Sample Preparation Procedures

Aiming to investigate the influence of the tire fraction content and its intensity on the creep and plastic behaviors, the two components of the mixture including sand and TDA were combined at various volumetric ratios depend on the deigned tests. For the first two tests which are the creep test and direct shear test the 5 different mixtures of sand-TDA were prepared at $\theta_p = 0.2, 0.4, 0.6, 0.8,$ and 1.0 , where θ_p represents the volume fraction of TDA per total volume of the mixture and the $\theta_p = 1$ reflects the sample which contains pure granulated tire rubber (100% TDA). For the triaxial test, 3 different mixtures of sand-TDA were prepared at $\theta_p = 0.50, 0.75, 1.0$ whereas for the small-scale foundation test a single mixture of $\theta_p = 80\%$ were prepared. Since, these mixtures involve two poorly graded materials and hence represent an undesirable field condition but a sensible one when running creep tests. The advantage is that the effect of creep, which this study shows to be inextricably linked to the TDA content, is more apparent when the fabric is unstable. Generally, in the field, well-graded sand is an important requirement if one wishes to obtain a stable mixture when combined with TDA. As shown in Figure 2.5, a phase diagram is plotted for the sand-TDA mixture and used to determine the initial void ratios that correspond to the five volumetric ratios mentioned previously. Note that this phase diagram illustrates the state of the sample before starting the test.

This was possible because both the weights of the TDA and sand phases, as well as the total volume they occupied were measured beforehand.

Table 2.1 Test sample specifications.

TDA Volume Content (%)	Volume of Sample (m³)	Mass of Sample (kg)	Density (ρ) (kg/m³)	Unit Weight (γ) (kN/m³)	Initial Void Ratio
20	0.000221	0.324	1466	14.37	0.64
40	0.000221	0.273	12355	12.10	0.74
60	0.000221	0.224	1013	9.93	0.83
80	0.000221	0.173	785	7.70	0.94
100	0.000221	0.124	561	5.50	1.05

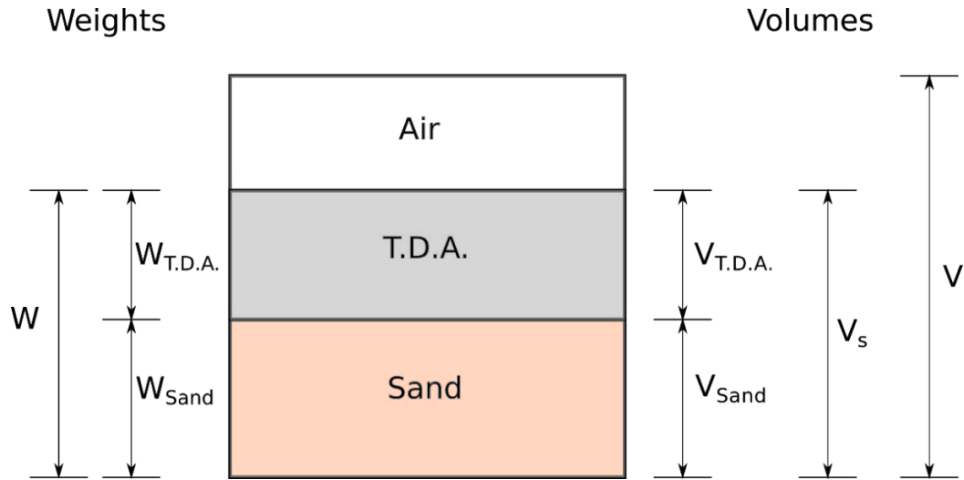


Figure 2.5 Phase diagram of TDA–sand mixture

For the calculations, the specific gravity of the TDA ($G_{TDA} = 1.15$) and Ottawa Sand ($G_{Sand} = 2.65$) were necessary. The phase volumes of the TDA and Sand were obtained respectively as $V_{TDA} = \frac{W_{TDA}}{G_{TDA} \gamma_{\omega}}$ and $V_{Sand} = \frac{W_{Sand}}{G_{Sand} \gamma_{\omega}}$. Consequently, the initial void ratio, e , and initial unit weight of the TDA-Sand mixture were known at the start of all tests. The values of density, unit weight and initial void ratio of the specimens with respect to their TDA volume fraction content have been calculated as shown in Table 2.1.

2.3 Description of the Creep Test for Determining the Creep Parameters of the Norton-Bailey Constitutive Model

In order to investigate the time-dependent creep response of sand specimens mixed with granulated tire rubber and also the pure granulated tire specimen the first step is to determine the necessary creep parameter for the above-mentioned materials. Hence, a creep test was designed to be run for a long duration aiming to achieve the long-term deformation parameters of the designed test materials. A total of 25 creep tests were performed on 5 different mixtures having various TDA fraction contents under 5 different vertical stresses. The different stages of the experiment including a description of the test materials, specifications of the cell (mold), mixture preparation, specifications of the specimens, sample placement, and compaction techniques, and test apparatus design and setup, as well as the test procedures, duration, and data recording method, have been explained within the following few subsections.

2.3.1 Description of the Samples and Test Apparatus Setup

The creep tests in this study were conducted via a modified version of the classical consolidometer typically used by geotechnical engineers. The consolidometer was primarily modified by replacing the consolidation ring with a cylindrical cell which consists of three parts (Figure 2.6). The cell is made of aluminum 6061 alloy and capable of accommodating a test sample measuring 50 mm in height and 75 mm in diameter (Figure 2.7). A cylindrical loading cap (loading cylinder) made of the same aluminum alloy having a diameter of 74 mm (Figure 2.7) was used in order to apply the vertical pressure to the test sample inside the cell. The two components of the test material were mixed on a clean paper at various mixing ratios and then placed inside the cell. A consistent procedure for preparing and testing dry samples of sand-TDA mixtures at a loose state was established. To avoid any unnecessary compaction of the sample, the loading cap is placed at the top of the sample right before the adjustment of the location of the cell within the consolidometer apparatus (Figure 2.8).

In order to investigate the influence of the magnitude of the vertical normal stress on the creep deformation behavior of the sand-TDA mixtures, five different normal stresses including $\sigma = 20, 35, 50, 75,$ and 100 kPa were applied vertically on the test samples for a long duration.

The setup of the consolidometer utilized for conducting the creep test in this study was carried out quite manually. Therefore, the preparation of the weights which are responsible to produce the vertical pressure is necessary prior to beginning of the consolidation test. For this reason, the required amounts of weights to produce each of the selected normal stresses must be calculated with respect to Eqs. (2.1) and (2.2).

$$w = \frac{\sigma \times 10^3 \times A_C \times k}{g} \quad (2.1)$$

$$w_R = w - w_C \quad (2.2)$$

Where, w is the total weight including mass of the loading cap, k is the constant of the testing apparatus (consolidometer constant), A_C is the cross-section area of the cylindrical loading cap (or the cross-section area of the test sample), g is gravitational acceleration, w_R are the required amounts of weights (Figure 2.9), and w_C is the weight of the aluminum cylinder. It must be noted that the mass of aluminum cylinder was measured to be $m_C = 0.32 \text{ kg}$.

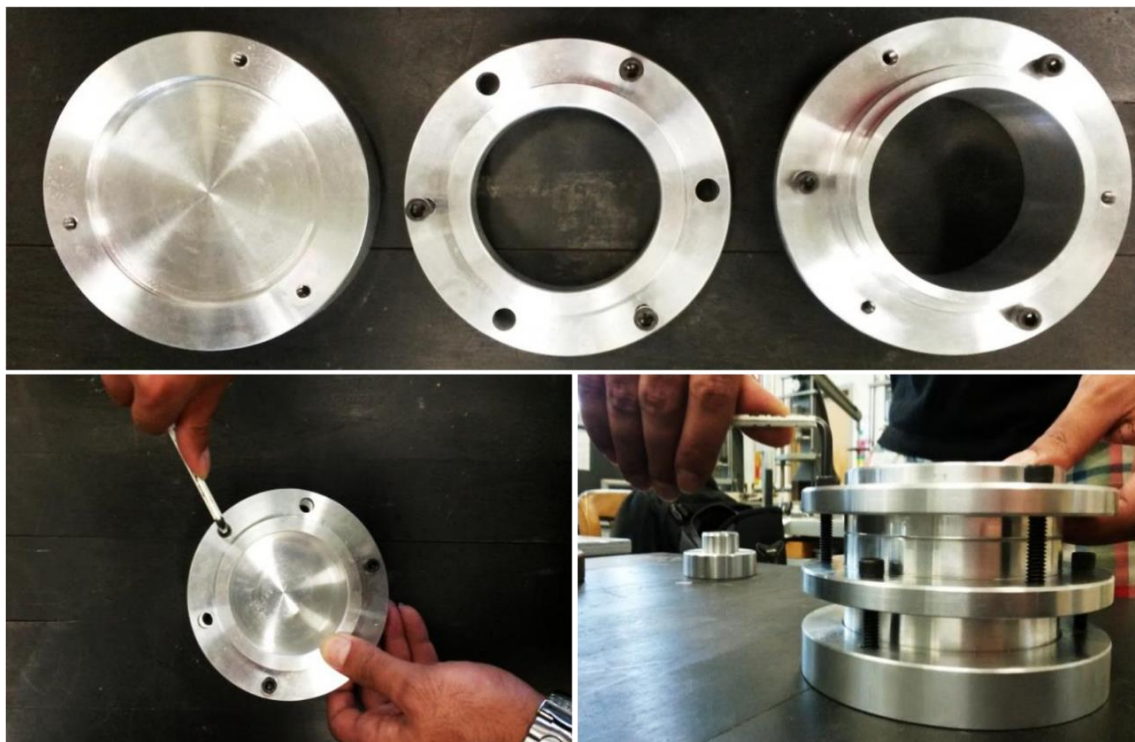


Figure 2.6 Preparation of the cylindrical aluminum cell

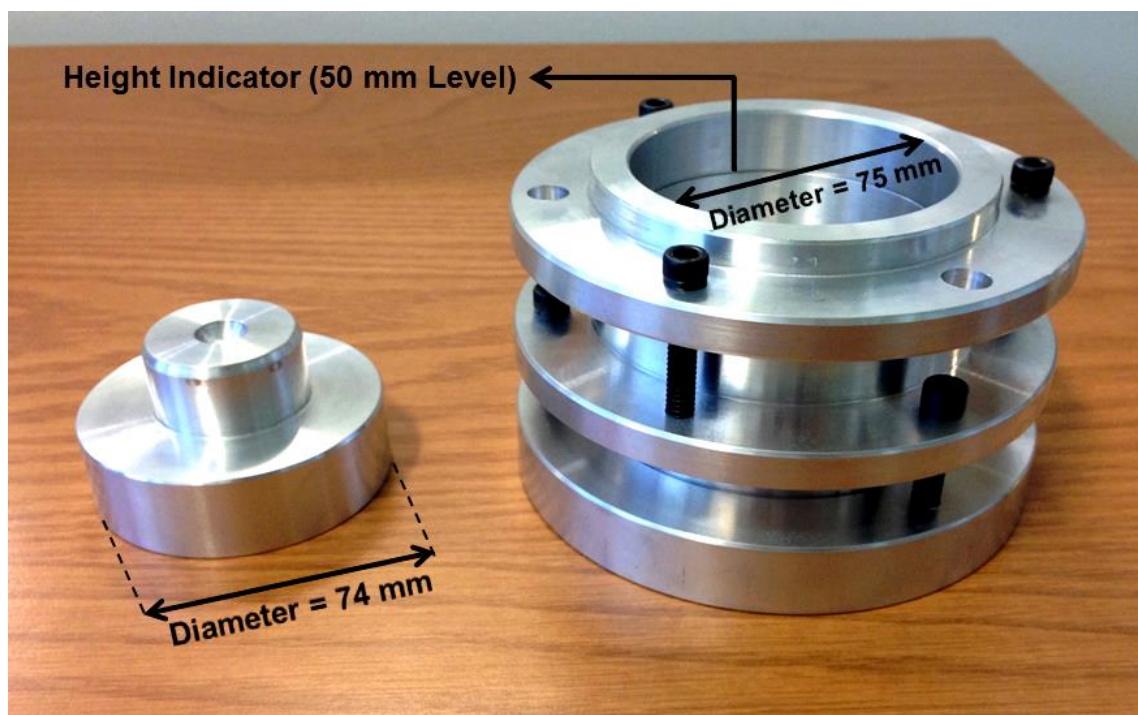


Figure 2.7 The cylindrical aluminum cell and loading cap with their dimensions



Figure 2.8 Placement of specimens inside the cylindrical cell before mixing



Figure 2.9 Measurement and preparation of the weights

As previously mentioned, a typical consolidometer was employed in order to conduct the creep test (Figure 2.10). After the preparation and placement of the test specimen inside the cell and also preparation of the weights to be added to the test apparatus, the loading cap was placed at the top of the sample inside the cell and the cell was placed and centered at its location in the test apparatus.

The apparatus was then leveled manually using a typical level and the side leveling jacks. The load is ready to be added to the system upon placement of the weights on the weight hanger. Although, an assistant must hold up the weights and the weight hanger to prevent unwanted early transmission of the load to the system and consequently to the sample.

As shown in Figure 2.10, the load is transmitted to the sample through a loading bar connected to a plate located at the bottom of the consolidation cell. Upon loading, two jacks which act as the connectors between loading bar and the plate, start to push up the sample while the loading cap is fixed within the apparatus. Hence, the load is transmitted to the test specimen vertically.

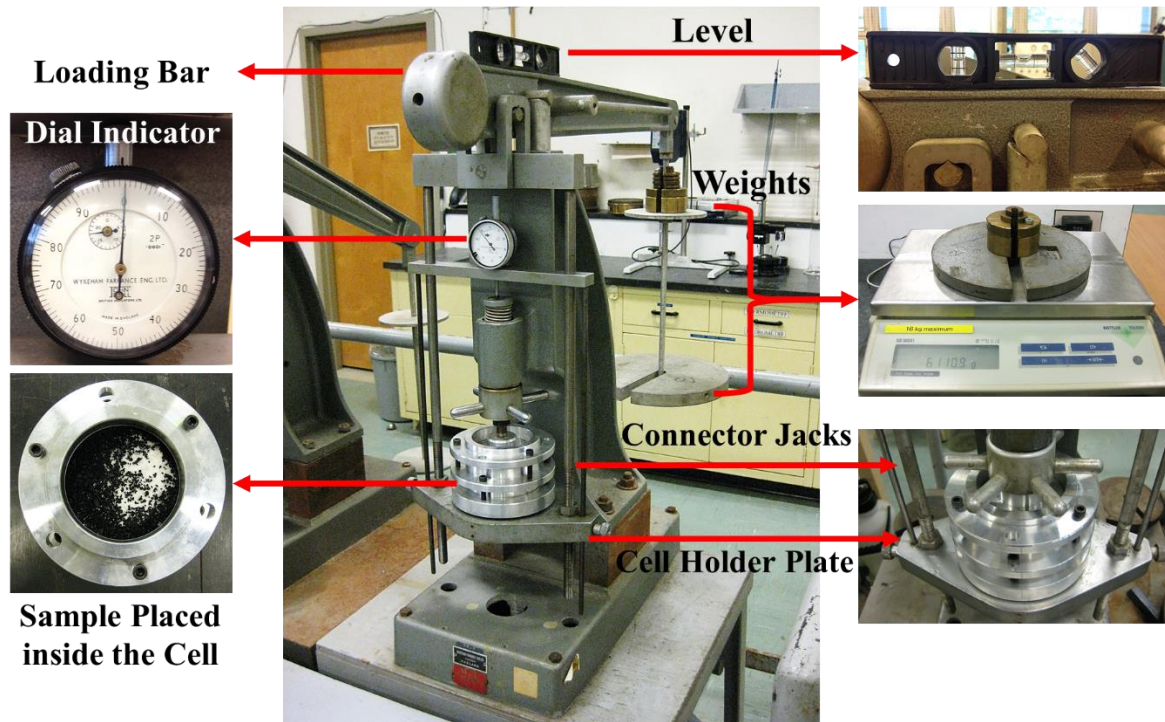


Figure 2.10 Creep test illustration

The data recording was performed manually using a digital chronometer installed right next to the deformation dial indicator. For the purpose of high accuracy, a digital camera was used in order to record the test data within the first minutes upon the beginning of the test. The camera was well adjusted in front of the apparatus, while able to capture the variations on the deformation dial indicator and the digital chronometer in a single frame.

After completion of all the above-mentioned preparations and adjustments, the test is ready to begin. To avoid missing the very first seconds of the test due to the possible inconsistency, the camera must start filming earlier right before loading the system and beginning of the test. The Consolidometer must be kept level within the entire of the test duration. To accomplish this, after applying the load a quick level adjustment is necessary in order to bring back the loading bar into its accurate horizontal position. The same procedure must be performed to keep the loading bar at

the horizontal position until the end of the test (Figure 2.10). The duration of all 25 creep tests was 6000 minutes. It must be noted that during the test when the rate does not change, we reached the secondary creep phase.

2.4 Description of the Triaxial Test for Determination of the Plasticity Parameters for the Constitutive Critical State Model

Aiming to determine the necessary elastic and plastic parameters of the sand-TDA mixtures, a series of triaxial tests were performed. These tests were conducted on sand-TDA samples with varying volumetric mixing ratios including $\theta_p = 0.50, 0.75, 1$, where θ_p represents the volume fraction of TDA per total volume of the mixture. Similar to the previous sample preparation practices, again a consistent procedure for preparing and testing dry samples of sand-TDA mixtures at a loose state was established. Comprehensive information on characteristics of the two granular materials including sand and TDA have been previously provided in Figure 2.1, Figure 2.2, Figure 2.3 and Figure 2.4 within section 2.2 (Test Materials) of this manuscript. Moreover, a phase diagram for the sand-TDA mixture which was employed to determine the initial void ratios that correspond to the above- mentioned three volumetric ratios ($\theta_p = 0.50, 0.75, 1$) has been illustrated in Figure 2.5.

2.4.1 Test Apparatus and Experimental Procedure

As shown in Figure 2.11, a standard triaxial apparatus, generally used for soils, was chosen for this study. The sand-TDA specimens which measured 35.1 mm in diameter and 67.5 mm in height were prepared to be tested (Figure 2.12). The required percentages of TDA were uniformly mixed with Ottawa sand in a dry condition. The sand-TDA mixture was then poured into a rubber membrane inside a split mold formerly under vacuum. The sand-TDA specimens when sheared were subjected to confining cell pressures of 50, 100 and 150 *kPa* for each volumetric ratio of $\theta_p = 0.50, 0.75, 1$.

A conventional drained triaxial test displacement rate of 0.0061 mm/min was maintained throughout the tests (tests were performed in dry state). Consequently, a total of 9 triaxial tests on sand-TDA dry granular mixtures were conducted. The vertical deformations of the specimen were measured by a LVTD installed vertically at the top of the cell and transmitted to the computer to be recorded (Figure 2.13). All the 9 tests continued to reach 23% strain.

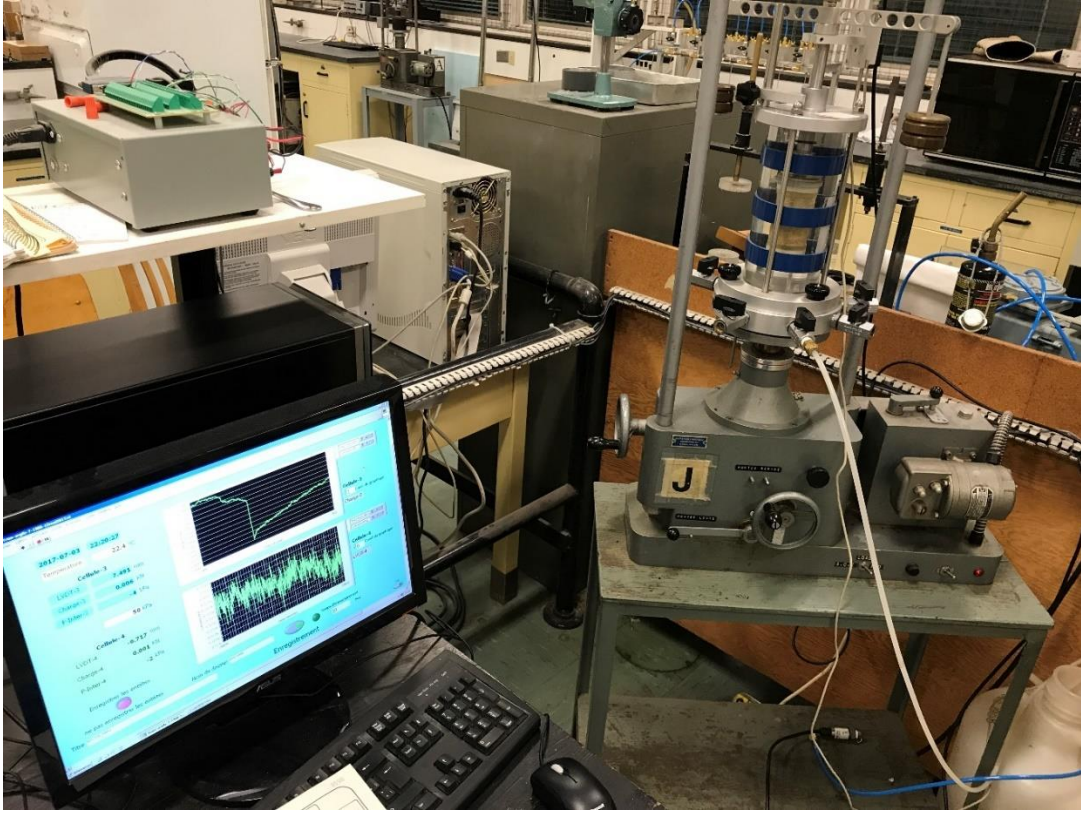


Figure 2.11 A whole perspective of the triaxial test



Figure 2.12 Test materials (sand and TDA) and triaxial test sample preparation

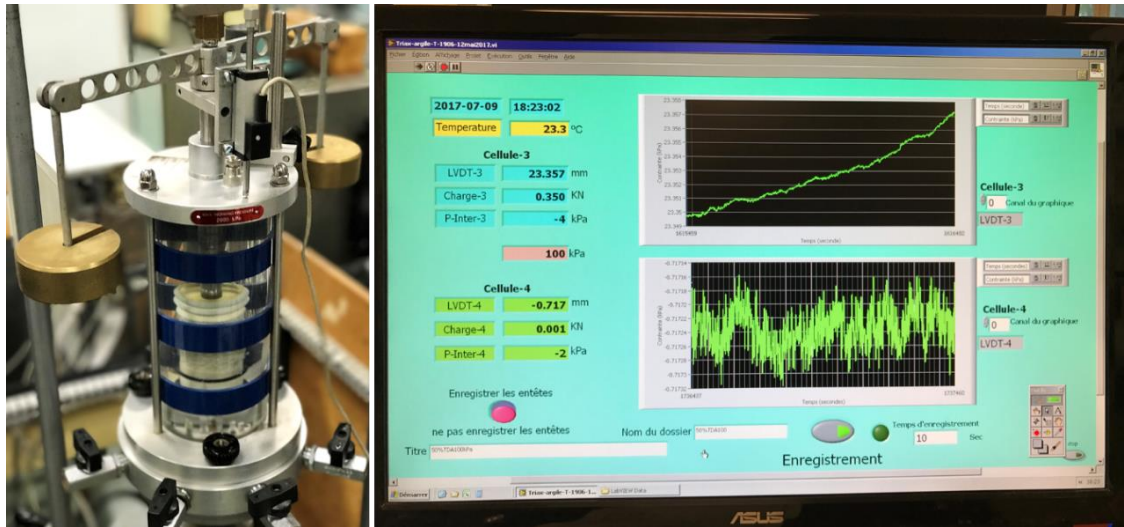


Figure 2.13 Illustration of the sample under triaxial testing while LVDT is connected to the PC to measure and record the vertical deformations occurred during the experiment

2.5 Direct Shear Tests for Determination of the True Stresses of the Creep Tests

It has been reported that the side friction must be considered as one of the major affecting factors within the compression tests. In fact, the vertical stress is reduced due to the generation of the opposite friction stresses during the compression process within the consolidation testing device. The friction loads are measured to be 10-40 percent of the original vertical applied load (CalRecycle. 2013).

In several studies conducted previously in which consolidation tests were carried out, the sidewalls of the cell were oiled up aimed at the removal of the friction influences on the magnitude of the applied loads. However, the mechanical properties of the soil sample may be affected by the oil compounds as soon as the oil inevitably reaches the soil particles. In particular, where rubber tire materials are included in the test sample as the only test material (pure tire samples) or as one of the two constituent components of the testing mixture (e.g., sand-tire mixture), the presence of oil poses significant impacts on the mechanical characteristics of the tire particles.

Hence, in this study instead of using any type of grease or lubricant gel, an appropriate distance was considered between the loading cap and the sidewalls of the cell secure the minimization of the friction influences while simultaneously avoid exiting the test materials out of the cell through the free space between cap sides and the cell sidewalls. The dimensions information including

internal the diameter of the cylindrical aluminum cell, as well as the diameter of the loading cap, have been provided earlier in section 2.3.1 and within Figure 2.7 on page 47 of this thesis manuscript.

In addition, a series of direct shear tests were performed aiming to determine the friction stress between the test materials and the sidewalls of the cylindrical aluminum cell. During the creep test, a friction force is produced between the test material and sidewalls of the cell which is made of Al 6061. Hence, a series of shear tests were necessary in order to measure opposite forces acting against applying vertical loads to the samples.

2.5.1.1 Shear Box Test Procedure

In this study, a typical shear box apparatus (in accordance with ASTM D 3080) was employed in order to perform direct shear tests on the sand-tire mixtures (Figure 2.14). To accomplish the determined target of the test, a well-polished cubic plate made of aluminum 6061 alloys was put in the interaction with the test samples of sand-TDA mixture with varying TDA contents (Figure 2.15).

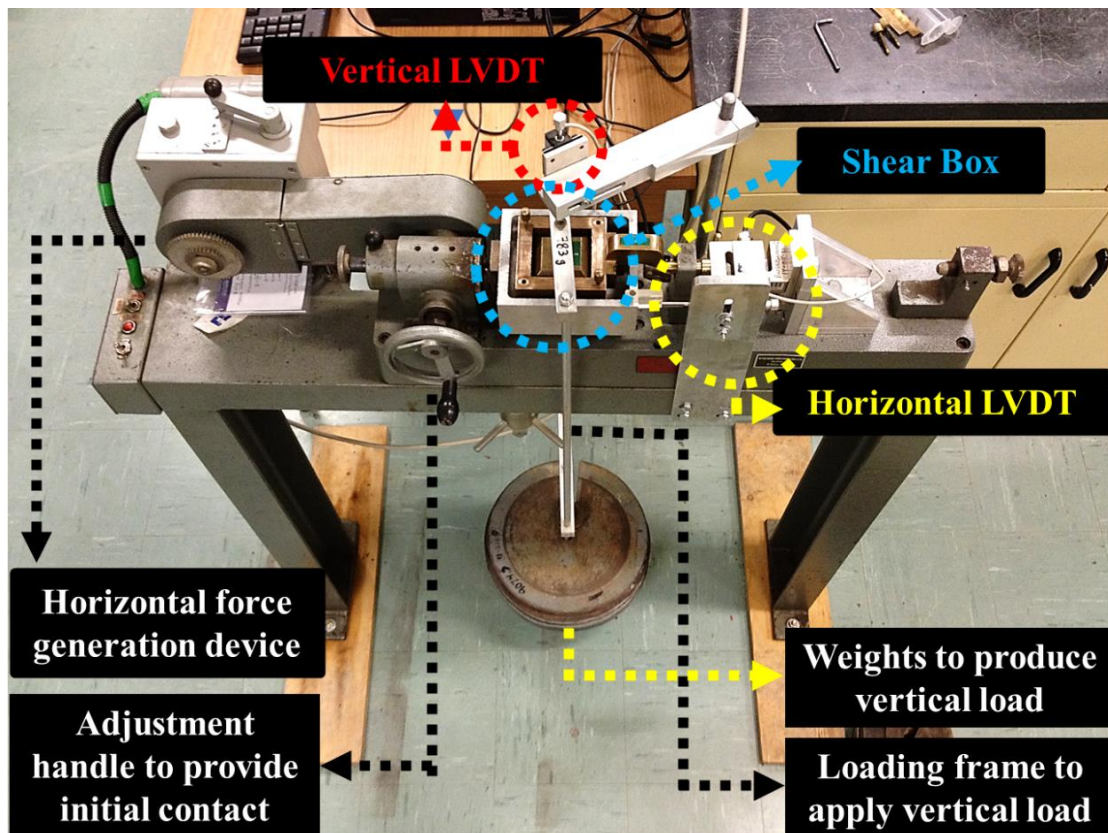


Figure 2.14 Illustration of direct shear test using shear box apparatus

As explained previously, in the creep tests a total of 25 tests including 5 different mixtures ($\theta_p = 0.2, 0.4, 0.6, 0.8, \text{ and } 1$) subjected to five different nominal stresses ($\sigma = 20, 35, 50, 75, \text{ and } 100 \text{ kPa}$) were conducted. Consequently, in order to comply with the creep test, here again a total of 25 direct shear tests were performed on Al 6061 in contact with the mixtures of sand-TDA in a similar condition to the creep test (same mixtures under the same nominal stresses). This enables the obtention of the relevant friction stresses and consequently calculation of true stresses applied to samples within the creep tests.

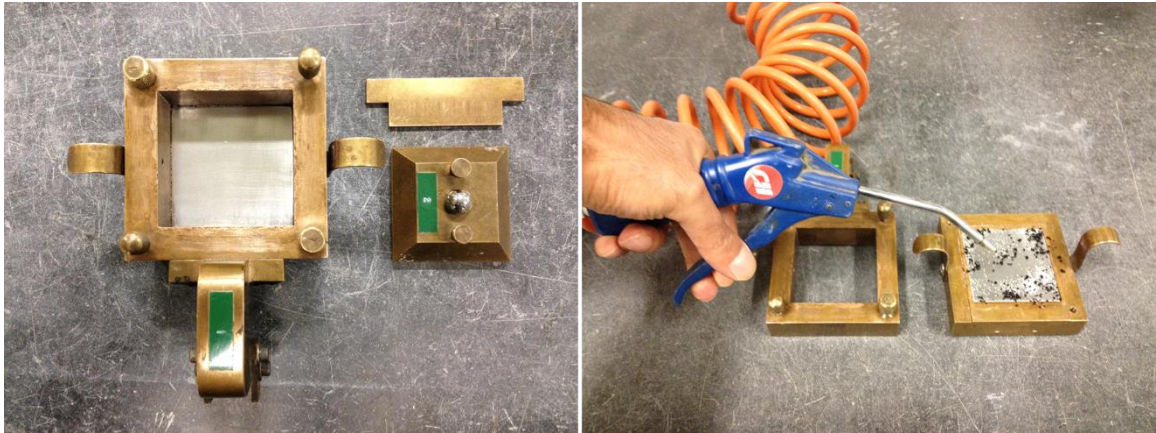


Figure 2.15 Shear box and the Al 6061 plate which is placed at the bottom of the box

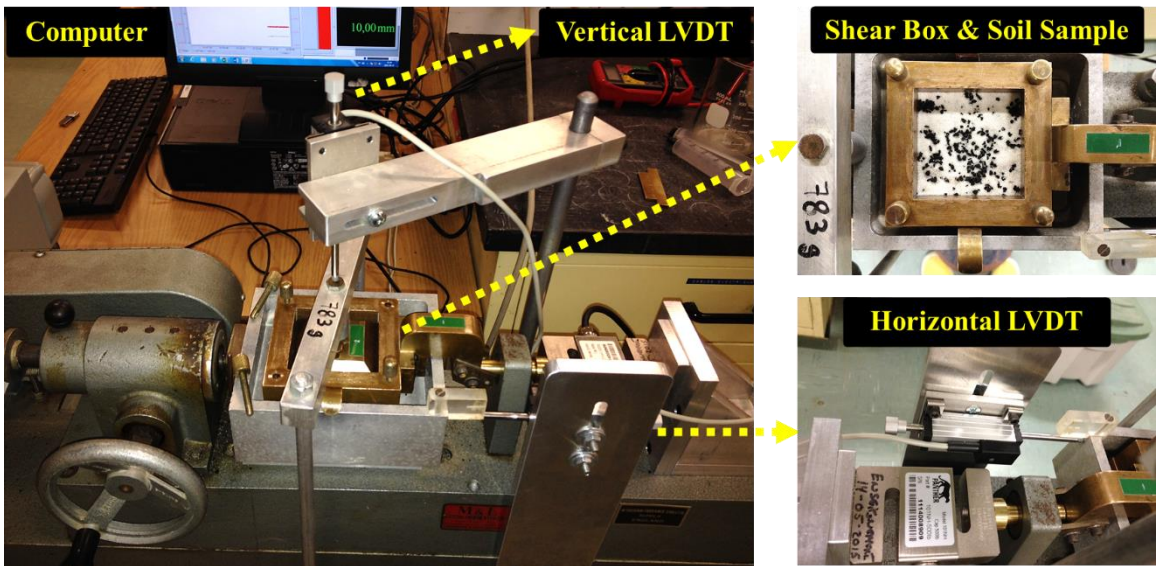


Figure 2.16 Illustration of the shear box and LVDTs positions as well as the data recording by computer during the direct shear testing

A consistent procedure for preparing and testing dry samples of sand-TDA mixtures at a loose state was established. As mentioned earlier this sample preparation and test procedure was carried out in accordance with the ASTM D 3080 hence one may study this standard specification for more detailed information. Once again, it must be noted that these direct shear tests were carried out in order to complete the results of the previously conducted creep tests.

After the preparation of the sample, it is placed in the shear box using a clean paper. The paper is then gently folded enough for the purpose of ease of Pouring material inside the box. The box is then located in its place in the apparatus. The surface of the sample must be flattened using a leveler, before placement of the loading cap on the sample (Figure 2.17).

The vertical load is produced through the weights and transmitted by a loading frame to the loading cap and consequently to the test sample. As shown in Figure 2.14, an adjustment handle is used to provide initial contact. The data recording button must be activated prior to the beginning of the test in order to secure a proper data recording from the very first seconds of the test beginning. The two LVDTs sensors including horizontal and vertical must be checked in order to provide appropriate contact prior to the beginning of the test.



Figure 2.17 Flattening of surface of the sample before placement of the loading cap

The test begins upon the switching on of the horizontal force generation device (engine). During the test, the horizontal displacements are detected by the horizontal LVDT sensor while the vertical deformations are measured by the vertical LVDT sensor, and these data are transferred to the computer to be recorded (Figure 2.16).

2.6 Small-Scale Foundation Test

In order to verify the robustness of the FEM creep model an independent creep test of long duration (18655 min), with different conditions and using a different stress path, was carried out where the values of the parameters were not obtained from the same test. Figure 3.27 illustrates FEM versus the small-scale foundation test results. As observed from this figure, a satisfactory match between the results of the finite element simulations and the small-scale foundation test is evident.

This laboratory test was conducted by subjecting a circular rigid plate having diameter of 74.65 mm (Figure 2.18) to a vertical load of a long duration. This enabled the measurement of the total vertical displacement as a function of time. As per the previously described creep tests, the friction components between different surfaces were accounted for in the determination of the total vertical displacement curve. The test was conducted at a vertical pressure of 100 *kPa* on a sand-TDA mixture having a TDA content of $\theta_p = 80\%$ volume fraction.

The two components of the specimen were partially placed in order to produce the mixture inside the cell which was made of plexiglass. The surface of the sample was then leveled accurately (Figure 2.18).

Figure 2.19 shows the experimental loading frame and the cylindrical cell which contains the rigid circular aluminum plate resting on the sand-TDA mixture. As it can be observed, the load is transmitted to the sample from a weight holder which is connected to a loading bar at the top of the cell through two jacks (left and right jacks) acting as the connectors. Upon the beginning of the test the load is transferred by the circular aluminum loading cap to the sample pushing/punching the sand-TDA mixture downward.

The data recording was performed manually using a digital chronometer installed right next to the deformation dial indicator. For the purpose of high accuracy, a digital camera was used in order to record the test data within the first minutes upon the beginning of the test. The camera was well adjusted in front of the apparatus, while able to capture the variations on the deformation dial indicator and the digital chronometer in a single frame (Figure 2.20).

To avoid missing the very first seconds of the test due to the possible inconsistency, the camera started filming earlier right before loading the system and beginning of the test. The data recording for small-scale foundation test continued for a long duration of 18655 minutes.



Figure 2.18 Test materials (sand and TDA) and the testing cell before and after the sample preparation and placement



Figure 2.19 Illustration of the small-scale test and the condition of the sample during the test



Figure 2.20 Data recording procedure during small-scale foundation test

CHAPTER 3 : FOREWORD

This chapter is written in accordance with a previously published journal paper. The entire of the materials and findings presented in this paper is taken from my PhD research project. Moreover, a permission has been already taken from the publisher of the journal to authorize the reuse of the mentioned paper as part of this PhD thesis. The information of this paper is briefly presented below.

Authors and affiliations

- Adolfo Foriero : Professor, Université Laval, Faculté des sciences et de génie, Département de génie civil et de génie des eaux.
- Nima Ghafari : PhD Student, Université Laval, Faculté des sciences et de génie, Département de génie civil et de génie des eaux.

Author contributions

General idea of the research project: The idea of conducting a research project on TDA materials was originally suggested by Mr. Charles Darwin-Annan (Professor at Laval University). This idea was further developed and suggested by Nima Ghafari to his new PhD director Mr. Adolfo Foriero.

Communication with industry: N. Ghafari conducted the communication with the industry.

Selection and provision of the testing materials: The selection of the type of TDA (e.g., shape and size) and sand (Ottawa sand) as well as the determination of the required quantity of the materials in order to conduct the entire experiments were carried out by Nima Ghafari in consultation with Adolfo Foriero.

Study conception and design: The project was designed by both of the authors while Adolfo Foriero was mostly involved in design of the theoretical parts and Nima Ghafari was mostly involved in design of the experimental parts of this study.

Research experiments and data collections: The experimental research work and the data collections were carried out by Nima Ghafari in consultation with Adolfo Foriero.

Test data processing: The calculations in order to process the row test results obtained from each of the tests were conducted by Nima Ghafari in consultation with Adolfo Foriero.

Test reports preparation: The tests report preparation was conducted by Nima Ghafari in consultation with Adolfo Foriero.

Analysis and interpretation of the results: The analysis and interpretation of the results obtained from the experiments as well as the numerical verifications were conducted by Adolfo Foriero and Nima Ghafari.

Draft manuscript preparation: The manuscript preparation was conducted by Adolfo Foriero and Nima Ghafari. The draft manuscripts were multiple times reviewed and modified by both of the authors before submission of the final version to the journal.

Status : Published

Date of acceptance : December 30, 2019

Journal : Indian Geotechnical Journal

Résumé français

L'étude présentée dans ce chapitre fait partie d'un programme expérimental qui a été menée pour déterminer les paramètres, élastique, plastique et de fluage des mélanges granulés TDA-sable. Cependant, ce chapitre ne met l'accent que sur l'obtention des paramètres de fluage à utiliser dans les équations constitutives. Les essais ont été réalisés en considérant des échantillons TDA-sable, à un contenu volumétrique donné en TDA, retenus latéralement et chargé axialement sous un incrément de contrainte totale de longue durée. Les résultats obtenus indiquent clairement une phase primaire de fluage qui se transforme rapidement en une phase de fluage secondaire stationnaire, n'atteignant jamais la phase tertiaire. L'amplitude de la déformation de fluage a été fortement affectée par la teneur volumétrique en TDA. De plus pour une valeur constante de celle-ci, le taux de déformation de fluage augmente avec la charge appliquée. Cette tendance a été observée dans tous les essais, à la différence que l'ampleur de la vitesse de déformation dépend de la contrainte appliquée et de la teneur volumétrique en TDA. Cette observation a conduit à l'adoption de la loi Bailey-Norton comme possibilité de modèle constitutif pour fluage des mélanges TDA-sable. Ensuite, l'extension multiaxiale de cette loi de fluage a été utilisée dans un

code MEF commercial pour la simulation du comportement de fluage d'une plaque circulaire rigide reposant sur un mélange TDA-sable. Finalement cette simulation a été vérifiée par le biais d'un essai de laboratoire à petite échelle du même problème.

Mots-clés : Mélange TDA–sable, teneur en fraction volumique de TDA, fluage non stationnaire, vitesse de déformation par fluage, équation constitutive, FEM.

3 Laboratory Creep Parameter Determination of Sand–TDA Mixtures with Subsequent FEM Validation

3.1 Abstract

This study is part of an experimental program that was conducted to determine the elastic, plastic and creep parameters of TDA-sand granulated mixtures. However, this paper emphasizes only the obtention of creep parameters for use in constitutive equations. This was attained by considering sand specimens, at a predetermined TDA volumetric content, which were restrained laterally and loaded axially with a total stress increment of long duration. The measured results clearly indicated a primary creep phase that rapidly transitioned into a secondary stationary creep phase, never attaining the tertiary phase. The magnitude of the creep strain was strongly affected by the TDA volume fraction content. Moreover, at a constant TDA volume fraction content the creep strain rate increased with applied load. This trend was observed in all of the tests, with the difference that the magnitude of the strain rate depends on the applied stress and TDA volume fraction content. This observation conduced the adoption of the Norton-Bailey law as a possible constitutive model for creep of TDA-sand mixtures. The multi-axial extension of this creep law was then used in a commercial FEM code to simulate the creep behaviour a rigid circular plate resting on a TDA-sand mixture. This simulation was then verified via a small-scale laboratory test of the same problem.

Keywords: TDA–sand mixture, TDA volume fraction content, Non-stationary creep, Creep strain rate, Constitutive equation, FEM.

3.2 List of Symbols

A	Creep parameter in the Norton-Bailey Law having units $(kPa)^{-n}(min)^{-b}$
β	Proportionality factor of the creep flow law
b	Creep parameter associated to time
δ_{ij}	The Kronecker delta
ϵ_{ij}^c	Tensorial representation of the creep strains

$\dot{\epsilon}_{ij}^c$	Tensorial representation of the creep strain rates
ϵ_e^c	The effective creep strain
$\dot{\epsilon}_e^c$	The effective creep strain rate having unit (min^{-1})
$\dot{\epsilon}_1^c$	The vertical creep strain rate having unit (min^{-1})
$\dot{\epsilon}_c$	Arbitrary reference strain rate having unit (min^{-1})
K_0	Coefficient of earth pressure at rest
n	Creep parameter associated to stress
S_{ij}	Tensorial representation of the deviatoric stress in (kPa)
σ_1	The total axial stress in (kPa)
σ_3	The total lateral stress in (kPa)
σ_{ij}	Tensorial representation of the total stress in (kPa)
σ_{co}	Extrapolated creep modulus σ_{cp} having units (kPa)
σ_{cp}	Power law creep parameter or creep modulus having units (kPa)
σ_e	The effective stress having units (kPa)
T	Variable representing the temperature in ($^{\circ}C$)
t	Variable representing time in minutes
θ_p	TDA percentage volume ratio

3.3 Introduction

The evergrowing disposal of automobile tires is a global issue. Stockpiling these tires presents various consequences. The most important one is that stockpiled tires are a fire hazard. Another is the undesirable fact they provide a breeding ground for mosquitoes and rodents. For this reason, scrap tire management requires innovative and efficient methods of tire disposal and use.

The most common forms of scrap tires are whole, halved, shredded and granulated. These in turn are found alone or mixed with different types of soils. Generally, the shredded and granulated forms of scrap tires are mixed with sand and/or silt to form what are commonly referred to as tire derived aggregate (TDA) soil mixtures.

Tire derived aggregates (TDA) are increasingly used in geotechnical applications. In most of these operations they are mixed with granular soil materials at various volumetric ratios. The employment of such mixtures as fill material for embankments (Humphrey 2008; Bosscher et al. 1997; Bosscher et al. 1992) and bridge abutments (Apex Companies 2008), as well as their use for backfilling retaining walls is well documented. In northern regions TDA-granular soil mixtures are also employed in pavement design. They primarily serve as an insulating layer (Humphrey and Eaton 1995) in order to prevent frost heave and hence degradation of the road surface. Moreover, a serendipity condition arises because this overlay mixture also acts as a damping layer against vibrations from the resulting traffic flow.

A review of the literature, related to past studies, exposes a lack of experimental as well as numerical investigations on long-term time-dependent constitutive behavior of TDA–sand mixtures. Engineering applications require such models for design purposes. One of these studies (Wartman et al. 2007) examined the immediate and time-dependent compression of tire chips and shreds. A characteristic relationship was shown to exist between the strain and time for TDA composites under one-dimensional compression. The time-dependent deformation was also shown to be inversely proportional to the sand content. Moreover, both the applied stress and tire particle size appear to have a negligible effect on time-dependent compression TDA. In the other study (Ngo and Valdes 2007), the one-dimensional compression of specimens, composed of sand and granulated tire rubber, was investigated. There again, results indicated that the time-dependent deformation is significant.

However, researchers have reported on the shear behavior of sand–TDA compositions (Foose et al. 1996; Ghazavi and Sakhi 2005; Sheikh et al. 2013; Zornberg, Cabral, and Viratjandr 2004). Other studies have investigated the compressibility behavior of such mixtures in relation to elasto-plasticity with emphasis on the reorientation and rearrangement of sand–TDA particles (Ahmed 1993; Meles et al. 2013; Wartman et al. 2007). The dynamic response of TDA backfill was also considered in order to evaluate its performance under dynamic loading applied to structures (Ahn and Cheng 2014).

In this study, the time-dependent creep response of sand specimens mixed with granulated tire rubber is also experimentally examined and verified numerically with FEM analyses. The FEM analyses considered both the creep tests and a small-scale rigid plate resting on a TDA– sand mixture. The next “Sand-TDA Mixtures of the Creep Tests”, “Apparatus for the Creep Tests”, “Testing procedure”, “Discussion of the Creep Test Results” sections describe the experimental investigation and discuss the creep test results.

3.4 Sand-TDA Mixtures of the Creep Tests

For the creep tests in this study, the specimens consisted of mixtures of two granular materials. One of these materials is Ottawa sand whose granulometric curve is shown in Figure 3.1. From the shape of this curve and with calculated values of $C_u = 2.1$ and $C_c = 1.26$, this sand is defined as a poorly graded sand (SP). The other material is a tire derived aggregate (TDA) obtained at *Shercom Industries Inc.* in Saskatoon, Saskatchewan, Canada, with calculated values of $C_u = 1.69$ and $C_c = 1.03$. This rubber granular material would also be considered as poorly graded if classified according to the Unified Soil Classification System. A granulometric curve for this material is also shown in Figure 3.1.

For the purpose of the tests these two materials were combined at five different volumetric ratios: $\theta_p = 0.2, 0.4, 0.6, 0.8, 1$, where θ_p represents the volume fraction of TDA per total volume of the mixture. As just mentioned, these mixtures involve two poorly graded materials and hence represent an undesirable field condition but a sensible one when running creep tests. The advantage is that the effect of creep, which this study shows to be inextricably linked to the TDA, is more apparent when the fabric is unstable. Generally, in the field, a well graded sand is an important requirement if one wishes to obtain a stable mixture when combined with TDA.

In Figure 3.2, a phase diagram for the sand-TDA mixture was used to determine the initial void ratios that correspond to the five volumetric ratios mentioned previously. This was possible because both the weights of the TDA and Sand phases, as well as the total volume they occupied were measured beforehand. For the calculations, the specific gravity of the TDA ($G_{TDA} = 1.15$) and Ottawa Sand ($G_{Sand} = 2.65$) were necessary. The phase volumes of the TDA and Sand were obtained respectively as $V_{TDA} = \frac{W_{TDA}}{G_{TDA} \gamma_w}$ and $V_{Sand} = \frac{W_{Sand}}{G_{Sand} \gamma_w}$. Consequently, the initial void ratio, e , and initial unit weight of the TDA-Sand mixtures were known at the start of all tests.

3.5 Apparatus for the Creep Tests

The creep tests in this study were conducted via a modified version of the classical consolidometer (Figure 3.3) normally used by geotechnical engineers. Typically, in these tests a sand specimen with a predetermined θ_p , is restrained laterally and loaded axially with a total stress increment of long duration. The stress increment is maintained throughout the primary creep phase, well into the secondary creep phase, but never attaining the tertiary phase. During the creep tests, measurements

are made of change in the specimen height versus time, and this data is used to determine the relationship between the stress, and the creep strain and strain rate.

The consolidometer was primarily modified by replacing the consolidation ring with a cylindrical aluminum cell (Figure 3.4). The cell is capable of accommodating a soil sample measuring 50 mm in height and 75 mm in diameter.

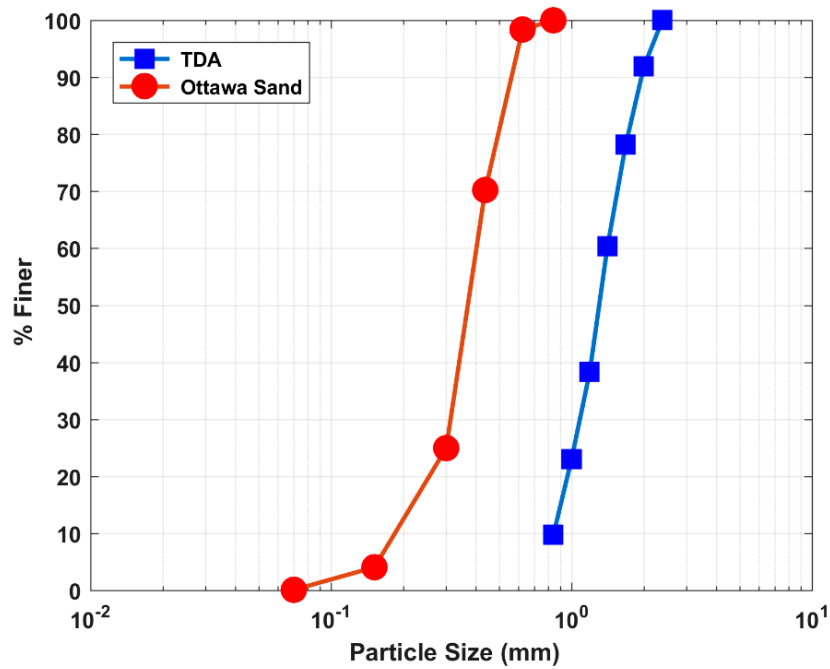


Figure 3.1 Grain-size distribution curves of materials used in the present study

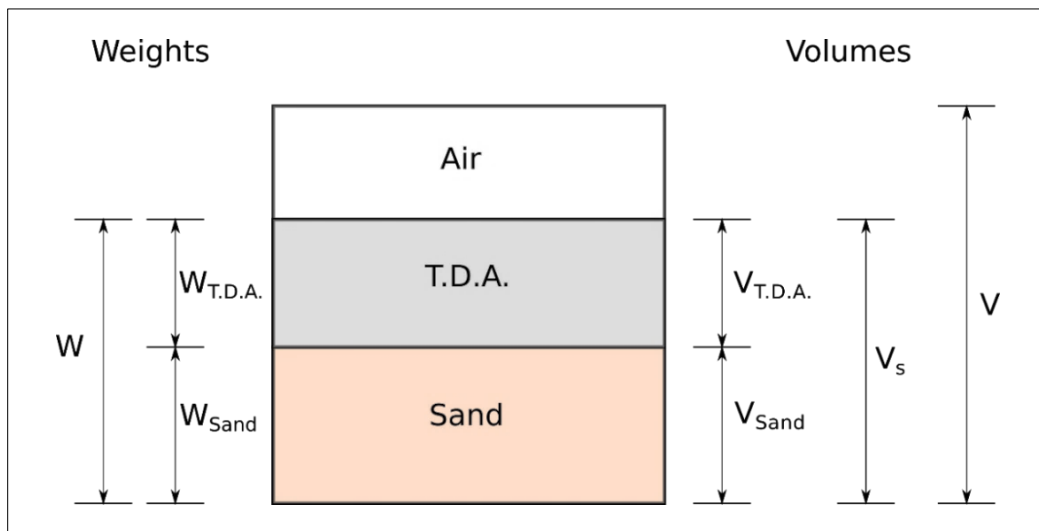


Figure 3.2 Phase diagram of TDA-sand mixture

3.6 Testing procedure

Placement of the TDA-sand mixture in the cell was carried out by pouring the sand from a minimal height in order to attain a loose state. There was no compaction afterwards. The height indicator in Figure 3.4 ensured the repeatability of the tests with respect to the unit weight. This was possible because the TDA-sand mixture was prepared based on the volume fraction of TDA per total volume of the mixture.

The walls of the cell were not coated with any form of silicon grease because of possible chemical reaction with the TDA. In fact, silicon grease generally softens rubber, and this would certainly change the characteristics of the granular TDA. Instead, a total of 25 shear box test (Figure 3.5) were carried out in order to determine the friction angle between the TDA-sand mixture and the same material that made up the aluminium cell. Typical results of the shear box tests are given in Figure 3.6. As shown in the Table 3.1, Table 3.2, and Table 3.3 an estimate of the wall friction, developed during the creep tests, enabled the determination of the true applied stresses in place of the applied nominal stress. A typical calculation is provided within the section 3.15 (Appendix).

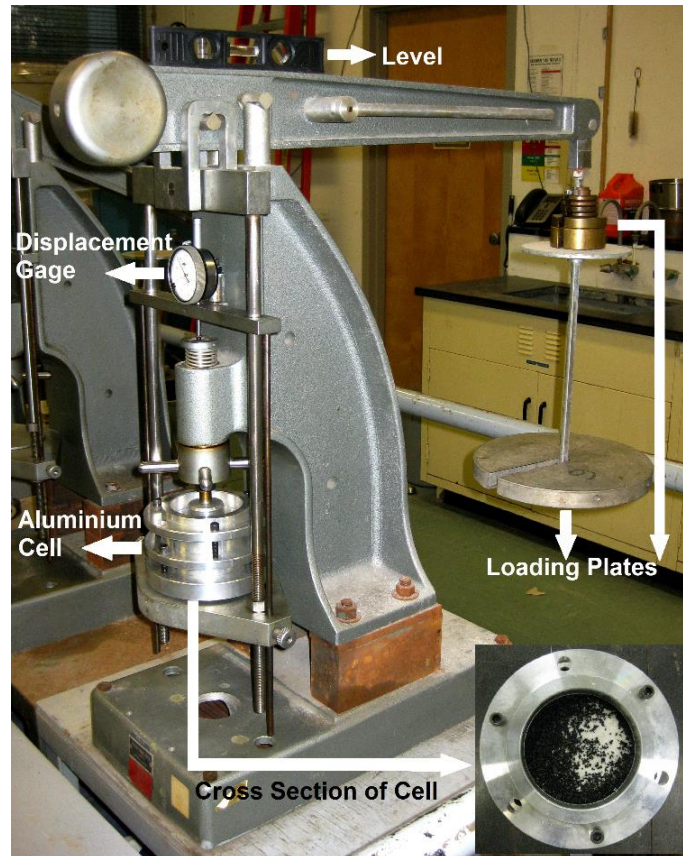


Figure 3.3 Consolidometer loading frame used for the creep tests

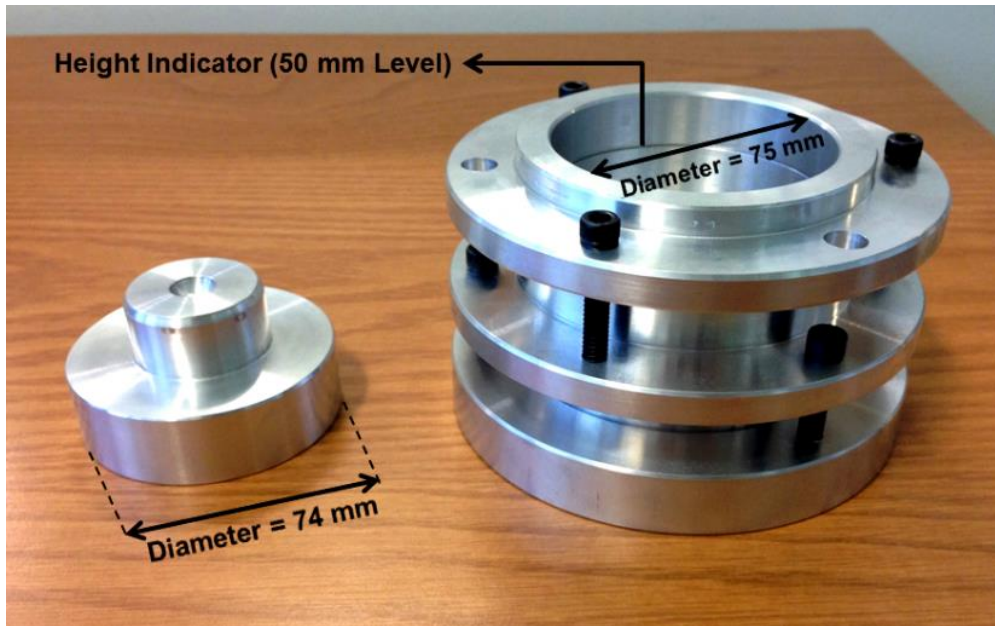


Figure 3.4 Loading cap and cylindrical aluminum cell (adapted for the consolidometer)



Figure 3.5 Typical shear box test setup to determine the friction angle between TDA–soil mixture and aluminum alloy 6061

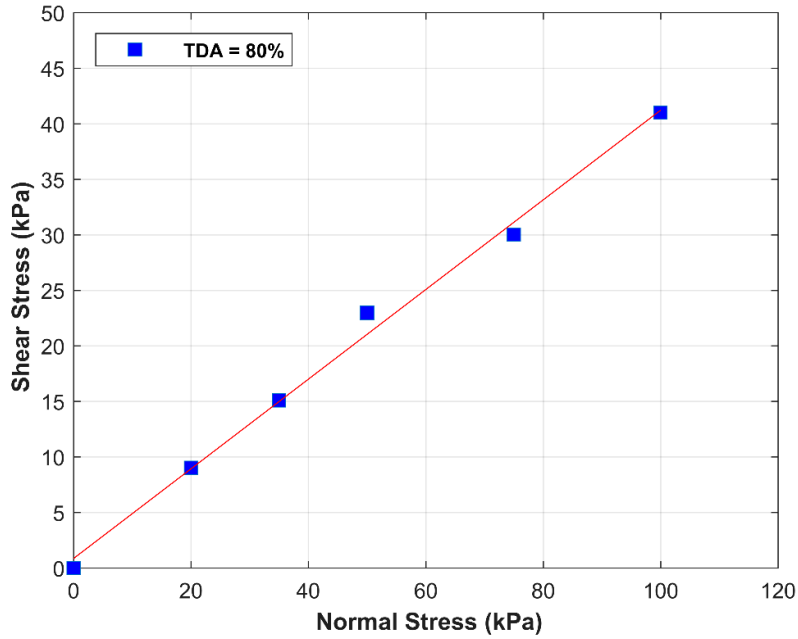


Figure 3.6 Typical shear box test result of a TDA–sand mixture resting

Table 3.1 Friction angle: shear box tests results (aluminum–Ottawa sand–TDA mixture)

TDA (%)	Friction Angle δ (Degrees)
20	22.15
40	21.79
60	22.37
80	21.97
100	26.89

Table 3.2 Net force calculation, based on the estimated wall friction obtained in shear box tests

Nominal Stress, σ_n (kPa)	Net Force (kN)				
	TDA = 20%	TDA = 40%	TDA = 60%	TDA = 80%	TDA = 100%
20	0.0880	0.0876	0.0864	0.0846	0.0788
35	0.1535	0.1529	0.1508	0.1513	0.1322
50	0.2198	0.2183	0.2152	0.2019	0.1835
75	0.3299	0.3259	0.3156	0.2979	0.2833
100	0.4399	0.4348	0.4243	0.3907	0.3990

Table 3.3 True Stress*, Based on Net Force Calculations

Nominal Stress, σ_n (kPa)	True Stress (kPa)				
	TDA = 20%	TDA = 40%	TDA = 60%	TDA = 80%	TDA = 100%
20	19.96092082	19.91471594	19.78039363	19.56947175	18.91816636
35	34.87842032	34.81344112	34.56188529	34.62328778	32.16018669
50	49.88059139	49.70683605	49.34118088	47.84735874	45.26697781
75	74.83717008	74.39235108	73.18824742	71.20596978	68.91468576
100	99.78289344	99.21112246	97.99060169	94.18786859	94.59083178

* An explanation on the calculation of the true stress is provided in the Appendix section.

3.7 Discussion of the Creep Test Results

A total of 25 creep tests and 25 shear box tests were carried out in the present study. As mentioned, the shear box tests were required in order to determine the friction between the TDA-sand mixture and the wall of the cell. Specifically, all mixtures were axially loaded at five different nominal stresses of long duration: $\sigma_v = 20, 35, 50, 75, 100$ (kPa).

The recorded total strain versus time curves, resulting from the applied stresses, were composed of an instantaneous strain and a delayed creep strain. A typical result for the case $\theta_p = 40\%$ is shown in Figure 3.7. In Figure 3.8 the total strain of Figure 3.7 is plotted as function of the applied stress for specific times of the test. These Figure 3.7 indicate the nonlinear nature of the creep response. The instantaneous strain may contain an elastic and plastic contribution and is unrelated to the time dependent creep strain. Consequently, for the purposes of isolating the creep strain and thereby determining the creep parameters, the instantaneous strain was subtracted from the total strain. The instantaneous strain is defined as the first point that could be captured immediately after the application of the load took by the pictures of the camera. Test results of the creep strain versus time, for two typical TDA volume fractions, are shown in Figure 3.9 and Figure 3.10. For example, Figure 3.10 depicts the creep behavior of pure TDA and is the test with the highest creep response. In fact, one observes from these figures that the magnitude of the creep strain is strongly affected by the TDA volume fraction θ_p .

In geotechnical engineering, creep is primarily associated to clays (Mitchel and Soga 2005; Fedea 1989; Mitchel et al. 1968). This form of creep produces a volume change just as consolidation. However, the driving mechanisms for volumetric creep and consolidation are different. In saturated

clays the driving mechanisms for consolidation is a pressure gradient. The response to this pressure gradient is flow (Darcy's Law) which produces a change in volume because water is ejected from the voids producing large strains (Foriero and Ladanyi 1998).

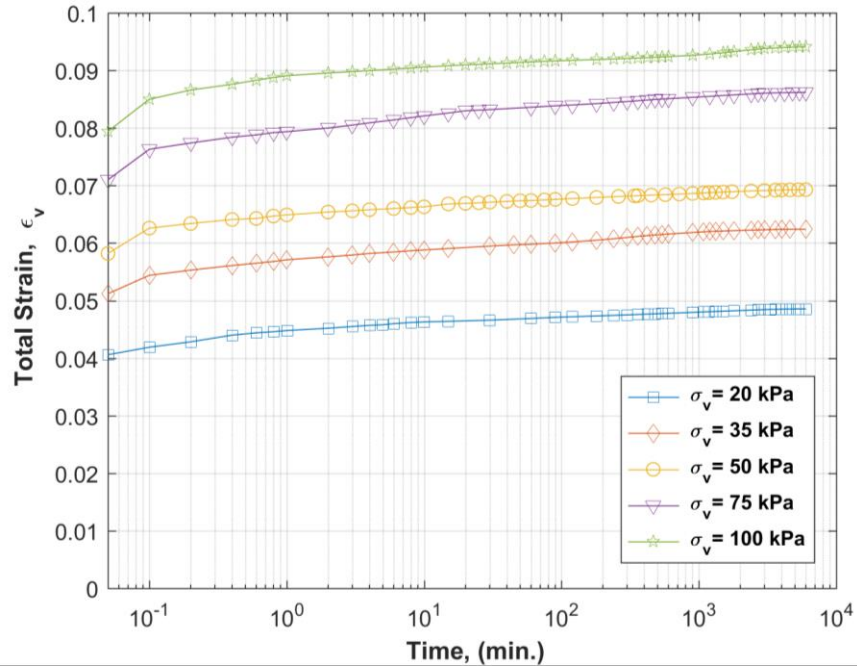


Figure 3.7 Constant stress logarithmic creep curves of the total strains (40% TDA)

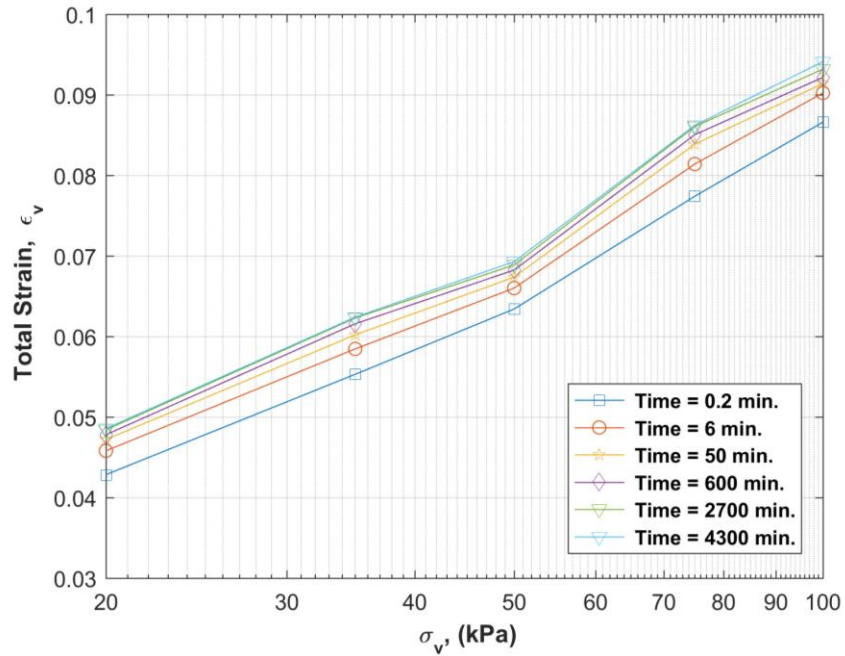


Figure 3.8 Total strain as a function of the applied vertical stress for specific times (40% TDA)

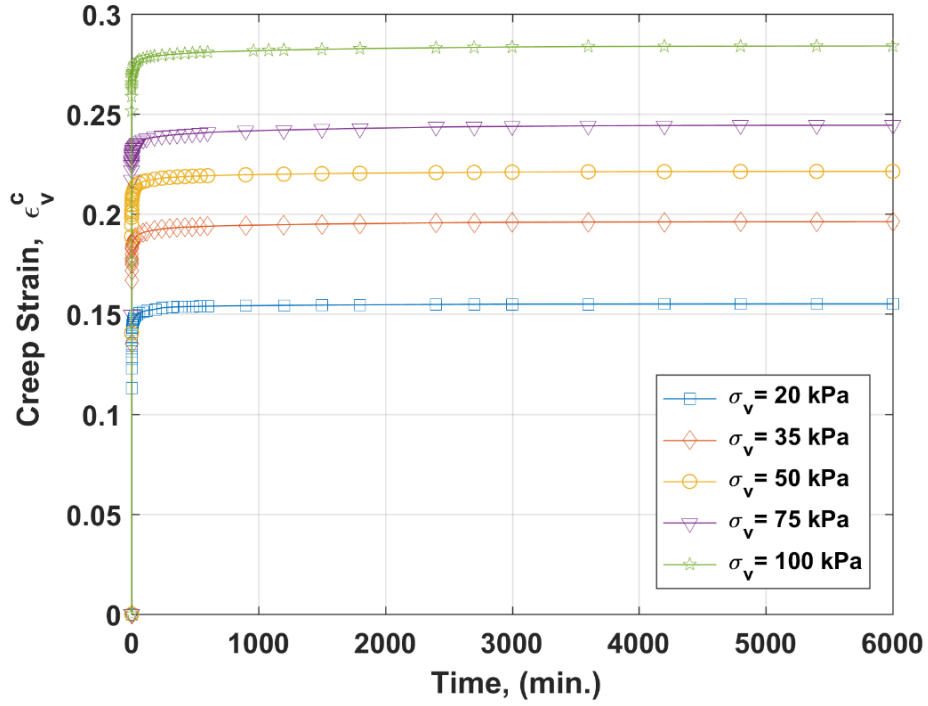


Figure 3.9 Constant stress creep curves of the creep strains (80% TDA)

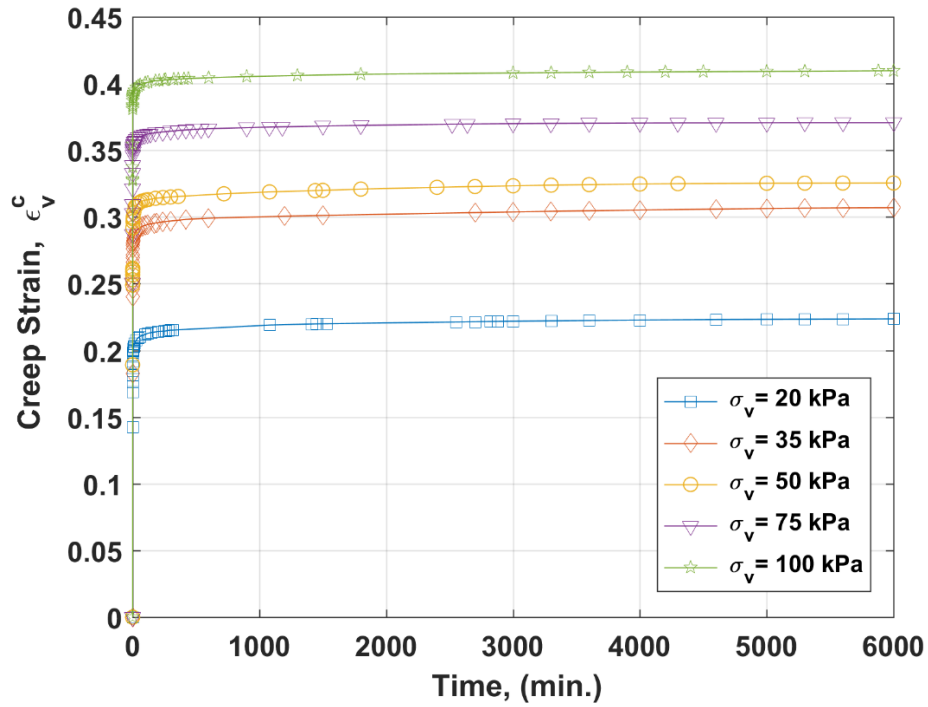


Figure 3.10 Constant stress creep curves of the creep strains (100% TDA)

Volumetric creep of clays also produces a volume change, but water is ejected from the voids because of a rearrangement of the soil particles. The cause or driving mechanisms of both consolidation and volumetric creep are different but the end result is a volume change.

Deviatoric creep on the other hand produces a distortion, not a volume change. In the problem being studied sand is mixed with rubber particles (TDA). Rubber does not flow out of the specimen, it does not flow like a liquid phase. TDA experiences distortion, which is attributed to the nature of the rubber phase. The sand particles being relatively incompressible with respect to the rubber particles. Upon vertical loading of the TDA-sand specimens, the rubber particles in the sand voids experience a contained relative displacement and distort occupying a different space of the sand structure. Contemporarily, the elastic properties of the TDA-Sand mixture system are responsible for both the volumetric as well as deviatoric elastic deformations. The overall result is a settlement of the surface.

It is important to mention here that saturated clays also experience deviatoric creep under undrained conditions (Foriero and Keviczky, 2000). Generally, this component of creep is rarely discussed because it occurs at the same time as consolidation and volumetric creep. The three forms of mechanisms are difficult to uncouple.

Generally, creep of pure sand alone is mainly due to particle crushing at very high confining pressures (Kampour and Lade 2013; Brzesowsky et al. 2014). That condition is not met in the present tests. Consequently, one presupposes that the rubber granular material is mainly responsible for the creep response of the sand-TDA mixture.

It is clear from Figure 3.9 and Figure 3.10 that the creep strain, at a constant TDA volume fraction, increases with the applied load. Moreover, in the very early stages of all tests, the creep rate decreases and then tends towards a stationary approximate creep strain rate. This trend is observed in all of the tests, with the difference that the magnitude of the strain rate depends on the applied stress and TDA volume fraction.

The initial phase of the tests, when the creep rate decreases, is generally called the primary creep phase. Subsequently, as time progresses the creep strain rate attains a predominantly near constant or stationary value, initiating what is commonly known in creep mechanics as the secondary phase. One cannot overemphasize that in the early stages of all tests, the creep rate decreases rapidly over a very short period of time. As mentioned, previously, for questions of brevity, only the particular cases pertaining to TDA volumetric ratios of $\theta_p = 0.8$ and $\theta_p = 1$, are shown in Figure 3.9 and Figure 3.10. For this reason, extraction of the creep parameters is better achieved by analyzing the

corresponding log-log plot of the creep rate versus time curves. This mapping of the test results for determining the creep parameters, in the context of the equation of state approach, is covered in the next section.

3.8 Equation of state approach to model creep of Sand-TDA mixtures

In this study the equation of state approach (defined hereafter) is utilized to model creep. The stress-strain state is determined by treating the TDA-sand mixture as a whole or as a quasi-continuous medium. It is tacitly assumed that changes in the proportions of individual phases per unit volume are negligible. Hence an expression for the creep strain in the form

$$\epsilon_e^c = A \sigma_e^n t^b \quad (\text{Norton-Bailey law}) \quad (3.1)$$

is chosen based on the observed creep test results such as those of Figure 3.9 and Figure 3.10. The Norton-Bailey law is known in the creep literature (Andersland and Ladanyi 1994) to model primary, followed by secondary creep only. Here σ_e and ϵ_e stand respectively for the equivalent or generalized stress and strain. These equivalent values are obtained via

$$\sigma_e = \sqrt{\frac{3}{2} S_{ij} S_{ij}} \quad (3.2)$$

and,

$$\epsilon_e^c = \sqrt{\frac{2}{3} \epsilon_{ij} \epsilon_{ij}} \quad (1 \leq i, j \leq 3) \quad (3.3)$$

where S_{ij} and ϵ_{ij} are respectively the tensorial representations of the deviatoric stresses and creep strains. The stress deviator tensor S_{ij} is determined from the stress tensor σ_{ij} by the definition of:

$$S_{ij} = \sigma_{ij} - \frac{1}{3} \sigma_{kk} \delta_{ij} \quad (1 \leq i, j \leq 3) \quad (3.4)$$

where δ_{ij} is the Kronecker delta. The use of the effective quantities is intended to satisfy the requirement that a multi-axial formulation must reduce to the conditions of the present tests (soil sample is restrained laterally and loaded axially).

In the creep law expression (3.1) the creep parameters A , n and b are all functions of the TDA volume fraction θ_p and the temperature, T ($^{\circ}C$).

However, in order to calculate the creep parameters, the law is rewritten in the form suggested by suggested by *Ladanyi* (Ladanyi 1972; Andersland and Ladanyi 1994; Foriero and Robitaille, 2016):

$$\epsilon_e^c = \left(\frac{\sigma_e}{\sigma_{cp}} \right)^n \left(\frac{\dot{\epsilon}_c t}{b} \right)^b \quad (3.5)$$

where equivalently in the Norton-Bailey law (3.1),

$$A = \left(\frac{1}{\sigma_{cp}} \right)^n \left(\frac{\dot{\epsilon}_c}{b} \right)^b \quad (3.6)$$

Consequently, the creep parameters determined in the tests are n , b and σ_{cp} . The parameter σ_{cp} (kPa) is defined as the creep modulus corresponding to an arbitrary reference strain rate, $\dot{\epsilon}_c$ (min^{-1}) and volume fraction of TDA, θ_p (%), in the sand-TDA mixture.

The effect of θ_p as well as temperature T ($^{\circ}C$) is included in the value of the creep modulus σ_{cp} , by means of an empirical power law provided below:

$$\sigma_{cp} = \sigma_{co} \left(1 + \frac{\theta_p}{100\%} \right)^p f(T) \quad (3.7)$$

where σ_{co} is the value of σ_{cp} extrapolated back to $\theta_p = 0$ and p is the slope in the log–log plot of σ_{cp} versus $\left(1 + \frac{\theta_p}{100\%} \right)$. All tests were performed in the soil mechanics laboratory at Laval University at room temperature. By considering the room temperature as the reference temperature, then $f(T) = 1$ for the present purposes. For the tests conducted at various temperatures, $f(T)$ describes a functional dependence in its own right. This functional dependence is normally based in numerous forms such as that of the theory of rate processes or a power law.

The Baily-Norton law (3.1) represents an equation of state approach, which means it limits the analyses to step changes of stress that are of long duration. In variable stress problems this law is

generally differentiated with respect to time because the creep strain rate is of interest. In doing so the time derivative of stress is ignored, even though one is dealing with a variable stress problem. This procedure characterizes the essence of an equation of state approach. Therefore, the time hardening formulations, equations (3.1) and (3.5) are differentiated with respect to time to yield the corresponding creep rates:

$$\dot{\epsilon}_e^c = A\sigma_e^n b t^{b-1} \quad (3.8)$$

and,

$$\dot{\epsilon}_e^c = \dot{\epsilon}_c \left(\frac{\sigma_e}{\sigma_{cp}} \right)^n \left(\frac{\dot{\epsilon}_c t}{b} \right)^{b-1} \quad (3.9)$$

3.9 Back-Calculation of the creep parameters based on the test results

As previously mentioned, the sand-TDA mixtures were confined to a cylindrical aluminum cell and thereby restrained laterally upon loading. It is noted that for axial symmetry, such as in the present tests, $\sigma_e = (\sigma_1 - \sigma_3)$ and $\dot{\epsilon}_e = \dot{\epsilon}_1$. For this reason, Eq. (3.9) is recast in the form:

$$\dot{\epsilon}_1^c = \dot{\epsilon}_c \left(\frac{\sigma_1 - \sigma_3}{\sigma_{cp}} \right)^n \left(\frac{\dot{\epsilon}_c t}{b} \right)^{b-1} \quad (3.10)$$

where $\sigma_3 = K_0 \sigma_1$. The K_0 coefficient is difficult to predict in such confined conditions. However, its value is not necessary for the determination of the creep parameters. If one plots the test result values of $\dot{\epsilon}_1^c$ versus t in a log-log space, then:

$$\log(\dot{\epsilon}_1^c) = \log \left[\left(\frac{\sigma_1 - \sigma_3}{\sigma_{cp}} \right)^n \left(\frac{\dot{\epsilon}_c}{b} \right)^b b \right] - (1 - b) \log(t) \quad (3.11)$$

and the value of the parameter b is calculated with the slope of the resulting test curves by virtue of:

$$b = 1 - \left(\frac{\Delta \log(\dot{\epsilon}_1^c)}{\Delta \log(t)} \right) \quad (3.12)$$

Typical results obtained with this Eq. (3.12) are shown in the log-log plots of Figure 3.11 and Figure 3.12. These two figures correspond to tests respectively at TDA volume fractions of $\theta_p = 0.6$ and $\theta_p = 1$, where the Sand-TDA mixtures are subject to axial stresses of long duration. The trend in all of these tests confirm that the creep rate versus time curves are, for all intense and purposes, parallel. As depicted in these Figure 3.11, the creep parameter b does vary with the axial stress, but the difference is imperceptible. Hence, from the engineering or practical point of view an average b value gives an adequate estimate of this creep parameter and is also shown in the figures. Essentially the creep parameter b increases with an increase in the TDA volume fraction θ_p . This creep parameter is associated with time in the creep laws previously mentioned [Eqs. (3.1) and (3.5)], and therefore the greater its value, the higher is the magnitude of the creep strains. As expected, the back calculated value of b is the highest in the case of pure TDA ($\theta_p = 100\%$).

As for the creep parameter, n , which is associated with the applied stress, a similar procedure is adopted. The expression containing the creep parameter n is extracted from ((3.11) and transformed with:

$$\log \left[\left(\frac{\sigma_1 - \sigma_3}{\sigma_{cp}} \right)^n \left(\frac{\dot{\epsilon}_c}{b} \right)^b b \right] = \log \left[\left(\frac{b}{\sigma_{cp}^n} \right) \left(\frac{\dot{\epsilon}_c}{b} \right)^b \right] + n \log (\sigma_1 - \sigma_3) \quad (3.13)$$

And, in order to obtain (at a constant t) the value of:

$$n = \frac{\Delta \log (Cb)}{\Delta \log (\sigma_1 - \sigma_3)} \quad (3.14)$$

here,

$$Cb = \left[\left(\frac{\sigma_1 - \sigma_3}{\sigma_{cp}} \right)^n \left(\frac{\dot{\epsilon}_c}{b} \right)^b b \right] \quad (3.15)$$

Figure 3.13 depicts the calculation of the n parameter for a particular TDA volume fraction $\theta_p = 0.6$. Since, as previously mentioned, the value of the confining stress $\sigma_3 = K_o \sigma_1$ is very difficult to measure but not necessary in such tests, typical K_o values for loose, medium and dense sand were assumed. As expected, these values do not affect the slope of the resulting line in a log-log plot of Cb versus $\sigma_v - \sigma_h$.

These results confirm that the n parameter decreases as the TDA volume fraction θ_p increases (Table 3.4). The only exception to this observation is the case of pure TDA which result yielded an increase in the n parameter. A plausible explanation is related to the possible mechanisms affecting creep of the TDA only. In addition to the sliding among the rubber particles, the particles themselves creep. The polymer chains in TDA rubber are mobile and slide past each other because they do not share chemical bonds with the other chains around them (Ward and Sweeney 2004). This time dependent movement of the chains in the rubber, which is closely linked to the stress field, is generally suppressed by the sand matrix. In the case of pure TDA this kinematic constraint is relaxed and thus creep is more pronounced.

Finally, the value of the creep parameter σ_{cp} , representing the creep modulus, is calculated for a selected value of $\dot{\epsilon}_c = 0.0001 \text{ min}^{-1}$ with:

$$\sigma_{cp} = (\sigma_1 - \sigma_3)_i \left[\frac{\left(\frac{\dot{\epsilon}_c}{b}\right)^b b}{\left(\left(\frac{\sigma_1 - \sigma_3}{\sigma_{cp}}\right)^n \left(\frac{\dot{\epsilon}_c}{b}\right)^b b\right)_i} \right]^{\frac{1}{n}} \quad (3.16)$$

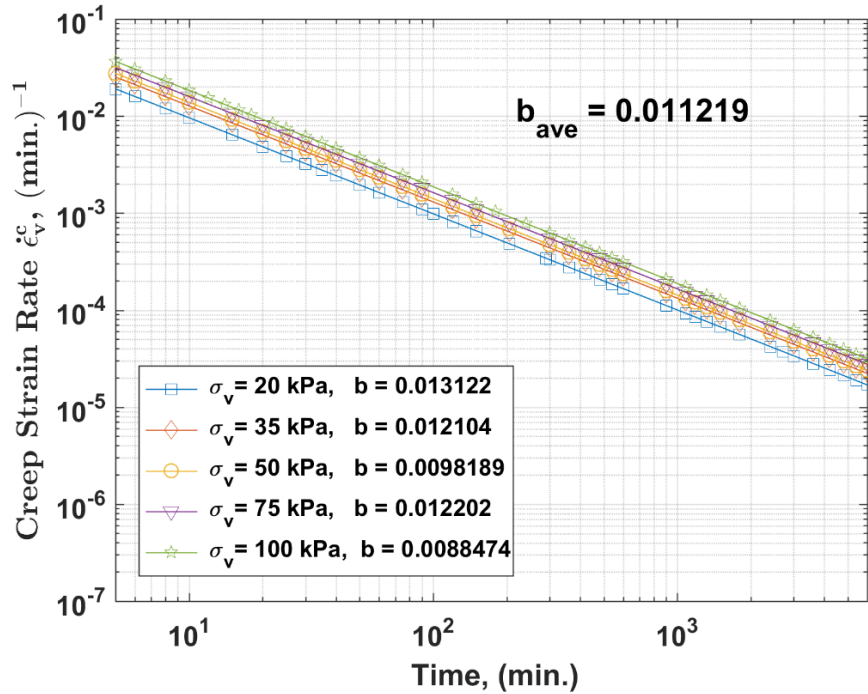


Figure 3.11 Determination of the time creep parameter b (60% TDA)

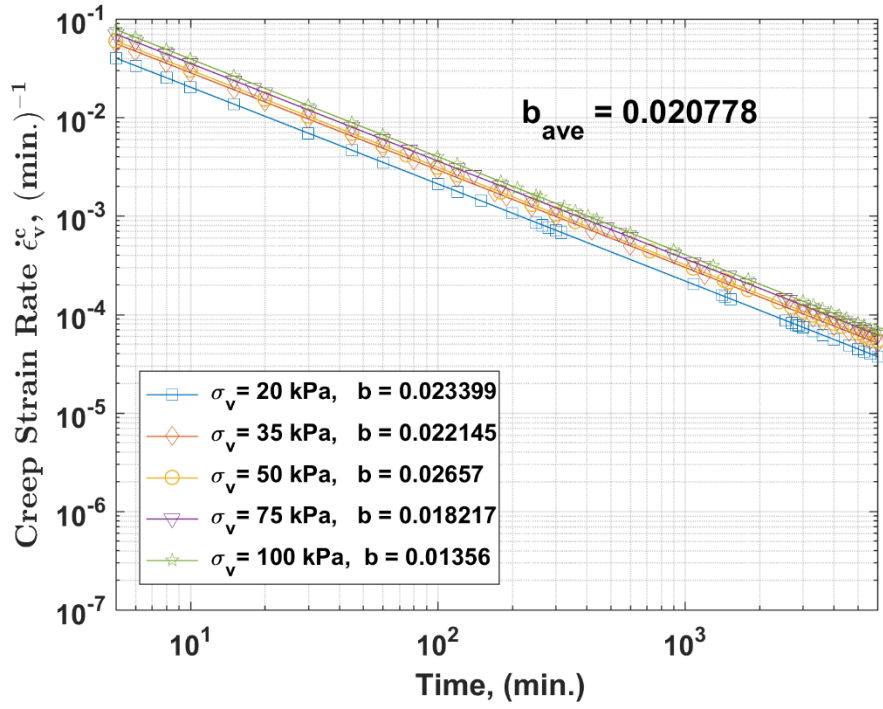


Figure 3.12 Determination of the time creep parameter b (100% TDA)

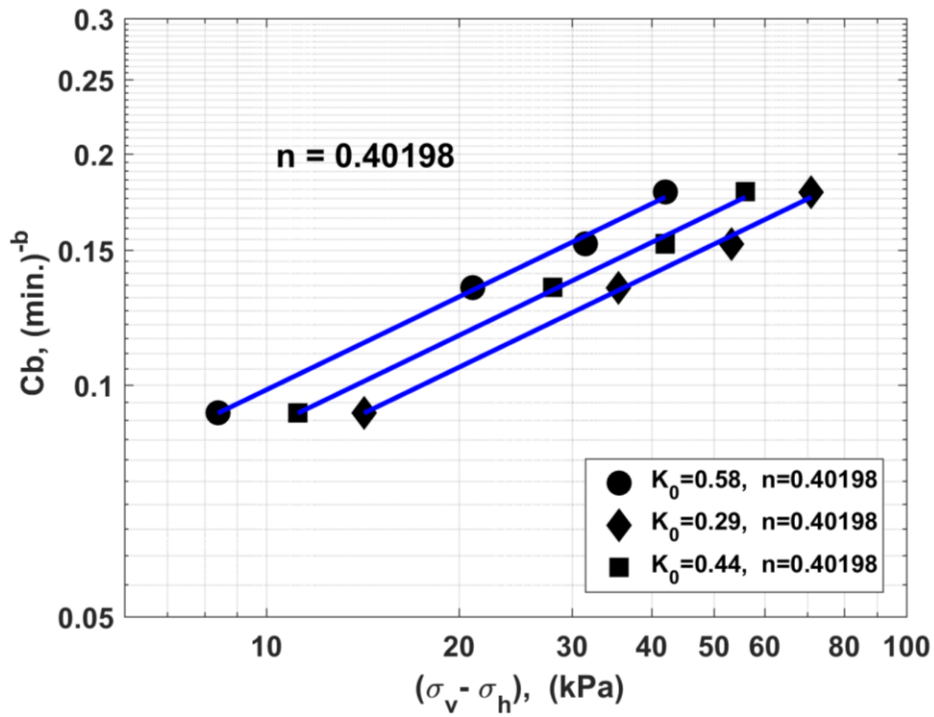


Figure 3.13 Determination of the creep parameter n (60% TDA)

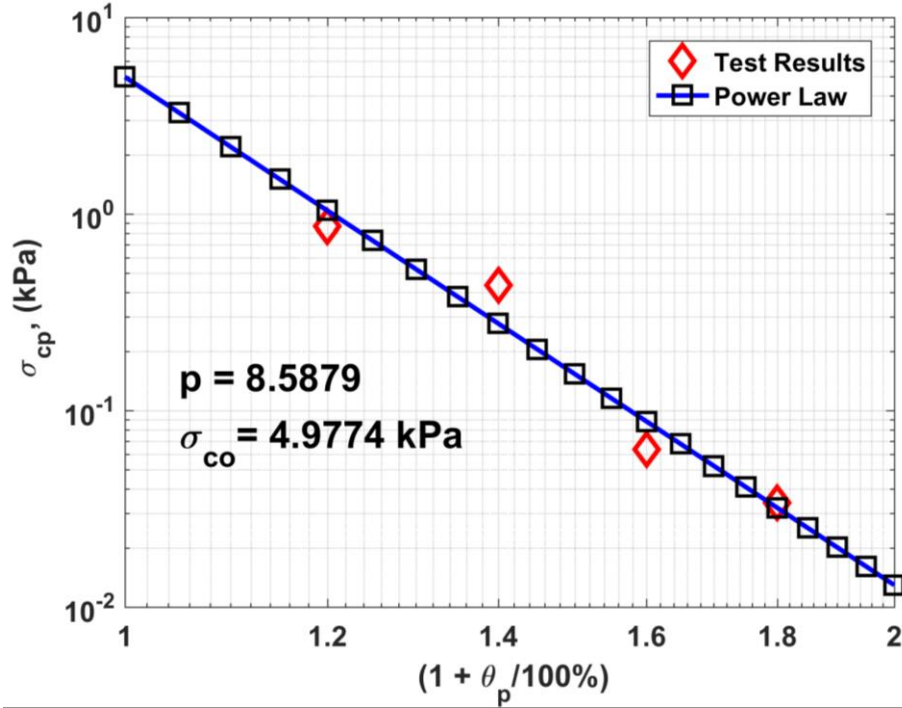


Figure 3.14 Determination of the creep modulus for the power law

Table 3.4 Creep parameters obtained from long duration tests at the reference strain rate ($\dot{\epsilon}_c = 0.0001 \text{ min}^{-1}$) and room temperature.

Volume ratio θ_p (%)	Unit weight $\gamma \left(\frac{kN}{m^3}\right)$	Void ratio e_o	Stress constant n	Time constant b	Power law $\sigma_{cp}(kPa)$	Bailey–Norton law A $[(kPa)^{-n}(min)^{-b}]$
20	14.37	0.6438	0.4342	0.0081	0.8644	1.0343
40	12.10	0.7362	0.4290	0.0109	0.4340	1.3540
60	9.93	0.8265	0.4019	0.0112	0.0636	2.8543
80	7.69	0.9351	0.3863	0.0168	0.0339	3.4158
100	5.50	1.05	0.4262	0.0208	0.0389	3.6278

The results of these calculations, for all TDA volume fractions θ_p , are plotted in a log-log plot of σ_{cp} versus $\left(1 + \frac{\theta_p}{100\%}\right)$ as shown in Figure 3.14. This plot, which demonstrates a functional dependence (Eq. (3.7)) of the creep modulus on the TDA volume fraction. This relationship (3.7) is necessary when estimating a creep modulus at a particular TDA volume fraction for use in the previously described creep laws [Eqs. (3.1) and (3.5)].

The full results of the just described parameter determinations are given in Table 3.4. Based on these results, one can observe that the Baily-Norton law parameter A (Eq. (3.6)) increases with the volume fraction of TDA (θ_p). Once again this is expected because the volume fractions of TDA is the primary cause of the creep deformations in the Sand-TDA mixture. Moreover, it must be noted that the sand does not creep. Hence, a test sample of pure Ottawa sand was not included in the experimental program of this study.

3.10 Assessment of the Creep Law Based on the Back-Calculated Creep Parameters

In order to verify the accuracy of the back-calculated creep parameters, the creep law (Eq. (3.9)) along with the test results are plotted in a log-log plot of $\dot{\epsilon}_c$ vs time. Figure 3.15 and Figure 3.16 depict that the curves obtained with this creep law give a good approximation of the test results for $\theta_p = 0.4$ and $\theta_p = 1$. These constitutive equations must now be incorporated in a FEM code in order to verify their efficiency when modeling a typical field problem involving TDA. However, it is very difficult to obtain field test results in the literature that are completely documented. For this reason, FEM simulations of the present lab tests represent a rational first start in the validation process. This sets the stage for the next sections where in the first step finite element analyses, using the commercial software COMSOL, are undertaken to model the creep tests (laterally restrained, axially loaded cylindrical TDA-soil samples). Subsequently a different FEM analysis, that considers a small scale rigid circular plate resting on a TDA-sand mixture, completes the assessment of the proposed creep law.

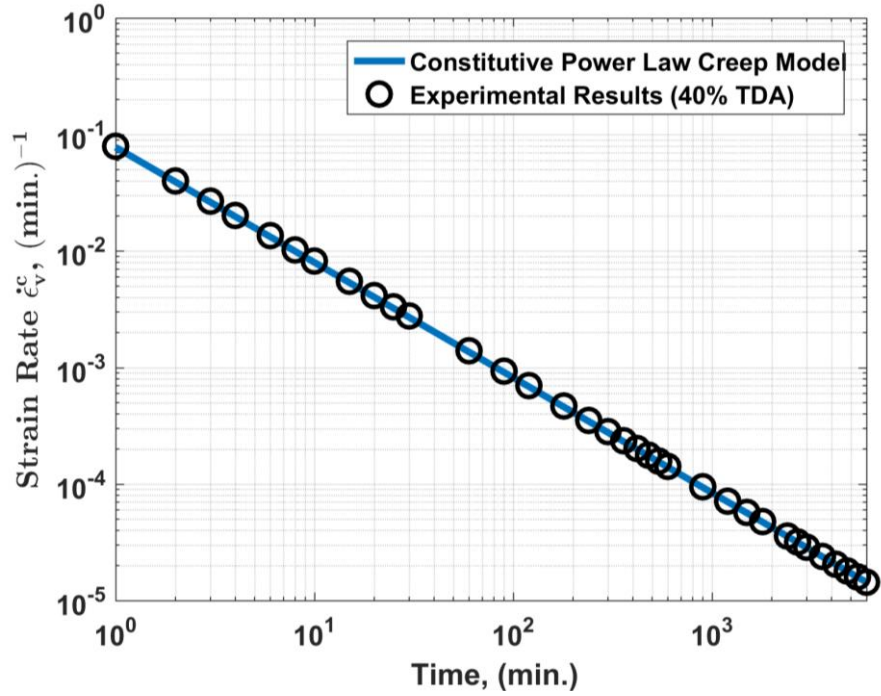


Figure 3.15 A comparison of the creep law with the test results for $\sigma_v = 75 \text{ kPa}$ (40% TDA)

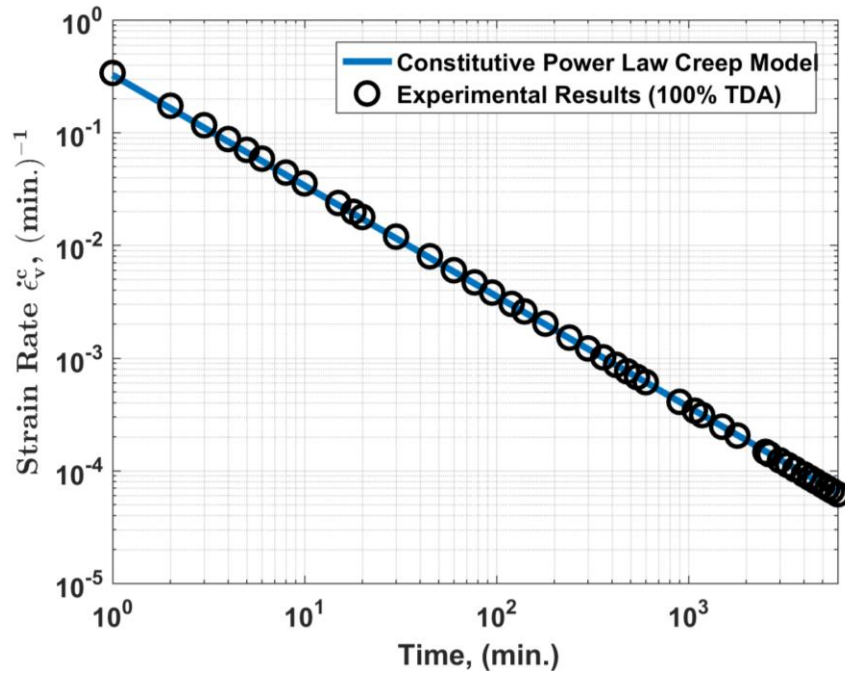


Figure 3.16 A comparison of the creep law with the test results for $\sigma_v = 75 \text{ kPa}$ (100% TDA)

3.11 Extension of the Creep Law for Multi-axial Deviatoric Creep FEM Formulations

Generally, incorporation of a creep law in a FEM formulation requires the adaptability of this law to multiaxial stress fields. Hence, in modeling of the deviatoric creep phenomenon the constitutive equations must satisfy certain requirements. For one, a multi-axial formulation must reduce to the correct uniaxial formulation when necessary. Secondly, the constitutive model should express constancy of volume (isochoric creep). Thirdly the constitutive equations must exemplify independence from a superimposed hydrostatic pressure and fourthly, the principal directions of stress and strain should coincide (Foriero and Robitaille 2016).

Generally, the rate of deformation tensor is written in terms of the stress deviator tensor in indicial notation via the flow rule:

$$\dot{\epsilon}_{ij}^c = \beta S_{ij} \quad (1 \leq i, j \leq 3) \quad (3.17)$$

where, β is a proportionality factor. The stress deviator S_{ij} is determined from the Cauchy stress tensor σ_{ij} with the definition of:

$$S_{ij} = \sigma_{ij} - \frac{1}{3} \sigma_{kk} \delta_{ij} \quad (1 \leq i, j, k \leq 3) \quad (3.18)$$

where δ_{ij} is the Kronecker delta (whose value equals 0 when $i \neq j$ and 1 when $i = j$).

The use of the deviator stress tensor renders the flow rule independent of the superimposed hydrostatic pressure thus satisfying the third requirement mentioned previously.

The flow rule in and of itself incorporates the fourth requirement of collinearity of stress and strain.

In order to determine the proportionality factor, β , one must define an effective stress and strain rate which are respectively given as:

$$\sigma_e = \sqrt{\frac{3}{2} S_{ij} S_{ij}} \quad (1 \leq i, j \leq 3) \quad (3.19)$$

and,

$$\dot{\epsilon}_{ij}^c = \sqrt{\frac{2}{3} \dot{\epsilon}_{ij}^c \dot{\epsilon}_{ij}^c} \quad (1 \leq i, j \leq 3) \quad (3.20)$$

Substituting (3.17) into (3.20) and by considering (3.19) and (3.8), yields for the proportionality factor,

$$\beta = \frac{3}{2\sigma_e} \dot{\epsilon}_e^c = \frac{3}{2} Ab \sigma_e^{n-1} t^{b-1} \quad (3.21)$$

Thus, a non-stationary time hardening multi-axial ow rule is represented by:

$$\dot{\epsilon}_{ij}^c = \frac{3}{2} S_{ij} Ab \sigma_e^{n-1} t^{b-1} \quad (1 \leq i, j \leq 3) \quad (3.22)$$

while a strain hardening one is rendered by:

$$\dot{\epsilon}_{ij}^c = \frac{3}{2} S_{ij} A \frac{1}{b} b \sigma_e^{\frac{n}{b}-1} \epsilon_e^{\frac{b-1}{b}} \quad (1 \leq i, j \leq 3) \quad (3.23)$$

For the FEM simulations in this study the time hardening formulation is adopted.

3.12 FEM Model to Simulate a Small-Scale Foundation Creep Test

The approach taken in this section is two-fold. First, a FEM simulation of the creep tests is performed using the creep law precisely obtained from these tests. This simulation is necessary in order to verify the robustness of the FEM creep model. Secondly, once the previous requirement is satisfied, this FEM model is applied to a practical case of a small-scale foundation (rigid circular plate) resting on a TDA-sand mixture. This was necessary in order to verify the constitutive model using a completely different stress path. The results confirm the applicability of the proposed constitutive creep law.

Precisely, we first examine the axisymmetric FEM model representation of a typical creep test. Geometrically, this type of analysis is justified because all the creep tests in this study meet the two

basic requirements of axial symmetry. First, it is clear that the cell is a body of revolution (Figure 3.4). Consequently, one adopts a cylindrical coordinate system having global coordinates r , θ and z . Moreover, since the geometry of the cell is invariant with respect to the θ coordinate, one considers only the remaining (r, z) coordinates. The second requirement is that the material properties as well as boundary conditions are not a function of θ . This last requirement is fulfilled because in all tests the specimens are restrained laterally and loaded axially. The analysis implies, for example, that an eight-node rectangular element is rotated by 2π radians. The actual elemental volume is then given by $dV = 2\pi r dr dz$.

A typical axisymmetric finite element mesh generated with the commercial FEM software COMSOL is shown in Figure 3.17. A thin layer elastic interface element was utilized in order to model the interface condition between the aluminum loading cap and the soil. It is very difficult to characterize the interface properties of this contact surface. For this reason, two extreme ideal conditions were modeled in order to bracket the real one. Both the cases of a completely smooth and rough interface were imposed by assigning respectively a very low and high value to the tangential spring constant of the thin layer elastic interface element. The mesh is also refined in the vicinity of this contact zone. The results of the FEM analyses indicate there is no difference when either of these two conditions are imposed.

In order to conduct the FEM creep analyses an estimate of the elastic parameters for both the TDA-sand mixtures and aluminum loading cap is also required. The elastic parameters for the TDA-sand mixtures were typically estimated based on the previously mentioned triaxial tests (applied cell stress of 100 kPa at $\theta_p = 80\%$ TDA) given in Figure 3.18. Consequently, an interpolated Young's modulus of $E = 17.75$ Mpa and a Poisson's ratio of $\mu = 0.3$ were used for the elastic properties of TDA-sand mixtures ($\theta_p = 80\%$). As previously mentioned, the TDA-sand creep parameters used in the simulations are given in Table 3.4. For the aluminum loading cap, one considers that its rigidity is much greater than that of the soil mixture. From the practical point of view the aluminum cap cannot creep and was modeled only as an elastic domain having a Young's modulus of $E = 68.9$ Gpa (Aluminum alloy 6061) and a Poisson's ration of $\mu = 0.33$.

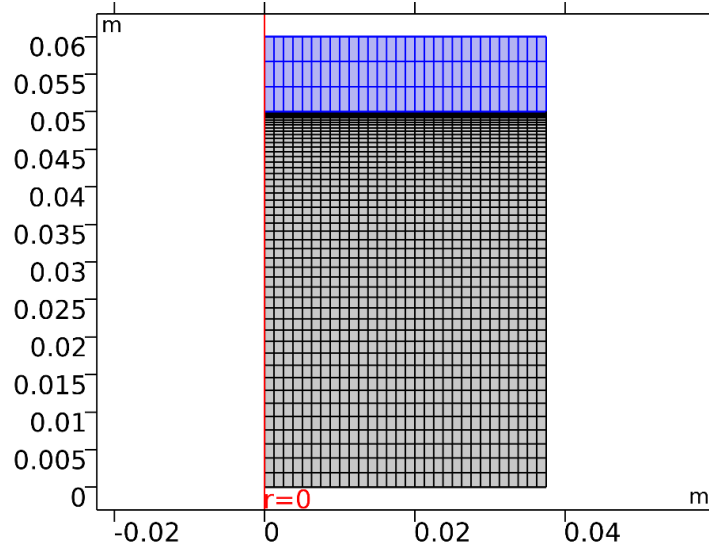


Figure 3.17 Axisymmetric finite element mesh used for the test

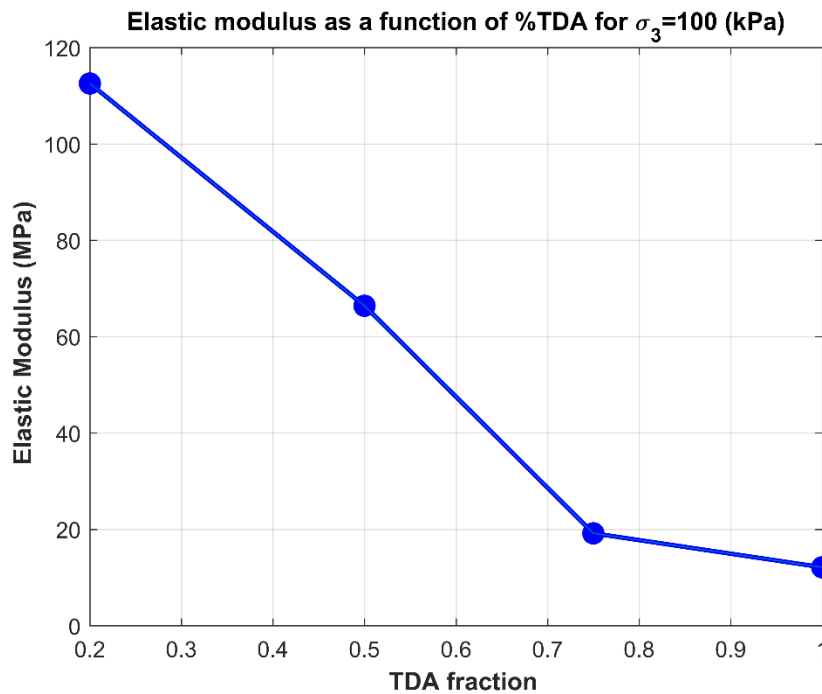


Figure 3.18 Triaxial test results of initial elastic modulus as a function of %TDA for $\sigma_v = 100$ kPa

Figure 3.19 and Figure 3.20 illustrate a typical FEM simulation for a vertically applied stress of 100 kPa at $\theta_p = 80\%$ and $\theta_p = 100\%$ TDA content. These figures show the axial creep strain rate as a function of time. The result of interest here is that the axial creep strain rate decreases with time at a nearly constant rate of change of the creep strain rate. Also shown in Figure 3.21 are the vertical displacement contours (vertically applied stress of 100 kPa at $\theta_p = 80\%$) at $t = 1000$ min.

It is very difficult to compare the creep strain rate of the test and FEM results because one cannot measure with certitude the initial strain rate at the very beginning of any of the present tests. The reason is that the load is applied instantly at the very beginning of the test not to mention that the results are plotted in a log-log plot in order to obtain the pertinent creep parameters. For this reason, in order to compare test and FEM results, the measured instantaneous creep strain rate is taken at $t = 0.1 \text{ min}$ and is used as the point of departure for both the tests and FEM simulations. The essence here is that the slopes of the creep strain rate curves are nearly equal when one compares the test results to the FEM simulations.

Finally, all of the FEM simulations of the creep tests confirmed the just previously discussed results. The only difference is that the magnitude of the creep strain rates depends on both the TDA volume fraction content (θ_p) and on the magnitude of the applied load. In order to show this general trend, typical results of simulations at lower axial loads and TDA contents are displayed in Figure 3.22 and Figure 3.23. As in the previous cases, the corresponding axial creep strain rate decreases with time at a nearly constant rate of change of the creep strain rate (Figure 3.22). At an even lower axial load and TDA content, a similar behavior is observed (Figure 3.23).

This fact confirms the validity of the FEM model with regards to the empirically determined creep strain rate law (3.8). Having established the robustness of the FEM model, one must now turn to a practical problem having a different stress path in order to assess the creep constitutive equation.

Consequently, in the second phase of the present section, one examines the creep behaviour of a small scale circular rigid plate (Figure 3.24 and Figure 3.25). A laboratory test was conducted by subjecting a circular rigid plate to a vertical load of long duration. This enabled the measurement of the total vertical displacement as a function of time. Figure 3.25 shows the experimental loading frame as well as the cylindrical cell which contains the rigid circular aluminum plate resting on the TDA-sand mixture. As per the previously described creep tests the friction component between the different surfaces was accounted for in the determination of the total vertical displacement curve. The test was conducted at a vertical pressure of 100 kPa for a TDA-sand mixture of $\theta_p = 80\%$.

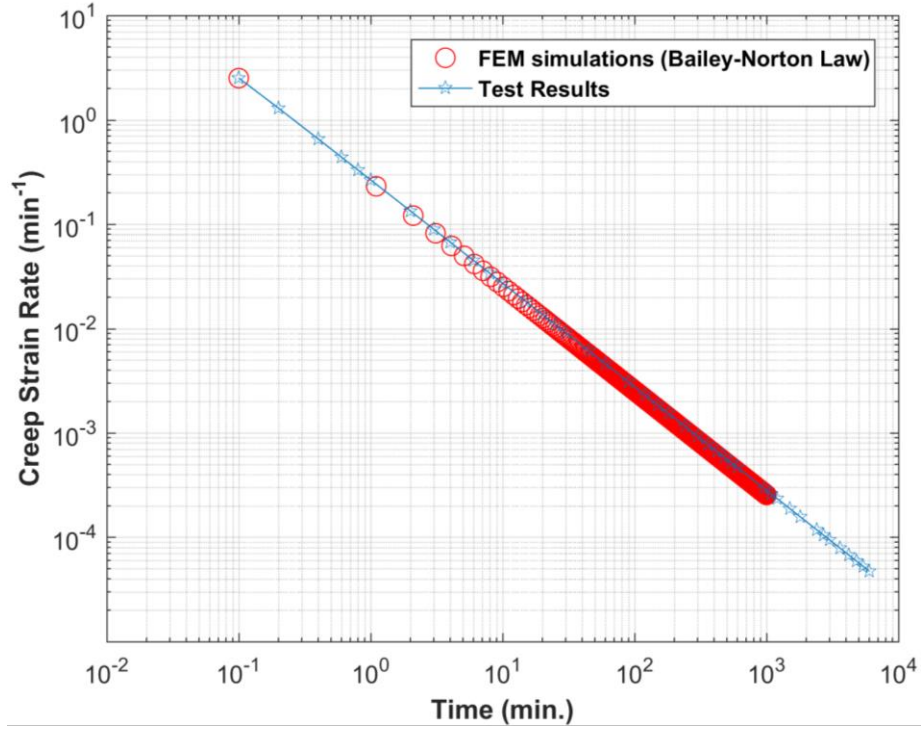


Figure 3.19 Comparison of a finite element simulation and test results for $\sigma_v = 100$ kPa at $\theta = 80\%$ TDA

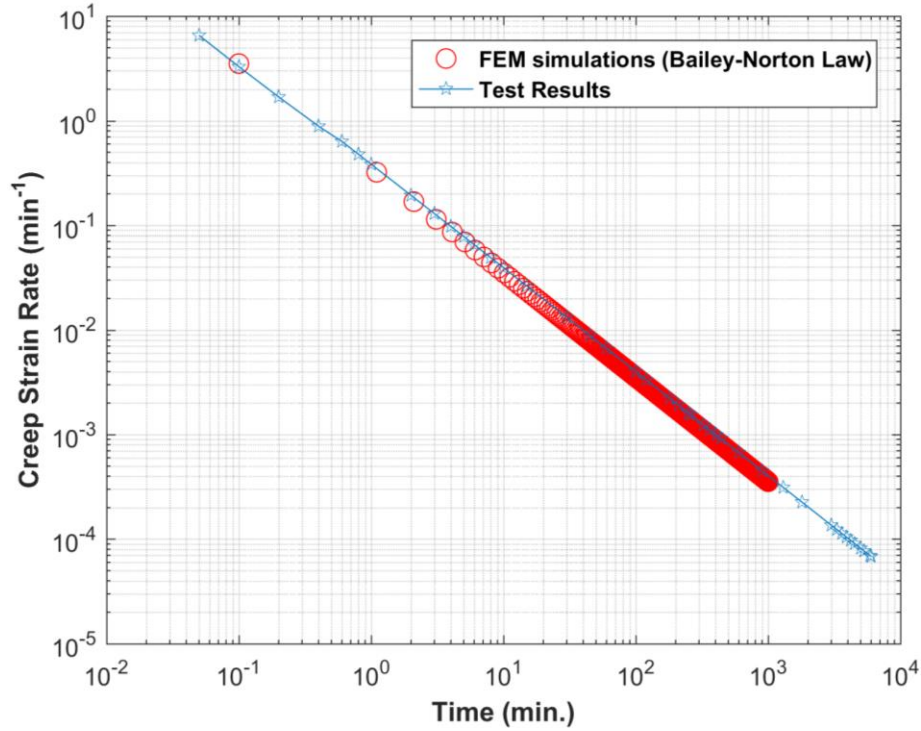


Figure 3.20 Comparison of a finite element simulation and test results for $\sigma_v = 100$ kPa at $\theta = 100\%$ TDA

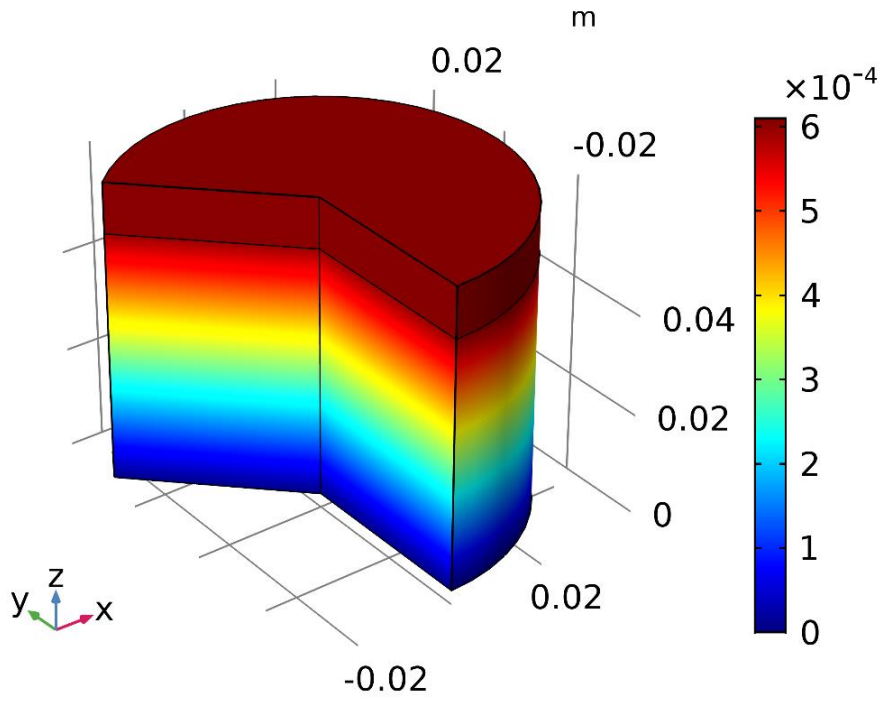


Figure 3.21 Typical result of vertical displacements obtained by finite element simulation for $\sigma_v = 100$ kPa at $\theta = 80\%$ TDA

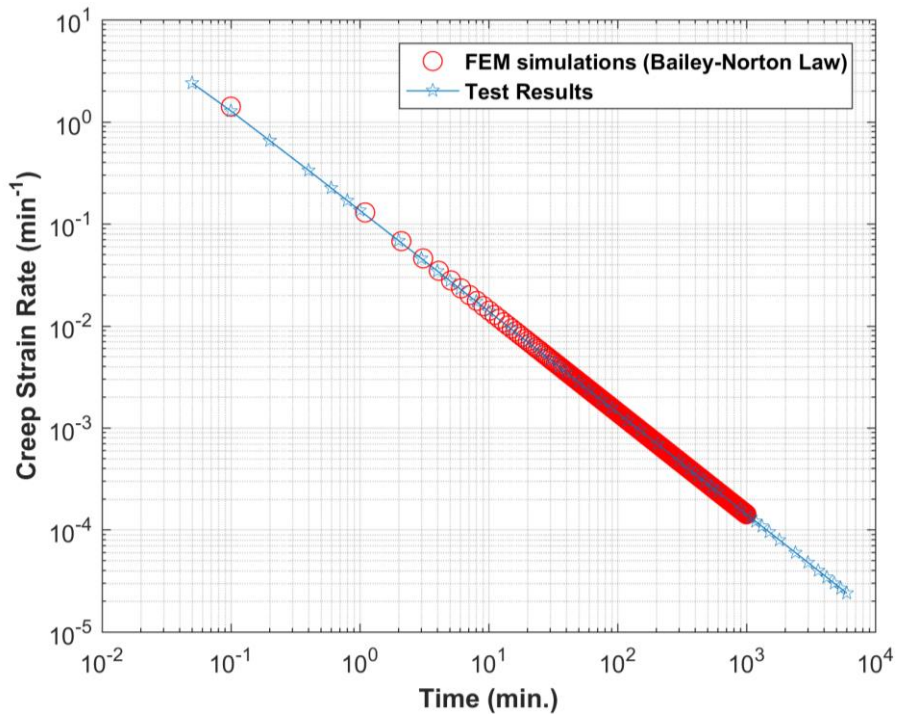


Figure 3.22 Comparison of a finite element simulation and test results for $\sigma_v = 50$ kPa at $\theta = 60\%$ TDA

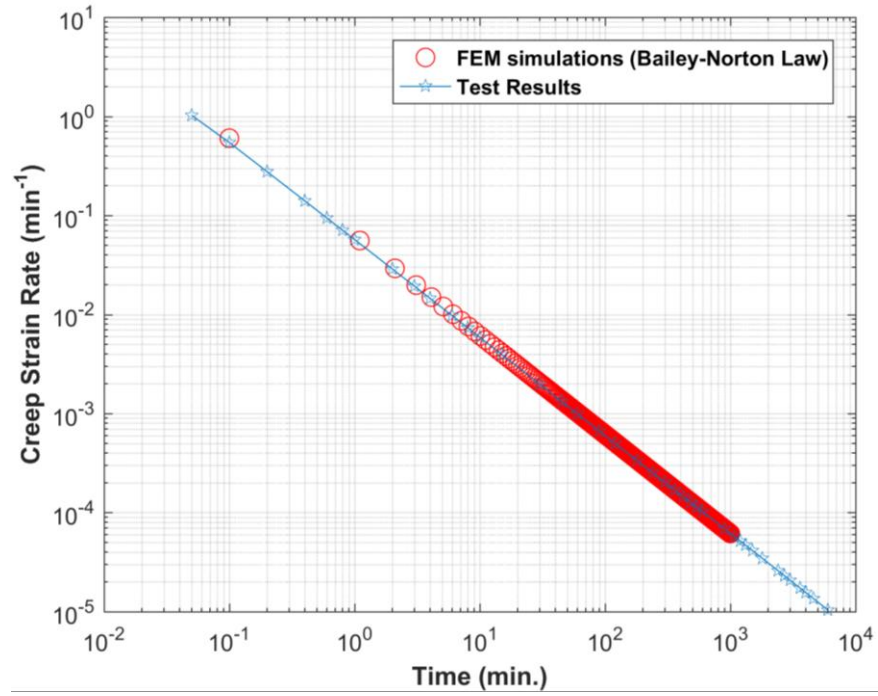


Figure 3.23 Comparison of a finite element simulation and test results for $\sigma_v = 35$ kPa at $\theta = 40\%$ TDA



Figure 3.24 Rigid circular plate resting on a TDA-sand mixture



Figure 3.25 Laboratory setup for small-scale circular rigid plate resting on a TDA–sand mixture

Again, for comparison purposes, a FEM simulation of the foundation test with the commercial software COMSOL was carried out. A typical finite element mesh for the ensuing analysis is shown in Figure 3.26. In order to comply with the previous creep tests the following entries were imposed: the creep parameters of the TDA-sand mixture $n = 0.3868$, $b = 0.0168$, $A = 3.4158 (kPa)^{-n}(\text{min})^{-b}$ (Norton-Bailey Law), the elastic parameters for the TDA-sand mixture, $E = 17.75 \text{ Mpa}$ and $\mu = 0.3$, and the elastic parameters of the aluminum plate $E = 68.9 \text{ Gpa}$ and $\mu = 0.33$. Moreover, in order to obtain the initial stress field, before application of the foundation load, input of the densities for both the aluminum circular rigid plate, $\rho = 2700 \text{ kg/m}^3$, and the TDA-sand mixture $\rho = 784.16 \text{ kg/m}^3$ were necessary.

The FEM simulation gives an acceptable result when compared with the measured experimental values as seen in Figure 3.27. FEM solutions are generally upper bounds to the actual solution and this fact is captured by the present model. Moreover, it is difficult to obtain a homogenous TDA-Sand mixture for testing and this could as well have affected the measured results. For the FEM simulations one assumes a homogeneous medium. It is interesting to note that the FEM model does

capture the pile-up that occurs along the cell wall (Figure 3.28 and Figure 3.29). These figures show respectively (for $t = 200$ and 18655 minutes) the vertical strain and displacement contours.

In order to completely assess the chosen constitutive model a large-scale field model is necessary. However, as previously mentioned, this requires a well-documented field case.

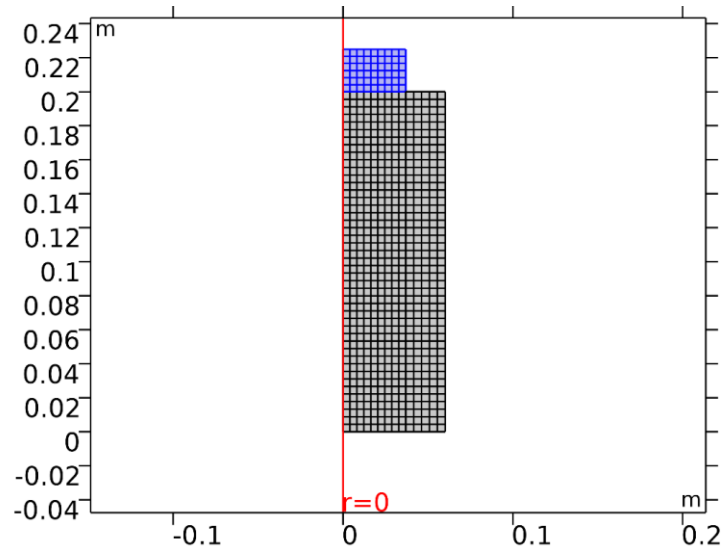


Figure 3.26 Axisymmetric finite element mesh used for the small-scale foundation simulations

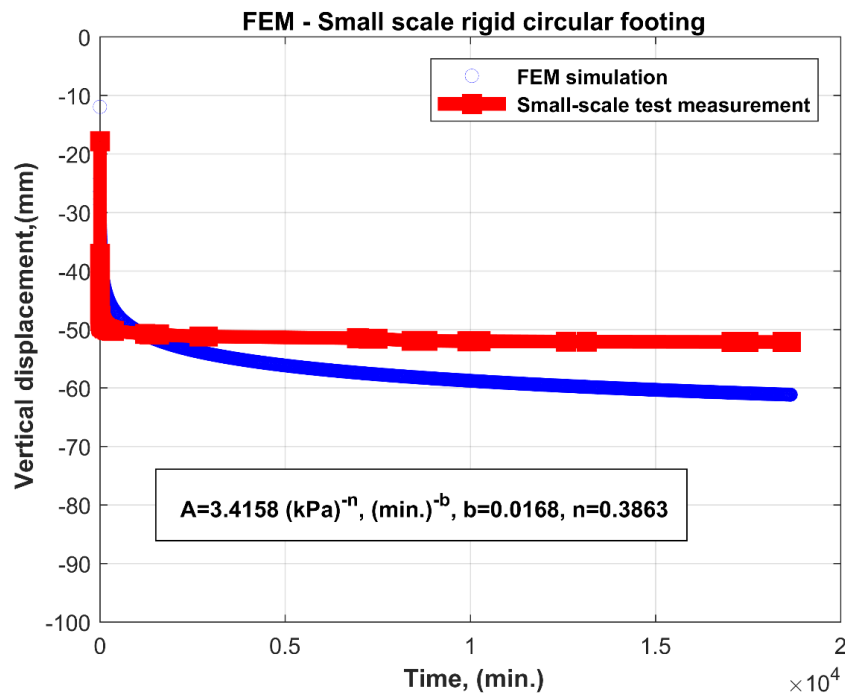


Figure 3.27 FEM simulation of rigid circular plate resting on a TDA–sand mixture

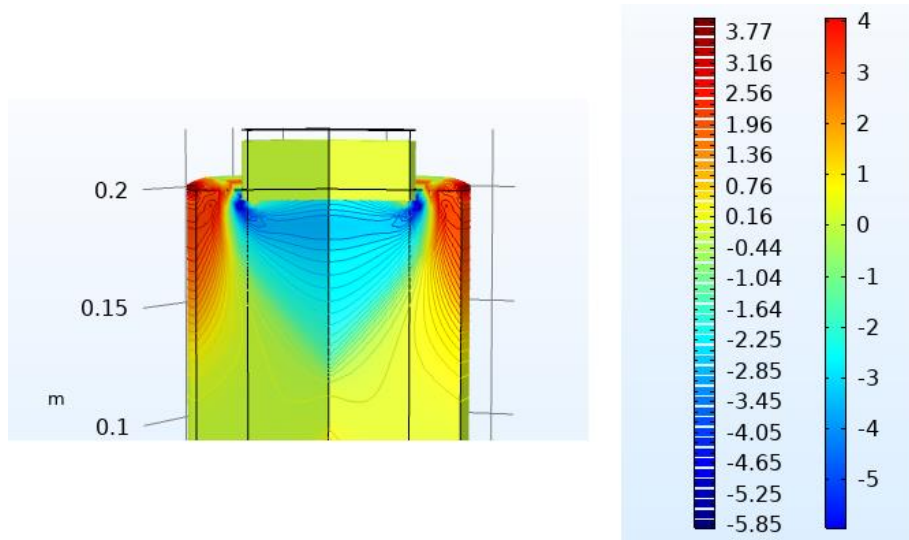


Figure 3.28 Vertical strain after 18,655 min: FEM simulation of rigid circular plate resting on a TDA-sand mixture

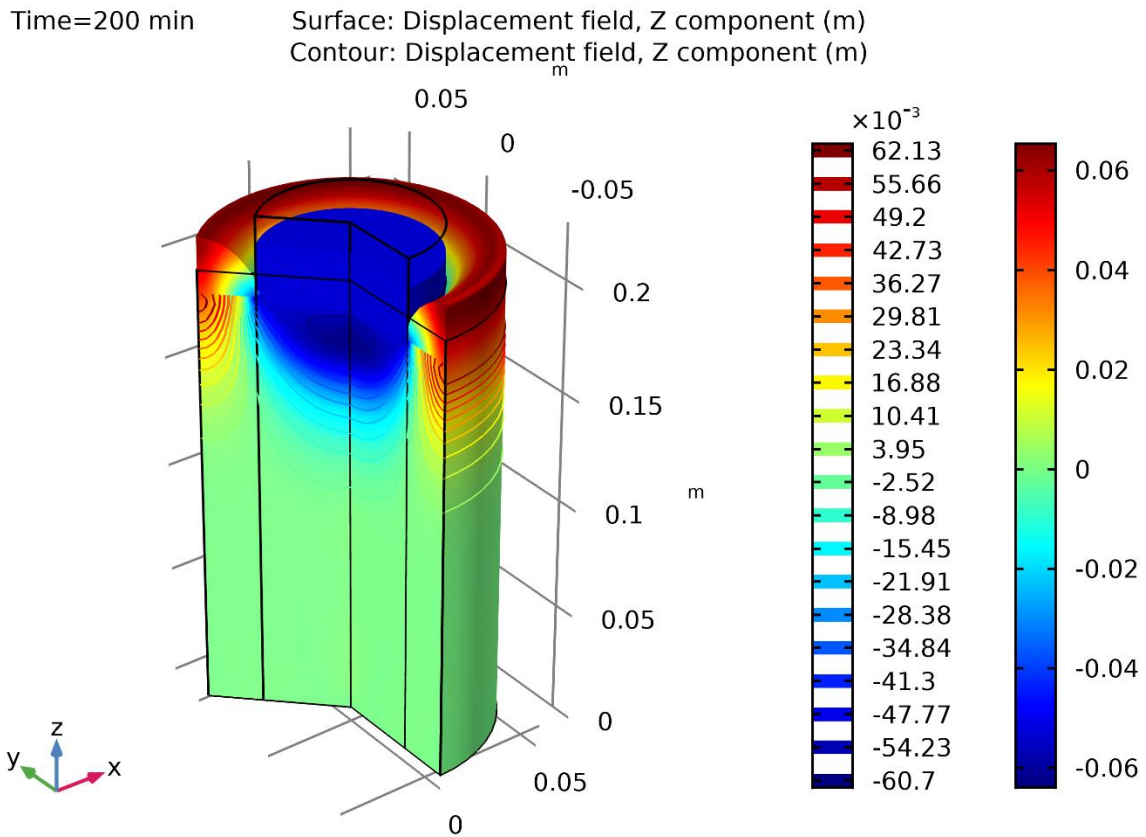


Figure 3.29 Total vertical displacements at 200 min: FEM simulation of rigid circular plate resting on a TDA-sand mixture

3.13 Conclusions

The experimental results obtained in this study have shown that granulated TDA-sand mixtures exhibit a time dependent deformation when subjected to a constant load. This manifestation of creep begins with an instantaneous strain, followed by a decreasing rate of strain (primary creep) which gradually attains a practically constant value (secondary creep). The Norton-Bailey law proved to be useful if one wishes to model a non-stationary creep phase that leads up to a stationary one. This law is effective even more so, because it is easily incorporated in commercial or programmed FEM codes.

The test results indicate that the magnitude of the creep strain is strongly affected by the TDA volume fraction content. Furthermore, the creep strain as well as strain rate, at a constant TDA volume fraction, increases with the applied load. This trend is observed in all of the tests, with the difference that the magnitude of the strain rate depends on the applied stress and TDA volume fraction.

The creep parameters were verified via FEM simulations of the laboratory tests. A satisfactory match of the creep strain rate was obtained, with the Norton-Bailey constitutive equation, in all of the tests. Finally, an FEM simulation of a rigid circular plate resting on a TDA-sand mixture, using the obtained creep parameters, yielded reasonable results.

3.14 Acknowledgments

The authors acknowledge and thank *Shercom Industries Inc.* in Saskatoon, Saskatchewan, Canada for their provision of the TDA used in the laboratory tests. Finally, the authors also acknowledge the technical support of *Christian Juneault* (Technicien en travaux d'enseignement et de recherche) of Département de génie civil et de génie des eaux, Université Laval.

3.15 Appendix

The true stress is calculated by assuming that full mobilization of the shear stress is produced along the cell wall for a length equal to the maximum displacement of the loading cap. The shear stress mobilized at the TDA–aluminum interface cell wall is obtained with,

$$f_W = \tau_f(2\pi\delta_{max})$$

where r and δ_{max} are, respectively, the internal radius of the cell and the maximum displacement of the loading cap. The mobilized shear stress is approximated with,

$$\tau_f = K_o \sigma_n \tan(\delta)$$

where K_o , σ_n and δ stand, respectively, for the coefficient of earth pressure at rest, the nominal stress and the angle of internal friction between the TDA–sand mixture (Table 3.1) and the aluminum cell wall. Values of K_o for loose granular soils generally range between 0.3 and 0.5. For the purposes of the present calculations, a value 0.5 was chosen. The true stress σ_t is calculated based on the net force divided by the projected area of loading and is given by,

$$\sigma_t = \frac{f_n - f_w}{\pi r^2}$$

where the nominal force is calculated with $f_n = \sigma_n \pi r^2$. Typical results of the calculated true stress are given in Table 3.3.

3.16 References

1. Ahmed I (1993) Laboratory study on properties of rubber-soils. *Publication FHWA/IN/JHRP 93/04*. Joint Highway Research Project, Indiana Department of Transportation and Purdue University, West Lafayette, Indiana.
2. Ahn IS, Cheng L (2014) Tire derived aggregate for retaining wall backfill under earthquake loading. *Constr Build Mater* 57:105–116.
3. Andersland OB, Ladanyi B (1994) An introduction to frozen ground engineering. *Chapman and Hall*, New York, p 10119.
4. Apex Companies (2008) Tarrtown bridge project case study guidance document for tire derived aggregate embankment construction and design strategic recycling contract No. 353R06 Pollution Prevention Section. Equad, LLC 269 Great Valley Parkway Malvern, Pennsylvania 19355.
5. Bosscher P, Edil T, Kuraoka S (1997) Design of highway embankments using tire chips. *J Geotech Geoenviron Eng.*, 123(4):295–304.
6. Bosscher P, Edil T, Eldin N (1992) Construction and performance of shredded waste tire embankments. *Transportation Research Record* 1345, Transportation Research Board. National Research Council, Washington, DC, pp 44–52.

7. Brzesowsky RH, Hangx SJT, Brantut N, Spiers CJ (2014) compaction creep of sands due to time-dependent grain failure: effects of chemical environment, applied stress, and grain size. *J Geophys Res Solid Earth* 119:7521–7541.
- Feda J (1989) Interpretation of creep of soils by rate of process theory. *Geotechnique* 39(4):667–677.
9. Foriero A, Robitaille K (2016) Time-scales for the redistribution of stress in the course of pressuremeter creep tests in permafrost. *Cold Reg Sci Technol* 132:44–59.
10. Foriero A, Keviczky A (2000) Steady state analysis of ice scouring via conformal mapping. *Riv Ital Geotech* 3:5–26.
11. Foriero A, Ladanyi B (1998) Finite element analysis for large strain consolidation of saturated clays under equilibrium conditions. *Riv Ital Geotech* 2:16–47.
12. Foose GJ, Benson CH, Bosscher PJ (1996) Sand reinforced with shredded waste tires. *J Geotech Eng.* 122(9):760–767.
13. Ghazavi M, Sakhi MA (2005) Influence of optimized tire shreds on shear strength parameters of sand. *Int J Geomech* 5(1):58–65.
14. Humphrey DN (2008) “Tire derived aggregates as lightweight fill for embankments and retaining wall. In: Hazarika H, Yasuhara K (eds) *Scrap tire derived geo-materials, opportunities and challenges: proceedings*.
15. Humphrey DN, Eaton RA (1995) Field performance of tire shreds as subgrade insulation for rural roads. In: Proceedings of the sixth international conference on low-volume roads, transportation research board, vol 2, pp 77–86.
16. Kampour H, Lade PV (2013) Creep behavior in Virginia Beach sand. *Can Geotech J* 50(11):1159–1178.
17. Ladanyi B (1972) An engineering theory of creep of frozen soils. *Can Geotech J* 9(1):63–80.
18. Meles D, Bayat A, Soleymani H (2013a) Compression behavior of large-sized tire-derived aggregate for embankment application. *J Mater Civ Eng.* 25(9):1285–1290
19. Mitchel J, Soga K (2005) Fundamental of soil behavior, chapter 12, 3rd edn. Wiley, Hoboken, pp 465–521.
20. Mitchel J, Campanella R, Singh A (1968) Soil creep as a rate process. *J Soil Mech Found Eng Div* 94(1):231–253.
21. Neaz Sheikh M, Mashiri M, Vinod J, Tsang H (2013) Shear and compressibility behavior of sand–tire crumb mixtures. *J Mater Civ Eng.* ASCE 25(10):1366–1374.
22. Ngo A, Valdez J (2007) Creep of sand–rubber mixtures. *J Mater Civ Eng.* 19(12):1101–1105.

23. Ward I. M., Sweeney J (2004) An introduction to the mechanical properties of solid polymers, 2nd edn. Wiley, New York. ISBN: 978-0-471-49626-7
24. Wartman J, Natale M, Strenk P (2007) Immediate and time-dependent compression of tire derived aggregate. *J Geotech. Geoenviron Eng.* 133(3):245–256.
25. Yi Y, Meles D, Nassiri S, Bayat A (2014) On the compressibility of tire derived aggregate: comparison of results from laboratory and field tests. *Can Geotech J* 52(4):442–458. <https://doi.org/10.1139/cgj-2014-0110>.
26. Zornberg, Jorge G., Alexandre R. Cabral, and Chardphoom Viratjandr. 2004. “Behaviour of Tire Shred - Sand Mixtures.” *Canadian Geotechnical Journal* 41 (2): 227–41. <https://doi.org/10.1139/t03-086>.

CHAPTER 4 : FOREWORD

This chapter is written in accordance with a previously published journal paper. The entire of the materials and findings presented in this paper is taken from my PhD research project. Moreover, a permission has been already taken from the publisher of the journal to authorize the reuse of the mentioned paper as part of this PhD thesis. The information of this paper is briefly presented below.

Authors and affiliations

- Adolfo Foriero : Professor, Université Laval, Faculté des sciences et de génie, Département de génie civil et de génie des eaux.
- Nima Ghafari : PhD student, Université Laval, Faculté des sciences et de génie, Département de génie civil et de génie des eaux.

Author contributions

The authors have confirmed contribution in the paper, **Critical State Model of Sand-Tire**

Derived Aggregate Mixtures Based on Triaxial Tests as follows (Foriero and Ghafari, 2021) :

Study conception and design: A. Foriero, N. Ghafari;

Data collection: N. Ghafari, A. Foriero;

Analysis and interpretation of results: A. Foriero, N. Ghafari;

Draft manuscript preparation: A. Foriero, N. Ghafari.

All authors reviewed the results and approved the final version of the manuscript.

A more detailed author contribution is given here in order to comply with the regulations of the FESP.

General idea of the research project: The idea of conducting a research project on TDA materials was originally suggested by Mr. Charles Darwin-Annan (Professor at Laval University). This idea was further developed and suggested by Nima Ghafari to his new PhD director Mr. Adolfo Foriero.

Communication with industry: N. Ghafari conducted the communication with the industry.

Selection and provision of the testing materials: The selection of the type of TDA (e.g., shape and size) and sand (Ottawa sand) as well as the determination of the required quantity of the materials in order to conduct the entire experiments were carried out by Nima Ghafari in consultation with Adolfo Foriero.

Study conception and design: The project was designed by both of the authors while Adolfo Foriero was mostly involved in design of the theoretical parts and Nima Ghafari was mostly involved in design of the experimental parts of this study.

Research experiments and data collections: The experimental research work and the data collections were carried out by Nima Ghafari in consultation with Adolfo Foriero.

Test data processing: The calculations in order to process the raw test results obtained from each of the tests were conducted by Nima Ghafari in consultation with Adolfo Foriero.

Test reports preparation: The tests report preparation was conducted by Nima Ghafari in consultation with Adolfo Foriero.

Analysis and interpretation of the results: The analysis and interpretation of the results obtained from the experiments as well as the numerical verifications were conducted by Adolfo Foriero and Nima Ghafari.

Draft manuscript preparation: The manuscript preparation was conducted by Adolfo Foriero and Nima Ghafari. The draft manuscripts were multiple times reviewed and modified by both of the authors before submission of the final version to the journal.

Status : Published

Date of acceptance : January 13, 2021

Journal : Transportation Research Record (TRR)

Résumé français

Cette étude s'inscrit dans le cadre d'un programme expérimental environnemental sur l'utilisation de pneus usés d'automobiles pour des applications géotechniques. Différents types d'essais de laboratoire ont été effectués pour déterminer les paramètres d'élasticité, de plasticité et de fluage de mélanges granulats dérivés de pneus (TDA) et de sable. Cependant, cet article met l'accent sur les paramètres de plasticité par le biais du développement d'un modèle d'état critique basé sur les résultats d'essais triaxiaux. Ceci a été atteint en considérant des échantillons de sable, à une teneur volumétrique prédéterminée de TDA, soumis à trois pressions de confinement différentes sous une vitesse de déplacement axial constante. Le modèle Cam-Clay modifié a simulé les courbes de contraintes déviatoriques par rapport à la déformation axiale avec une réponse élastoplastique non linéaire obtenue dans les essais. Les résultats ont indiqué un niveau de résistance au cisaillement important qui dépend de l'angle de frottement à l'état critique et qui à son tour dépend de la teneur volumétrique en TDA. Pour les mélanges TDA-sable utilisés dans la présente étude, l'effet de la teneur volumétrique en TDA démontre un renforcement de la matrice de sable. Cependant, ce renforcement diminue à mesure que la teneur en TDA augmente.

4 A Critical State Model of Sand-TDA Mixtures Based on Triaxial Tests

4.1 Abstract

This study is part of an environmental experimental program on the use of scrap automobile tires for geotechnical applications. Different types of laboratory tests were conducted to determine the elastic, plastic and creep parameters of TDA-sand granulated mixtures. However, this paper emphasizes the plasticity parameters via the development of a critical state model based on the results of triaxial tests. This was attained by considering loose sand specimens, at a predetermined TDA volumetric content, subject to three different confining pressures under a constant axial displacement rate. The calculated deviatoric stress versus axial strain curves, obtained via the modified Cam Clay model, captured the non-linear elastoplastic response obtained in the tests. Results indicated that the level of the shear strength is highly dependent on critical state friction angle which in turn depends on the TDA content. For the loose TDA-sand mixtures used in the present study, the effect of the TDA content demonstrates a reinforcement of the sand matrix. However, this reinforcement diminishes as the TDA content increases.

4.2 Introduction

Environmental as well as economic conditions have given rise to the use of recycled tires as construction materials. There are various reasons for this. One of them is that stockpiles of discarded tires are on the rise and constitute a real fire hazard, not to mention a breeding ground for rodents. Another reason is that natural resources like sand, clay, gravel and other mineral aggregates are being depleted throughout the world because of the opening of new quarries. Finally, when shredded, tire derived aggregates (TDA) could be mixed with traditional construction aggregate materials. The basic characteristics of such mixtures are that they are lightweight and frictionally resistant precisely as a result of the TDA. Another important property of sand-TDA mixtures is their low thermal conductivity. This constitutes an economic and engineering advantage over traditional materials.

Granular material mixed with TDA is increasingly used in geotechnical applications. In many of these operations sand is mixed with TDA at various volumetric ratios. The resultant sand-TDA mixture have been used in such applications as highway embankment and bridge abutments (Bosscher

et al. 1992; Bosscher et al. 1997; Apex Companies 2008). In northern regions TDA-granular soil mixtures are also employed in pavement design. They primarily serve as an insulating layer (Humphrey and Eaton 1995) in order to prevent frost heave and hence degradation of the road surface.

A review on the related past studies, exposes a lack of experimental as well as numerical investigations on long-term time dependent constitutive behavior of sand-TDA mixtures. A recent study on sand-TDA mixtures clearly indicates a primary creep phase that rapidly transitioned into a secondary stationary creep phase, never attaining the tertiary phase (Foriero, A. and Ghafari, N. 2020). The magnitude of the creep strain was strongly affected by the TDA volume fraction content (Schofield and Wroth 1968). This observation conduced the adoption of the Norton-Bailey law as a possible constitutive model for creep of TDA-sand mixtures. Other studies such as Wartman et al., examined the immediate and time dependent compression of tire chips and shreds (Roscoe and Burland 1968). The time-dependent deformation of the mixture was also shown to be inversely proportional to the sand content. In another study, the one-dimensional compression of specimens, composed of sand and granulated tire rubber, was investigated (Ngo and Valdez 2007). There again, results indicated that the time dependent deformation is significant. However, a complete constitutive model must consider, in addition to time dependent deformations, the shear strength of the sand-TDA mixtures.

In the past decades, most of the laboratory research with regards to shear strength was conducted on sand reinforced with tire chips (generally from 10 to 300 mm in size) (Apex-Companies 2008; A Foriero and Ghafari 2020; Ward and Sweeney 2004; AbdelRazek et al. 2018; Foose et al. 1996). The direct shear box test and the triaxial test were the apparatuses mostly used to test these mixtures. The overall research emphasized that the shear strength of sand is increased by the tire chips.

Direct shear box tests by Bosscher et al. and Foose et al. show an increase in shear strength with a rubber content of up to 50 % (Humphrey and Eaton 1995; AbdelRazek et al. 2018). Foose et al. also reported that the failure envelope of sand-rubber mixtures containing dense sand is non-linear (AbdelRazek et al. 2018). Yang et al. also observed a non-linear failure envelope of the shear stress but in the cases of granulated rubber and not tire chips (Mitchel, and Soga 2005). However, most studies of sand mixed with granulated rubber, using the direct shear box, show inconsistencies in the results. For example, Anbazhagan et al. (2007) determined an increase of the shear strength when granulated rubber is mixed with uniform sand. However, the shear strength decreased when the granulated rubber was mixed with poorly graded sand. Ghazavi (2004) reported an insignificant increase in shear strength of the mix with an increase in granulated rubber.

Experimental studies on the shear strength measured in the triaxial apparatus also show considerable inconsistencies in the test results. A study by Noorzad and Raveshi (2017), in which tire crumbs act as reinforcement of a sand-tire mixture, found that the shear strength decreases with increase in the amount of tire crumbs. A similar conclusion was obtained for mixtures of sand and granulated rubber by Youwai and Bergrado (2013) and Madhusudhan et al. (2017). On the other hand, a study by Venkatappa R. and Dutta, R.K. (2006) determined some improvement in strength on additions of rubber inclusions. Tyre chips with an aspect ratio of 2 showed the best improvement for low confining pressures and chip content.

Numerous laboratory investigations have considered sand reinforced with tire chips whereas, only a few have considered sand-TDA granular mixtures. Although, none of the previous studies have considered a critical state model for interpretation of the test results.

4.3 Sand-TDA Mixtures of the Triaxial Tests

For the triaxial tests in this study, the specimens consisted of mixtures of two granular materials. One of these materials is Ottawa sand whose granulometric curve is shown in Figure 4.1. From the shape of this curve and with calculated values of $C_u = 2.1$ and $C_c = 1.26$, this sand is defined as a poorly graded sand (SP). The other material is tire derived aggregate (TDA) obtained at *Shercom Industries Inc.* in Saskatoon, Saskatchewan, Canada, with calculated values of $C_u = 1.69$ and $C_c = 1.03$. This rubber granular material would also be considered as poorly graded if classified according to the Unified Soil Classification System. A granulometric curve for this material is also shown in Figure 4.1.

For the purpose of the tests these two materials were combined at three different volumetric ratios: $\theta_p = 0.50, 0.75, 1.00$, where θ_p represents the volume fraction of TDA per total volume of the mixture. In Figure 4.2, a phase diagram for the sand-TDA mixture was used to determine the initial void ratios that correspond to the five volumetric ratios mentioned previously.

This was possible because both the weights of the TDA and Sand phases, as well as the total volume they occupied were measured beforehand. For the calculations, the specific gravity of the TDA ($G_{TDA} = 1.15$) and Ottawa Sand ($G_{Sand} = 2.65$) were necessary. The phase volumes of the TDA and Sand were obtained respectively as $V_{TDA} = \frac{W_{TDA}}{G_{TDA} \gamma_\omega}$ and $V_{Sand} = \frac{W_{Sand}}{G_{Sand} \gamma_\omega}$. Consequently, the initial void ratio, e , and initial unit weight, γ , of the TDA-Sand mixtures were known at the start of all tests (Table 4.1).

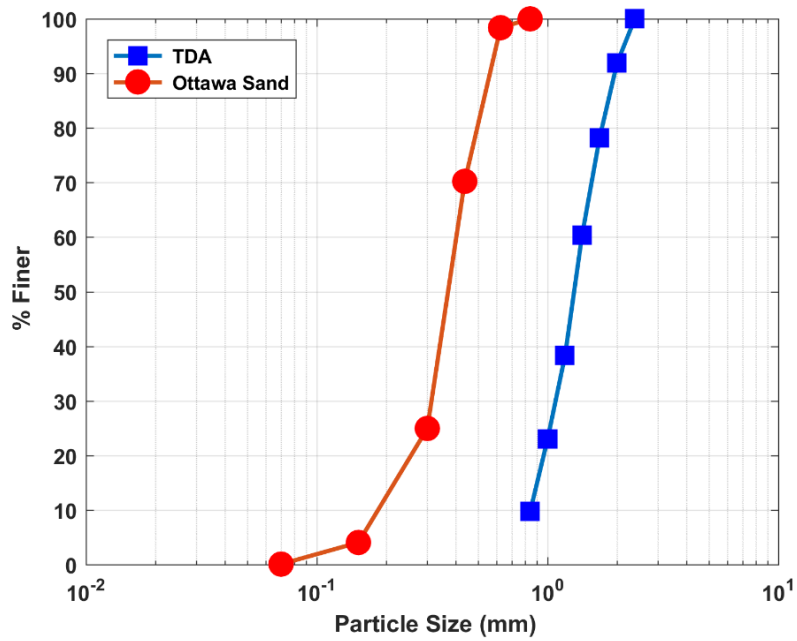


Figure 4.1 Grain-size distribution curves of materials used in the present study

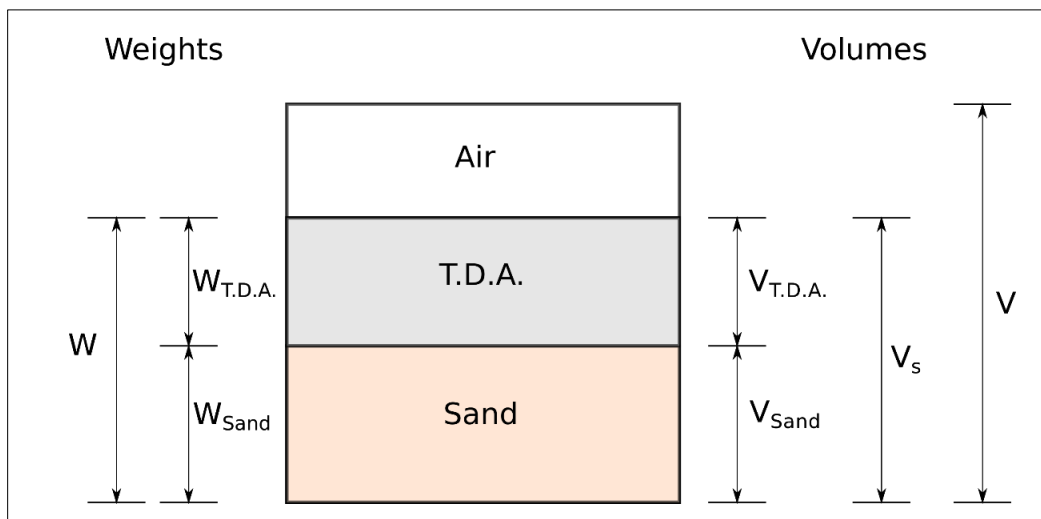


Figure 4.2 Phase diagram of TDA-sand mixture

Table 4.1 Initial void ratio and unit weight of Ottawa Sand-TDA mixture

TDA (%)	Void Ratio, e_o	Unit Weight, $\gamma, \frac{kN}{m^3}$
50	0.78	11.02
75	0.91	8.25
100	1.05	5.5

4.4 Test Equipment and Experimental Procedure

A standard triaxial apparatus, generally used for soils, was chosen for this study (Figure 4.3). The sand-TDA specimen measured 35.1 mm in diameter and 67.5 mm in height. A consistent procedure for preparing and testing dry samples of sand-TDA mixtures at a loose state was established. The required percentages of TDA were uniformly mixed with Ottawa sand in a dry condition. The sand was then poured into a rubber membrane inside a split mold former under vacuum. The sand-TDA specimens when sheared were subjected to confining cell pressures of 50, 100 and 150 kPa for each volumetric ratio $\theta_p = 0.50, 0.75, 1.0$. A conventional drained triaxial test displacement rate of 0.0061 mm/min was maintained throughout the tests.

4.5 Test Results and Observations

A total of 9 triaxial tests on sand-TDA dry granular mixtures were completed in the present study. Test samples at three different TDA volumetric ratios $\theta_p = 0.50, 0.75, 1.0$ were subjected to three different confining pressures of 50, 100 and 150 kPa.

Typical stress-strain curves for the cases pertaining to $\theta_p = 0.50$ and 0.75 are exhibited in Figure 4.4 and Figure 4.5. Results show, as one would expect, that for a constant TDA volumetric ratio, the deviatoric stress increases with the confining stress.



Figure 4.3 Triaxial test configuration

However, from these two Figure 4.4s, an increase in the TDA volumetric content tends to lower the shear strength of the sand-TDA mixture. Moreover, both Figure 4.5 and Figure 4.6 depict a strain hardening behavior.

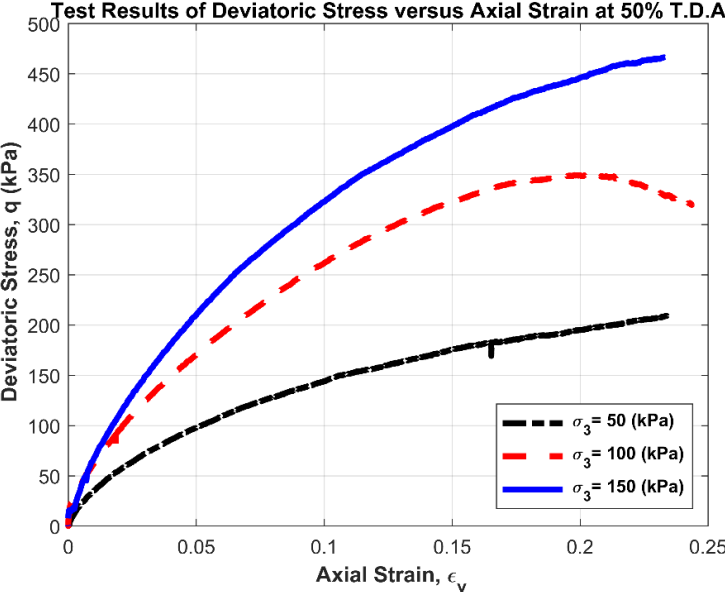


Figure 4.4 Test results of deviatoric stress versus axial strain at 50 % TDA

Although, it is evident from these two figures that an increase in the TDA volume fraction content (θ_p) tends to lower the shear strength of the sand-TDA mixture. Furthermore, a strain hardening behavior is evident in both Figure 4.5 and Figure 4.6

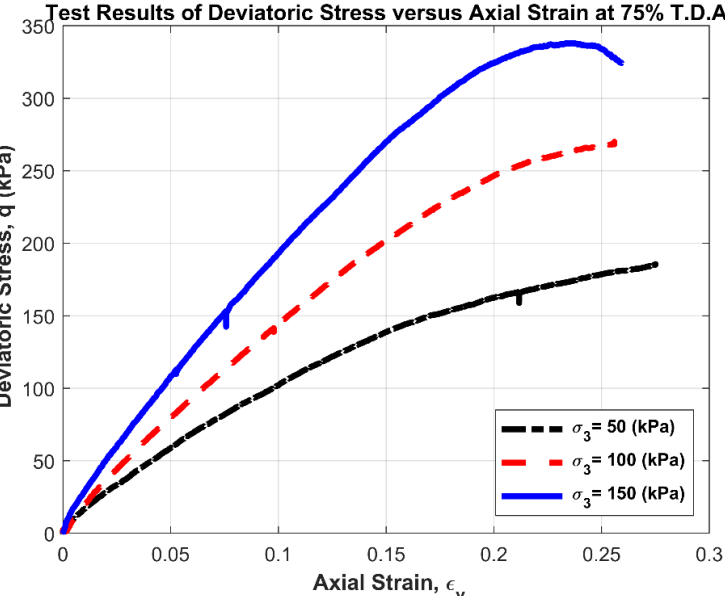


Figure 4.5 Test results of deviatoric stress versus axial strain at 75 % TDA

This was confirmed by the barrel shape of the specimen at the end of the test (Figure 4.6) which occurred at an axial strain of approximately 23%.

An interesting result for the triaxial tests with pure TDA particles $\theta_p = 1.0$ is given in Figure 4.7. Here again the deviatoric stress increases with the confining stress but for the lower confining stresses this increase is minimal. The stress-strain behavior in this instance and for practical purposes appears to be linear. It is obvious that, for this case in which the sample is prepared from 100% TDA the behavior is elastic.

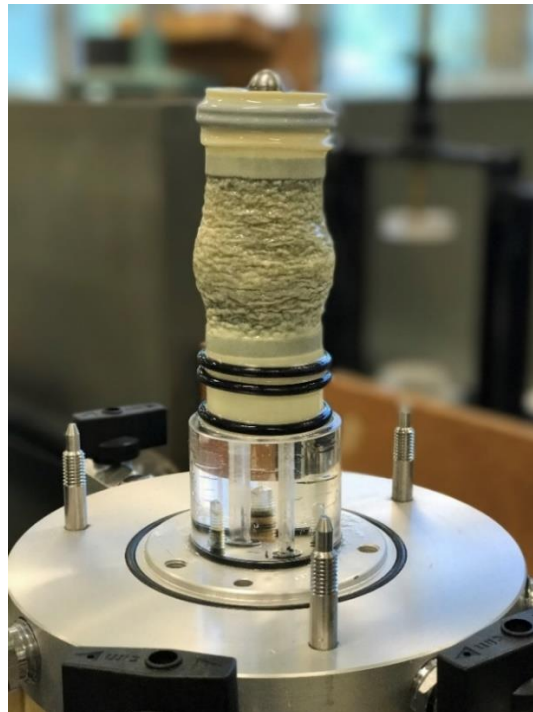


Figure 4.6 The shape of the sand-TDA sample having 75% TDA at the end of the triaxial test

In all of these tests one must define the value of the failure strain. At approximately 23% of the axial strain, the sand-TDA specimen is severely distorted as previously mentioned (Figure 4.6). Hence, the critical state, which is reached when no further changes in shear stress and volume occurs under continuous shearing, cannot be attained. Several studies on triaxial testing have defined failure based on a predetermined strain in the range of 10 to 20 % (Yang et al.,2002; Noorzad and Raveshi, 2017). Thus, in this study, 4 different values of the vertical strain ($\epsilon_v = 10\%$, 15%, 20%, 23%) were considered (Figure 4.8, Figure 4.9, Figure 4.10) in order to examine the effect of the TDA content on the presumable deviatoric stress at failure. As seen in these Figure 4.8s, for a constant confining pressure, an increase in the TDA content lowers the deviatoric stress. Again, the deviatoric stress increases with the confining cell pressure at one particular TDA volumetric ratio.

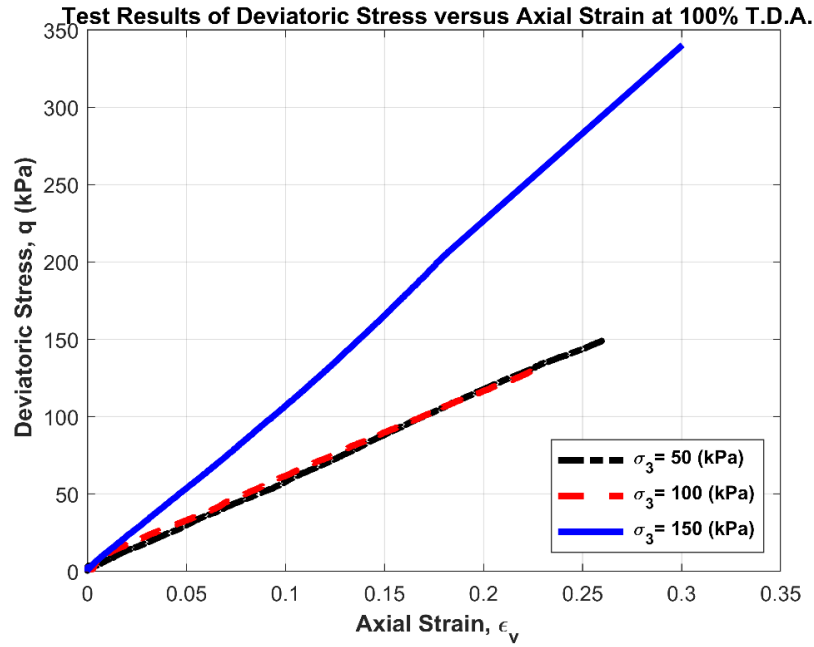


Figure 4.7 Test results of deviatoric stress versus axial strain at 100 % TDA

As observed from these figures, for a constant confining pressure, an increase in the TDA volume fraction content (θ_p) results to reduction in the deviatoric stress. Once more, it is evident from these figures that the deviatoric stress increases with the confining cell pressure at one particular TDA volumetric ratio.

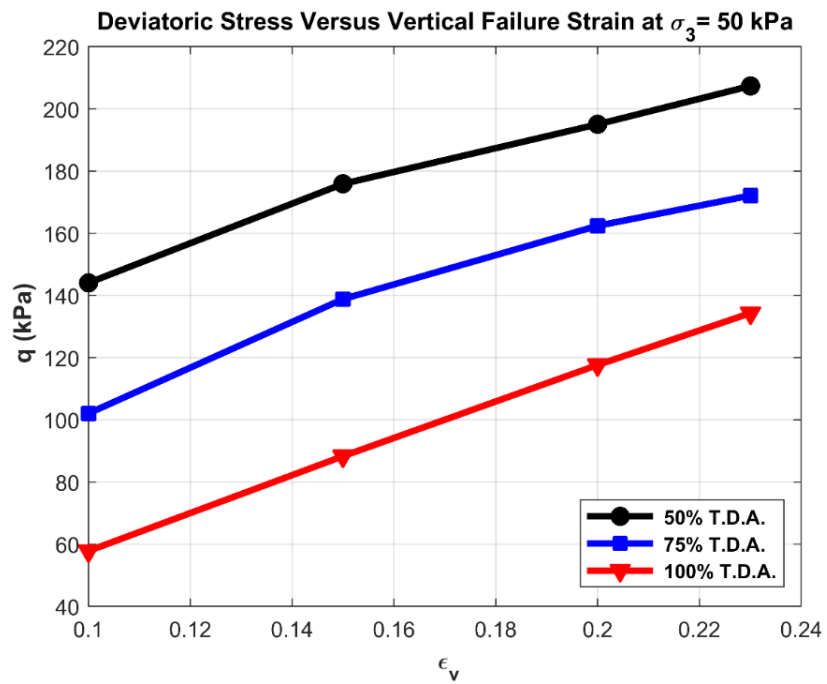


Figure 4.8 Deviatoric stress versus axial strain at failure for $\sigma_3 = 50$ kPa

The previous stress-strain curves (Figure 4.4, Figure 4.5 and Figure 4.7) showed a reduction in the stiffness of the sand-TDA mixtures as the TDA content increased. An average representation of stiffness for non-linear behavior is through the secant modulus.

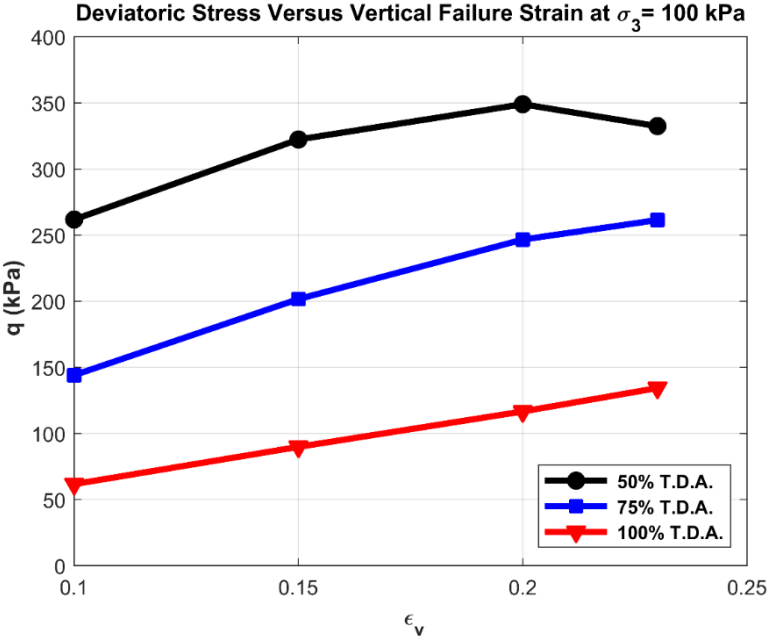


Figure 4.9 Deviatoric stress versus axial strain at failure for $\sigma_3 = 100 \text{ kPa}$

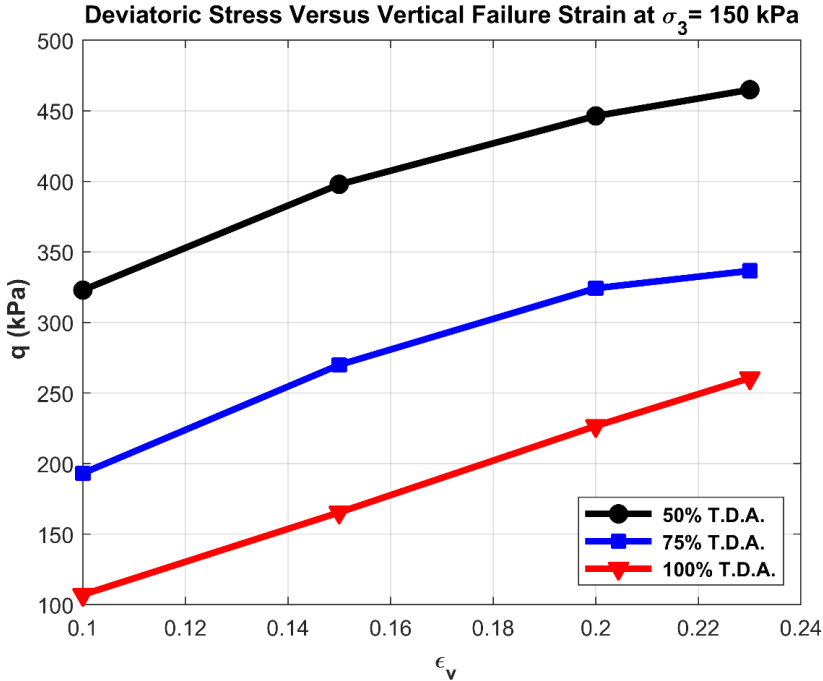


Figure 4.10 Deviatoric stress versus axial strain at failure for $\sigma_3 = 150 \text{ kPa}$

Figure 4.11, Figure 4.12 and Figure 4.13 exhibit the secant modulus at the vertical failure strains previously cited. As confirmed by the previous results, the trend is analogous. The secant moduli decrease with an increase in TDA and a decrease of the confining pressure.

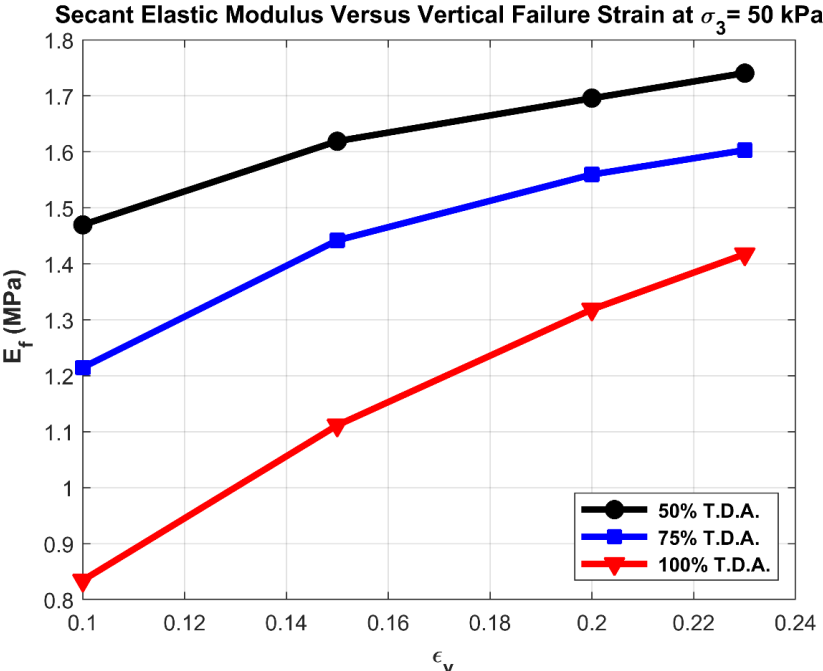


Figure 4.11 Secant elastic modulus versus axial strain at failure for $\sigma_3 = 50 \text{ kPa}$

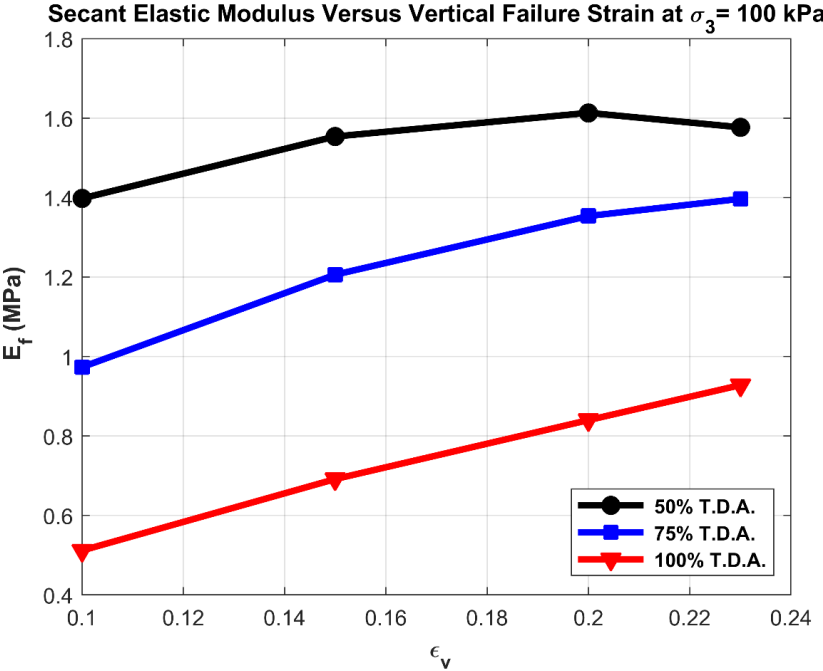


Figure 4.12 Secant elastic modulus versus axial strain at failure for $\sigma_3 = 100 \text{ kPa}$

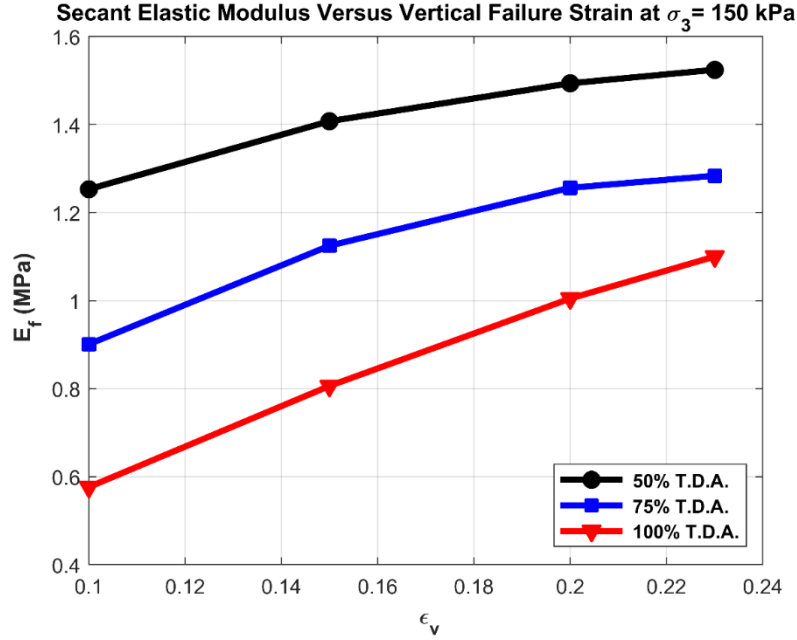


Figure 4.13 Secant elastic modulus versus axial strain at failure for $\sigma_3 = 150 \text{ kPa}$

It is clear from the previous experimental results that the TDA volumetric ratio plays an important role as far as the behavior of the mixture is concerned. A constitutive equation is therefore needed that accounts for this. Consequently, the next section of this paper is devoted to the development of a simple framework capable of describing, interpret and anticipate the sand-TDA mixture response to loading.

4.6 A Critical State Model to Interpret TDA-Sand Mixtures

As a preliminary attempt in understanding TDA-sand mixtures, it is tacitly assumed that such mixtures are quasi-single phased. This means that deformation causes no change, or negligible change, in the phase ratio per unit volume. In this particular case one refers to the sand-TDA phase ratio, implying that the TDA does not flow out of the sand matrix. Consequently, the term effective stress shall be indiscriminately used from hereon.

The fundamental concept of a unique failure surface is adopted in the present approach. Moreover, the terms failure and critical state are taken as synonymous. From hereon, the failure line will be referred to the critical state line (CSL) (Schofield and Wroth 1968). The yield surface is an ellipse whose equation in (p', q, e) space is

$$(p')^2 - p'p'_c + \frac{q^2}{M(\theta)^2} = 0 \quad (4.1)$$

and is a function of the TDA volumetric content through the friction constant M . The other variables p', p'_c, q are respectively the effective mean stress, the maximum past effective mean stress and the deviatoric stress. In geotechnical engineering this surface is better known as the modified Cam-Clay yield surface (Roscoe, K.H., and Burland, J.B., 1968).

The Mohr-Coulomb failure criterion is written in terms of the previously mentioned stress invariants as

$$q_f = M(\theta)p'_f \quad (4.2)$$

where p'_f, q_f are respectively the effective mean stress and the deviatoric stress at failure. Since the triaxial testing program in the present study dealt with axisymmetric compression only, the expression for the friction parameter is specialized to

$$M(\theta) = M_c(\theta) = \frac{6 \sin(\varphi'_{cs}(\theta))}{3 - \sin(\varphi'_{cs}(\theta))} \quad (4.3)$$

where the critical state friction angle φ'_{cs} is back-calculated from the present triaxial tests with

$$\sin(\varphi'_{cs}(\theta)) = \frac{3 M_c(\theta)}{6 - M_c(\theta)} \quad (4.4)$$

The equation for the critical state line in $(e - p')$ space is represented by

$$e_f = e_\Gamma - \lambda \ln(p'_f) \quad (4.5)$$

where $e_f, e_\Gamma, \lambda, p'_f$ are respectively the void ratio at failure, the void ratio on the critical state line when $\ln(p') = 1$, the slope of the critical state line and effective mean stress at failure. One determines e_Γ from the initial state of the soil with

$$e_\Gamma = e_o + (\lambda - k) \ln\left(\frac{p'_c}{2}\right) + k \ln(p'_o) \quad (4.6)$$

here k is the unloading/reloading index or the recompression index.

In order to calculate the elastic response, the elastic modulus E' is required. This modulus is obtained from the triaxial tests. One can approximate this modulus by a secant modulus (Figure 4.11, Figure 4.12, Figure 4.13) over the stress increment of interest. However, an estimate of this modulus is also possible using the critical state model through the bulk modulus. The bulk modulus is calculated with

$$K' = \frac{p'(1 + e_o)}{k} \quad (4.7)$$

and since $E' = 3K'(1 - 2\mu')$ one obtains that

$$E' = \frac{3p'(1 + e_o)(1 - 2\mu')}{k} \quad (4.8)$$

Consequently, the elastic shear modulus, G , is also estimated as

$$G = \frac{3p'(1 + e_o)(1 - 2\mu')}{2k(1 + \mu')} \quad (4.9)$$

Eqs. (4.7) and (4.8) indicate a non-linear elastic behaviour because both are functionally dependent on the mean effective stress. Consequently, calculations must be carried out incrementally.

The total volumetric strain is the sum of the elastic and plastic volumetric strain and is written as

$$\Delta\epsilon_v = \Delta\epsilon_v^e + \Delta\epsilon_v^p \quad (4.10)$$

where the superscripts e and p indicate the elastic and plastic components. If the soil yields at a void ratio of e_1 and a small increment of stress causes the yield surface to expand to a void ratio of e_2 , then the corresponding total change in volumetric strain is given by

$$\Delta\epsilon_v = \frac{\Delta e}{1 + e_o} = \frac{|e_2 - e_1|}{1 + e_o} = \frac{\lambda}{1 + e_o} \ln\left(\frac{p'_2}{p'_1}\right) \quad (4.11)$$

where p'_1 and p'_2 are the applied mean effective stresses producing the overall stress increment.

For the same stress increment the volumetric elastic strain increment is calculated with (4.7) as

$$\Delta\epsilon_v^e = \frac{p'_2 - p'_1}{K'} \quad (4.12)$$

or via

$$\Delta\epsilon_v^e = \frac{k}{1 + e_o} \ln\left(\frac{p'_2}{p'_1}\right) \quad (4.13)$$

by considering the unloading/reloading line associated with the maximum mean effective stress for the yield surface on which unloading initiates. The change in volumetric plastic strain is now calculated as $\Delta\epsilon_v^p = \Delta\epsilon_v - \Delta\epsilon_v^e$ and is expressed as

$$\Delta\epsilon_v^p = \frac{k - \lambda}{1 + e_o} \ln\left(\frac{p'_2}{p'_1}\right) \quad (4.14)$$

The shear strains are calculated from the representation of the yield surface. Furthermore, for the purposes of the present study, these strains are calculated by assuming that the plastic potential function and the yield function are the same. In other words, a normality condition is assumed. The resulting plastic deformation produces a volumetric and a deviatoric plastic strain components. The volumetric plastic deformation was given in (4.14), the deviatoric component of the volumetric plastic strain is obtained as

$$d\epsilon_s^p = d\epsilon_v^p \frac{q}{(M(\theta))^2 (p' - \frac{p'_c}{2})} \quad (4.15)$$

by considering the normal to the yield surface. Finally, the elastic deviatoric strains are obtained with

$$\Delta\epsilon_s^e = \frac{\Delta q}{3G} \quad (4.16)$$

One must use all the above strains (Eqs. (4.10) to (4.16)) in incremental calculations, because they are only valid for small changes in stress.

4.7 Calculation Procedure for The Stress-Strain Response of The Sand-TDA Mixture

From the equations of the last section one can determine the stress-strain response and the volume changes from the initial stress state. The required parameters are $p'_o, e_o, p'_c, \lambda, k, \theta, \varphi'_{cs}(\theta)$ and μ' .

The procedure used in this study to simulate the stress-strain response of the present triaxial tests results is as follows: a) Determine the TDA volumetric content θ of the sand-TDA mixture; b) Determine the mean effective stress and the deviatoric stress at initial yield by finding the coordinates of the initial yield surface with the effective stress path. This is achieved numerically by finding the root of the resulting coupled Eq. (4.1) and $p' = p'_o + \frac{q}{3}$ of the particular test; c) Determine the mean effective stress and deviatoric stress at failure with $p'_f = \frac{3p'_o}{3-M(\theta)}$ and $q'_f = \frac{3M(\theta)p'_o}{3-M(\theta)}$; d) Calculate the non-linear elastic modulus G using (9); e) Calculate the initial elastic volumetric strain with ((4.13) and initial elastic deviatoric strain using ((4.14); f) Discretize the stress path from the initial stress point to the failure point into a number of equal sufficiently small stress increments; g) Determine the major axis of the ellipse, using the current mean effective stress, for each stress increment via (4.1) with $p'_c = p' + \frac{q^2}{(M(\theta))^2 p'}$; h) Calculate the volumetric strain increment for each stress increment using (4.11); i) Calculation of the plastic volumetric strain for each stress increment using (4.14); j) Calculate the plastic deviatoric strain increment for each stress increment using (4.15); k) Calculate the elastic deviatoric strain increment for each stress increment via (4.16); l) Sum the elastic and plastic deviatoric strains increments to give the total deviatoric strain increment; m) Sum the total volumetric strain increments; n) Calculation of $\epsilon_1 = \epsilon^q + \frac{\epsilon}{3}$, $\sigma'_1 = \frac{2q}{3} + p'$ and $\sigma'_3 = p' - \frac{q}{3}$.

This procedure was coded and carried out numerically with the MATLAB software (Foriero, A. 2019).

4.8 Comparison of The Critical State Model with The Triaxial Test Results

The TDA-sand mixture parameters p'_o, e_o, p'_c, θ and $\varphi'_{cs}(\theta)$ were known for all the triaxial tests carried out in this study. The parameters λ, k and μ' were estimated.

In general, for soils $\frac{1}{10} \leq \frac{k}{\lambda} \leq \frac{1}{5}$ and $0.1 \leq \mu' \leq 0.4$ (Schofield, A. and Wroth, C.P., 1968). For the simulations, a ratio of $\frac{k}{\lambda} = 0.15$ and a value of $\mu' = 0.3$ were taken. Numerous simulations showed that the level-value of the shear strength at the critical state was insensitive to the values of these

parameters. It was also observed that these values affect mostly the initial portion of the stress-strain curve. The reason being that the critical state shear strength, obtained with the Modified Cam Clay model, is strongly affected by the critical state friction angle $\phi'_{CS}(\theta)$ through the Mohr-Coulomb relation $q_f = M(\theta)p'_f$. On the other hand, the yield surface, represented by the elliptic locus, is responsible for the elastic wall at a particular void ratio thus affecting the stress-strain curve mostly before failure. Consequently, emphasis will be placed from hereon on the shear strength of sand-TDA mixtures.

As previously mentioned, in this study the failure state is synonymous with the critical state. Moreover, we reiterate that establishment of the failure state of a sand-TDA mixture depends on a chosen strain criterion (Yang et al.,2002; Noorzad and Raveshi, 2017). In order to determine a value for the critical state friction angle, 4 different values of the vertical strain ($\epsilon_v = 10\%, 15\%, 20\%, 23\%$) were considered at 3 different TDA contents. Figure 4.14, Figure 4.15, Figure 4.16 and Figure 4.17 show typical determinations of the value of a mobilized friction angle $\phi'_{mob}(\theta)$ based on the triaxial test curves of Figure 4.5 and Figure 4.6. These values were obtained, for a particular TDA content, by linear regression based on the picked-off (p_f, q_f) pair at the 4 previously stated vertical strains.

The critical state friction angle is determined from a plot of the mobilized friction angles versus the vertical strains at which these mobilized values were obtained (Figure 4.18 and Figure 4.19). As previously mentioned, the critical state was difficult to attain because of the excessive deformations achieved during the tests (Figure 4.6).

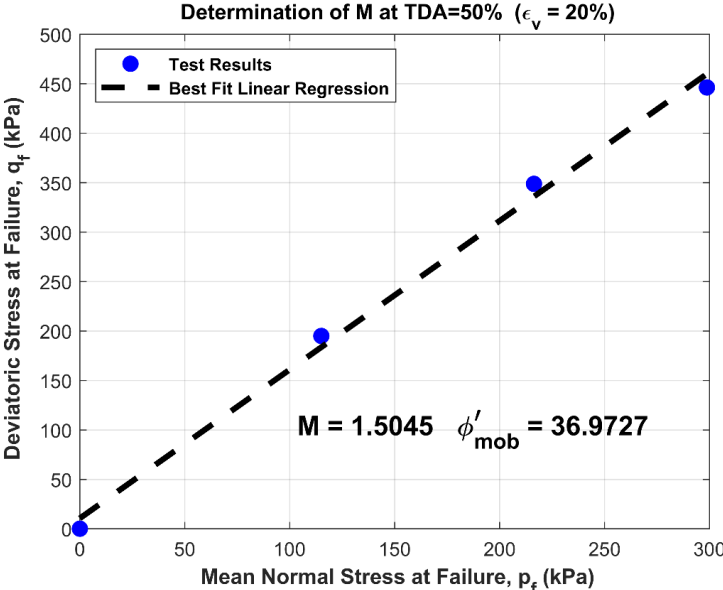


Figure 4.14 Determination of the frictional constant M at a TDA of 50 % and $\epsilon_v = 20\%$

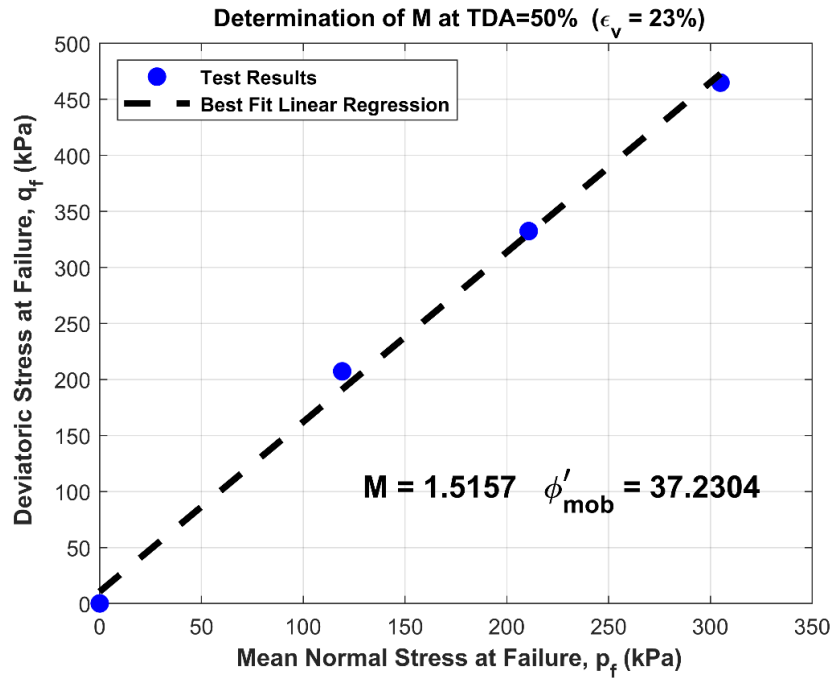


Figure 4.15 Determination of the frictional constant M at a TDA of 50 % and $\epsilon_v = 23$ %

The critical state friction angle is unique and generally obtained when the stress-strain curve attains a limiting value of the shear stress.

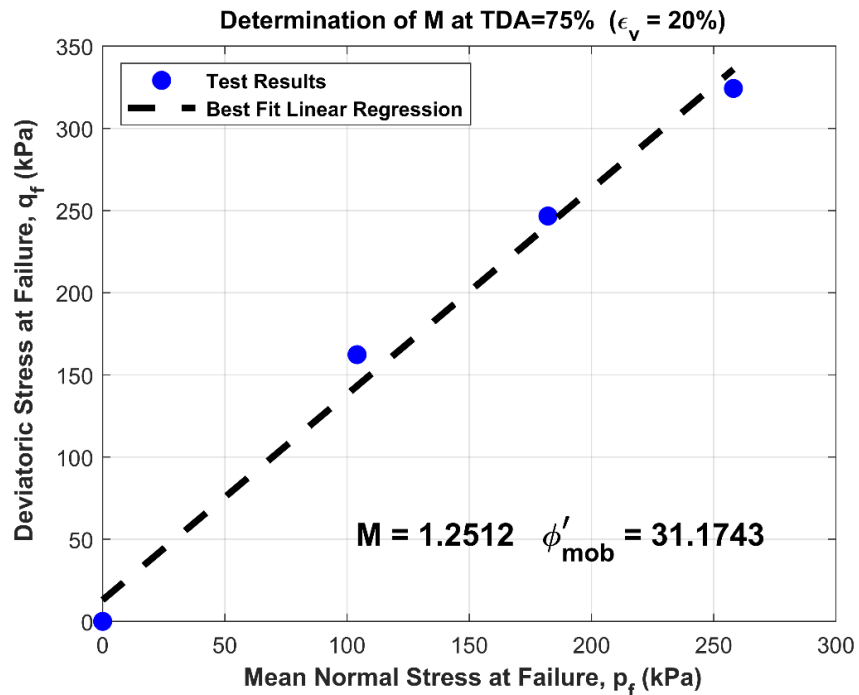


Figure 4.16 Determination of the frictional constant M at a TDA of 75 % and $\epsilon_v = 20$ %

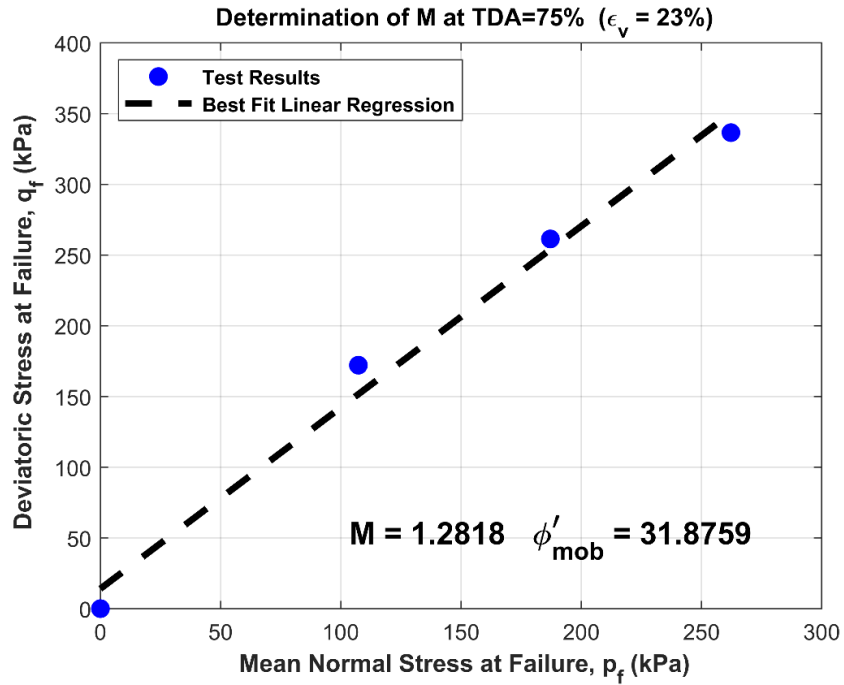


Figure 4.17 Determination of the frictional constant M at a TDA of 75 % and $\epsilon_v = 23$ %

Figure 4.18 and Figure 4.19 show that a critical state friction angle is asymptotically approached at very high vertical strains, where the value of the mobilized friction angles begin to level off. This leveling of the mobilized friction angle depends on the TDA content.

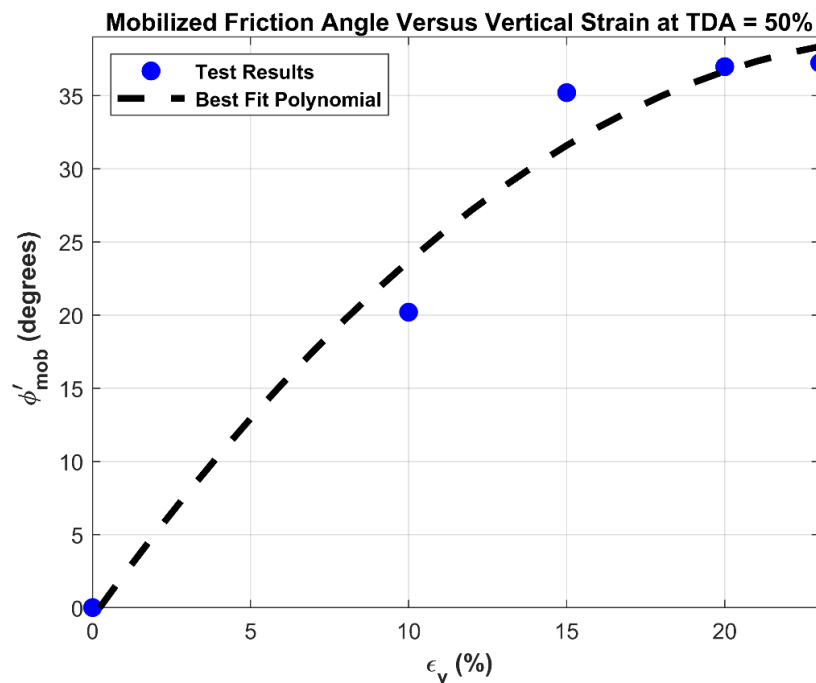


Figure 4.18 Mobilized friction angle versus vertical strain at TDA = 50 %

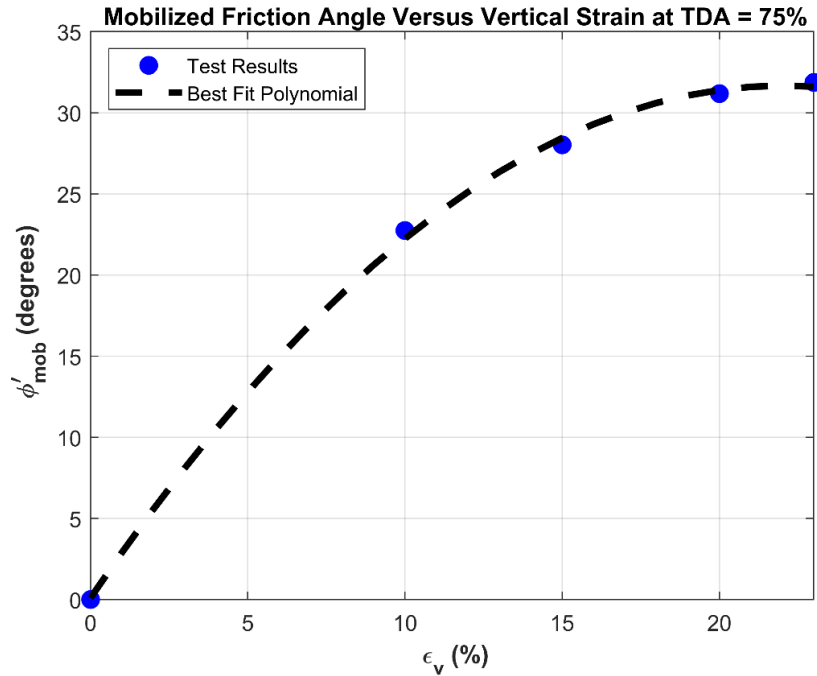


Figure 4.19 Mobilized friction angle versus vertical strain at TDA = 75 %

For a TDA volumetric ratio of $\theta = 50\%$ (Figure 4.18) a critical state friction angle greater than 38° is realistic since this value continues to grow. On the other hand, Figure 4.19, for the case $\theta = 75\%$, shows that a value of 34° could be taken as a lower bound. Consequently, in the simulations that follow, the critical state friction angle is bracketed in order to capture the measured shear strength of the triaxial tests.

The MCC yield surface as well as the CSL, for Ottawa sand and a typical Ottawa Sand-TDA mixture at $\theta = 50\%$, are shown in Figure 4.20. It is clear from this figure that the TDA reinforces the sand matrix because the yield surface is expanded and the critical state line assumes a greater inclination.

In all of the following simulations a sand-TDA sample is sheared at its current mean effective stress, p'_o , by increasing the axial stress, while keeping the cell pressure σ_3 constant. The imposed effective stress path has a slope of $\frac{q}{p'} = 3$. The load is incremented along the effective stress path until the sand-TDA mixture fails. Figure 4.21, Figure 4.22, Figure 4.23 and Figure 4.24 show the results of four triaxial test simulations using the MCC. These simulations were conducted at confining cell pressures of 100 and 150 kPa and TDA contents of 50% and 75%.

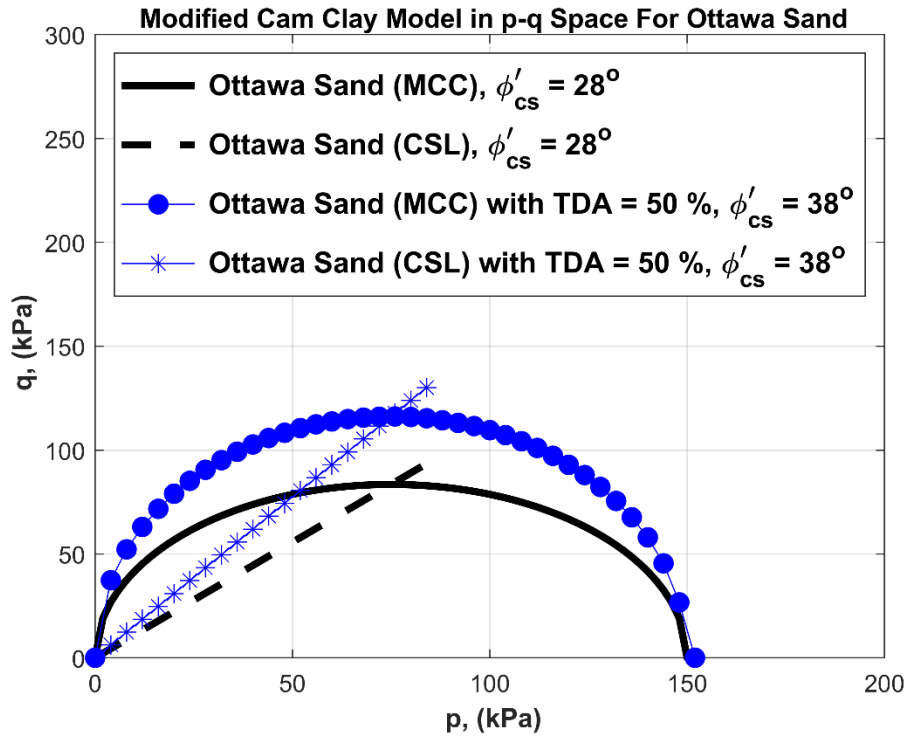


Figure 4.20 Modified Cam Clay Model in p-q Space for Ottawa Sand

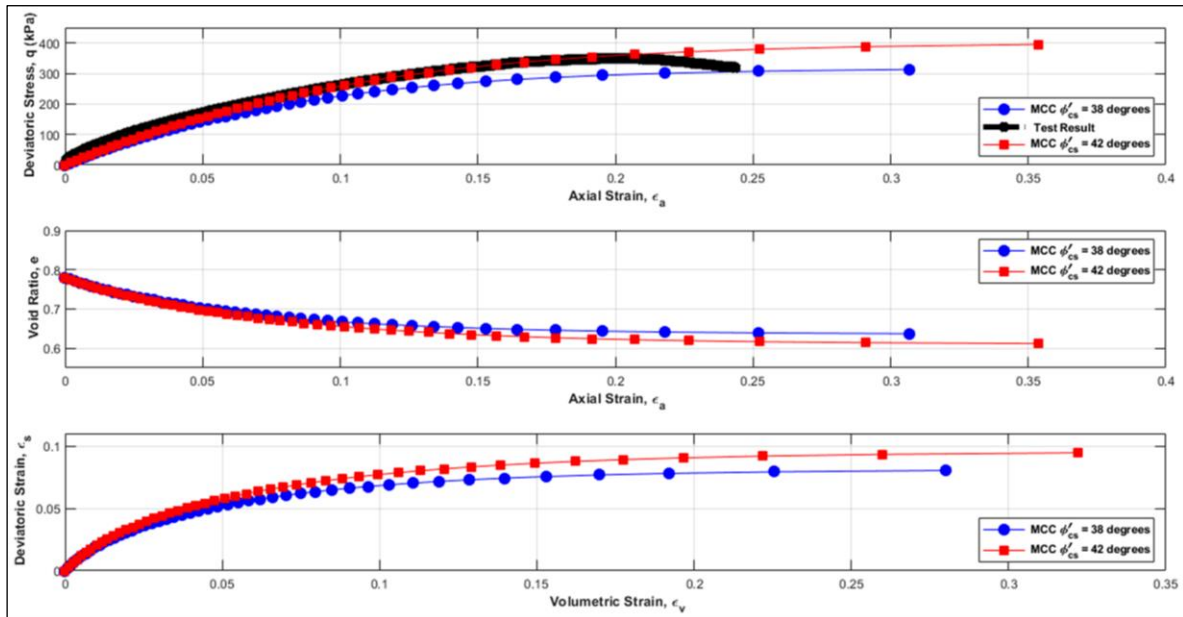


Figure 4.21 Deviatoric stress versus axial strain, void ratio versus axial strain, and deviatoric strain versus volumetric strain at 50% tire derived aggregate (TDA) and $\sigma_3 = 100 \text{ kPa}$.

Note: MCC = modified Cam Clay.

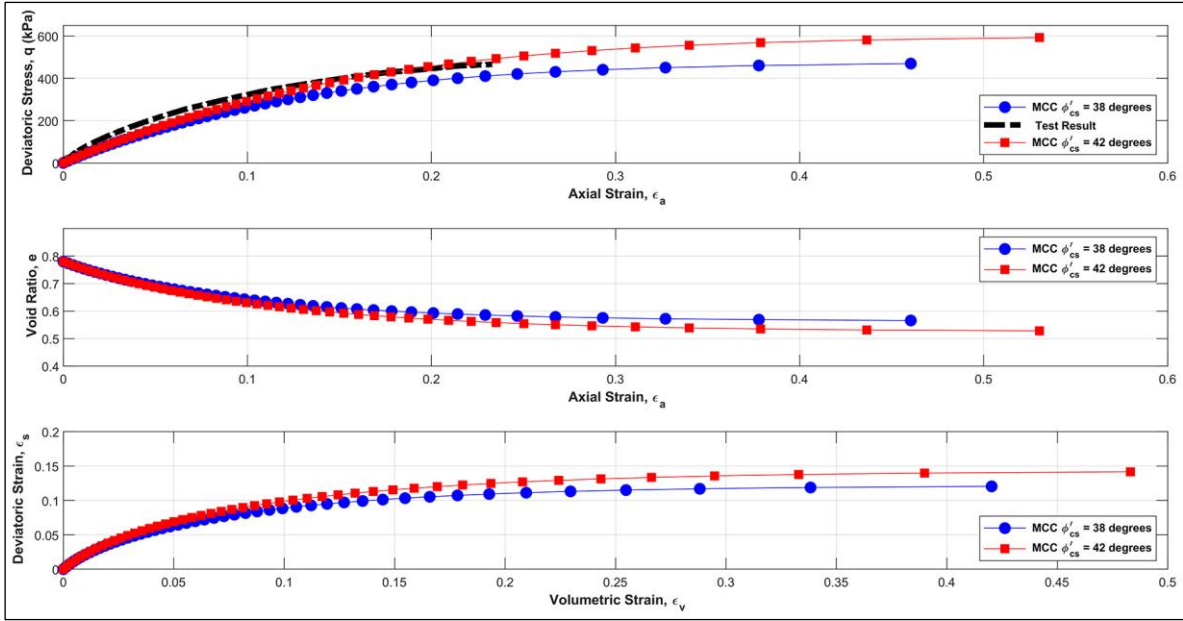


Figure 4.22 Deviatoric stress versus axial strain, void ratio versus axial strain, and deviatoric strain versus volumetric strain at 50% tire derived aggregate (TDA) and $\sigma_3 = 150 \text{ kPa}$.
 Note: MCC = modified Cam Clay.

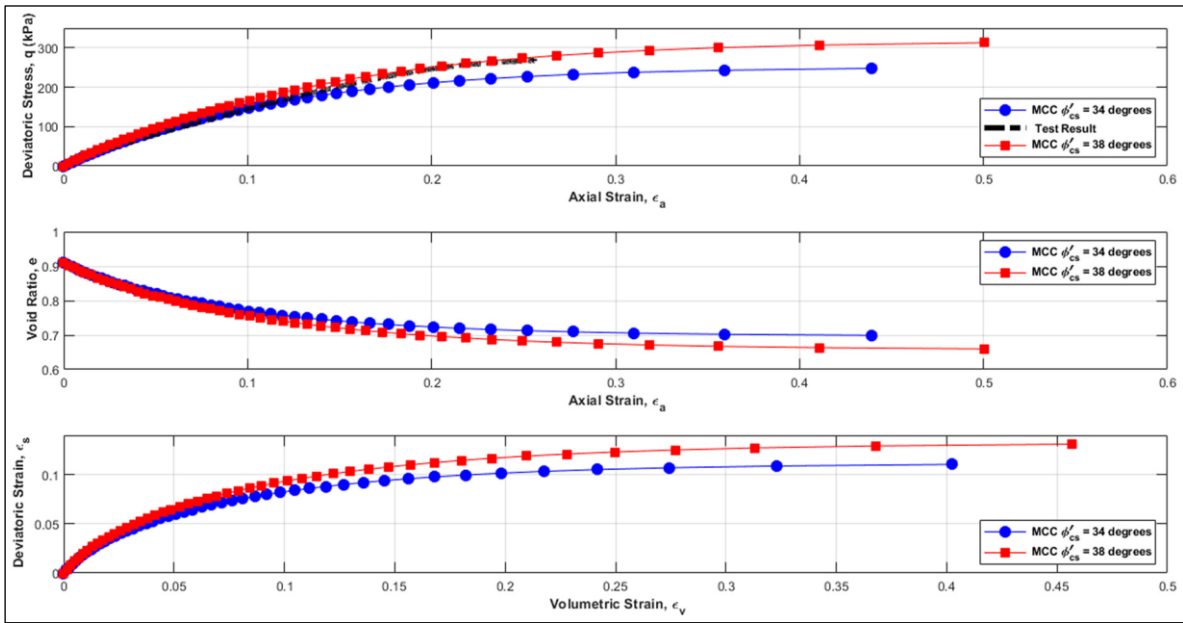


Figure 4.23 Deviatoric stress versus axial strain, void ratio versus axial strain, and deviatoric strain versus volumetric strain at 75% tire derived aggregate (TDA) and $\sigma_3 = 100 \text{ kPa}$.
 Note: MCC = modified Cam Clay.

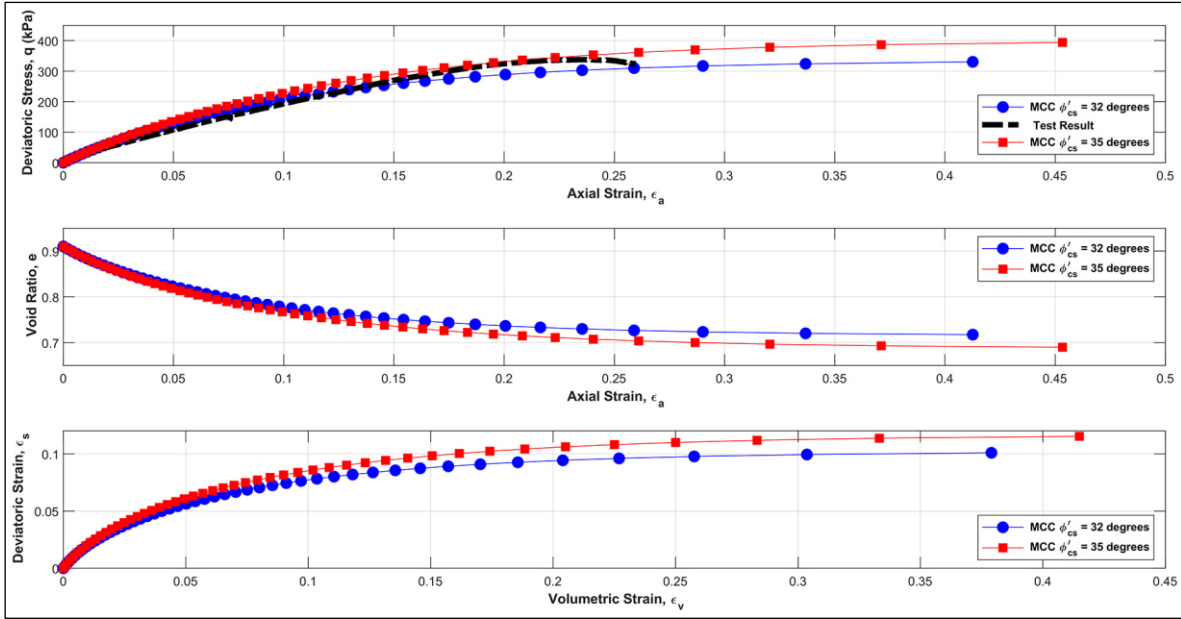


Figure 4.24 Deviatoric stress versus axial strain, void ratio versus axial strain, and deviatoric strain versus volumetric strain at 75% tire derived aggregate (TDA) and $\sigma_3 = 150 \text{ kPa}$. Note: MCC = modified Cam Clay.

Figure 4.21, Figure 4.22, Figure 4.23 and Figure 4.24 depict, for each of the four tests, the calculated deviatoric stress versus axial strain in comparison with the test results. The initial yield surface expands, and the stress-strain response is a curved path because the sand-TDA mixture behaves elastoplastically. As previously stated, the level of the shear strength is highly dependent on critical state friction angle which in turn depends on the TDA content. In all of these cases the deviatoric stresses obtained in the tests are bracketed by the theoretical curves generated with the MCC.

In all simulations, the curves of the void ratio versus vertical strain (Figure 4.21, Figure 4.22, Figure 4.23 and Figure 4.24) show an overall compression of the specimen. The initial void ratio attenuating towards a critical void ratio. Again, this behaviour conforms with that of loose granular materials. The resulting barrel shaped specimen (Figure 4.6) at the end of the test is a manifestation of this type of behaviour.

Finally, the curves of the deviatoric strain versus volumetric strain confirm that distortion increases with the volumetric strain. The curve assuming a non-linear shape with no peaks. In other words, no dilation is predicted by the MCC because all of the sand-TDA mixtures were in a loose state at the start of the test.

Overall, the critical state model is satisfactory if one wishes to predict the overall magnitude of the shear strength of initially loose sand-TDA mixtures. The model is highly dependent on the critical

state friction angle, φ'_{cs} , which in turn depends on the TDA volumetric content. For the loose TDA-sand mixtures used in the present study, the effect of the TDA content demonstrates a reinforcement of the sand matrix. However, this reinforcement diminishes as the TDA content increases.

Finally, triaxial tests on dense sand-TDA specimens are warranted because such samples will sustain higher stresses than loose samples. Moreover, one expects a peak value of the deviatoric stress at low vertical strains followed by a decrease with increasing strain, attaining a critical deviatoric stress. The determination of the critical friction angle in such tests will be evident provided the critical state is attainable. Moreover, since it is well known in the literature that the MCC model performs less well when dilation is present (Jefferies and Been, 2006), a new constitutive model capable of capturing this effect will be required.

4.9 Conclusions

Based on the triaxial test results obtained in this study the following conclusions transpired. In general, TDA content reinforces a sand matrix when compared with the original sand. For loose sand-TDA mixtures, results show that for a constant TDA volumetric ratio, the deviatoric stress increases with the confining stress. However, an increase in the TDA volumetric content tends to lower the shear strength of the sand-TDA mixture. A strain hardening behaviour was confirmed by the stress-strain curves, and by the barrel shape of the specimen at the end of the test which occurred at an axial strain of approximately 23%. Consequently, the critical state is difficult to attain in such cases.

Test results also showed a reduction in the stiffness of the sand-TDA mixtures as the TDA content increased. In particular the secant moduli decreased with an increase in TDA and a decrease of the confining pressure.

It is clear from the previous experimental results that the TDA volumetric ratio plays an important role as far as the behaviour of a mixture is concerned. A constitutive equation based on a critical state model (MCC) is satisfactory in predicting the level of the shear strength offered by a sand-TDA mixture. The calculated deviatoric stress versus axial strain curves, obtained via the model, captured the non-linear elastoplastic response obtained in the tests. The level of the shear strength is highly dependent on critical state friction angle which in turn depends on the TDA content. In all of these cases the deviatoric stresses obtained in the tests are bracketed by the theoretical curves generated with the MCC.

In all simulations, the curves of the void ratio versus vertical strain show an overall compression of the specimen. The initial void ratio attenuating towards a critical void ratio. Again, this behaviour conforms with that of loose granular materials.

Finally, the curves of the deviatoric strain versus volumetric strain confirm that distortion increases with the volumetric strain. The curves assume a non-linear shape with no peaks. In other words, no dilation is predicted by the MCC because all of sand-TDA mixtures were in a loose state at the start of the test.

4.10 List of Symbols

e_o	Initial void ratio
e_f	Void ratio at failure
e_Γ	Void ratio on the critical state line when $\ln(p_f) = 1$
ϵ_s	Total deviatoric strain
ϵ_s^e	Elastic deviatoric strain
ϵ_s^p	Plastic deviatoric strain
ϵ_v	Total volumetric strain
ϵ_v^e	Elastic volumetric strain
ϵ_v^p	Plastic volumetric strain
ϕ'_{cs}	Friction angle at the critical state
γ	Unit weight having unit $\frac{kN}{m^3}$
κ	Unloading/reloading index
p'	Mean effective stress in (kPa)
p'_o	Initial mean effective stress in (kPa)
p'_y	The mean effective stress at yield in (kPa)
p'_c	Maximum past mean effective stress in (kPa)
p'_f	Mean effective stress at failure in (kPa)
λ	Compression index
M	Friction constant

q	Deviatoric stress in (kPa)
q_f	Deviatoric stress at failure in (kPa)
q_y	Deviatoric stress at yield in (kPa)
σ_1	The total axial stress in (kPa)
σ_3	The total lateral stress in (kPa)
θ_p	TDA percentage volume ratio

4.11 Acknowledgments

The authors acknowledge and thank *Shercom Industries Inc.* in Saskatoon, Saskatchewan, Canada for their provision of the TDA used in the laboratory tests. Finlay, the authors also acknowledge the technical support of Christian Juneault (Technicien en travaux d'enseignement et de recherche) of Département de génie civil et de génie des eaux, Laval University.

4.12 Author Contributions

The authors confirm contribution to the paper as follows: study conception and design: A. Foriero, N. Ghafari; data collection: N. Ghafari, A. Foriero; analysis and interpretation of results: A. Foriero, N. Ghafari; draft manuscript preparation: A. Foriero, N. Ghafari. All authors reviewed the results and approved the final version of the manuscript.

4.13 Declaration of Conflicting Interests

The author(s) declared no potential conflicts of interest with respect to the research, authorship, and/or publication of this article.

4.14 References

- Anbazhagan, P., Monobar, D.R., Rohit, D. (2017). Influence of size of granulated rubber and tyre chips on the shear strength characteristics of sand-rubber mix. *Geomechanics and Geoengineering*, 12 (4), 266-278. doi:10.1080/1748025.2016.1222454.
- Apex Companies, (2008), Tarrtown bridge project case study guidance document for tire derived aggregate embankment construction and design strategic recycling contract No.353R06 Pollution Prevention Section", Equad, LLC 269 Great Valley Parkway Malvern, Pennsylvania 19355.

Bosscher, P.J., Edil, T.B., and Eldin, N., (1992). Construction and performance of shredded waste tire test embankment. *Transportation Research Record*, 1345, 44-52.

Bosscher, P., Edil, T. and Kuraoka, S., (1997), Design of highway embankments using tire chips", *Journal of Geotechnical and Geoenvironmental Engineering*, 123(4), pp. 295-380 304.

Foriero, A. (2019). Exposé MATLAB, Faculté des sciences et de génie, Informatique pour l'ingénieur, pp. 1-323.

Foriero, A. and Ghafari, N., (2020), Laboratory Creep Parameter Determination of Sand-TDA Mixtures and Subsequent FEM Validation", *Indian Geotechnical Journal*, doi.org/10.1007/s40098-019-00407-0.

Foose, G.J., Benson, C.H., and Bosscher, P.J. (1996). Sand Reinforced with Shredded Waste Tires". *Journal of Geotechnical Engineering*, 122(9), 760-767.

Ghazavi, (2004). Shear strength characteristics of sand mixed with granular rubber". *Journal of Geotechnical and Geological Engineering*, 22, 401-416.doi:10.1023/B:GEGE.0000025035.74092.6c

Humphrey, D.N. and Eaton, R.A., (1995), Field Performance of Tire Shreds as Subgrade Insulation for Rural Roads", *Proceedings of the Sixth International Conference on Low-Volume Roads*, Transportation Research Board, Vol. 2, pp. 77-86.

Jefferies, M., Been, K. (2006). Soil Liquefaction: A Critical State Approach (1st ed.). CRC Press. <https://doi.org/10.4324/9780203301968>.

Madhusudhan, B.R., Boominathan, A. and Banerjee, S. (2017). Static and large-strain dynamic properties of sand-rubber tire shred mixtures. *Journal of Materials in Civil Engineering*, 29 (10), 04017165. doi:10.1061/(ASCE) MT.1943-5533.0002016.

Mitchel, J. and Soga, K., (2005), "Fundamental of soil behaviour", 3rd ed., Chap. 12, Wiley, Hoboken, N.J., pp. 465-521.

Ngo, A. and Valdez, J., (2007), "Creep of Sand-Rubber Mixtures", *Journal of Materials in Civil Engineering*, Vol. 19, No. 12, pp.1101-1105.

Noorzad, R., Raveshi, M., (2017). Mechanical behaviour of Waste Tire Crumbs-Sand Mixtures Determined by Triaxial Tests., *Geotech Geol Eng.*, Vol. 35, pp. 1793-1802.

Rao, G.V., Dutta, R.K. (2006). Compressibility and Strength Behaviour of Sand-tyre Chip Mixtures. *Geotech Geol Eng* 24, 711-724. <https://doi.org/10.1007/s10706-004-4006-x>.

Roscoe, K.H., and Burland, J.B. (1968). On the generalized stress-strain behaviour of wet clay. Engineering Plasticity, J. Heyman and F. Leckie (eds.). *Cambridge University Press*, Cambridge, pp. 535-609.

Schofield, A. and Wroth, C.P. (1968). Critical State Soil Mechanics. McGraw-Hill, London.

Ward, J.I. and Sweeney, J., (2004), \An Introduction to the Mechanical Properties of Solid Polymers", 2nd Ed., John Wiley and Sons.

Wartman, J., Natale, M. and Strenk, P., (2007), "Immediate and Time-Dependent Compression of Tire Derived Aggregate", *Journal of Geotechnical and Geoenvironmental Engineering*, Vol. 133(3), pp. 245-256.

Yang, S., Lohnes, R.A., and Kjartanson, B.H. (2002). Mechanical Properties of Shredded Tires. *Geotechnical Testing Journal*, 25(1), 44-52. doi:10.1520/GT11078.

CHAPTER 5

5 Results and Discussion

The majority of the results and findings achieved through the experimental and numerical investigations conducted within the present study have been presented within chapters 3 and 4 of this thesis. Additional results that have not been earlier stated in previous chapters are presented in the present chapter. The main objective of this chapter is to discuss and validate the obtained results from chapters 3 and 4.

5.1 Results of Creep Parameter Determination

This section discusses the results achieved from the two laboratory experimental works including the creep tests of long duration and the direct shear tests simultaneously. Since the direct shear tests have been performed in order to modify the values of nominal stress and consequently achieve the values of the true stresses applied to the samples during the creep tests, hence, their results may not be presented individually. Therefore, a combination of the results of the two lab experiments has been rendered within the same section.

5.1.1 Results of Direct Shear Tests for Determination of the Nominal Stresses

The direct shear tests were performed aiming to determine the friction stress between the test materials and the side walls of the cylindrical aluminum cell. During the creep test, a friction force was produced between the test material and side walls of the cell which is made of Al 6061.

Therefore, a total of 25 direct shear tests were conducted on Al 6061 in contact with 5 different mixtures of sand and rubber having a TDA volume fraction content of $\theta_p = 0.2, 0.4, 0.6, 0.8, 1.0$ (same mixtures used in creep tests) subjected to 5 different nominal stresses including $\sigma = 20, 35, 50, 75, 100 \text{ kPa}$ (same nominal stresses applied during creep tests) in order to achieve the relevant friction stresses and consequently calculation of true stresses applied to samples within the creep tests.

The typical results of the direct shear tests between Al6061 and the test material having the TDA volume fraction content of $\theta_p = 0.6$ has been depicted in Figure 5.1. The same graph shows the typical

results for the test material of $\theta_p = 0.8$ was illustrated previously within section 3.6, as Figure 3.6. Moreover, the value of the friction angle obtained during the shear box tests have been provided within Table 3.1. As it can be observed the resulted friction angles between Al6061 and the four mixtures of $\theta_p = 0.2, 0.4, 0.6, 0.8$ are very similar and close to approximately 22 degrees. However, the values of friction angle obtained from the last series of tests between Al6061 and the sample containing pure TDA ($\theta_p = 1.0$) indicates an increase to reach approximately 27 degrees. The result was quite predictable. Rubber is considered as a *high friction material* which makes it suitable for the production of automobile tires and shoes. The soft and adhesive nature of the rubber makes it capable of intimate contact with the opposite surfaces. When mixed with rubber, the sand particles attach to the surface of the granulated rubber particles which prevents direct contact between the TDA and the aluminum walls. In return, test material made from pure TDA exhibits high friction in contact with the inner walls of the mold.

The values of the net forces (related to the creep tests) have been calculated in accordance with the estimated friction angles achieved at the end of the shear box tests (Table 3.1) and provided in Table 3.2, within section 3.6.

Consequently, the values of true stresses, which have been vertically applied during the creep tests, were calculated in accordance with the obtained net forces (Figure 5.2). The achieved values of the true stresses are stated within section 3.6 as Table 3.3.

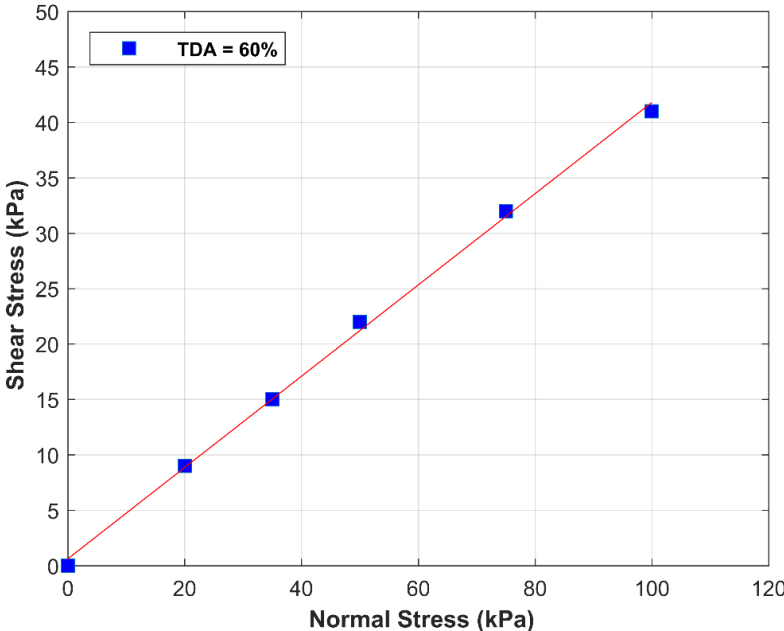
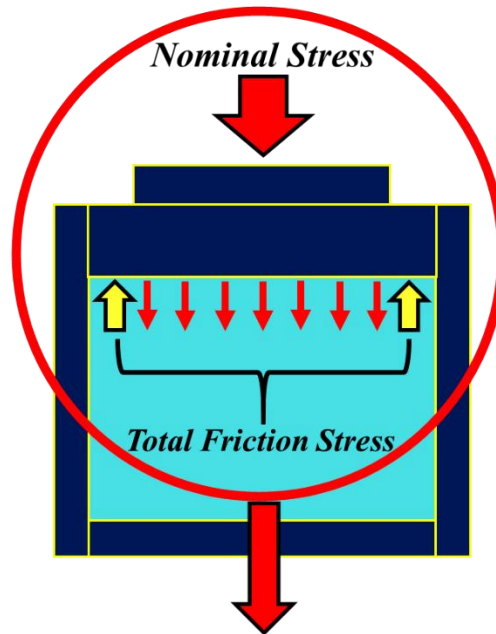


Figure 5.1 Direct shear test results of sand-TDA mixture ($\theta_p = 0.6$) resting on a plate made of aluminum alloy 6061



$$\text{True Stress} \times A_C = (\text{Nominal Stress} \times A_C) - (\text{Total Friction Stress} \times A_S)$$

Figure 5.2 Calculation of true stresses based on the nominal stresses and friction stresses (A_C : area of cylinder (cap) A_S : cross-section area of soil)

5.1.2 Discussion on the Creep Test Results

As mentioned earlier in the methodology section, a series of creep tests were performed for a long duration in order to determine the value of the creep parameters essential for conducting a numerical modeling of time dependent deformation behavior of the geomaterials composed of sand and TDA. Hence, a total of 25 creep tests were performed on 5 different mixtures having various TDA volume contents ($\theta_p = 0.2, 0.4, 0.6, 0.8, 1.0$) under 5 different vertical stresses including ($\sigma_v = 20, 35, 50, 75, 100 \text{ kPa}$) for the duration of 6000 minutes.

Figure 5.3 and Figure 5.4 illustrate the typical movements of the loading cap inside the cell during the different stages of the creep test. As it can be observed from Figure 5.3, the test is started simultaneously through the beginning of the vertical load application. As illustrated the load is applied to the specimen via the loading cap. It is evident from this figure that the first stage of the volumetric strain begins with an instantaneous strain which occurs simultaneously with applying the load.

Owing to the low dry density and the soft and flexible nature of the rubber, the TDA materials have a high compressibility characteristic in comparison with the typical soils such as Ottawa sand. Therefore, when the mixtures composed of sand and TDA are subjected to vertical loads, in particular the instantaneous strain occurs in a large scale and immediately.

After the completion of the instantaneous strain, the development of the creep strain begins (Figure 5.4). Although the magnitude of the creep strain is often less than the instantaneous strain and it occurs in a long period of time at a very low rate, it must be accurately estimated and carefully considered by the engineers as one of the design key-factors. By the beginning of the creep stage the strain rate starts to decrease considerably.

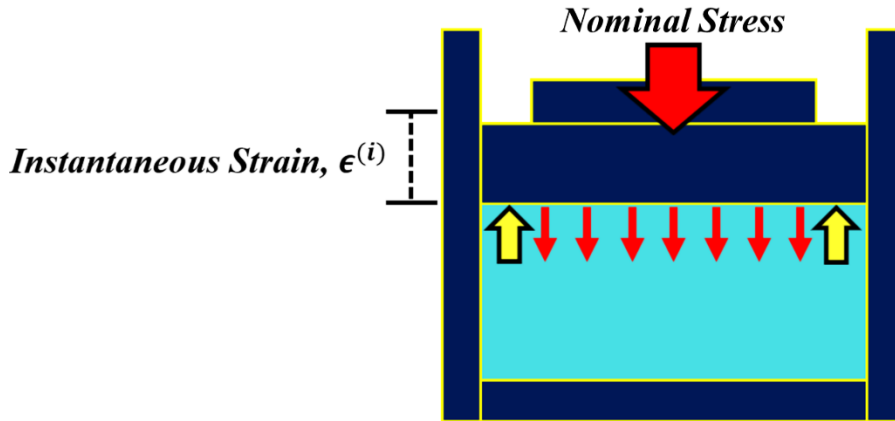


Figure 5.3 Instantaneous strain occurs simultaneously with applying the vertical load

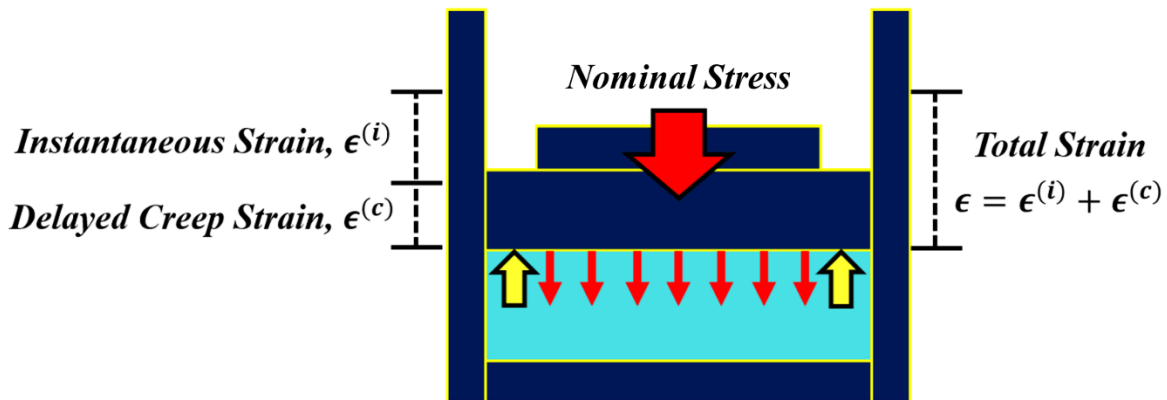


Figure 5.4 Illustration of the total strain which is sum of Instantaneous strain and creep strain

Consequently, as illustrated in Figure 5.4 the total strain is calculated through the sum of the instantaneous strain and the creep strain of the sample.

The test results of the creep strain versus time, for four samples having different TDA volume fractions content of $\theta_p = 0.4, 0.6, 0.8, 1.0$, and subjected to the five different constant stresses of

$\sigma_v = 20, 35, 50, 75, 100 \text{ kPa}$, are presented within Figure 5.5, Figure 5.6, Figure 5.7, and Figure 5.8, respectively.

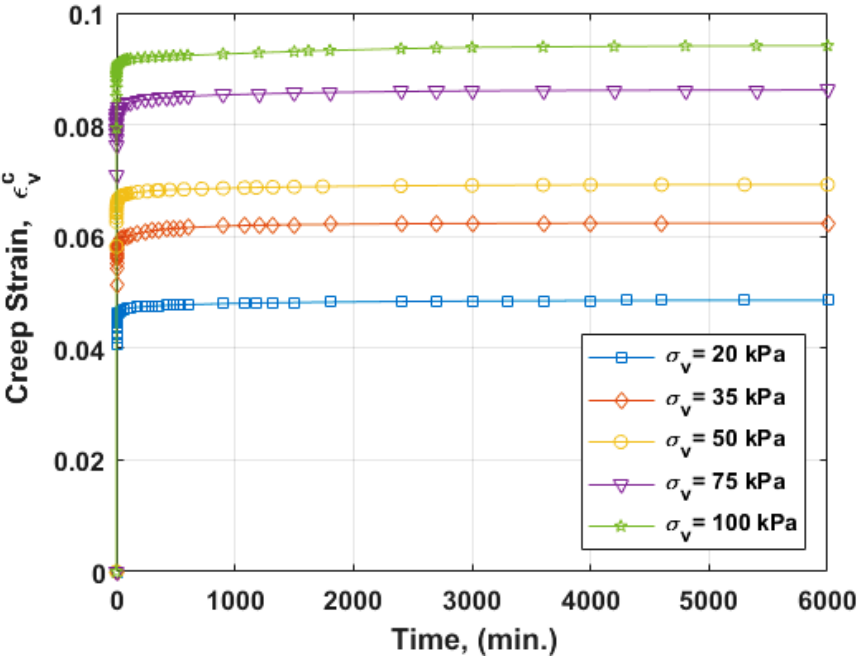


Figure 5.5 Creep strain versus time curves of sample having 40% TDA under 5 constant stresses

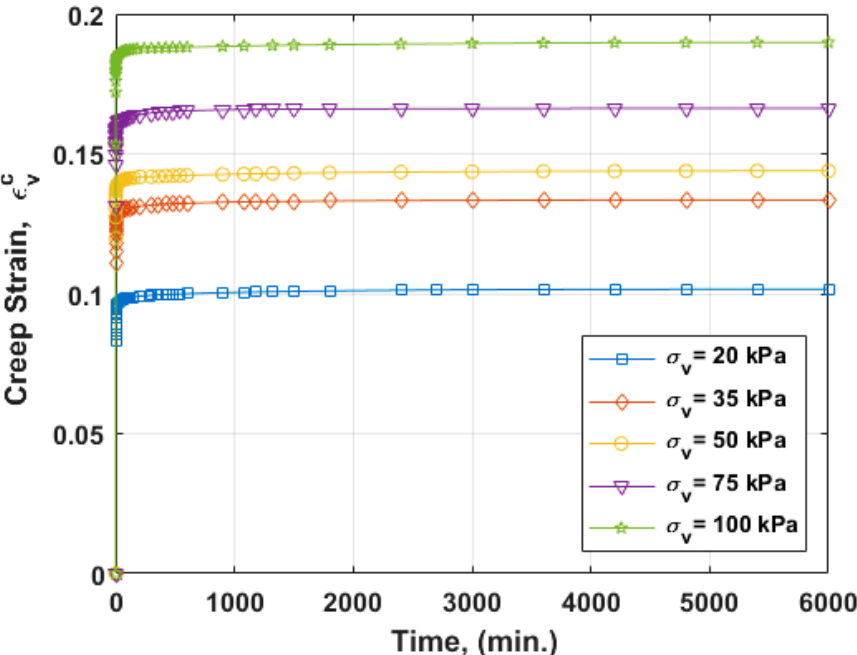


Figure 5.6 Creep strain versus time curves of sample having 60% TDA under 5 constant stresses

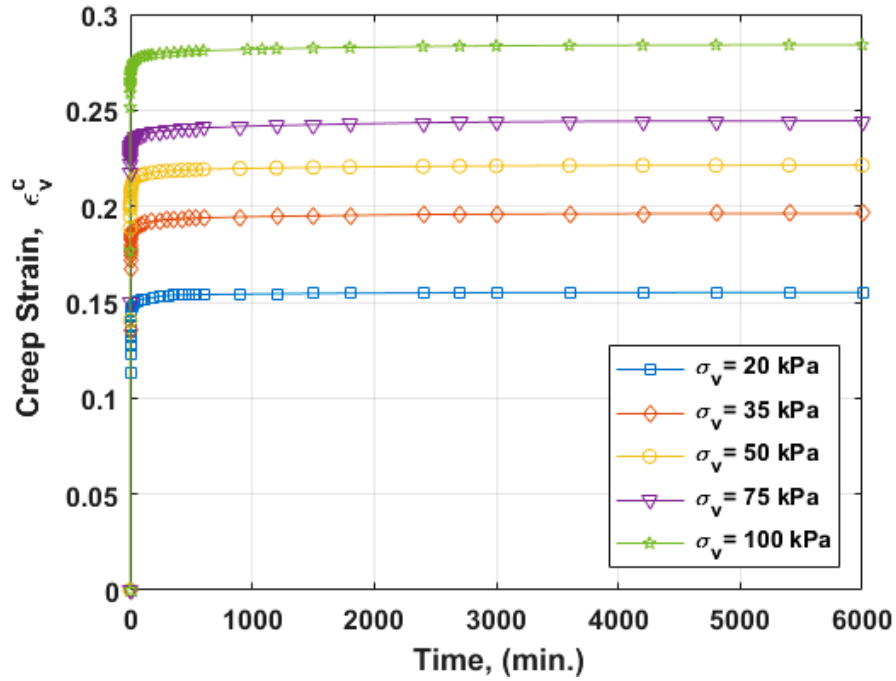


Figure 5.7 Creep strain versus time curves of sample having 80% TDA under 5 constant stresses

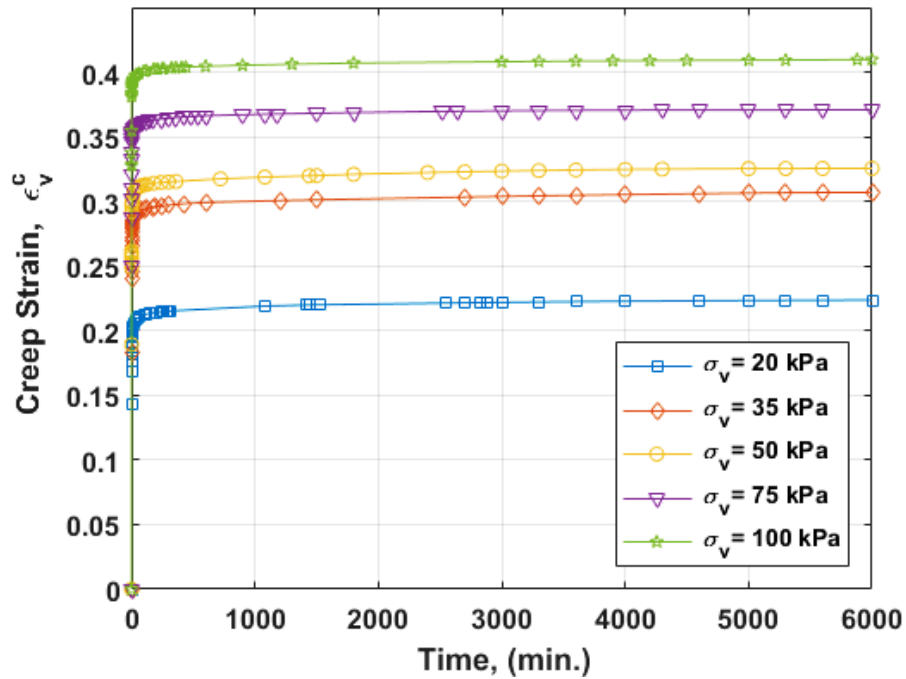


Figure 5.8 Creep strain versus time curves of sample having 100% TDA under 5 constant stresses

It is apparent from these figures that the magnitude of the creep strain increases with the increase in the intensity of the applied vertical stresses. Moreover, it is obvious from these figures that the

intensity of the creep strain increases with the increase in the TDA volume fraction content (θ_p). As it can be observed the creep strain ranged from 0.04 to 0.1 for the sample having 40% TDA (Figure 5.5), from 0.075 to 0.2 for the sample having 60% TDA (Figure 5.6), from 0.1 to 0.3 for the sample having 80% TDA (Figure 5.7) and finally, from 0.14 to 0.41 for the sample having 100% TDA (Figure 5.8). For instance, Figure 3.10, which was presented earlier in chapter 3, depicts the creep behavior of pure TDA and is the test with the highest creep response. Hence, one observes from these figures that the magnitude of the creep strain is highly influenced by the TDA volume fraction content (θ_p).

In chapter 3, within section 3.7, Figure 3.7 and Figure 3.9 have illustrated the plots of constant stress creep curves of the total strains respectively for the samples having TDA volume fraction content of $\theta_p = 0.4, 0.8$, in accordance with the obtained results from the creep tests. As it can be observed in these figures the total strains are plotted over the logarithmic time aiming to clearly and perceptibly depict the first part which is related to the instantaneous strain.

It is obvious from these figures that as expected the magnitude of the total strain increases with the increase in intensity of the applied vertical stresses. Moreover, it is evident from these figures that the intensity of the instantaneous strain and the creep strain and consequently the total strain is increased with the increase in the TDA volume fraction content (θ_p).

Through a closer look at the Y axis, it can be observed that the ascending slope of the curves at the secondary deformation phase (creep strain curves) where the $\theta_p = 0.8$ (Figure 3.9) is slightly steeper than the ascending slope of the creep strain curves plotted for the sample with $\theta_p = 0.4$ (Figure 3.7). Although, the difference in the intensity of the instantaneous strain occurred in the two above-mentioned samples is obviously apparent.

Furthermore, the curves in Figure 3.8 are the total strain of Figure 3.9 which are plotted as function of the applied stress for specific times of the test. All these figures (Figure 3.7, Figure 3.8 and Figure 3.9) reveal the nonlinear nature of the creep response. As it has been discussed earlier in chapter 4, the instantaneous strain may contain an elastic and plastic contribution and is totally unrelated to the time-dependent creep strain. Hence, in order to isolate the creep strain and thereby determining the creep parameters, as mentioned previously in section 3.7, the instantaneous strain was subtracted from the total strain. The instantaneous strain is determined from the images of the dial indicator recorded by a camera at $t = 6$ s. This time ($t = 6$ s) is determined in accordance with the logarithmic plots of creep curves of the total strains drawn for samples containing different TDA content (Figure 3.7 and Figure 3.9). The observations and analysis of the mentioned camera recording images from dial

movement rate confirm the time $t = 6$ s which determined from the logarithmic plots of creep curves of the total strains.

As discussed in chapter 3 under section 3.9, the values of the time creep parameter b are calculated using the slope of the curves obtained from the creep tests through the equation $b = 1 - \left(\frac{\Delta \log(\dot{\epsilon}_1^c)}{\Delta \log(t)} \right)$. The typical results of time creep parameter b calculated through the above-mentioned equation for two samples of $\theta_p = 0.6$ and 1.0 and illustrated previously in chapter 4 (Figure 3.11 and Figure 3.12). The curves of the parameter b for two other samples of $\theta_p = 0.4$ and 0.8 are plotted here and shown in Figure 5.9 and Figure 5.10, respectively. The trend in all of these tests confirms that the creep rate versus time curves, for all purposes, are parallel.

As it can be observed from these figures, the creep rate versus time curves is parallel together and the creep parameter b is variable in accordance with the magnitude of the axial stress and the TDA volume fraction content (θ_p). Although, as reported earlier in this study, the axial stress related variations are negligible as the plotted curves associated with parameter b are situated very close to each other in all the figures. Therefore, as mentioned earlier, from the engineering and practical point of views, an average b value gives an appropriate estimate of this creep parameter as presented in the figures. Moreover, parameter b is associated with time in the creep laws, previously stated in chapter 3, hence, the greater its value, the higher is the magnitude of the creep strains.

As previously discussed in chapter 3 under section 3.9, the values of the stress associated creep parameter n are calculated using the slope of the curves obtained from the creep tests through the equation $n = \frac{\Delta \log(Cb)}{\Delta \log(\sigma_1 - \sigma_3)}$ where $Cb = \left[\left(\frac{\sigma_1 - \sigma_3}{\sigma_{cp}} \right)^n \left(\frac{\dot{\epsilon}_c}{b} \right)^b \right]$.

The typical results of creep parameter n calculated through the above-mentioned equation for the sample of $\theta_p = 0.6$ and illustrated previously in chapter 4 (Figure 3.13). The curves of the parameter n for three other samples of $\theta_p = 0.4, 0.8$ and 1.0 are plotted here and shown in Figure 5.11, Figure 5.12 and Figure 5.13, respectively.

Since as previously mentioned, the value of confining stress $\sigma_3 = K_0 \sigma_1$ is very difficult to measure but not necessary in such tests, typical K_0 values for loose, medium and dense sand were assumed. As expected, these values do not influence the slope of the resulting line in a log-log plot of Cb versus $\sigma_v - \sigma_h$. The K_0 values obtained from the experiments are shown in Figure 5.11, Figure 5.12, and Figure 5.13

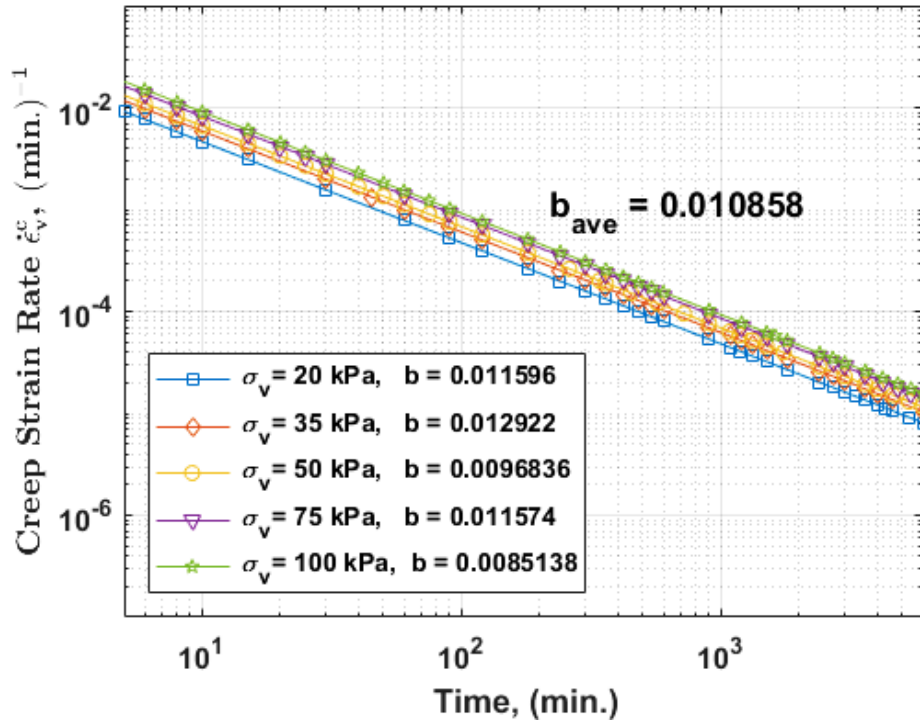


Figure 5.9 Determination of the time creep parameter b (40% TDA)

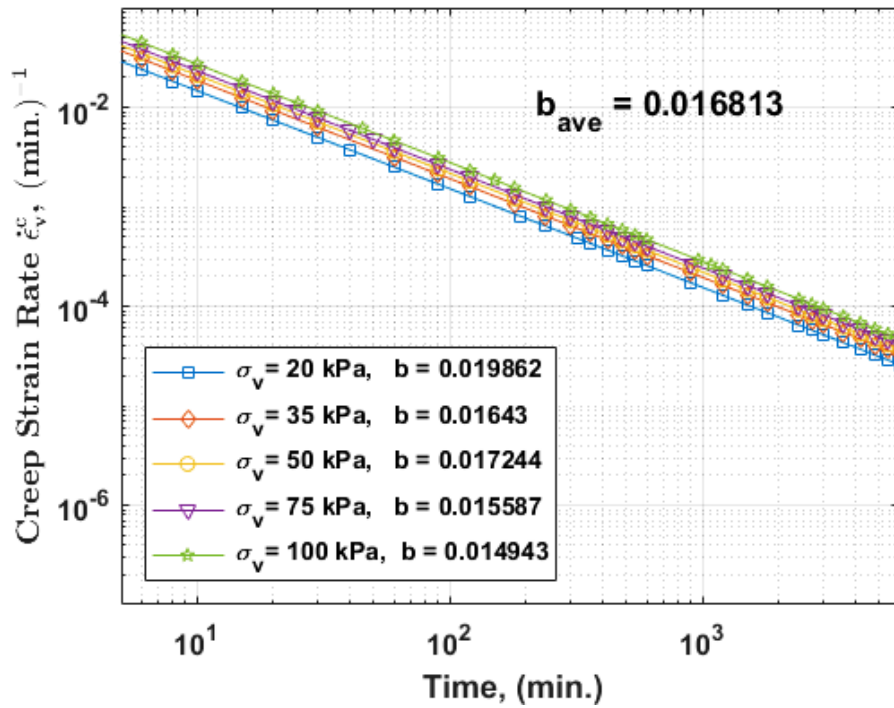


Figure 5.10 Determination of the time creep parameter b (80% TDA)

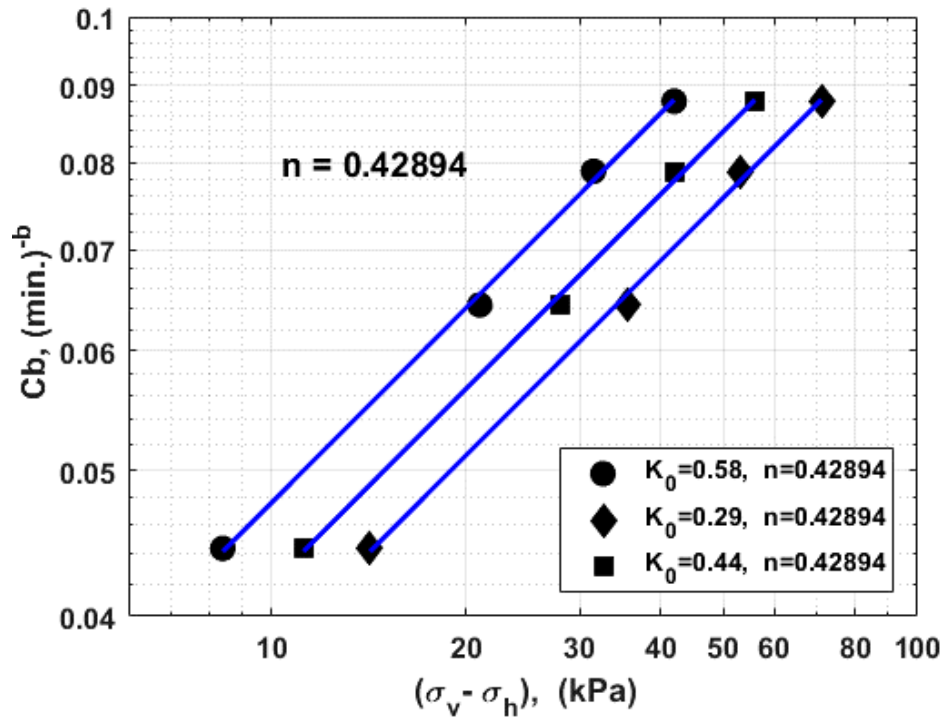


Figure 5.11 Determination of the creep parameter n (40% TDA)

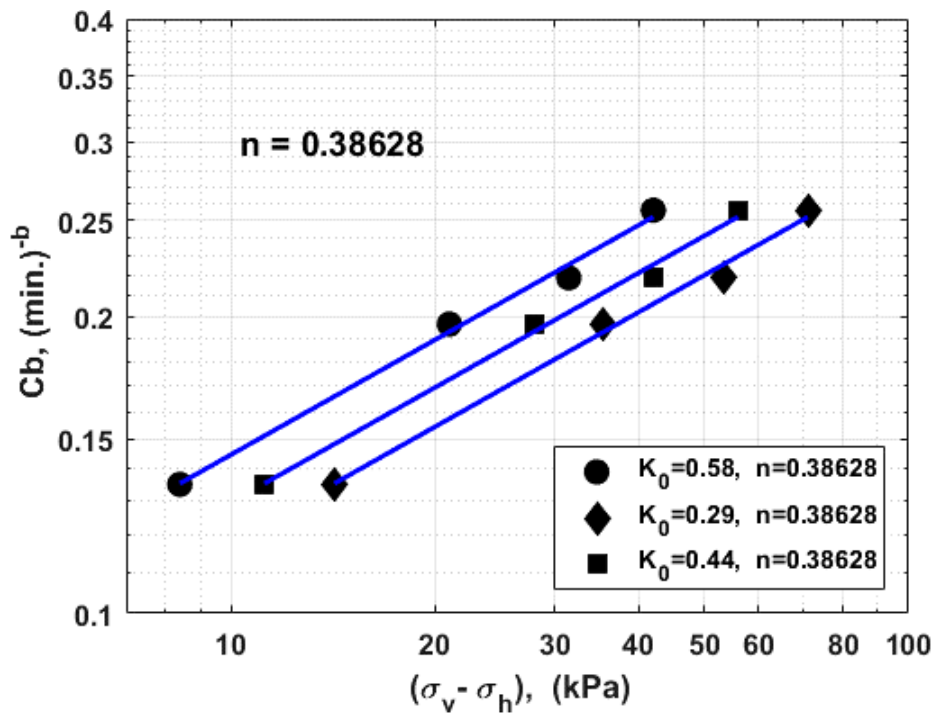


Figure 5.12 Determination of the creep parameter n (80% TDA)

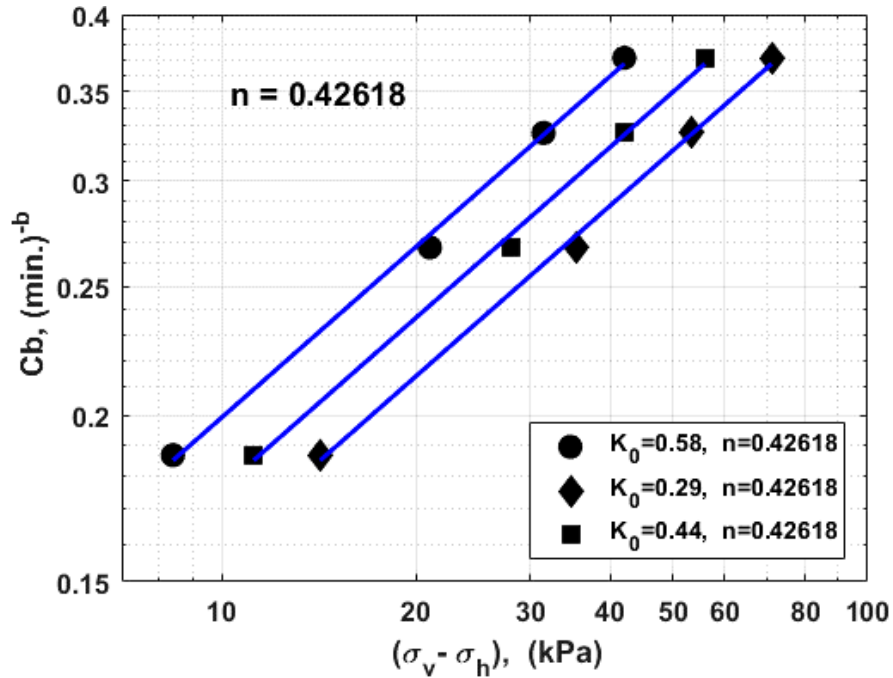


Figure 5.13 Determination of the creep parameter n (100% TDA)

5.2 Evaluation of the Creep Law Based on the Back-Calculated Creep Parameters

Owing to verify the precision of the back-calculated creep parameters, the creep law (Eq. (3.9)) together with the test results are plotted in a log-log plot of $\dot{\epsilon}_c$ vs time. Figure 5.14 and Figure 5.15 illustrate the comparisons of the results of creep law with the lab test results for samples having TDA volume fraction content of $\theta_p = 0.6, 0.8$ respectively. It is obvious from these figures that the curves obtained through this creep law give a good approximation of the test results.

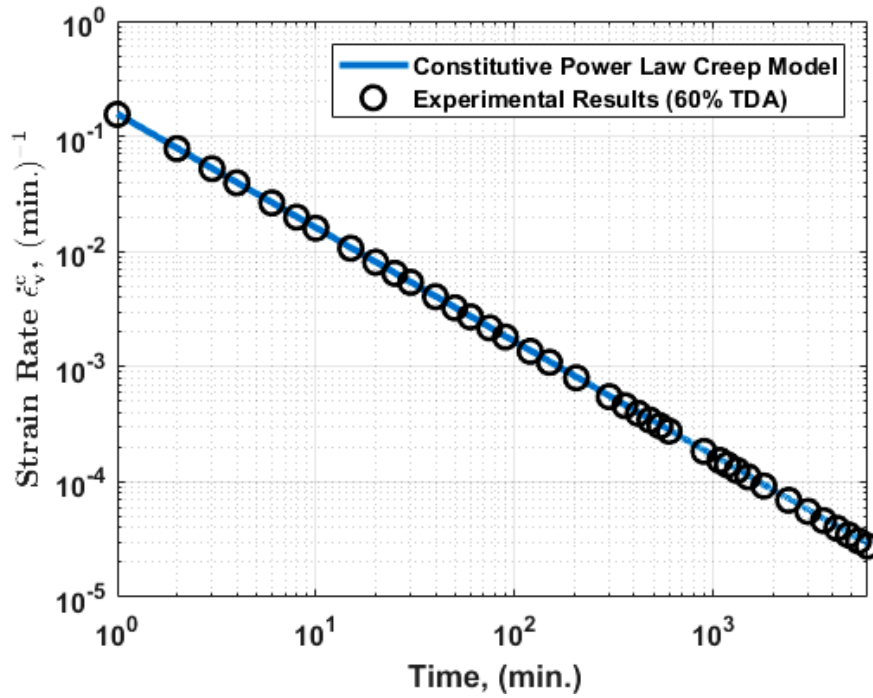


Figure 5.14 A comparison of the creep law with the test results for $\sigma_v = 75 \text{ kPa}$ (60% TDA)

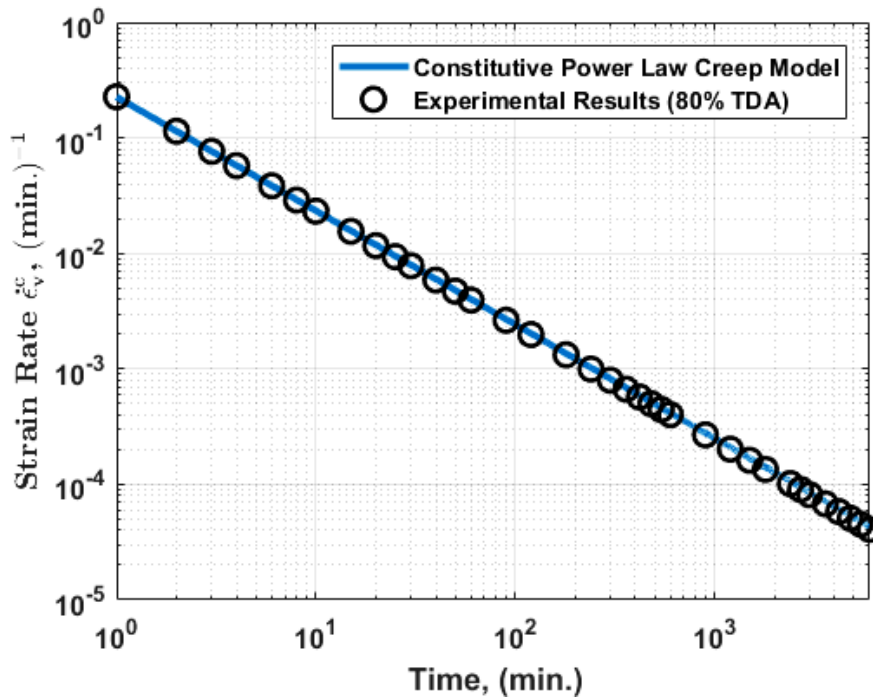


Figure 5.15 A comparison of the creep law with the test results for $\sigma_v = 75 \text{ kPa}$ (80% TDA)

5.3 Rebound Behavior of a Sand-TDA Sample Under Triaxial Testing

Aiming to investigation of the rebound behavior of sand-TDA mixtures under triaxial loading, a sand-TDA sample containing 60% TDA ($\theta_p = 0.6$) was prepared and subjected to the $\sigma_3 = 300 \text{ kPa}$ for a long duration of approximately 5000 min within the same triaxial apparatus. The sample was prepared through the same procedure as previously employed for other sample preparation that has been explained in chapter 2. Moreover, the size of the sample was similar to that of other previously tested samples (35.1 mm in diameter and 67.5 mm in height). Again here, a conventional drained triaxial test displacement rate of 0.0061 mm/min was maintained throughout the entire of the test including unloading stage. A constant $\sigma_3 = 300 \text{ kPa}$ was applied to the sample during the entire of the test while the sample was axially loaded and unloaded (deviatoric stress was changing) in order to record the rebound behavior of the mixture.

The resulting curve of deviatoric stress versus axial strain during axial loading and unloading has been illustrated in Figure 5.16, whereas the obtained curve of axial strain versus time is plotted within the Figure 5.17. These figures demonstrate the nonlinear behavior of the sand-TDA mixture during the rebound process. Hence, it is obvious from these figures that the deformation and rebound behaviors of the sand-TDA mixtures during axial loading and unloading are very similar.

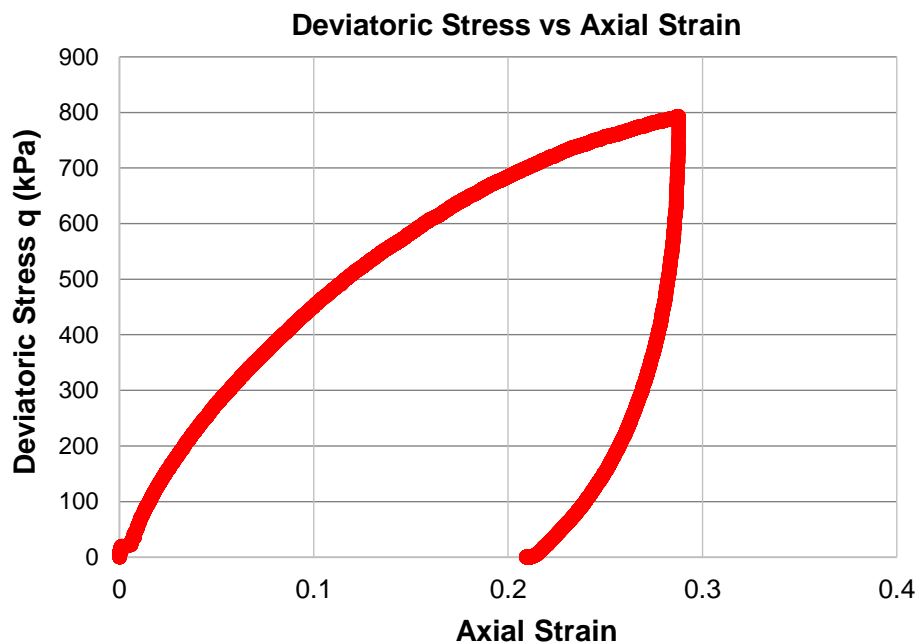


Figure 5.16 Rebound behavior of sand-TDA mixture having $\theta_p = 0.6$ under $\sigma_3 = 300 \text{ kPa}$ triaxial loading

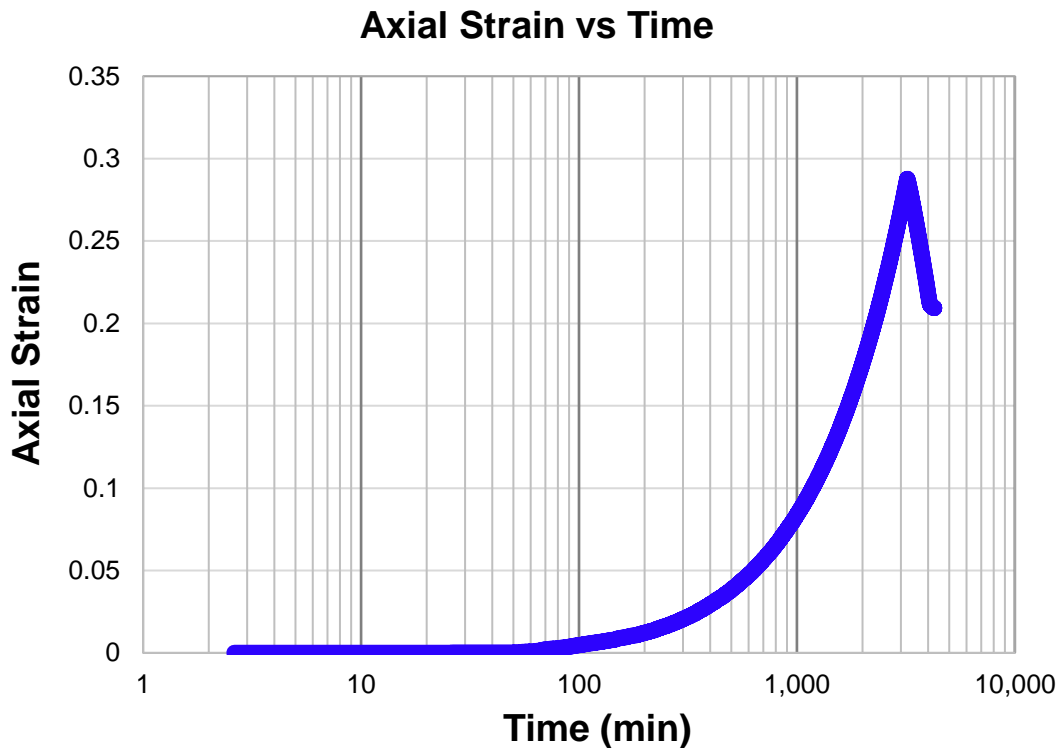


Figure 5.17 Axial strain vs time during triaxial loading and rebound for sand-TDA mixture of $\theta_p = 0.6$ under $\sigma_3 = 300 \text{ kPa}$

5.4 Simulation of the Behavior of the Sand-TDA Mixtures During a Tunnel Excavation

5.4.1 Introduction

This example simulates the behavior of a soil-tire aggregate mixture during the tunnel excavation. The surface settlement and the extent of the plastic region around the tunnel are important parameters required to predict the necessary reinforcements during the excavation.

In order to calculate the in-situ stresses, two steps are performed in COMSOL. In the first step of this study, the state of the soil before the excavation of the tunnel is computed. In the second step, the elastoplastic behavior is examined once the soil is removed. For comparison purposes, this example also considers the soil without TDA reinforcement.

In order to speed up the calculations, the soil in the first step is considered elastic whereas in the second step the soil is modeled with the Drucker-Prager soil plasticity model. The simulations will be limited to 2D.

5.4.2 Finite Element Mesh

The geometry consists of a soil layer that is 60 m deep and 90 m wide. A zone measuring 20 m in width and 40 m in height is filled with a mixture of soil-tire-derived aggregates. This zone will host the tunnel after excavation. A circular cavity measuring 20 m in diameter is excavated at a depth of 30 m on the axis of symmetry. A bedrock is assumed to be 60 m below the surface and constraints the vertical displacements. A roller boundary condition is used for simulating an infinite extension of the soil in the lateral direction.

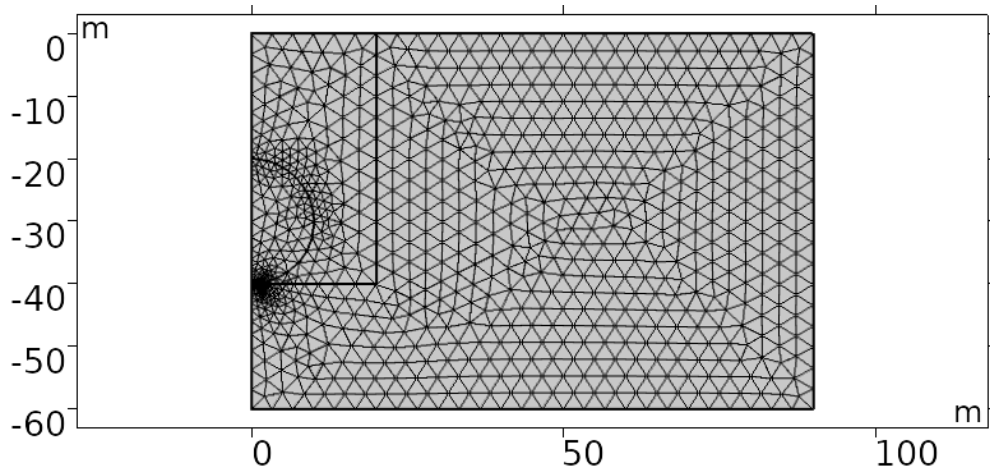


Figure 5.18 Finite Element Mesh

5.4.3 Soil Properties Aggregate

Young's Modulus, $E = 20 \text{ MPa}$ and Poisson's ratio $\mu = 0.3$

Cohesion $c = 150 \text{ kPa}$ and angle of internal friction $\varphi' = 28^\circ$

Density = 2000 kg/m^3

The Drucker-Prager criterion matches the material parameters to the Mohr-Coulomb criterion

5.4.4 Properties of Soil-Tire Aggregate Mixture

Young's Modulus, $E = 20 \text{ MPa}$ and Poisson's ratio $\mu = 0.3$

Cohesion $c = 150 \text{ kPa}$ and angle of internal friction corresponding to 50 % TDA is $\varphi' = 38^\circ$

Density = 1500 kg/m^3

The Drucker-Prager criterion matches the material parameters to the Mohr-Coulomb criterion

5.4.5 Results and Discussion

The next figures show the stress distribution due to gravity for the cases with and without TDA (first step of the analyses). The roller and symmetric boundaries conditions cannot create a homogeneous vertical variation for the soil deposit with the TDA (Figure 5.20) because of the 20 by 40 m zone which will eventually host the excavation.

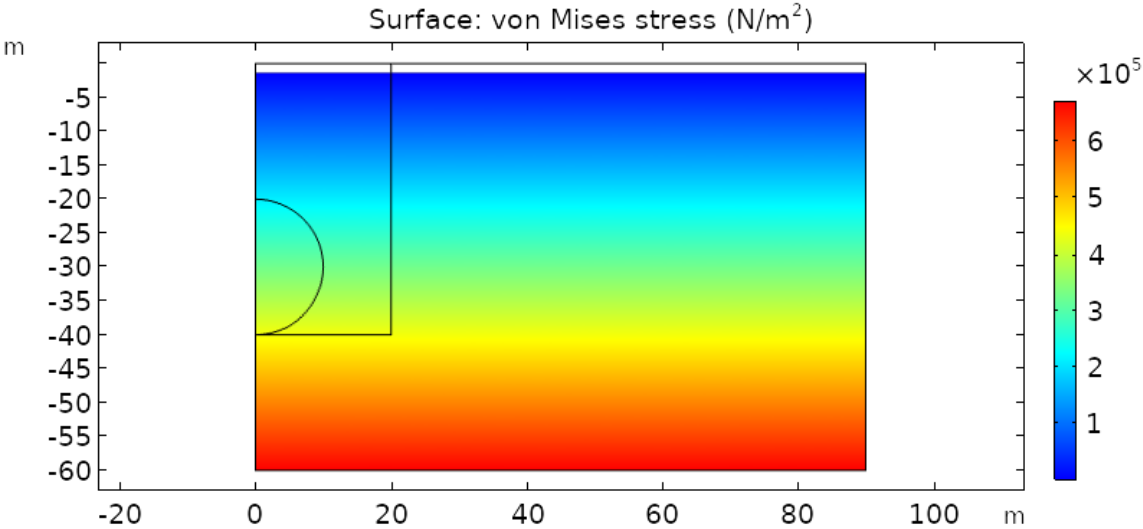


Figure 5.19 The initial stress field for a soil deposit with no TDA

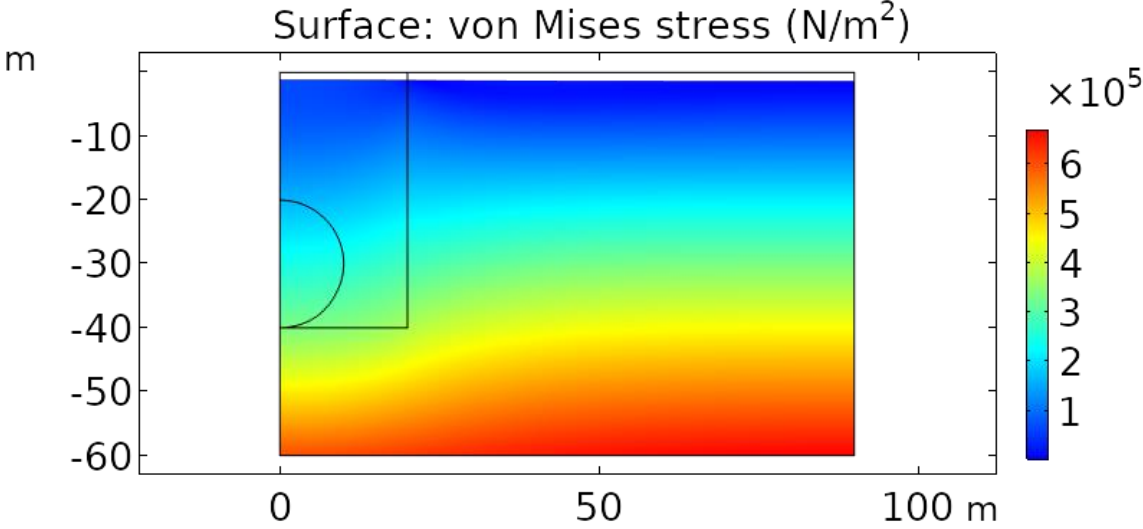


Figure 5.20 The initial stress field at 50% TDA

In the second step, the tunnel domain or the excavation zone of the soil-TDA mixture is extracted. The plasticity analyses using the Drucker-Prager plasticity model is implemented for both the cases

with and without TDA. In Figure 5.21 and Figure 5.22 the Von Mises stress contours are shown respectively before and after the excavation. The extent of the region that experiences plasticity, in both cases, is also shown in Figure 5.23 and Figure 5.24. It is evident from these Figures that the soil-TDA mixture produces a more limited plastic zone.

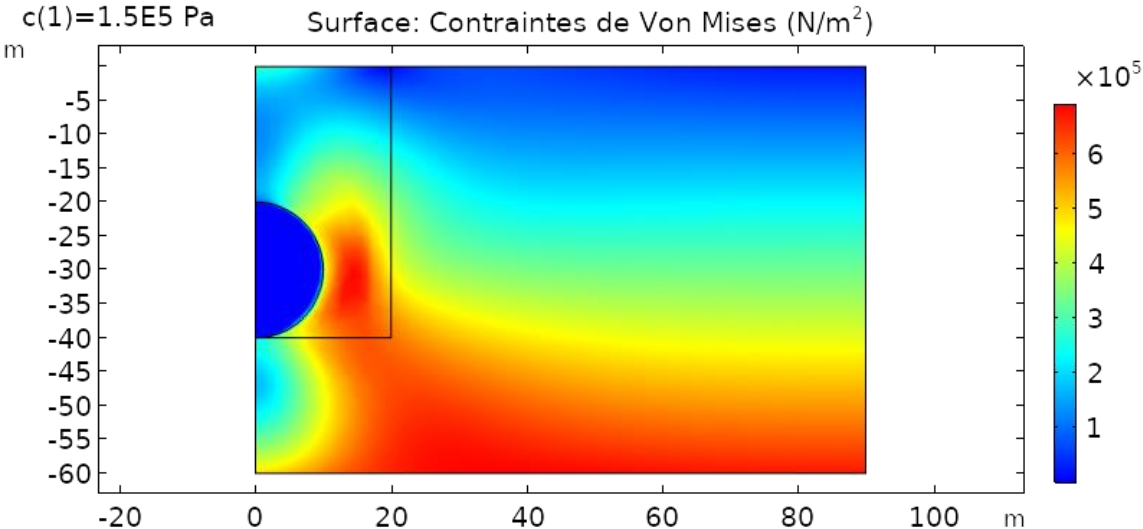


Figure 5.21 The stress field after excavation with no TDA

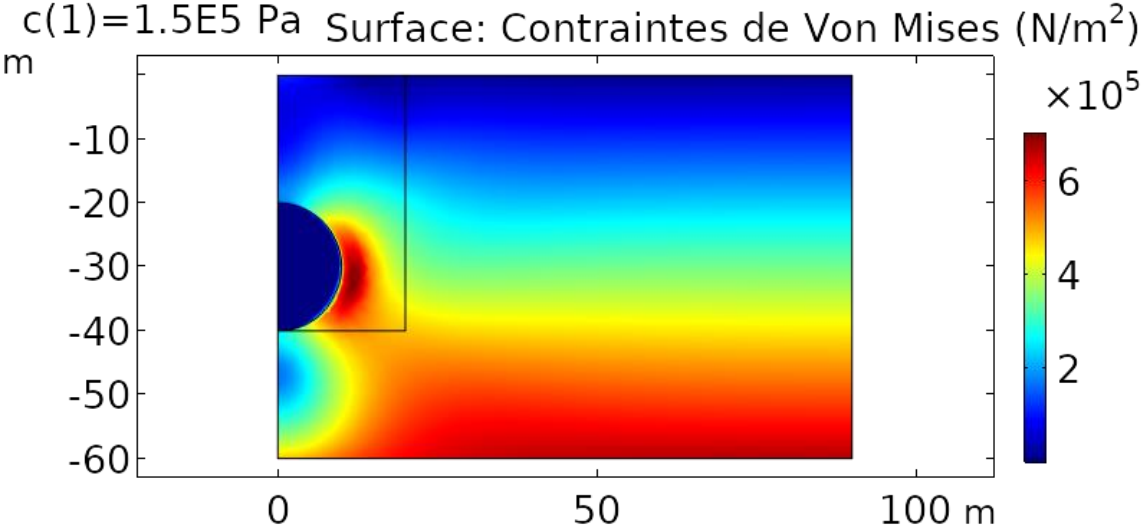


Figure 5.22 The stress field after excavation at 50% TDA

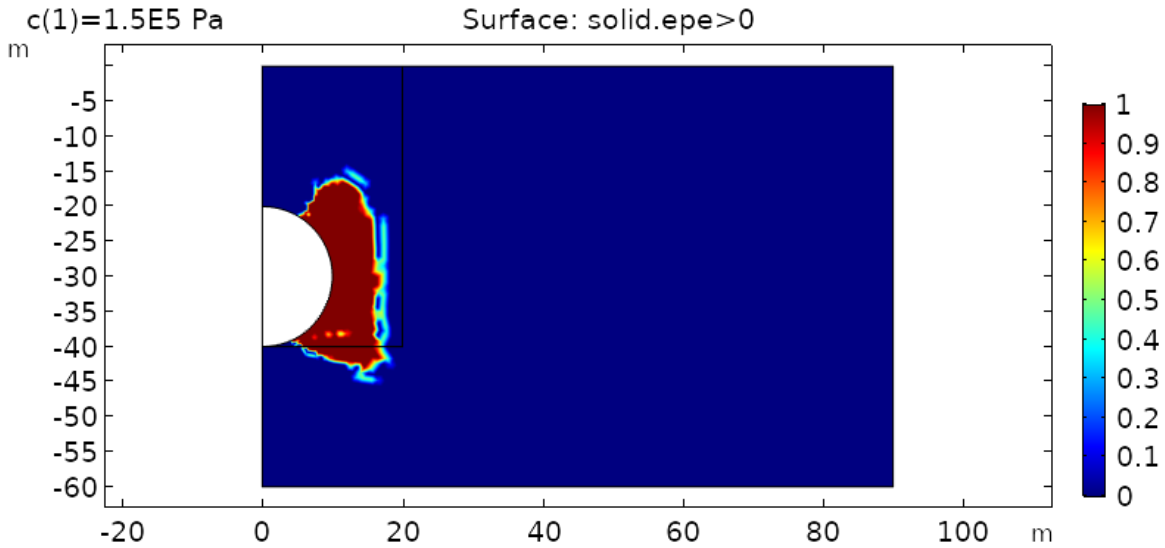


Figure 5.23 The effective plastic deformations after excavation with no TDA

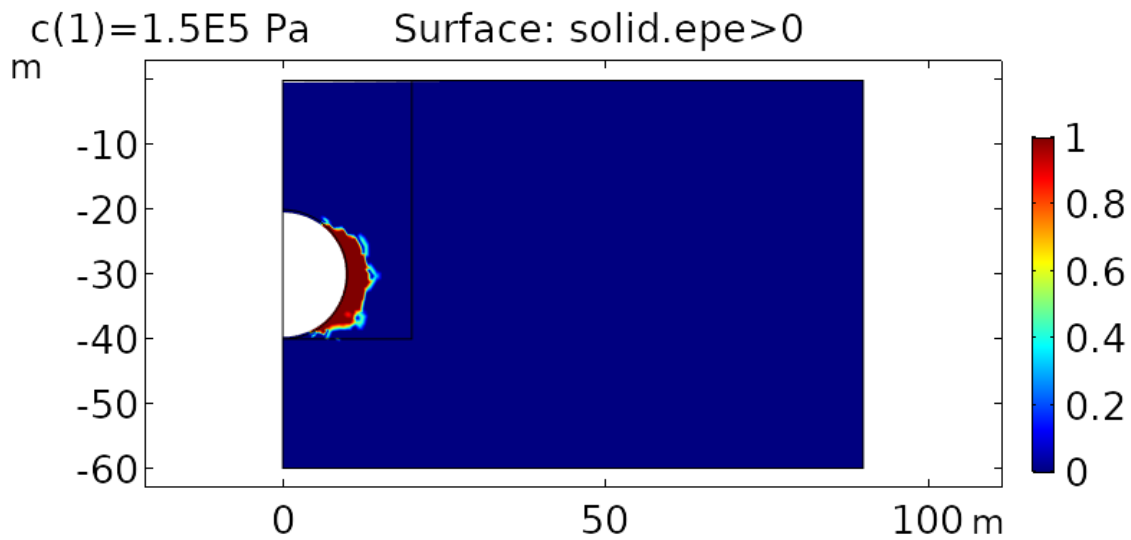


Figure 5.24 The effective plastic deformations after excavation with 50 % TDA

The horizontal displacement and the subsidence of the top surface due to excavation are shown respectively in Figure 5.25, Figure 5.26, Figure 5.27 and Figure 5.28. Again, here the effect is significant and the soil-TDA mixture produces much less displacements in the lateral as well as vertical directions.

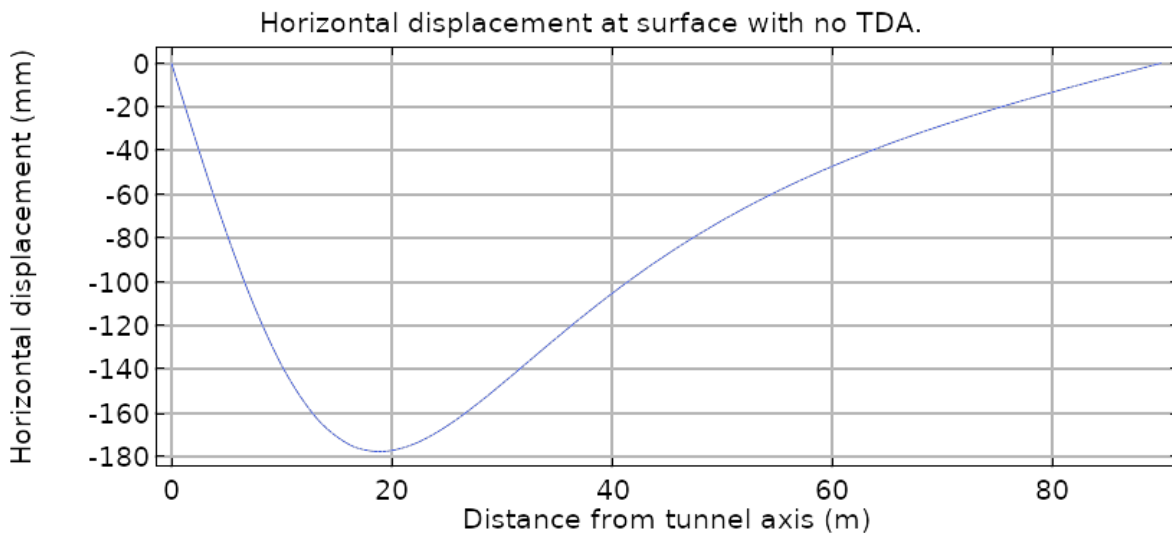


Figure 5.25 Horizontal displacement from the axis of symmetry of tunnel after excavation with no TDA

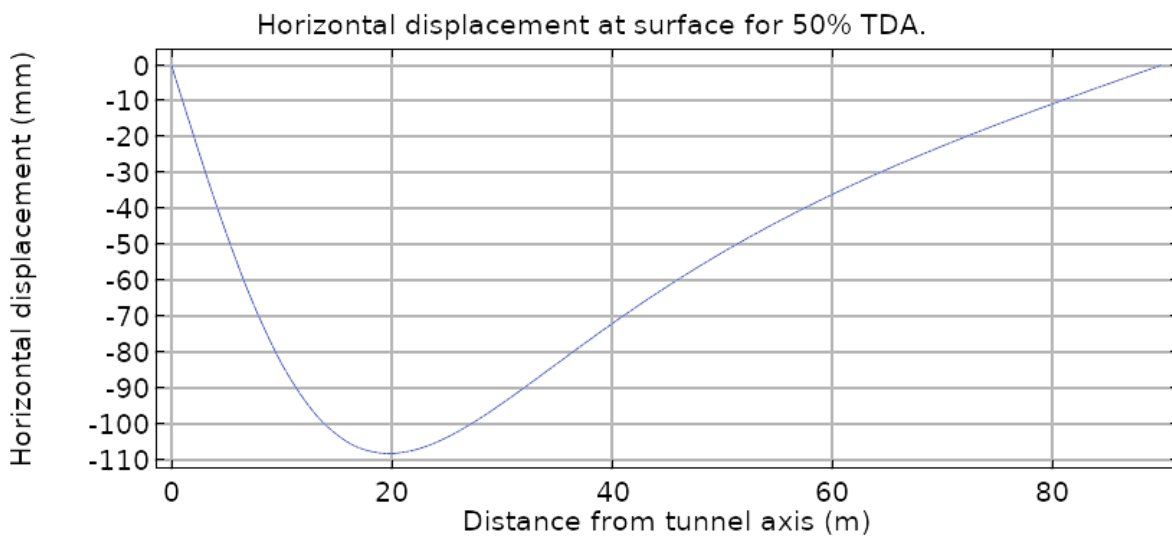


Figure 5.26 Horizontal displacement from the axis of symmetry of tunnel after excavation with 50% TDA

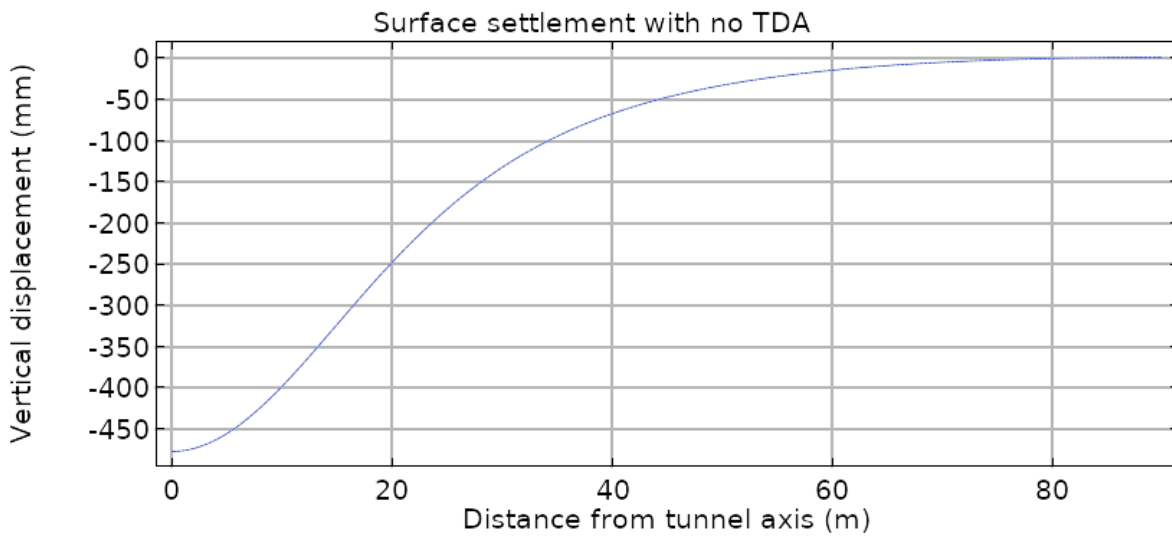


Figure 5.27 Surface displacement of tunnel after excavation with no TDA

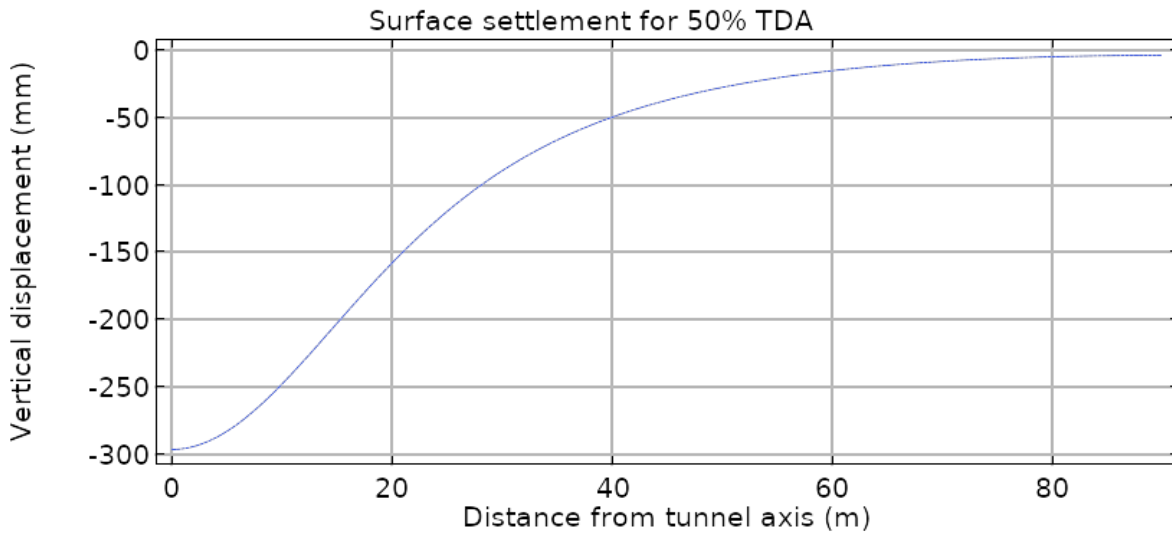


Figure 5.28 Surface displacement of tunnel after excavation with 50% TDA

CONCLUSION

Owing to the phenomenon of mechanization of societies the auto industry is growing faster than expected, which has led to the precipitate production of massive amounts of waste tire across the world. The dependence of people on to daily use of automobiles and consequently generation of higher quantities of scrap tire in such vast countries as Canada, that is additionally located in a cold region, is more highlighted. With careful and particular considerations to the disastrous experiences of two landfill tire fires that took place previously in the Ontario and Quebec provinces, recently a nationwide consensus has been developed aiming to reduce the illegal scrap tire landfills through recycling of these waste materials.

Application of processed scrap tire in form of Tire Derived Aggregate (TDA) for the various civil engineering purposes not only helps to remove vast quantities of scrap tire from the environment but additionally offers engineering advantages to the project designs and consequently the built-up structures.

In particular, when used as geomaterial in backfilling projects, mixtures of TDA with conventional soils especially sand have demonstrated to offer such unique mechanical and thermal properties as lightweight owing to its low unit weight, good thermal insulation due to its low thermal conductivity, appropriate drainage because of its great hydraulic conductivity, and removal of vast quantities of scrap tire thanks to the often mega projects and consequently demand to enormous volumes of geomaterials.

One of the main and all-time concerns of geotechnical engineers regarding the use of novel geomaterials is the long-term performance of the material which directly influences the service life of the civil engineering structures.

Owing to the low elastic modulus of tire rubber, geomaterials containing TDA are extremely compressible, making the excessive instantaneous and creep deformations a major concern for the geotechnical engineers. Hence, appropriate measures are necessary to be taken in order to achieve a reliable prediction of the long-term mechanical behavior of such materials. In order to prevent plausible failures these predictions are essential to be carried out by the design engineers and the results must be considered within the designs of the projects.

In order to obtain the objectives of the study, a series of laboratory experiments including direct shear tests, creep tests, triaxial tests, and a small-scale foundation test was carried out, finite element

simulations were conducted and consequently, a critical state model and constitutive equations have been proposed.

In accordance with the findings of the *creep parameter determination and the developed constitutive model* the following conclusions have been achieved:

1. The achieved laboratory testing results have demonstrated that the granulated materials containing sand-TDA mixtures while under a constant load experience a time-dependent creep deformation. This manifestation of creep begins with an instantaneous strain, followed by a decreasing rate of strain (primary creep) which gradually attains a practically constant value (secondary creep).
2. The Norton-Bailey law proved to be useful if one wishes to model a non-stationary creep phase that leads up to a stationary one. Furthermore, since the law is simply incorporated into commercial or programmed FEM codes, hence, it is even more effective.
3. Moreover, the test results reveal that the magnitude of the creep strain is highly influenced by the TDA volume fraction content (θ_p). Additionally, at a constant TDA volume fraction, the creep strain along with the strain rate increases with the vertical applied load. This trend is observed in all of the tests, with the difference that the magnitude of the strain rate is influenced by the intensity of the applied stress and TDA volume fraction (θ_p).
4. The creep parameters were verified via FEM simulations of the laboratory tests. A satisfactory match of the creep strain rate was obtained, with the Norton-Bailey constitutive equation, in all of the tests. Eventually, the FEM simulation of a rigid circular plate resting on a TDA-sand mixture, which employed the creep parameters achieved, gave satisfactory results.
5. The magnitude of the delayed creep deformation (long-term settlement) of the sand-TDA mixtures has been found to be significant. Therefore, an accurate estimation of the creep strain of such mixtures should be considered by the design engineers in geotechnical field projects.

In accordance with the findings of the *plasticity parameter determination and the developed critical state model* the following conclusions have been achieved:

6. It is evident from the triaxial test results that typically, TDA inclusion reinforces a sand matrix when compared with the sand without reinforcement (original sand). The results show that as

TDA volumetric ratio is constant, the magnitude of the deviatoric stress increases with confining stress for loose sand-TDA mixtures. Although, an increase in the TDA volumetric content tends to reduce the shear strength of the sand-TDA mixture.

7. By observing the stress-strain curves and simultaneously the barrel shape of the specimen at the end of the experiment that eventuated at an axial strain of approximately 23%, a strain hardening behaviour is evident for the specimen with TDA volumetric ratio of 75%. Therefore, the critical state appears to be complicated to obtain in such cases.
8. The test results depict that an increase in the TDA volumetric content results in a decrease in the stiffness of the sand-TDA mixtures. Especially, an increase in TDA volumetric ratio and a decrease of the confining pressure cause reduction of the secant moduli.
9. It is evident from the earlier discussed test results that the TDA volume fraction content plays a significant role as long as the behavior of the mixture is concerned. A constitutive equation, while in accordance with a critical state model (MCC), can adequately predict the amount of shear strength available in the sand-TDA mixture. The calculated deviatoric stress versus axial strain curves, achieved through the model, captured the non-linear elastoplastic response obtained in the tests. The level of the shear strength is significantly linked to the critical state friction angle which in turn depends on the TDA fraction content. In all these cases, the deviatoric stresses achieved from the tests are bracketed with the theoretical curves generated with the MCC.
10. In all simulations, the curves of the void ratio versus vertical strain indicate an overall compression of the sample. Initial void ratio mitigates towards a critical void ratio. This pattern is similar to that of loose granular materials.
11. The curves of the deviatoric strain versus volumetric strain confirm that distortion increases as the volumetric strain increment. The curves assume a non-linear shape with no peaks. In other words, no dilation is predicted by the MCC since all of sand-TDA mixtures were in a loose state at the beginning of all tests.
12. The plotted curve of deviatoric stress versus axial strain obtained from the results of axial loading and unloading of the specimen within the triaxial apparatus has been demonstrated the nonlinear behavior of the sand-TDA mixture during the rebound process. Hence, it can be concluded from the plotted curves that the deformation and rebound behaviors of the sand-TDA mixtures during axial loading and unloading are very similar.

In accordance with the findings of the *Simulation of the Behavior of the Sand-TDA Mixtures During a Tunnel Excavation* the following conclusions have been achieved:

This example presented a 2D simulation on the behavior of a sand-TDA mixture during a tunnel excavation. It must be noted that the surface settlement and the extent of the plastic region around the tunnel are important parameters which are essential in order to predict the required reinforcement during the excavation. For comparison purposes, this example considers both soil and soil-TDA ($\theta_p = 0.50$) reinforcement. The conclusions are as follows.

13. It was observed from the results that the sand-TDA mixture (50% TDA by volume) produces a significantly limited plastic zone in comparison with the simulation that considers sand without reinforcement.
14. Furthermore, it is evident from the simulations that the magnitude of the horizontal and vertical displacements over the tunnel experience a significant reduction, in the case of sand-TDA mixtures (50% TDA by volume), when compared with that of sand without reinforcement.

REFERENCES

- AbdelRazek, Ahmed, Rami M. El-Sherbiny, and Hani A. Lotfi. 2018. "Mechanical Properties and Time-Dependent Behaviour of Sand-Granulated Rubber Mixtures." *Geomechanics and Geoengineering* 13 (4): 288–300. <https://doi.org/10.1080/17486025.2018.1440013>.
- Abdrabbo, F. M., H. M. Abouseeda, K. E. Gaaver, and M. A. El-Marassi. 2005. "Behavior of Strip Footings Resting on Sand Reinforced with Tire-Chips." In *Geo-Frontiers Congress 2005*, edited by Mohamed A. Gabr, John J. Bowders, David Elton, and Jorge G. Zornberg, 14. Austin, Texas: ASCE. [https://doi.org/10.1061/40787\(166\)6](https://doi.org/10.1061/40787(166)6).
- Ahmed, Imtiaz. 1993. "Laboratory Study on Properties of Rubber-Soils. Publication FHWA/IN/JHRP-93/04. Joint Highway Research Project." *Indiana Department of Transportation and Purdue University*. West Lafayette, Indiana. <https://doi.org/10.5703/1288284314210>.
- Ahn, Il Sang, and Lijuan Cheng. 2014. "Tire Derived Aggregate for Retaining Wall Backfill under Earthquake Loading." *Construction and Building Materials* 57: 105–16. <https://doi.org/10.1016/j.conbuildmat.2014.01.091>.
- Anastasiadis, Anastasios, Kostas Senetakis, Kyriazis Pitolakis, Chrysanthi Gargala, and Iphigeneia Karakasi. 2012. "Dynamic Behavior of Sand/Rubber Mixtures. Part I: Effect of Rubber Content and Duration of Confinement on Small-Strain Shear Modulus and Damping Ratio." *Journal of ASTM International* 9 (2). <https://doi.org/10.1520/JAI103680>.
- Andersland, Orlando B., and Branko Ladanyi. 1994. *An Introduction to Frozen Ground Engineering. An Introduction to Frozen Ground Engineering*. Springer US. <https://doi.org/10.1007/978-1-4757-2290-1>.
- Apex-Companies. 2008. "Tarrtown Bridge Project Case Study: Guidance Document for Tire Derived Aggregate Embankment Construction and Design." *Commonwealth of Pennsylvania Department of Transportation*. Pennsylvania.
- Asadi, Mohsen, and Ahmad Mahboubi. 2019. "Three-Dimensional Numerical Simulation of Mechanical Properties of Soil-Tire Mixture by Discrete Element Method." *E3S Web of Conferences* 92: 1–4. <https://doi.org/10.1051/e3sconf/20199214011>.
- Asadi, Mohsen, Klaus Thoeni, and Ahmad Mahboubi. 2018. "An Experimental and Numerical Study on the Compressive Behavior of Sand-Rubber Particle Mixtures." *Computers and Geotechnics* 104 (July): 185–95. <https://doi.org/10.1016/j.compgeo.2018.08.006>.
- ASTM. 2008. "ASTM D6270 - 08 Standard Practice for Use of Scrap Tires in Civil Engineering Applications." In *Annual Book of ASTM Standards*. West Conshohocken, PA: ASTM. <https://doi.org/10.1520/D6270-08>.
- ASTM D 3080. 2003. "ASTM D 3080 - 03 Direct Shear Test of Soilds Under Consolidated Drained Conditions." *Astm International* 04: 7. www.astm.org.
- Atech Group. 2001. *A National Approach to Waste Tyres*. Enivronment Australia. https://books.google.ca/books/about/A_National_Approach_to_Waste_Tyres.html?id=opzIAAACA AJ&redir_esc=y.

- Attom, Mousa F. 2006. "The Use of Shredded Waste Tires to Improve the Geotechnical Engineering Properties of Sands." *Environmental Geology* 49 (4): 497–503. <https://doi.org/10.1007/s00254-005-0003-5>.
- Azizian, Mohammad F., Peter O. Nelson, Pugazhendhi Thayumanavan, and Kenneth J. Williamson. 2003. "Environmental Impact of Highway Construction and Repair Materials on Surface and Ground Waters: Case Study. Crumb Rubber Asphalt Concrete." *Waste Management* 23 (8): 719–28. [https://doi.org/10.1016/S0956-053X\(03\)00024-2](https://doi.org/10.1016/S0956-053X(03)00024-2).
- Bailey, R. W. 1935. "The Utilization of Creep Test Data in Engineering Design." [Http://Dx.Doi.Org/10.1243/PIME_PROC_1935_131_012_02](http://dx.doi.org/10.1243/PIME_PROC_1935_131_012_02) 131 (1): 131–349. https://doi.org/10.1243/PIME_PROC_1935_131_012_02.
- Balunaini, Umashankar, Varenya Kumar D. Mohan, Monica Prezzi, and Rodrigo Salgado. 2014. "Shear Strength of Tyre Chip–Sand and Tyre Shred–Sand Mixtures." *Proceedings of the Institution of Civil Engineers: Geotechnical Engineering* 167 (GE6): 585–95. <https://doi.org/10.1680/geng.13.00097>.
- Basel Convention. 2007. "Revised Technical Guidelines on the Environmentally Sound Management of Used Tyres, UNEP/CHW/OEWG/6/INF/6." Geneva, Switzerland. <http://archive.basel.int/meetings/oewg/oewg7/docs/i09e.pdf>.
- Basheer, Imad A., Yacoub M. Najjar, Robert W. Day, Paul S. H. Poh, and Bengt B. Broms. 1996. "Discussions and Closure: Slope Stabilization Using Old Rubber Tires and Geotextiles." *Journal of Performance of Constructed Facilities* 10 (1): 40–41. [https://doi.org/10.1061/\(ASCE\)0887-3828\(1996\)10:1\(40\)](https://doi.org/10.1061/(ASCE)0887-3828(1996)10:1(40)).
- Belabdelouahab, F., and H. Trouzine. 2014. "Research and Enhancement of Used Tyres, Such as Material Innovative in Algeria." *Physics Procedia* 55: 68–74. <https://doi.org/10.1016/j.phpro.2014.07.011>.
- Benessalah, Ismail, Ahmed Arab, Marwan Sadek, and Rachid Bouferra. 2019. "Laboratory Study on the Compressibility of Sand–Rubber Mixtures under One Dimensional Consolidation Loading Conditions." *Granular Matter* 21 (1): 7. <https://doi.org/10.1007/s10035-018-0860-8>.
- Bernal, Andres, C. W. Lovell, and Rodrigo Salgado. 1996. "Laboratory Study on the Use of Tire Shreds and Rubber-Sand in Backfilled and Reinforced Soil Applications. Publication FHWA/IN/JHRP-96/12." *Joint Highway Research Project, Indiana Department of Transportation and Purdue University*. West Lafayette, IN. <https://doi.org/10.5703/1288284313259>.
- Bosscher, Peter J., Tuncer B. Edil, and Senro Kuraoka. 1997. "Design of Highway Embankments Using Tire Chips." *Journal of Geotechnical and Geoenvironmental Engineering* 123 (4): 295–304. [https://doi.org/10.1061/\(ASCE\)1090-0241\(1997\)123:4\(295\)](https://doi.org/10.1061/(ASCE)1090-0241(1997)123:4(295)).
- Bosscher, Peter J, Tuncer B Edil, and Neil N Eldin. 1992. "Construction and Performance of a Shredded Waste Tire Test Embankment." *Transportation Research Record*, no. 1345: 44–52. <https://trid.trb.org/view/370717>.
- Boyle, J. T. (James T.), and J. (John) Spence. 1983. *Stress Analysis for Creep*. Butterworths.
- Cal-Recycle. 2009. "Continuing Education and University Curricula of Rubberized Asphalt Concrete and Civil Engineering Application of Waste Tires," no. May.

- Cal.Recycle. 2019. "Tire-Derived Aggregate (TDA)." California Department of Resources Recycling and Recovery (CalRecycle). January 28, 2019. <https://www.calrecycle.ca.gov/Tires/TDA>.
- CalRecycle. 2013. "DRRR-2014-1489 - Properties of Tire-Derived Aggregate For Civil Engineering Applications." *California Department of Resources Recycling and Recovery (CalRecycle)*. Sacramento, CA. <http://www.calrecycle.ca.gov/>.
- CalRecycle. 2016. "DRRR-2016-1545 - Usage Guide - TDA (Tire-Derived Aggregate)." *California Department of Resources Recycling and Recovery (CalRecycle)*. Sacramento, CA. <http://www.calrecycle.ca.gov/>.
- CARID. 2020. "The Hidden Secrets of Tires." 2020. <https://www.carid.com/articles/the-hidden-secrets-of-tires.html>.
- CATRA. 2019. "CATRA Annual Report 2019." *Canadian Association of Tire Recycling Agencies*. British Columbia. <https://www.catraonline.ca/>.
- CBC. 2019. "1990 Was the Year of the Tire Fire in Canada | CBC Archives." *CBC Archives*, May 16, 2019. <https://www.cbc.ca/archives/1990-was-the-year-of-the-tire-fire-in-canada-1.5126271>.
- Celauro, Bernardo, Clara Celauro, Davide Lo Presti, and Antonio Bevilacqua. 2012. "Definition of a Laboratory Optimization Protocol for Road Bitumen Improved with Recycled Tire Rubber." *Construction and Building Materials* 37: 562–72. <https://doi.org/10.1016/j.conbuildmat.2012.07.034>.
- Chamberlin, William P, and Prasanta K Gupta. 1986. "Use of Scrap Automobile Tire Rubber In Highway Construction, REPORT FHWA/NY/SR-86/85." *New York State Department of Transportation*. New York.
- Cheng, Lijuan, and Il-Sang Ahn. 2014. "Retaining Wall Shake-Table Test and Design Using Tire Derived Aggregates as Backfill." *California Department of Resources Recycling and Recovery, Publication # DRRR-2018-1640*. Sacramento, CA.
- Computype. 2020. "Parts of a Tire," 2020. <https://www.computype.com/>.
- Dammala, Pradeep K., Bali R. Sodom, and Murali K. Adapa. 2015. "Experimental Investigation of Applicability of Sand Tire Chip Mixtures as Retaining Wall Backfill." In *IFCEE 2015*, edited by Magued Iskander, Muhannad T. Suleiman, J. Brian Anderson, and Debra F. Laefer, 1420–29. San Antonio, Texas. <https://doi.org/10.1061/9780784479087.128>.
- Dickson, Todd H, Donald F Dwyer, and Dana N Humphrey. 2001. "Prototype Tire-Shred Embankment Construction." *Transportation Research Record* 1755 (01): 160–67. <https://doi.org/10.3141/1755-17>.
- Dorn, J. E. 1955. "Some Fundamental Experiments on High Temperature Creep." *Journal of the Mechanics and Physics of Solids* 3 (2): 85–116. [https://doi.org/10.1016/0022-5096\(55\)90054-5](https://doi.org/10.1016/0022-5096(55)90054-5).
- Downard, Jared, Ashish Singh, Robert Bullard, Thilina Jayarathne, Chathurika M. Rathnayake, Donald L. Simmons, Brian R. Wels, et al. 2015. "Uncontrolled Combustion of Shredded Tires in a Landfill - Part 1: Characterization of Gaseous and Particulate Emissions." *Atmospheric Environment* 104: 195–204. <https://doi.org/10.1016/j.atmosenv.2014.12.059>.

- Edeskar, T. 2006. "Use of Tyre Shreds in Civil Engineering Applications: Technical and Environmental Properties." *Theses*. <http://epubl.ltu.se/1402-1544/2006/67/index-en.html>.
- Edil, TB, and PJ Bosscher. 1994. "Engineering Properties of Tire Chips and Soil Mixtures." *Geotechnical Testing Journal* 17 (4): 453–64. <https://doi.org/10.1520/gtj10306j>.
- Edinçliler, Ayşe, Gökhan Baykal, and Altug Saygili. 2010. "Influence of Different Processing Techniques on the Mechanical Properties of Used Tires in Embankment Construction." *Waste Management* 30 (6): 1073–80. <https://doi.org/10.1016/j.wasman.2009.09.031>.
- Edinçliler, Ayse, Ali Firat Cabalar, Abdulkadir Cevik, and Haluk Isik. 2018. "New Formulations for Dynamic Behavior of Sand-Waste Tire Mixtures in a Small Range of Strain Amplitudes." *Periodica Polytechnica Civil Engineering* 62 (1): 92–101. <https://doi.org/10.3311/PPci.8698>.
- Ehsani, M., N. Shariatmadari, and S. M. Mirhosseini. 2015. "Shear Modulus and Damping Ratio of Sand-Granulated Rubber Mixtures." *Journal of Central South University* 22 (8): 3159–67. <https://doi.org/10.1007/s11771-015-2853-7>.
- Ehsani, M, N Shariatmadari, and S M Mirhosseini. 2017. "Experimental Study on Behavior of Soil-Waste Tire Mixtures." *Scientia Iranica, Transactions A: Civil Engineering* 24 (1): 65–71. <https://doi.org/10.24200/SCI.2017.2377>.
- Eldin, By Neil N, and Ahmed B Senouci. 1992. "USE OF SCRAP TIRES IN ROAD CONSTRUCTION." *Journal of Construction Engineering and Management* 118 (3): 561–76. [https://doi.org/10.1061/\(asce\)0733-9364\(1992\)118:3\(561\)](https://doi.org/10.1061/(asce)0733-9364(1992)118:3(561)).
- Eldin, Neil N., and Julian A. Piekarski. 1994. "SCRAP TIRES: MANAGEMENT AND ECONOMICS." *Journal of Environmental Engineering* 119 (6): 1217–32. [https://doi.org/10.1061/\(ASCE\)0733-9372\(1993\)119:6\(1217\)](https://doi.org/10.1061/(ASCE)0733-9372(1993)119:6(1217)).
- Eldin, Neil N., and Ahmed B. Senouci. 1993. "Rubber-Tire Particles as Concrete Aggregate." *Journal of Materials in Civil Engineering* 5 (4): 478–96. [https://doi.org/10.1061/\(ASCE\)0899-1561\(1993\)5:4\(478\)](https://doi.org/10.1061/(ASCE)0899-1561(1993)5:4(478)).
- EPA. 1997. "AIR EMISSIONS FROM SCRAP TIRE COMBUSTION, EPA-600/R-97-115." *U.S. Environmental Protection Agency (EPA)*. Washington, DC.
- EPA. 2010. *Scrap Tires: Handbook on Recycling Applications and Management for the U.S. and Mexico, EPA530-R-10-010*. Edited by Intergovernmental Panel on Climate Change. *U.S. Environmental Protection Agency*. Cambridge: Cambridge University Press. <https://doi.org/10.1128/AAC.03728-14>.
- Esmaeili, Morteza, and Nazanin Rezaei. 2016. "In Situ Impact Testing of a Light-Rail Ballasted Track with Tyre-Derived Aggregate Subballast Layer." *International Journal of Pavement Engineering* 17 (2): 176–88. <https://doi.org/10.1080/10298436.2015.1007226>.
- Feng, Zheng Yi, and Kevin G. Sutter. 2000. "Dynamic Properties of Granulated Rubber/Sand Mixtures." *Geotechnical Testing Journal* 23 (3): 338–44. <https://doi.org/10.1520/gtj11055j>.
- FHWA. 2016. "FHWA-RD-97-148 - User Guidelines for Waste and Byproduct Materials in Pavement Construction." Washington.
- Foose, Gary J., Craig H. Benson, and Peter J. Bosscher. 1996. "Sand Reinforced with Shredded Waste Tires." *Journal of Geotechnical Engineering* 122 (9): 760–67.

[https://doi.org/10.1061/\(asce\)0733-9410\(1996\)122:9\(760\)](https://doi.org/10.1061/(asce)0733-9410(1996)122:9(760)).

- Foriero, A, and N Ghafari. 2020. "Laboratory Creep Parameter Determination of Sand-TDA Mixtures with Subsequent FEM Validation." *Indian Geotechnical Journal*.
<https://doi.org/10.1007/s40098-019-00407-0>.
- Foriero, Adolfo, and Nima Ghafari. 2020. "Laboratory Creep Parameter Determination of Sand-TDA Mixtures with Subsequent FEM Validation." *Indian Geotechnical Journal* 50 (5): 710–725. <https://doi.org/10.1007/s40098-019-00407-0>.
- Garcia, Mauricio, Miguel A. Pando, and Brett Tempest. 2011. "Tire Derived Aggregates as a Sustainable Recycled Material for Retaining Wall Backfills." In *IICSDC 2011: Integrating Sustainability Practices in the Construction Industry*, edited by Wai Kiong Oswald Chong and Christopher Hermreck, 542–52. Kansas City, Missouri: ASCE.
<https://doi.org/10.1061/9780784412046>.
- Garga, Vinod K., and Vince O'Shaughnessy. 2000. "Tire-Reinforced Earthfill. Part 1 : Construction of a Test Fill, Performance, and Retaining Wall Design." *Canadian Geotechnical Journal* 37 (1): 75–96. <https://doi.org/10.1139/t99-084>.
- GeoSyntec. 2008. "Guidance Manual for Engineering Uses of Scrap Tires, ME0012-11/MD04173." *Maryland Department of the Environment*. Baltimore, Maryland.
- Ghazavi, Mahmoud. 2004. "Shear Strength Characteristics of Sand-Mixed with Granular Rubber." *Geotechnical and Geological Engineering* 22 (3): 401–16.
<https://doi.org/10.1023/B:GEGE.0000025035.74092.6c>.
- Ghazavi, Mahmoud, and Masoud Amel Sakhi. 2005. "Optimization of Aspect Ratio of Waste Tire Shreds in Sand-Shred Mixtures Using CBR Tests." *Geotechnical Testing Journal* 28 (6): 564–69. <https://doi.org/10.1520/GTJ12126>.
- Ghazavi, Mahmoud, and Masoud Amel Sakhi. 2005. "Influence of Optimized Tire Shreds on Shear Strength Parameters of Sand." *International Journal of Geomechanics* 5 (1): 58–65.
[https://doi.org/10.1061/\(ASCE\)1532-3641\(2005\)5:1\(58\)](https://doi.org/10.1061/(ASCE)1532-3641(2005)5:1(58)).
- Grubb, Dennis G., Wanxing Liu, Allen W. Cadden, and Dana N. Humphrey. 2007. "BULKHEAD DESIGN USING RECYCLED MATERIALS AS BACKFILL." In *11th Triennial International Conference on Ports*, edited by Wade Watson, 11. San Diego, California: ASCE.
[https://doi.org/10.1061/40834\(238\)90](https://doi.org/10.1061/40834(238)90).
- Guo, Peijun, and Xubin Su. 2007. "Shear Strength, Interparticle Locking, and Dilatancy of Granular Materials." *Canadian Geotechnical Journal* 44 (5): 579–91. <https://doi.org/10.1139/T07-010>.
- Guo, Shuaicheng, Qingli Dai, Ruizhe Si, Xiao Sun, and Chao Lu. 2017. "Evaluation of Properties and Performance of Rubber-Modified Concrete for Recycling of Waste Scrap Tire." *Journal of Cleaner Production* 148: 681–89. <https://doi.org/10.1016/j.jclepro.2017.02.046>.
- Harry, Kraus. 1980. *Creep Analysis*. New York: Wiley.
- Hazarika, Hemanta, Kazuya Yasuhara, Yoshiaki Kikuchi, Ashoke K. Karmokar, and Yoshio Mitarai. 2010. "Multifaceted Potentials of Tire-Derived Three Dimensional Geosynthetics in Geotechnical Applications and Their Evaluation." *Geotextiles and Geomembranes* 28 (3): 303–15. <https://doi.org/10.1016/j.geotexmem.2009.10.011>.

- Heimdahl, Thor C., and Andrew Drescher. 1999. "Elastic Anisotropy of Tire Shreds." *Journal of Geotechnical and Geoenvironmental Engineering* 125 (5): 383–89. [https://doi.org/10.1061/\(ASCE\)1090-0241\(1999\)125:5\(383\)](https://doi.org/10.1061/(ASCE)1090-0241(1999)125:5(383)).
- Hoor, Azadeh, and R. Kerry Rowe. 2012. "Application of Tire Chips to Reduce the Temperature of Secondary Geomembranes in Municipal Solid Waste Landfills." *Waste Management* 32 (5): 901–11. <https://doi.org/10.1016/j.wasman.2011.12.026>.
- Hoppe, Megan, and Matthew Oman. 2013. "Use of Tire Derived Products (TDP) in Roadway Construction, Report: 2013-20." St. Paul, MN.
- Humphrey, D. 2003. "CIVIL ENGINEERING APPLICATIONS OF TIRE SHREDS, Publication No. DRRR-2011-038." *California Integrated Waste Management Board*, 2003.
- Humphrey, D. N. 2008. "Tire Derived Aggregate as Lightweight Fill for Embankments and Retaining Walls." In *Proceedings of the International Workshop on Scrap Tire Derived Geomaterials - Opportunities and Challenges, IW-TDGM 2007*, 59–81. Taylor & Francis Group.
- Humphrey, Dana, and Michael Blumenthal. 2010. "The Use of Tire-Derived Aggregate in Road Construction Applications." In *Green Streets and Highways 2010: An Interactive Conference on the State of the Art and How to Achieve Sustainable Outcomes*, edited by Neil Weinstein, 299–313. Denver, Colorado: ASCE. [https://doi.org/10.1061/41148\(389\)25](https://doi.org/10.1061/41148(389)25).
- Humphrey, Dana N., and Robert A. Eaton. 1995. "Field Performance of Tire Chips as Subgrade Insulation for Rural Roads." In *SIXTH INTERNATIONAL CONFERENCE ON LOW-VOLUME ROADS*, 77–86. Minneapolis, Minnesota: NATIONAL ACADEMY PRESS, WASHINGTON, D.C. <https://trid.trb.org/view/426010>.
- Humphrey, Dana N., Thomas C. Sandford, Michelle M. Cribbs, and William P. Manion. 1993. "Shear Strength and Compressibility of Tire Chips for Use as Retaining Wall Backfill." *Transportation Research Record*, no. 1422: 29–35.
- Humphrey, Dana N, and Michael Swett. 2006. "LITERATURE REVIEW OF THE WATER QUALITY EFFECTS OF TIRE DERIVED AGGREGATE AND RUBBER MODIFIED ASPHALT PAVEMENT." *U.S. Environmental Protection Agency (USEPA)*. Orono, Maine. https://www.ustires.org/sites/default/files/LEA_013_USTMA.pdf.
- Jamshidi Chenari, Reza, Reza Alaie, and Behzad Fatahi. 2019. "Constrained Compression Models for Tire-Derived Aggregate-Sand Mixtures Using Enhanced Large Scale Oedometer Testing Apparatus." *Geotechnical and Geological Engineering* 37 (4): 2591–2610. <https://doi.org/10.1007/s10706-018-00780-2>.
- Jamshidi Chenari, Reza, Behzad Fatahi, Mohammad Ali Akhavan Maroufi, and Reza Alaie. 2017. "An Experimental and Numerical Investigation into the Compressibility and Settlement of Sand Mixed with TDA." *Geotechnical and Geological Engineering* 35 (5): 2401–20. <https://doi.org/10.1007/s10706-017-0255-3>.
- Jang, Ji Won, Taek Soo Yoo, Jae Hyun Oh, and Iwao Iwasaki. 1998. "Discarded Tire Recycling Practices in the United States, Japan and Korea." *Resources, Conservation and Recycling* 22 (1–2): 1–14. [https://doi.org/10.1016/S0921-3449\(97\)00041-4](https://doi.org/10.1016/S0921-3449(97)00041-4).
- JATMA. 2019. "TYRE INDUSTRY OF JAPAN 2019." *The Japan Automobile Tyre Manufacturers*

Association, August 2019. <https://www.jatma.or.jp/>.

- K. H. Roscoe and J. B. Burland. 1968. "On the Generalized Stress-Strain Behavior of 'Wet' Clay: 60. K. H. Roscoe and J. B. Burland. Engineering Plasticity (Papers for a Conference Held in Cambridge, Mar. 1968), Cambridge, University Press, 535–609 (1968)." *Cambridge University Press*, 535–609. [https://doi.org/10.1016/0022-4898\(70\)90160-6](https://doi.org/10.1016/0022-4898(70)90160-6).
- Kiran Sonti, Sanjaya Senadheera, P.W. Jayawickrama, Phillip T. Nash, and And Douglas D. Gransberg. 2003. "FHWA/TX-03/0-1808-1: Evaluate the Uses for Scrap Tires in Transportation Facilities." Austin, TX. <https://www.depts.ttu.edu/>.
- Kobelev, V. 2014. "Some Basic Solutions for Nonlinear Creep." *International Journal of Solids and Structures* 51 (19–20): 3372–81. <https://doi.org/10.1016/j.ijsolstr.2014.05.029>.
- Lee, J. H., R. Salgado, A. Bernal, and C. W. Lovell. 1999. "Shredded Tires and Rubber-Sand as Lightweight Backfill." *J. Geotech. Geoenviron. Eng.* 125 (2): 132–41. [https://doi.org/10.1061/\(ASCE\)1090-0241\(1999\)125:2\(132\)](https://doi.org/10.1061/(ASCE)1090-0241(1999)125:2(132)).
- Li, W., C. Y. Kwok, C. S. Sandeep, and K. Senetakis. 2019. "Sand Type Effect on the Behaviour of Sand-Granulated Rubber Mixtures: Integrated Study from Micro- to Macro-Scales." *Powder Technology* 342: 907–16. <https://doi.org/10.1016/j.powtec.2018.10.025>.
- Lopera Perez, J. C., C. Y. Kwok, and K. Senetakis. 2016. "Effect of Rubber Size on the Behaviour of Sand-Rubber Mixtures: A Numerical Investigation." *Computers and Geotechnics* 80: 199–214. <https://doi.org/10.1016/j.compgeo.2016.07.005>.
- Lopera Perez, J. C., C. Y. Kwok, and K. Senetakis. 2017a. "Investigation of the Micro-Mechanics of Sand-Rubber Mixtures at Very Small Strains." *Geosynthetics International* 24 (1): 30–44. <https://doi.org/10.1680/jgein.16.00013>.
- Lopera Perez, J. C., C. Y. Kwok, and K. Senetakis. 2017b. "Micromechanical Analyses of the Effect of Rubber Size and Content on Sand-Rubber Mixtures at the Critical State." *Geotextiles and Geomembranes* 45 (2): 81–97. <https://doi.org/10.1016/j.geotexmem.2016.11.005>.
- Ma, Yunming, Hongchang Wang, Kang Zhao, Lizhu Yan, and Dagang Yang. 2022. "Study of a Modified Time Hardening Model for the Creep Consolidation Effect of Asphalt Mixtures." *Materials* 15 (8). <https://doi.org/10.3390/ma15082710>.
- Madhusudhan, B. R., A. Boominathan, and Subhadeep Banerjee. 2019a. "Engineering Properties of Sand-Rubber Tire Shred Mixtures." *International Journal of Geotechnical Engineering*, 1–17. <https://doi.org/10.1080/19386362.2019.1617479>.
- Madhusudhan, B. R., A. Boominathan, and Subhadeep Banerjee. 2019b. "Factors Affecting Strength and Stiffness of Dry Sand-Rubber Tire Shred Mixtures." *Geotechnical and Geological Engineering* 37 (4): 2763–80. <https://doi.org/10.1007/s10706-018-00792-y>.
- Mahgoub, Ahmed, and Hany El Naggar. 2019. "Using TDA underneath Shallow Foundations: Simplified Design Procedure." *International Journal of Geotechnical Engineering* 00 (00): 1–15. <https://doi.org/10.1080/19386362.2019.1690415>.
- Marto, Aminaton, Nima Latifi, Raziieh Moradi, Mohsen Oghabi, and Sayyed Yaghouh Zolfeghari. 2013. "Shear Properties of Sand – Tire Chips Mixtures." *Electronic Journal of Geotechnical Engineering* 18 (B): 325–34.

- Masad, Eyad, Ramzi Taha, Carlton Ho, and Thomas Papagiannakis. 1996. "Engineering Properties of Tire/Soil Mixtures as a Lightweight Fill Material." *Geotechnical Testing Journal* 19 (3): 297–304. <https://doi.org/10.1520/gtj10355j>.
- Mashiri, M. S., J. S. Vinod, and M. Neaz Sheikh. 2016. "Constitutive Model for Sand-Tire Chip Mixture." *International Journal of Geomechanics* 16 (1): 1–10. [https://doi.org/10.1061/\(ASCE\)GM.1943-5622.0000472](https://doi.org/10.1061/(ASCE)GM.1943-5622.0000472).
- Mashiri, M. S., J. S. Vinod, M. Neaz Sheikh, and Hing Ho Tsang. 2015. "Shear Strength and Dilatancy Behaviour of Sand-Tyre Chip Mixtures." *Soils and Foundations* 55 (3): 517–28. <https://doi.org/10.1016/j.sandf.2015.04.004>.
- Mashiri, Maria Soledad. 2014. "Monotonic and Cyclic Behaviour of Sand-Tyre Chip (STCh) Mixtures." University of Wollongong. <http://ro.uow.edu.au/theses/4267>.
- Mawhinney, J. R. 1990a. "The Hagersville Tire Fire February 12 to 28, 1990." *National Research Council of Canada (NRC)*. <https://doi.org/10.4224/20378062>.
- Mawhinney, J. R. 1990b. "The Tire Fire at Saint Amable, Quebec, May 16 to 19, 1990, NRC-IRC-1805." *National Research Council of Canada (NRC)*. <https://doi.org/10.4224/20377250>.
- MDE. 2011. "MARYLAND SCRAP TIRE ANNUAL REPORT 2011." *MARYLAND DEPARTMENT OF THE ENVIRONMENT (MDE)*. Baltimore, MD. <https://www.maryland.gov>.
- Meles, Daniel, Alireza Bayat, and Hamid Soleymani. 2013. "Compression Behavior of Large-Sized Tire-Derived Aggregate for Embankment Application." *Journal of Materials in Civil Engineering* 25 (9): 1285–90. [https://doi.org/10.1061/\(ASCE\)MT.1943-5533.0000675](https://doi.org/10.1061/(ASCE)MT.1943-5533.0000675).
- Merry, Scott M., and Jonathan D. Bray. 1997. "Time-Dependent Mechanical Response of HDPE Geomembranes." *Journal of Geotechnical and Geoenvironmental Engineering* 123 (1): 57–65. [https://doi.org/10.1061/\(ASCE\)1090-0241\(1997\)123:1\(57\)](https://doi.org/10.1061/(ASCE)1090-0241(1997)123:1(57)).
- Moghaddas Tafreshi, S. N., and A. H. Norouzi. 2012. "Bearing Capacity of a Square Model Footing on Sand Reinforced with Shredded Tire - An Experimental Investigation." *Construction and Building Materials* 35: 547–56. <https://doi.org/10.1016/j.conbuildmat.2012.04.092>.
- Mohamad, Edy Tonnizam, Nima Latifi, Aminaton Marto, Razieh Moradim, and Seyed Vahid Alavi Nezhad Khalil Abad. 2013. "Effects of Relative Density on Shear Strength Characteristics of Sand-Tire Chips Mixture." *Electronic Journal of Geotechnical Engineering* 18 (D): 623–32.
- Mujibur Rahman. 2004. "CHARACTERISATION OF DRY PROCESS CRUMB RUBBER MODIFIED ASPHALT MIXTURES, A Thesis Submitted to the University of Nottingham." *University of Nottingham*. Nottingham.
- Naggar, A. El, P. Sadeghian, and H. El Naggar. 2019. "Using TDA to Partially Replace Coarse Aggregates in Concrete Mixtures." *Proceedings, Annual Conference - Canadian Society for Civil Engineering* 2019-June: 1–7.
- Naggar, Hany El, Pendar Soleimani, and Amirnezam Fakhroo. 2016. "Strength and Stiffness Properties of Green Lightweight Fill Mixtures." *Geotechnical and Geological Engineering* 34 (3): 867–76. <https://doi.org/10.1007/s10706-016-0010-1>.
- Nantung, Tommy, Nayyar Zia, Monica Prezzi, Uma Balunaini, and Minsang Lee. 2009. "Use of

- Tire Shreds in Lightweight Fill Construction. Publication FHWA/IN/JTRP-2009/36.” FHWA/IN/JTRP-2009/36. *Joint Transportation Research Program, Indiana Department of Transportation and Purdue University*. Joint Transportation Research Program Technical Report Series. West Lafayette, IN: Indiana Department of Transportation and Purdue University. <https://doi.org/10.5703/1288284314331>.
- Ngo, Anh T, and Julio R Valdes. 2007. “Creep of Sand – Rubber Mixtures.” *Journal of Materials in Civil Engineering* 19 (12): 1101–5. [https://doi.org/10.1061/\(ASCE\)0899-1561\(2007\)19:12\(1101\)](https://doi.org/10.1061/(ASCE)0899-1561(2007)19:12(1101)).
- Noorzad, Reza, and Masoud Raveshi. 2017. “Mechanical Behavior of Waste Tire Crumbs–Sand Mixtures Determined by Triaxial Tests.” *Geotechnical and Geological Engineering* 35 (4): 1793–1802. <https://doi.org/10.1007/s10706-017-0209-9>.
- Norton, F.H. 1929. *The Creep of Steel at High Temperatures*. London: McGraw-Hill book company, inc. https://openlibrary.org/books/OL23291700M/The_creep_of_steel_at_high_temperatures.
- NYSDOT. 2015. “GEM-20, Guidelines for Project Selection, Design, and Construction of Tire Shreds in Embankments.” New York. www.dot.ny.gov/.
- Oikonomou, N., and S. Mavridou. 2009. “The Use of Waste Tyre Rubber in Civil Engineering Works.” In *Sustainability of Construction Materials*, edited by Jamal M. Khatib, 213–38. Woodhead Publishing. <https://doi.org/10.1533/9781845695842.213>.
- Pacheco-Torgal, F., Yining Ding, and Said Jalali. 2012. “Properties and Durability of Concrete Containing Polymeric Wastes (Tyre Rubber and Polyethylene Terephthalate Bottles): An Overview.” *Construction and Building Materials* 30: 714–24. <https://doi.org/10.1016/j.conbuildmat.2011.11.047>.
- Penny, R.K., and D.L. Marriott. 1995. *Design for Creep*. 2nd ed. London: SPRINGER-SCIENCE+BUSINESS MEDIA, B.V. <https://doi.org/10.1007/978-94-011-0561-3>.
- Platzer, Auriane, Salman Rouhanifar, Patrick Richard, Bogdan Cazacliu, and Erdin Ibrahim. 2018. “Sand–Rubber Mixtures Undergoing Isotropic Loading: Derivation and Experimental Probing of a Physical Model.” *Granular Matter* 20 (4). <https://doi.org/10.1007/s10035-018-0853-7>.
- Presti, Davide Lo. 2013. “Recycled Tyre Rubber Modified Bitumens for Road Asphalt Mixtures: A Literature Review.” *Construction and Building Materials* 49 (December 2013): 863–81. <https://doi.org/10.1016/j.conbuildmat.2013.09.007>.
- Promptthangkoon, Panu, and Bancherd Karnchanachetanee. 2013. “Geomaterial Prepared from Waste Tyres, Soil and Cement.” *Procedia - Social and Behavioral Sciences* 91: 421–28. <https://doi.org/10.1016/j.sbspro.2013.08.439>.
- Raffoul, Samar, Reyes Garcia, David Escolano-Margarit, Maurizio Guadagnini, Iman Hajirasouliha, and Kypros Pilakoutas. 2017. “Behaviour of Unconfined and FRP-Confined Rubberised Concrete in Axial Compression.” *Construction and Building Materials* 147: 388–97. <https://doi.org/10.1016/j.conbuildmat.2017.04.175>.
- Rao, G.Venkatappa, and R. K. Dutta. 2006. “Compressibility and Strength Behaviour of Sand-Tyre Chip Mixtures.” *Geotechnical and Geological Engineering* 24 (3): 711–24. <https://doi.org/10.1007/s10706-004-4006-x>.

- RECYC-QUÉBEC. 2019. “Indicateurs de Performance 2019, PROGRAMME QUÉBÉCOIS DE GESTION DES PNEUS HORS D’USAGE.” Québec. <https://www.recyq-quebec.gouv.qc.ca/>.
- Recycling Research Institute. 2020. “Tire Derived Aggregate - Scrap Tire News: Tire and Rubber Recycling News and Information.” Recycling Research Institute. 2020. <https://scraptirenews.com/information-center/tda/>.
- Reddy, S. Bali, A. Murali Krishna, and Krishna R. Reddy. 2018. “Sustainable Utilization of Scrap Tire Derived Geomaterials for Geotechnical Applications.” *Indian Geotechnical Journal* 48 (2): 251–66. <https://doi.org/10.1007/s40098-017-0273-3>.
- Reddy, Sodom Bali, and Adapa Murali Krishna. 2017. “Tyre Chips as Compressible Inclusions in Earth-Retaining Walls.” *Proceedings of the Institution of Civil Engineers: Ground Improvement* 170 (3): 137–48. <https://doi.org/10.1680/jgrim.16.00034>.
- Rodríguez, Luis Medina, Marcos Arroyo, and Miguel Martín Cano. 2018. “Use of Tire-Derived Aggregate in Tunnel Cut-and-Cover.” *Canadian Geotechnical Journal* 55 (7): 968–78. <https://doi.org/10.1139/cgj-2017-0446>.
- Schofield, Andrew, and Peter Wroth. 1968. *Critical State Soil Mechanics*. McGraw-Hill. New York: McGraw-Hill. <http://www-civ.eng.cam.ac.uk/>.
- Schwab Tire Center, Les. 2020. “Tire Size Explained: Reading the Sidewall - Les Schwab.” 2020. <https://www.lesschwab.com/article/tire-size-explained-reading-the-sidewall.html>.
- Scott, Ewan. 2016. “ETRMA 2015 END-OF-LIFE TYRE REPORT.” *European Tyre & Rubber Manufacturers Association (ETRMA)*. Brussels. <https://www.etrma.org/>.
- Senetakis, Kostas, Anastasios Anastasiadis, and Kyriazis Ptilakis. 2012. “Dynamic Properties of Dry Sand/Rubber (SRM) and Gravel/Rubber (GRM) Mixtures in a Wide Range of Shearing Strain Amplitudes.” *Soil Dynamics and Earthquake Engineering* 33 (1): 38–53. <https://doi.org/10.1016/j.soildyn.2011.10.003>.
- Senoro, D.B., S.L. Maravillas, N. Ghafari, C.C. Rivera, E.C. Quiambao, and M.C.M. Lorenzo. 2016. “Modeling of the Residue Transport of Lambda Cyhalothrin, Cypermethrin, Malathion and Endosulfan in Three Different Environmental Compartments in the Philippines.” *Sustainable Environment Research* 26 (4): 168–76. <https://doi.org/10.1016/j.serj.2016.04.010>.
- Sheikh, M. Neaz, M. S. Mashiri, J. S. Vinod, and Hing Ho Tsang. 2013. “Shear and Compressibility Behavior of Sand-Tire Crumb Mixtures.” *Journal of Materials in Civil Engineering* 25 (10): 1366–74. [https://doi.org/10.1061/\(ASCE\)MT.1943-5533.0000696](https://doi.org/10.1061/(ASCE)MT.1943-5533.0000696).
- Shercom Industries Inc. 2015. “Tire Derived Aggregate (TDA).” Saskatoon, Saskatchewan, Canada. 2015. <https://www.shercomindustries.com/>.
- Siddika, Ayesha, Md Abdullah Al Mamun, R. Alyousef, Y. H. Mugahed Amran, Farhad Aslani, and Hisham Alabduljabbar. 2019. “Properties and Utilizations of Waste Tire Rubber in Concrete: A Review.” *Construction and Building Materials* 224 (November): 711–31. <https://doi.org/10.1016/j.conbuildmat.2019.07.108>.
- Singh, Ashish, Scott N. Spak, Elizabeth A. Stone, Jared Downard, Robert L. Bullard, Mark Pooley, Pamela A. Kostle, et al. 2015. “Uncontrolled Combustion of Shredded Tires in a Landfill - Part 2: Population Exposure, Public Health Response, and an Air Quality Index for Urban Fires.” *Atmospheric Environment* 104: 273–83.

<https://doi.org/10.1016/j.atmosenv.2015.01.002>.

- Singh, Awtar, and James K. Mitchell. 1968. "General Stress-Strain-Time Function for Soils." *Journal of the Soil Mechanics and Foundations Division* 94 (1): 21–46.
- Tanchaisawat, T., D. T. Bergado, and P. Voottipruex. 2008. "Numerical Simulation and Sensitivity Analyses of Full-Scale Test Embankment with Reinforced Lightweight Geomaterials on Soft Bangkok Clay." *Geotextiles and Geomembranes* 26 (6): 498–511.
<https://doi.org/10.1016/j.geotexmem.2008.05.005>.
- Tatliso, N., T. B. Edil, and C. H. Benson. 1998. "Interaction between Reinforcing Geosynthetics and Soil-Tire Chip Mixtures." *Journal of Geotechnical and Geoenvironmental Engineering* 124 (11): 1109–19. [https://doi.org/10.1061/\(ASCE\)1090-0241\(1998\)124:11\(1109\)](https://doi.org/10.1061/(ASCE)1090-0241(1998)124:11(1109)).
- Tatliso, N, CH Benson, and TB Edil. 1997. "Effect of Fines on Mechanical Properties of Soil-Tire Chip Mixtures." In *Testing Soil Mixed with Waste or Recycled Materials*, edited by M. Wasemiller and K. Hoddinott, 93–108. West Conshohocken, PA: ASTM International.
<https://doi.org/10.1520/stp15645s>.
- Thakur, Disha, and M K Kaushik. 2016. "Assessment of Drainage Properties of Tires Derived Aggregates to Be Used As Drainage Layer Material in Leachate Collection System of MSW Landfill." *International Journal of Innovative Research in Science, Engineering and Technology* 5 (2): 2219–30. <https://doi.org/10.15680/IJRSET.2016.050114>.
- Thomas, Blessen Skariah, and Ramesh Chandra Gupta. 2015. "Long Term Behaviour of Cement Concrete Containing Discarded Tire Rubber." *Journal of Cleaner Production* 102: 78–87.
<https://doi.org/10.1016/j.jclepro.2015.04.072>.
- Torretta, Vincenzo, Elena Cristina Rada, Marco Ragazzi, Ettore Trulli, Irina Aura Istrate, and Lucian Ionel Cioca. 2015. "Treatment and Disposal of Tyres: Two EU Approaches. A Review." *Waste Management* 45: 152–60. <https://doi.org/10.1016/j.wasman.2015.04.018>.
- Tsiavos, Anastasios, Nicholas A. Alexander, Andrea Diambra, Erdin Ibrahim, Paul J. Vardanega, Alicia Gonzalez-Buelga, and Anastasios Sextos. 2019. "A Sand-Rubber Deformable Granular Layer as a Low-Cost Seismic Isolation Strategy in Developing Countries: Experimental Investigation." *Soil Dynamics and Earthquake Engineering* 125 (May): 105731.
<https://doi.org/10.1016/j.soildyn.2019.105731>.
- Tweedie, J. J., D. N. Humphrey, and T. C. Sandford. 1998. "Tire Shreds as Lightweight Retaining Wall Backfill: Active Conditions." *Journal of Geotechnical and Geoenvironmental Engineering* 124 (11): 1061–70. [https://doi.org/10.1061/\(ASCE\)1090-0241\(1998\)124:11\(1061\)](https://doi.org/10.1061/(ASCE)1090-0241(1998)124:11(1061)).
- Tweedie, Jeffrey J., Dana N. Humphrey, Michael H. Wight, David E. Shaw, and John H. Stetson. 2004. "Old Town – Mud Pond Inlet Bridge, Rehabilitation of a Timber Structure with Tire Shreds." In *Geotechnical Engineering for Transportation Projects*, 740–49. Reston, VA: ASCE. [https://doi.org/10.1061/40744\(154\)61](https://doi.org/10.1061/40744(154)61).
- Tweedie, Jeffrey J, Dana N Humphrey, and Thomas C Sandford. 1998. "Tire Chips as Lightweight Backfill for Retaining Walls - Phase II, NETCR-8." *The New England Transportation Consortium*, March 11, 1998. <https://rosap.nhl.bts.gov/view/dot/42351>.
- USTMA. 2018. "2017 U.S. Scrap Tire Management Summary." *U.S. Tire Manufacturers*

- Association (USTMA). Washington. <https://www.ustires.org/>.
- Wang, Can, An Deng, and Abbas Taheri. 2018. "Three-Dimensional Discrete Element Modeling of Direct Shear Test for Granular Rubber–sand." *Computers and Geotechnics* 97 (January): 204–16. <https://doi.org/10.1016/j.compgeo.2018.01.014>.
- Ward, I. M., and J. Sweeney. 2004. *An Introduction to the Mechanical Properties of Solid Polymers*. 2nd ed. John Wiley & Sons.
- Wartman, Joseph, Mark F. Natale, and Patrick M. Strenk. 2007. "Immediate and Time-Dependent Compression of Tire Derived Aggregate." *Journal of Geotechnical and Geoenvironmental Engineering* 133 (3): 245–56. [https://doi.org/10.1061/\(ASCE\)1090-0241\(2007\)133:3\(245\)](https://doi.org/10.1061/(ASCE)1090-0241(2007)133:3(245)).
- Williams, Paul T., Serpil Besler, and David T. Taylor. 1990. "The Pyrolysis of Scrap Automotive Tyres. The Influence of Temperature and Heating Rate on Product Composition." *Fuel* 69 (12): 1474–82. [https://doi.org/10.1016/0016-2361\(90\)90193-T](https://doi.org/10.1016/0016-2361(90)90193-T).
- World Business Council for Sustainable Development (WBCSD), Geneva, Switzerland. 2020. "End-of-Life Tires - World Business Council for Sustainable Development (WBCSD)." World Business Council for Sustainable Development, Geneva, Switzerland. 2020. <https://www.wbcscd.org/>.
- Wu, Wei Y., Christopher C. Benda, and Robert F. Cauley. 1997. "Triaxial Determination of Shear Strength of Tire Chips." *Journal of Geotechnical and Geoenvironmental Engineering* 123 (5): 479–82. [https://doi.org/10.1061/\(ASCE\)1090-0241\(1997\)123:5\(479\)](https://doi.org/10.1061/(ASCE)1090-0241(1997)123:5(479)).
- Xiao, Ming, Jan Bowen, Mathew Graham, and Jesus Larralde. 2012. "Comparison of Seismic Responses of Geosynthetically Reinforced Walls with Tire-Derived Aggregates and Granular Backfills." *Journal of Materials in Civil Engineering* 24 (11): 1368–77. [https://doi.org/10.1061/\(ASCE\)MT.1943-5533.0000514](https://doi.org/10.1061/(ASCE)MT.1943-5533.0000514).
- Xiao, Ming, Martin Ledezma, and Corbin Hartman. 2014. "Large-Scale Shear Testing of Tire Derived Aggregates (TDA)." In *Geo-Congress 2014*, edited by Murad Abu-Farsakh, Xiong Yu, and Laureano R. Hoyos, 3744–53. Atlanta, Georgia: ASCE. <https://doi.org/10.1061/9780784413272>.
- Yao, Hua Tang, Fu Zhen Xuan, Zhengdong Wang, and Shan Tung Tu. 2007. "A Review of Creep Analysis and Design under Multi-Axial Stress States." *Nuclear Engineering and Design* 237 (18): 1969–86. <https://doi.org/10.1016/j.nucengdes.2007.02.003>.
- Yoon, Sungmin, Monica Prezzi, Nayyar Zia Siddiki, and Bumjoo Kim. 2006. "Construction of a Test Embankment Using a Sand-Tire Shred Mixture as Fill Material." *Waste Management* 26 (9): 1033–44. <https://doi.org/10.1016/j.wasman.2005.10.009>.
- Yoon, Yeo Won, Sung Han Cheon, and Dae Seong Kang. 2004. "Bearing Capacity and Settlement of Tire-Reinforced Sands." *Geotextiles and Geomembranes* 22 (5): 439–53. <https://doi.org/10.1016/j.geotextmem.2003.12.002>.
- Yoon, Yeo Won, Seung Beom Heo, and Keun Soo Kim. 2008. "Geotechnical Performance of Waste Tires for Soil Reinforcement from Chamber Tests." *Geotextiles and Geomembranes* 26 (1): 100–107. <https://doi.org/10.1016/j.geotextmem.2006.10.004>.
- Youwai, Sompote, and Dennes T. Bergado. 2003. "Strength and Deformation Characteristics of Shredded Rubber Tire - Sand Mixtures." *Canadian Geotechnical Journal* 40 (2): 254–64.

<https://doi.org/10.1139/t02-104>.

Zornberg, Jorge G., Alexandre R. Cabral, and Chardphoom Viratjandr. 2004. "Behaviour of Tire Shred - Sand Mixtures." *Canadian Geotechnical Journal* 41 (2): 227–41.
<https://doi.org/10.1139/t03-086>.